

Sheffield Hallam University

Fundamentals studies of a magnetically steered vacuum arc.

WALKE, Paul.

Available from the Sheffield Hallam University Research Archive (SHURA) at:

<http://shura.shu.ac.uk/20482/>

A Sheffield Hallam University thesis

This thesis is protected by copyright which belongs to the author.

The content must not be changed in any way or sold commercially in any format or medium without the formal permission of the author.

When referring to this work, full bibliographic details including the author, title, awarding institution and date of the thesis must be given.

Please visit <http://shura.shu.ac.uk/20482/> and <http://shura.shu.ac.uk/information.html> for further details about copyright and re-use permissions.



BRN 309754

Sheffield Hallam University
REFERENCE ONLY

Fines are charged at 50p per hour

16 APR 2002 4.59pm	26 JUN 2002 4.18pm
17 APR 2002 9.00	26 NOV 2002 5.33
18 APR 2002 5.52	27 NOV 2002 8.54
18 APR 2002 9.00pm	
19 APR 2002 4.18pm	

ProQuest Number: 10701129

All rights reserved

INFORMATION TO ALL USERS

The quality of this reproduction is dependent upon the quality of the copy submitted.

In the unlikely event that the author did not send a complete manuscript and there are missing pages, these will be noted. Also, if material had to be removed, a note will indicate the deletion.



ProQuest 10701129

Published by ProQuest LLC (2017). Copyright of the Dissertation is held by the Author.

All rights reserved.

This work is protected against unauthorized copying under Title 17, United States Code
Microform Edition © ProQuest LLC.

ProQuest LLC.
789 East Eisenhower Parkway
P.O. Box 1346
Ann Arbor, MI 48106 – 1346

**Fundamental studies
of a
magnetically steered vacuum arc**

Paul Walke, BSc

A thesis submitted in partial fulfilment of the requirements of
Sheffield Hallam University for the degree of Doctor of Philosophy

September 1994

The Division of Applied Physics, Sheffield Hallam University
in collaboration with Hauzer Techno Coating, Europe B.V.

Abstract

In recent years demand from production industry for high performance cutting tools, aero and automobile engine parts has prompted research into both existing and novel methods of laying down hard, low friction coatings. A key process for the production of such coatings has been Physical Vapour Deposition (PVD) which has proved to be a consistent and reliable tool for industry. For this technique to continue to be improved and more advanced coatings to be produced, research at the fundamental level is required. This thesis describes research investigating the behaviour of the steered arc cathode spot and methods of improving existing steered arc coating technology.

The majority of existing steered arc systems use either permanent magnets or a combination of permanent and electromagnets to steer the arc. Described here is a novel system which employs a pair of electromagnetic coils of cylindrical geometry which enable the arc to be positioned on a circular orbit through a range of continuously variable radii. In addition to this the coils are capable of controlling the transverse and normal magnetic field profiles independently of the steering radius selected. This enables the behaviour of the arc spot to be investigated under a range of magnetic field conditions thus allowing the comparison of measured arc behaviour with a new model of arc motion.

Care has described the motion of the arc spot as a biased random walk and has derived an analytical solution to describe the time dependent, probability density function for the arc position in two dimensions. Two distributions are proposed (one in each dimension); the first describes the probability density for the arc position in the direction of driven motion, the second the probability density in the direction of arc confinement. The shape of these distributions is dependent upon the transverse and normal components of the applied magnetic field.

A series of experiments are described here that measure the shape of these distributions as a function of either magnetic field, cathode material or both. In the case of the distribution of the arc position in the direction of confinement the width of the distribution is measured as a function of normal and transverse field components. In the direction of steered motion, distributions of arc orbital transit times are measured for a number of cathode materials: analysis of these distributions allow the determination of a mean macroscopic spot velocity and the spot diffusion coefficient. In both cases comparison with Care's model reveals good agreement between experiment and theory to the limits of the experimental apparatus. A further experiment was also conducted to test the prediction that the diffusion coefficient (measured in the direction of steered motion) is independent of the applied field. In this case results are inconclusive and further work is recommended.

The mean spot velocity and diffusion coefficients for four materials were measured; titanium, zirconium, aluminium and 316 stainless steel. The results for aluminium and stainless steel compared favourably with some measurements performed by other workers, whilst those for titanium and zirconium are new results with no data available for comparison.

Advanced studies

As part of the course of study I attended two workshops. The first of these was a two day event on Physical Vapour Deposition techniques and research which is run on an annual basis at the University of Hull. The second was the three day 1st European Workshop on Plasma Ion Surface Engineering held in Toulouse. I have also attended a number of research seminars on a variety of topics, these were presented at Sheffield Hallam University by resident or visiting academics.

The following conference was attended:

The Third International Conference on Plasma Surface Engineering (PSE '92),
Garmisch-Partenkirchen, Germany, October 1992.

Publications

The following papers were presented at conference and accepted for publication in the named journal.

'The behaviour of a steered cathodic arc as a function of steering magnetic field',
Presented at The Third International Conference on Plasma Surface
Engineering, PSE '92, Garmisch-Partenkirchen, Germany, October 1992.
Published in Surface and Coating Technology, **59**, 126, (1993).

'The distribution of transit times in a magnetically steered cathodic arc',
Presented at The International Conference on Metallurgical Coatings and Thin
Films,
ICMCTF '94, San Diego, USA, April 1994
Accepted for publication in Surface and Coating Technology.

Acknowledgements

Firstly, I would like to thank my supervisors at the University, Dr. R. New and Professor C.M. Care, for their time in the form of helpful discussions throughout the period of study (and giving me a few pointers in the basics of the English language). I would also like to thank Messrs R. Day and G. Robinson for their enthusiastic and expert technical advice and assistance (whilst I provided the cabaret) and Mr L. Donohue for issuing the challenge to include the words 'moist' and 'fluffy' in this thesis.

I would also like to offer my thanks to both The Science and Engineering Research Council for funding the research and also for sponsoring my trip to The PSE '92 Conference and also to all the technical staff in Physics for putting up with me for four years (especially Glenn Miller for breaking off his last European gig to supply me with computing hardware).

Finally I would like to thank my wife Karen for years of selfless support (financial and other wise) and also the late Dr David Allen-Booth for re-admitting me to the University to study for my first degree against his better judgement.

'It never fails to amaze me
why people get excited and vexed.
You'll always be late for the previous train
and always in time for the next'

Piet Heyn

Contents

Chapter One:	Introduction to Physical Vapour Deposition.	1
1.1	Arc coating methods	1
1.1.1	The random arc	1
1.1.2	The steered arc	4
1.1.3	Arc evaporation using segmented cathodes	6
1.1.4	Filtered arc	6
1.2	Present work	8
Chapter Two	Experimental studies of the cathode spot.	12
2.1	The spot life cycle	13
2.1.1	Surface explosion	14
2.1.2	Melting and deformation	16
2.1.3	Crater formation and steady state	17
2.1.4	New spot ignition	18
2.2	The type of cathode spot	19
2.2.1	The Type I cathode spot	19
2.2.2	The Type II cathode spot	20
2.3	The spot diameter and current density	20
2.4	The total current per spot (spot splitting)	23
2.5	The type of erosion	25
2.6	Spot motion	27
2.6.1	Random spot motion	27
2.6.2	The arc motion in a magnetic field	35
2.7	Summary	40

Chapter Three	Theoretical models of the arc.	47
3.1	An introduction to spot models	47
3.1.1	Heating processes	49
3.1.2	Cooling processes	50
3.1.3	Summary	53
3.2	Models of the evolution of a random cathode spot	54
3.2.1	Computer based numerical solutions	54
3.2.2	Ionic bombardment and Joule heating models	57
3.2.3	Conical protrusion model	64
3.2.4	Models of the spot motion as a random walk	65
3.3	Models of the cathode spot in a magnetic field	67
3.3.1	Asymmetric confinement	68
3.3.2	Movement of the space charge	70
3.3.3	Movement of the spot plasma	72
3.3.4	Bending of the plasma column	76
3.4	Summary	79
Chapter Four	The design of the steered arc system	86
4.1	The electromagnetic steering array	88
4.1.1	Confinement of the cathode spot	88
4.1.2	A two coiled steering system	90
4.1.3	Modelling of the coil fields	95
4.1.4	Testing of the field modelling program	97
4.1.5	The design of the coils	99
4.1.6	The manufacture of the coils	103

4.2	The arc chamber and associated systems	104
4.2.1	The main chamber and pumping system	104
4.2.2	The power supplies	105
4.2.3	The gas flow control	107
4.2.4	The cathode assembly	108
4.3	Summary of system and system performance	110
Chapter Five	Experimental studies of arc motion	113
5.1	Introduction	115
5.2	Measurement of arc confinement	117
5.2.1	Introduction	117
5.2.2	Experimental details	118
5.2.3	Results and discussion	119
5.3	Measurement of the distribution of orbital transit times	125
5.3.1	Introduction	125
5.3.2	Experimental details	127
5.3.3	Analysis of results	133
5.3.4	Results and discussion	138
5.4	The field dependence of the diffusion constant	153
5.5	Summary of chapter	156
Chapter Six	Summary and further work	160
6.1	Summary	160
6.2	Recommendations for further work	164
Appendix I	The Biot-Savart Model	168
Appendix II	Program documentation	172
Appendix III	A summary of coil parameters and experiments	191

Chapter One

Introduction to Physical Vapour Deposition

Physical Vapour Deposition has been used for a number of years as a method of laying down hard, low friction coatings [1, 2, 3, 4]. Applications range from use as thermal barrier coatings in jet turbine engines to its purely decorative use in the jewellery industry. The term PVD embraces a number of coating methods which share the common feature that all are carried out under partial vacuum conditions and one, if not more, of the coating species are vaporised from a solid within the chamber, see Figure 1.1.

The cathodic arc process, often referred to as a vacuum arc, is characterised by the striking of a high current, low voltage arc on the surface of the material to be evaporated (the cathode). Two coating techniques have evolved from this basic process, random and steered arc PVD. This thesis describes work carried out on the development of new steered arc equipment and experiments conducted, using this equipment, to characterise the cathodic arc. By way of introduction this chapter outlines the two coating methods, discusses improvements made upon the basic systems and also describes the areas studied and the reasons for interest in these areas.

1. 1 Arc coating methods

1.1.1 The random arc.

The striking of a cathodic arc gives rise to a small, but highly active, emitting area (the cathode spot or spots) which produces a high velocity jet of vaporised cathode material. The jet contains atoms, both neutral and ionised, and various sized macro-particles or clusters of atoms, see Figure 1.2. The plasma jet generated peaks in a direction normal to the cathode surface and is very energetic with a high proportion of multiply charged ions [5]. The arc is supported in this flux and can be maintained under high vacuum

conditions. If a suitable reactive gas is introduced into the vacuum chamber (Figure 1.1) then excitation of the gas by the ion flux occurs, followed by the deposition of a compound film upon a substrate placed within the chamber. Dense, uniform and adhesive coatings are achieved at relatively low deposition temperatures. Furthermore, the coating quality may be improved by the application of a negative bias voltage to the substrate.

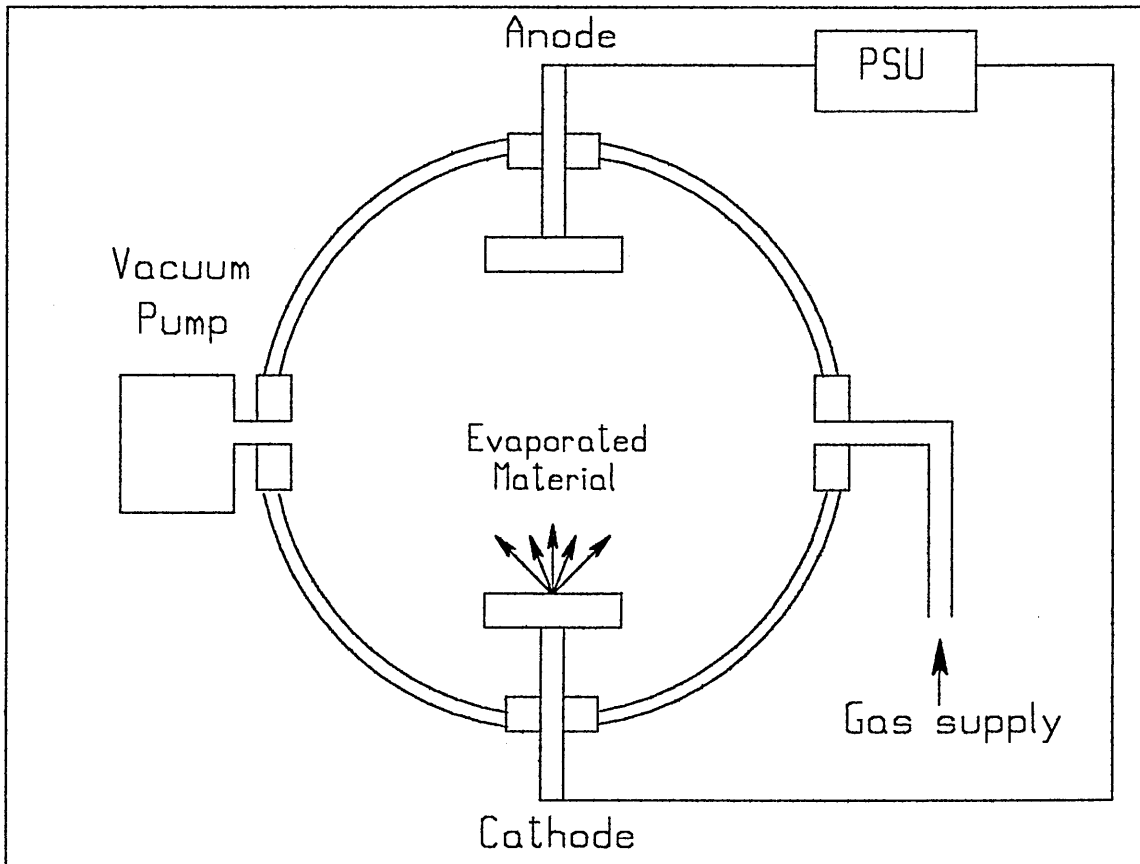


Figure 1.1 Schematic diagram of PVD apparatus.

The random arc technique was developed in the United States [2] and the Soviet Union [3] in the early 1970's and was successful in laying down hard, adherent and durable coatings. The success of the method is thought to be due in part to the high energy of the ions liberated by the arc, the high degree of ionisation at the substrate and the ability to etch the substrate and provide a clean surface for coating species [6]. These high energies are due in turn to the intense heating conditions prevailing at the cathode

surface. Unfortunately, it is these conditions which limit the random arc in its application; in the absence of a steering magnetic field the cathode spot wanders at random over the entire cathode surface. Consequently, the spot tends to spend longer at single sites than when driven by a field. This has the effect of increasing the yield of macro particles which, if deposited upon the substrate, can have an extremely detrimental effect on the coating quality. In addition to this, more recently, problems due to corrosion and premature delamination of the coating have been experienced when attempting to coat certain types of tool, particularly those requiring a very adherent or corrosion resistant coating.

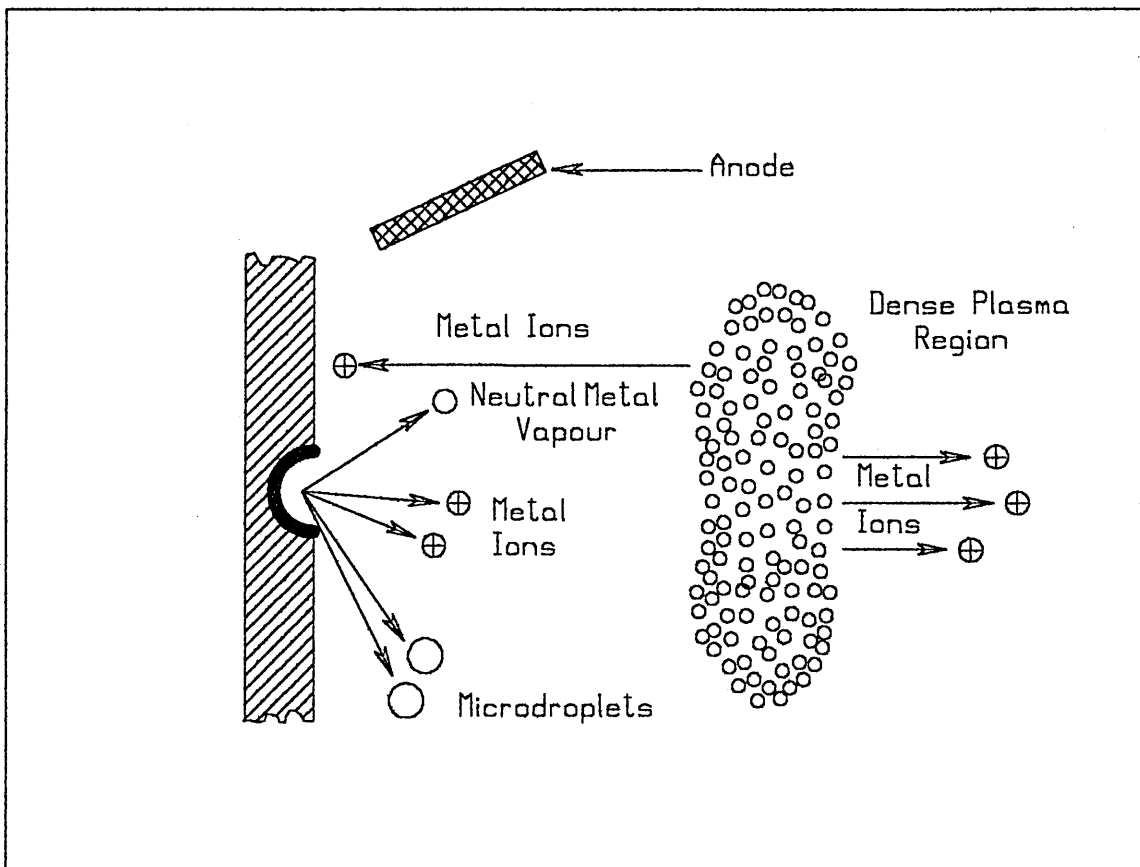


Figure 1.2, The spot region of a cathodic arc after Ref. 7.

This has necessitated research into multi-layered and compound coatings. It is hoped that problems of premature component failure will be alleviated by laying down thin, soft but adherent coatings and then building on top of these with variable composition

compounded coatings [8, 9, 10]. Unfortunately, partly due to the problem of macro particles and partly due to the inability to accurately control the mix of the ion flux, the random arc does not lend itself readily to these applications. However, the development of the steered arc has already significantly reduced some of the problems experienced with depositing reliable coatings and will, in the future, hopefully alleviate others.

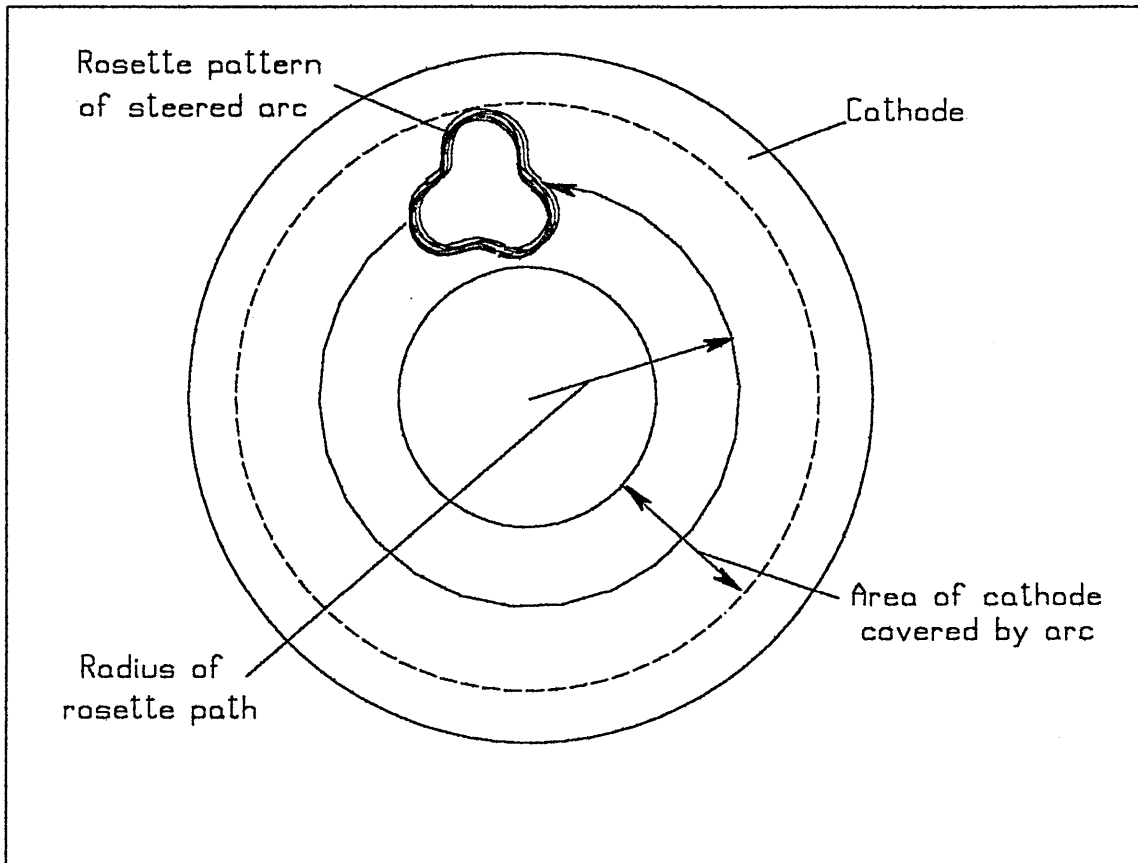


Figure 1.3, Interatom's steered arc.

1.1.2 The steered arc.

The steered arc system uses a magnetic field to control the motion of the arc (which is essentially a current carrying conductor) and to force the cathode spot along a predetermined closed path. The arc spot follows the normal field component zero and moves in the non-amperian or retrograde direction. The first such system was developed by Ramalingam [11] in the 1980's, and uses a permanent magnet to steer the arc in a simple circular orbit. Later systems developed by Interatom use motors to rotate the

magnet in eccentric orbits which produces rosette shaped arc paths upon the cathode, see Figure 1.3, thus utilising a greater proportion of the cathode surface. More recent developments by Morrison [12] use transient steering fields generated by electromagnetic coils to "bounce" the arc back and forth along a channel, see Figure 1.4, this has the benefits of a reduction in the number of moving parts and the possibility of a more complete control of the arc.

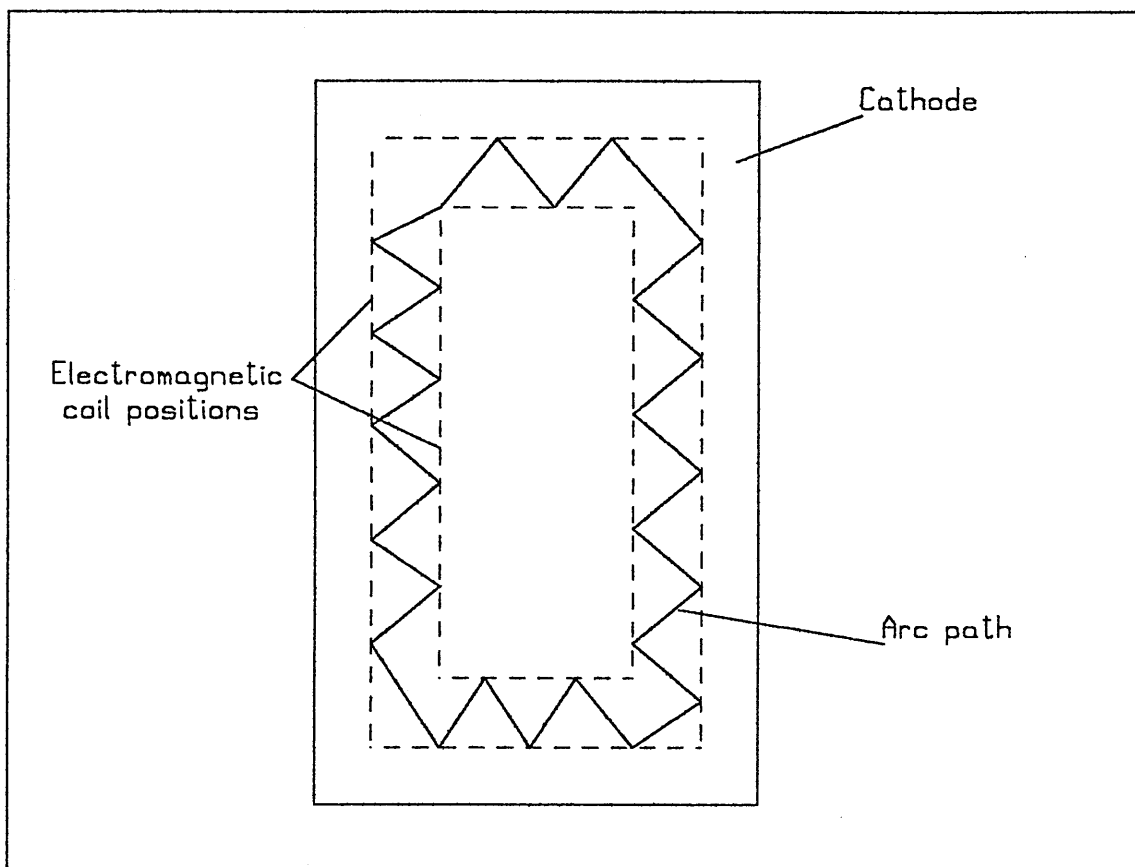


Figure 1.4, Morrison's steered arc after Ref. 12.

The steered arc as a commercial coating system offers several advantages over the random arc process: there is a significant improvement in coating quality due to reductions in size and frequency of macro particle emission coupled with improved surface finish and adhesion; better control of the system is established with the elimination of periodic arc quenching (caused by the arc attempting to travel beyond the edge of the cathode) and the confinement of arc cathode spots to a pre-selected closed

path. This improved control provides the possibility of the production of multi-layered and/or alloyed coatings..

1.1.3 Arc evaporation using segmented cathodes

By the use of segmented multi-part cathodes and by controlling the location and residence time of the arc on the various segments, it is theoretically possible to produce coatings with variable or graded compositions [13]. These ternary and quaternary coatings have generally demonstrated improved tribological properties when compared to simple binary coatings, for example improved hardness, corrosion resistance and coefficient of friction [14]. However, to date, little success has been enjoyed when employing a steered arc upon a multi-part cathode. The arc experiences difficulty when crossing the boundaries between dissimilar metals, appearing to dither at the junction, occasionally there is complete loss of control of the arc [15]. Establishing a more complete control of the cathode spot using a controllable steered arc system may offer the possibility of overcoming this problem.

1.1.4 Filtered arc.

In an effort to alleviate the macro particle problems associated with random arc (and to a lesser extent steered arc) processes employing various methods of "filtering" the particles out of the plasma stream have been employed.

(i) Shielding [16]. The simplest method employed is to use a screen to block the macro particles path to the substrate. The substrate and shield are biased to attract the plasma onto them. This has the advantage of producing particle free coatings but suffers from a low deposition rate.

(ii) Magnetic filtering [17]. A number of magnetic filtering devices have been described in the literature, these use magnetic fields of varying geometry and complexity to filter out the macro particles [18, 19].

(iii) **Magnetic plasma duct filtering [20]**. This filtering device consists of a quarter torus with the magnetic field parallel to the walls of the torus, see Figure 1.5. The plasma is transported along the duct to be deposited upon the substrate, whilst the macro particles remain unaffected by the magnetic field and follow their normal trajectory out of the line of sight of the substrate.

Of these methods, plasma duct filtering has shown the best results, eliminating the macro particle problem whilst laying down extremely corrosion resistant films.

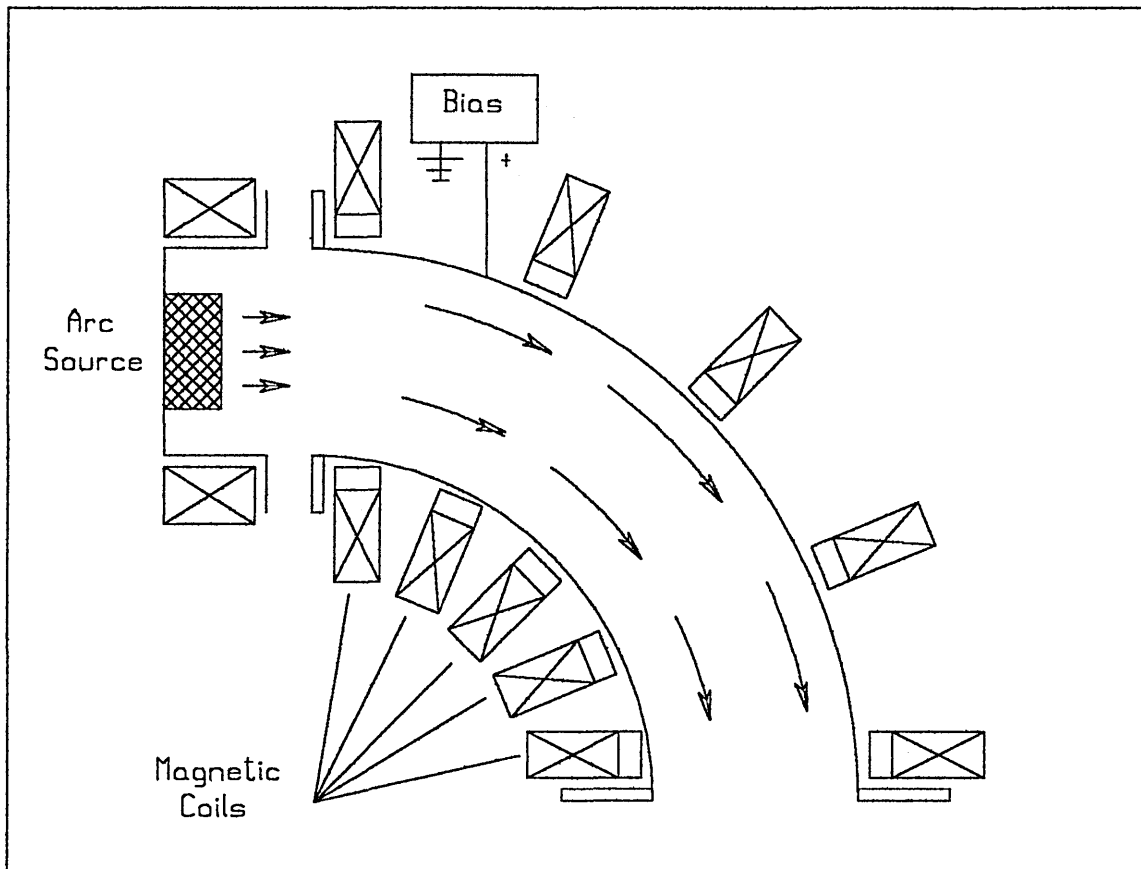


Figure 1.5, Magnetic plasma duct after Ref. 20.

1.2 Present work.

At present knowledge about the movement of and conditions at the cathode spot is far from complete. A large number of mathematical models have been developed for both the steered and random arc, the validity of which is not easy to assess without detailed knowledge of certain spot parameters. These models are discussed in detail in Chapter 3. Matters are further complicated by large discrepancies between existing experimental data from various sources. These discrepancies are discussed in detail in Chapter 2. Only when there is certainty about these parameters will it be possible to produce an accurate and comprehensive model of spot motion. Considering the information presented here so far and following a review of current literature, which is presented in Chapters 2 and 3. The following three areas were identified in which further research is required, these were;

- (i) To develop a novel steered arc system using electromagnets to produce the steering fields, thus allowing a more complete control of the magnetic field in which the arc is moving. Specifically to control the degree of confinement and the orbital radius (on a continuously variable basis) of the arc.

- (ii) To use the steering system designed in (i) to carry out experimental measurements of certain spot parameters (spot confinement and distributions of spot velocities) and to compare these observations with those predicted by a new mathematical model that describes the motion of the arc as a biased stochastic process [21].

- (iii) To use the comparison of experimental data and theoretical predictions to understand more clearly the physical mechanisms governing spot behaviour under the control of a magnetic field..

This thesis describes work performed in these areas and consists of a further five chapters;

- Chapter 2 is a review of experimental data obtained from the literature and reviews investigations of spot size, current density, spot life time and spot type.
- Chapter 3 is a review of mathematical models of the cathodic arc and is divided into three main parts; the first part describes physical inputs to the spot, i.e. heating and cooling processes occurring at the spot; the second part summarises models describing the behaviour of the random arc; the third part summarises models of the steered arc, including the new model of arc motion mentioned above.
- Chapter 4 is a description of the development of the experimental apparatus; firstly the design and assembly of the vacuum chamber and associated systems, i.e. gas supply and regulation, arc power supply and cooling systems and secondly the design and implementation of the electromagnetic steering coils.
- Chapter 5 consists of a description of experimental work performed, a presentation and the analysis of the results obtained. Comparisons are also made between measured data and predictions made by a new model of arc motion [21].
- Chapter 6 contains a summary of the literature reviewed, experimental work performed and conclusions drawn from this work. In conclusion, suggestions are made of relevant areas for further research.

References.

- [1] "Vacuum arcs, Theory and applications."
J.M. Lafferty, Editor, Wiley-Interscience, (1980).
- [2] A.A. Snaper,
United States Patent Nos. **3,625, 848** and **3,836,451**, (1971) and (1974).
- [3] Sablev et al.,
United States Patent No. **3,783,231**, (1974).
- [4] "Gaseous conductors",
J.D. Cobine, Dover publications, New York, (1958).
- [5] J. Kutzner, H. C. Miller,
IEEE, Trans. on Plasma Science, **17(5)**, 688, (1989).
- [6] A.A Plyutto, V.N. Ryzhkov, A.T. Kapin,
Sov. Phys. JETP, **20**, 328, (1965).
- [7] J.E. Daalder,
PhD Thesis; Eindhoven University of Technology, (1978).
- [8] H. Holleck, M. Lahres, P. Woll,
16th Int Conf. on Metallurgical Coatings, San Diego, (1988),
Surface and Coatings Technology, **41**, 179, (1990).
- [9] Surface and Coatings Technology, **43** and **44(1-3)**, 245, (1990).
- [10] P. Jewsbury, S. Ramalingam, R.F. Chang,
Engineering for Advanced Friction Wear Applications Conf., (1988).
- [11] S. Ramalingam,
United States Patent No. **4,763,477**, (1987).
- [12] J.R. Morrison,
United States Patent No. **4,724,058**, (1988).
- [13] D.P. Monaghan, D.G. Teer, K.C. Lang, I. Efeoglu, R.D. Arnell,
Surf. Coat. Tech., **59(1-3)**, 21, (1993).

- [14] W-D. Munz,
J. Vac. Sci. Technol., **A6**(4), 2717, (1986).
- [15] L. Donohue, J. Cawley, J.S. Brooks,
Surface Coating and Technology, **63**, 49, (1994).
- [16] H. Brandoff,
United States Patent No. **4,511,593**, (1985).
- [17] D.M. Sanders,
J. Vac. Sci. Technol., **A6**, 1929, (1987).
- [18] G.V. Kljuchko, V.G. Padalka, L.P. Sablev, R.I. Stupak,
United States Patent No., **4,492,845**, (1985).
- [19] J Storer, J.E. Galvin, I.G. Brown,
J. Appl. Phys., **66**, 5245, (1989).
- [20] P.J. Martin, R.P. Netterfield, A. Bendavid, T.J. Kinder,
Surface and Coatings Technology, **54** and **55**, 136, (1992).
- [21] C.M. Care,
J. Phys. D Appl. Phys., **25**(12), 1841, (1992).

Chapter Two

Experimental studies of the cathode spot

The cathode spots of vacuum arcs have been studied for a number of years and a large amount of data has been amassed concerning their behaviour. Unfortunately the tiny dimensions of the spot, its swift and random movement over the cathode and the emission of a metal vapour cloud that obscures direct observation of the spot cast doubt on the accuracy of some of these data. It is the purpose of this chapter to summarise the literature dealing with the experimental measurement of some of the more relevant spot parameters, to present a concise review of the results of this work and where appropriate give a more detailed picture of important results. Also presented is a description of a spot life cycle which introduces a number of interesting ideas about spot motion which are discussed in detail in Chapter 3. It is significant to note the wide range of values reported by different authors for the cathode spot size and hence current density (perhaps the two most important spot parameters) and also the apparent existence of two types of cathode spot.

A major review by Rakhovskii [1] characterises the cathode spot in terms of the following parameters;

- (i) The diameter of the spot.
- (ii) The type and velocity of the spot.
- (iii) The type of erosion of the cathode.
- (iv) The current density in the spot.
- (v) The lifetime of the spot.
- (vi) The total current per spot.
- (vii) The mass loss rate.

Some of these parameters are readily measured and are not the subject of any great contention. The following subjects, however, will be discussed in some detail either because of the general significance of the parameter or because there is some dispute over its measured value.

- (1) The spot life cycle (the lifetime of the spot).
- (2) The type of spot.
- (3) The spot diameter and current density.
- (4) The total current per spot.
- (5) The type of erosion.
- (6) The spot motion

In addition in Section 2.6 a separate heading is introduced devoted to mean spot time step and mean spot displacement (Section 2.6.1). These topics will be discussed in detail not only because of their particular relevance to the later part of this thesis (Section 3.2.2 and Chapter 5) but also because the important concept of a spot diffusion constant is introduced. This parameter is derived by several authors (Section 3.2.4) and may be measured experimentally enabling a direct comparison between theory and experiment to be made. In addition to this, knowledge of the diffusion constant allows the estimation of other spot parameters such as erosion rates, mean spot velocities and the ratio of the thermal conductivity time scale to spot formation time scale.

2.1 The spot life cycle.

The spot lifetime, according to Guile and Jüttner [2], may be conveniently broken into four stages (see Figure 2.1);

- (i) Surface explosion.
- (ii) Melting and deformation of liquid.
- (iii) Crater formation and quasi-steady state.
- (iv) New spot ignition.

These will be discussed individually.

2.1.1 Surface explosion.

The application of high voltage between anode and cathode when placed in a vacuum causes an extremely rapid and energetic evaporation of cathode material leading to the formation of a plasma cloud and breakdown of the vacuum. It is observed that the macroscopic field at breakdown is at least two orders of magnitude below that required for the onset of field emission, which is the mechanism widely quoted to be responsible for the maintenance of the arc [3, 4, 5, 6, 14, 18, 19]. However, values for the breakdown voltage vary over a range of several hundred percent for identical experimental conditions (electrode spacing, material and size [20]).

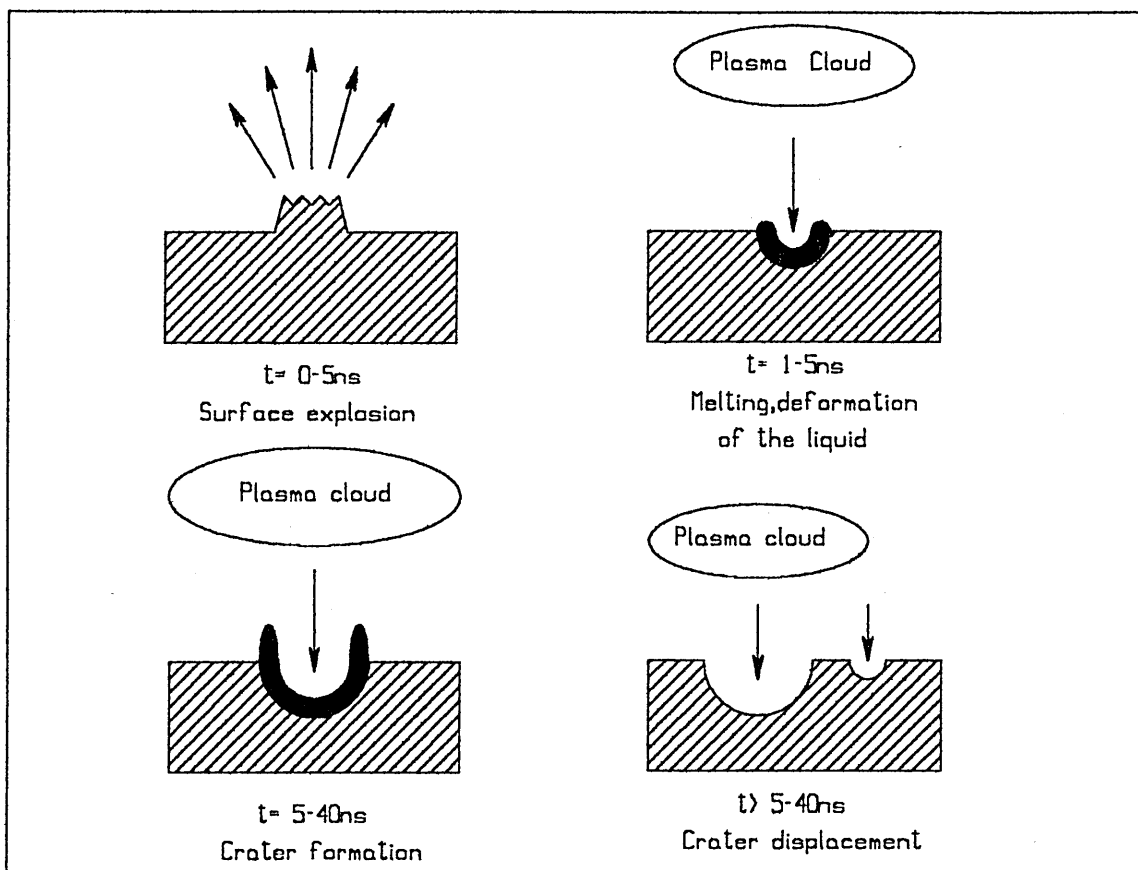


Figure 2.1, The spot life cycle after Ref. 2.

This apparent inconsistency may be reconciled in two ways, firstly the existence of a micro structure on the surface of the cathode, i.e. the surface is composed of many micro protrusions of varying shape, and secondly the effect of contaminants within the chamber being adsorbed onto the cathode. Dealing with these individually.

(a) The existence of micro protrusions causes an enhancement of the applied electric field by a factor β (the field enhancement factor) at the tip of the protrusion [7]. Varying degrees of artificially roughened cathode surface have led to values for β of between 200 and 800 being experimentally measured [8] thus giving the sufficient local field gradients required for field emission.

(b) The existence of a residual gas in the vacuum chamber affects the condition of the cathode surface by adsorption. This has the effect of lowering the work function of the metal surface thus increasing the likelihood of electron emission. In addition to this the adsorbed atoms are desorbed very efficiently by electron, ion or photon impact, thus providing an additional plasma source at the point of arc ignition [9, 10, 17].

The existence of both surface contamination and structure then combine to produce conditions conducive for field emission. It is generally agreed that the breakdown occurs along the following general lines [5, 7, 12, 13, 14]. In the pre-breakdown stage, due to the enhancement of the local electric field [8, 14], field emission occurs from the tip of a protrusion leading to localised resistive heating, which may then allow the thermal and secondary emission of electrons to take place again causing extreme and rapid heating of the tip [5]. Such is the thermal loading that emission is quickly followed by an explosive evaporation of the feature producing a rapidly expanding plasma flare. After a short period the flare then settles into a cloud above the cathode spot.

2.1.2 Melting and deformation.

It is suggested by several authors [12, 15, 16] that in the case of complete explosive destruction of the micro protrusion, with only a flat cathode surface remaining, that pressure from the plasma cloud is responsible for the burrowing of a hemispherical crater into the cathode. Indeed such a process is necessary to observe the formation of a crater on such a scale [16]. In the case of a portion of the protrusion remaining after explosion Ecker [12] suggests that, depending upon the relative dimensions of the feature, a combination of plasma pressure with either field rupture or surface tension will destroy it leaving a molten pool which may then be displaced by the plasma cloud. The total time for this process has been estimated as 1-5ns [15].

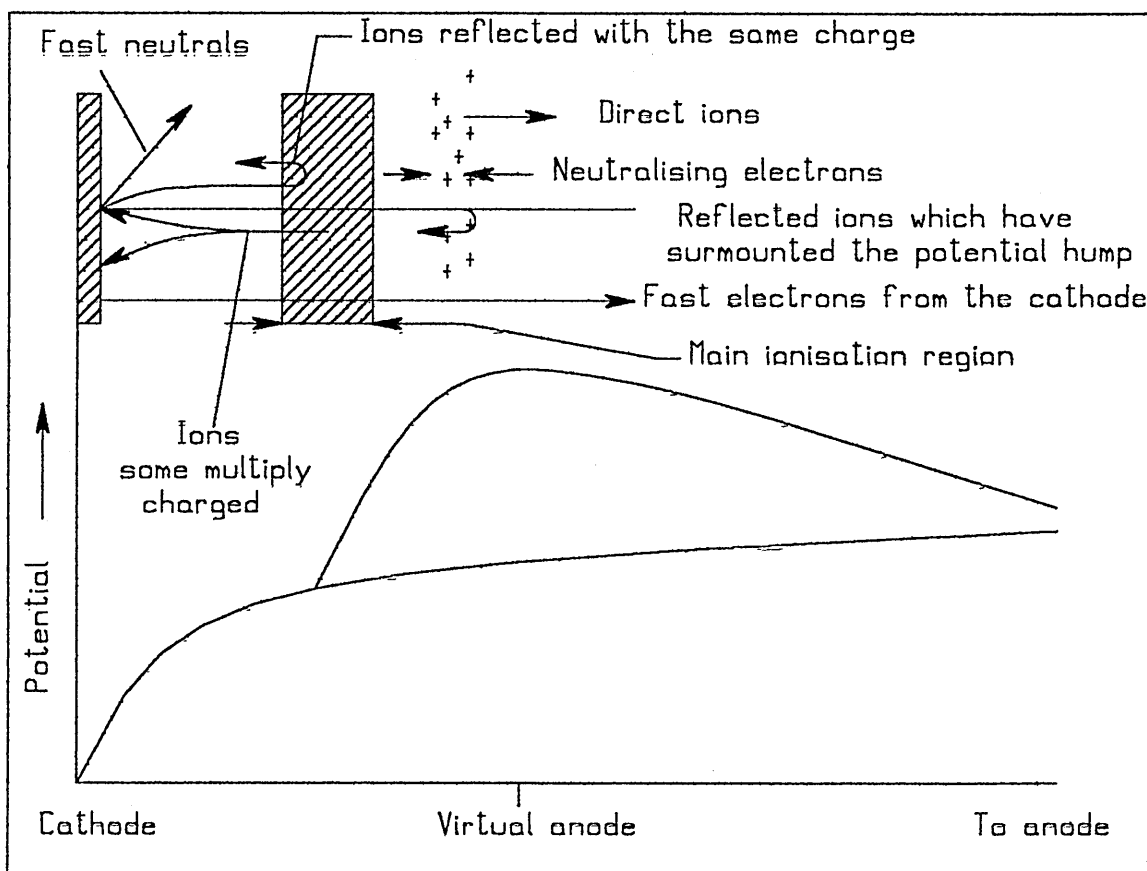


Figure 2.2, A Potential Hump model after Ref. 23.

2.1.3 Crater formation and steady state.

After initial formation of the crater by plasma pressure the main lifetime of the spot is spent as a crater that is constantly evaporating material into the plasma cloud. A considerable ion flux (most ions are multiply charged [25]) is emitted from the cathode spot with a spatial distribution that can be approximated as an exponential function of the solid angle. Observations by Plyutto et al [21] first established that ions with greater than expected energy, i.e. larger than the arc potential, are present in this flux. This was confirmed by further work on the energies of individual ions present [22]. Two theories have been presented to explain this phenomena; the potential hump (PH) theory and the gas dynamic (GD) theory.

The PH theory (see Figure 2.2) explains the anomalously high ion energies by way of the existence of a region of positive space charge near the cathode surface [21, 23]. Ions, created in the main ionisation zone, fall through the cathode potential (which is dropped across a narrow collision free zone, the sheath [30, 31]) towards the cathode where a substantial proportion of them are reflected elastically, some with a reduction in charge.

Quoting an example given by Lloyd [23]; a doubly charged ion which loses negligible energy upon reflection would have energy $2eV_c$ (where V_c is approximately the cathode fall voltage) as it leaves the cathode surface. If it gains an electron during reflection then it will apparently have been accelerated through $2V_c$ and after surmounting the cathode fall will still have energy equivalent to nearly V_c . If more fast ions surmount the cathode fall than are necessary to neutralise the negative space charge (caused by fast electrons from the cathode) then a positive space charge will build up which will only let through enough of the highest energy ions to neutralise the electron space charge.

The GD theory proposes that ions are accelerated by collisions with the higher velocity electron flux from the spot i.e. there is a net transfer of energy from the electron flux to the ion flux. There is also conversion of thermal energy to directed kinetic energy due to the cooling effect of the expanding plasma cloud. This leads to uniform flow of ions being established i.e. all ions having the same velocity

Thus the PH theory predicts a charge state dependent ion energy and velocity (increasing energy and velocity with increasing charge state Z) with a constant potential, whilst the GD theory predicts a decreasing ion potential and constant energy and velocity with increasing charge. Results using both models have agreed well with experimental results for average ion energy, average ion potential and ion charge state. However, when individual ion parameters are measured large discrepancies appear, indicating the failure of both models to give a more detailed description of the ion flux [25]. Several extensions of these theories have since been published, those of Harris [24], Ya Moizhes and Nemchinskii [26] and Wieckert [27] appear promising but have not been tested against individual ion parameters. The modified GD theory of Sizonenko et al. [28] by Aksenov et al [29] has been subjected to such a test and agreement with experiment is good (for a general review of these models see Kutzner and Miller [25]).

2.1.4 New spot ignition.

After some time it is believed that the spot dies and a new one ignites to take its place. Ecker [12] suggests that this occurs when local heating of the cathode material causes the resistance to rise to such a point that a voltage increase is needed to maintain emission levels (the rise in local resistance is also exaggerated by deviations from Ohm's law at high current densities [32]). This implies that a new lower voltage site may exist that has already been heated to a favourable temperature by the plasma cloud of the old spot. A balance must be achieved between the level of heating required to start the new spot and the unfavourable conditions offered by the rise in local resistance. The new spot igniting at the more energetically favourable site now supplies the plasma cloud with the matter needed to sustain the arc and the old spot extinguishes no longer having sufficient current density to evaporate cathode material, and a new cycle begins. It is interesting to note that were there a protrusion in the vicinity of the new ignition site it, presumably, would be the favoured site for ignition. This is of particular significance as the surface condition of the cathode has important implications for the operation of the arc and is discussed in detail in Section 2.6.

The time scale for the full lifetime of the spot is the subject of a great deal of debate with values ranging from 1-20 μ s from Rakhovskii [1] and Djakov and Holmes [34] to 10ns from Jüttner [16]. For a detailed discussion see Section 2.6.

2.2 The type of cathode spot.

As indicated previously there is almost certainly more than one form of cathode spot. This was first observed by Rakhovskii [1] who identified what he termed the type I and type II spots. This observation is supported by experimental work by a large number of authors [1, 8, 36, 37] and was also predicted by theoretical modelling work by Ecker [12, 39, 40, 41] that allows the existence of RSI (Rough Surface with Individual features) and RSA (Rough Surface with Average structure effects) spots, subject to conditions at the cathode surface. The existence of the types I and II spot is of great consequence when considering experimental data on spot parameters. The behaviour and physics of the two types is very different (the primary emission mechanism for the type I spot being field emission, whilst that for the type II spot is thermal emission). Additionally, as will be shown, orders of magnitude difference may exist between parameters measured under otherwise identical conditions.

2.2.1 The Type I cathode spot.

Type I spots occur only on contaminated cathodes with some degree of surface roughness and are characterised by a sequence of breakdowns between spot plasma and cathode surface: the essential mechanism being the field emission of electrons from micro-protrusions beneath the spot plasma. The explosion of a protrusion supplies ionised material to the spot plasma which continues to expand until causing another protrusion to explode at the edge of the cloud. The spot moves jumping from feature to feature with a velocity determined by the expansion of the plasma [36]. The average distance moved is larger than the radius of the crater produced and the colour of the arc is not characteristic of the cathode material (indicating a weak interaction with the bulk material). The existence of such spots on contaminated and/or rough cathodes is

consistent with the effects of such conditions on the enhancement of the local electric field noted in Section 2.1.1. These observations compare very favourably with a spot type predicted by Ecker's RSI model (Rough Surface with Individual features) [12].

2.2.2 The type II cathode spot.

The type II cathode spot may exist in tandem with a type I spot or on a cathode surface that has been cleaned and repeatedly arced upon i.e. the arc has a cleaning effect upon the cathode surface removing adsorbed gases and eroding micro protrusion so that there is a change from one spot type to another during the arcing process [42]. Characteristic of this type of spot is a relatively low velocity active area which relies upon thermal emission of electrons from a large crater area to sustain it. The distance moved by the spot is of the order of a crater radius (the lips of the crater acting as small surface features to move to) and the colour of the arc is characteristic of the cathode material [36]. Work by Ecker [12] predicts a spot type of the RSA (Rough Surface with Average effects) mode which follows the behaviour of the type II spot closely. In this case the arc is slower moving, and evaporation is thermal.

2.3 The spot diameter and current density.

In this section the two parameters of current density and spot size are discussed together (the current density depending on the determination of spot size). The cathode spot, which appears as a single small highly luminous region, has been observed to be made up of a number of sub-spots or cells [24]. It is the movement of these sub-spots which gives rise to the movement of the spot as a whole. It is vital that the spot should be studied at this level as the current density and surface temperature are increased by several orders of magnitude when considering the spot as a collection of smaller sub-spots with the corresponding reduction in emitting area.

The cathode spot size is usually determined by one of two methods; the autograph method [1] which examines the trail of craters left behind to estimate spot size and the fast registry method [48] which uses high speed camera techniques to examine the size of

the luminescent area (the plasma cloud) over the spot to achieve the same. The fast registry method gives typical spot diameters of the order of $1 \times 10^{-4} \text{m}$, whilst the autograph method gives substantially different values of the order of $1 \times 10^{-5} \text{m}$. There is a great deal of contention surrounding the accuracy of the differing methods. Whilst the autograph method is easily used, Rakhovskii [1] holds that the emitting area (and hence spot size) may be much larger than the molten crater produced, the method therefore underestimating spot size. Hantzsche and Jüttner [48], however, are of the opinion that the crater size represents an upper limit to the emitting area and that the fast registry method is limited in spatial resolution and the luminous plasma cloud photographed is larger than the emitting area underneath it, the method overestimating spot size.

Daalder [49] in a major experimental investigation of crater size measured the distribution of crater diameters for single and multiple discharges on a copper cathode. The resulting distribution was found to be a log-normal distribution determined only by the arc current. In the case of a multiple discharge two or more overlapping distributions were found corresponding to the discharge current at each spot. The lognormal distribution is given by,

$$dP(a) = \frac{1}{\alpha\sigma\sqrt{2\pi}} e^{-\frac{(\log a - \mu)^2}{2\sigma^2}} da \quad (2.1)$$

Where a is the crater diameter and μ and σ for copper are given by,

$$\sigma = 0.22I^{0.19} \quad (2.2)$$

$$\mu = 1.28e^{7 \times 10^{-3} I} \quad (2.3)$$

Where I is the arc current expressed in amps. These distributions combined with further experimental work on molybdenum enabled Jüttner [68] to make approximations for r_c , the mean crater radius for copper and molybdenum based upon the arc current in amps.

$$r_c \approx 0.06I \mu m \text{ for copper} \quad (2.4)$$

$$r_c \approx 0.1I \mu m \text{ for molybdenum} \quad (2.5)$$

Current densities at the cathode spot depend upon a number of parameters. These include; cathode material, the type of cathode spot and current growth rate. Most authors report current densities of between 10^{10} and 10^{14} Am⁻². The literature surveyed is summarised in Tables 2.1 and 2.2.

The determination of spot size and current density would seem to suffer similar problems to the determination of arc velocity. The majority of research does not quote either a spot type or whether the spot exhibits a cellular sub-structure, both of which are likely to affect the measured spot size and hence the current density. If micro protrusions are being explosively evaporated then the current density is likely to be changing on a very short time scale. This is another area in which further work would be profitable. The effects of cathode roughness on spot size, for example, would be of great interest.

Table 2.1
Summary of crater diameters found.

Author	Autograph method, (m)	Fast Registry method, (m)
Daalder, [49] (4.7A)	3.8×10^{-6}	-----
Daalder, [49] (105A)	12×10^{-6}	-----
Jüttner, [50] (100A)	15×10^{-6}	-----
Smith et al., [51] (main spot)	-----	1.3×10^{-4} to 8×10^{-4}
Smith et al., [51] (sub-spots)	-----	1.6×10^{-4}
Drouet and Grouber, [52] (sub-spots)	1×10^{-7}	-----

Table 2.2

Summary of values for current density found.

Author	Type I, type II, sub-spot(s) or none declared (N)	Own work, (O) or review (R)	Average current density (Am ²)
Mitterauer, [19]	N	R	10 ⁶ to 10 ¹³
Lyubimov and Rakhovskii, [53]	I	R	2x10 ¹⁰ to 7x10 ¹⁰
Lyubimov and Rakhovskii, [53]	II, S	R	5x10 ¹¹
Djakov and Holmes, [34]	N	O	5x10 ¹² to 10 ¹⁷
Djakov and Holmes, [34]	S	O	10 ¹¹ to 5x10 ¹³
Rakhovskii, [54] (autograph method)	N	O	10 ¹³ to 10 ¹⁴
Rakhovskii, [54] (registry method)	N	O	4x10 ¹⁰ to 10 ¹²
Hantzsche and Jüttner, [48]	N	O	5x10 ¹¹ to 10 ¹²
Pucharev and Murzkayev, [55]	N	O	5x10 ¹¹ to 10 ¹²
Ecker, [12]	Theoretical	O	10 ¹¹ to 10 ¹²
Drouet, [56] and Jüttner, [16]	N	O	7.5x10 ¹² to 10 ¹⁴
Prock, [57]	Theoretical	O	7x10 ¹² to 10 ¹⁴

2.4 The total current per spot (spot splitting).

As mentioned previously, closer inspection of the cathode spot reveals a structure of sub-spots or cells [52, 34, 58, 59]. As the current delivered to the spot increases so too does the number of cells up to a limit where another large spot begins to form. The behaviour of the arc is highly dynamic with spots splitting extinguishing and reigniting on a rapid and continuous basis. Drouet and Gruber [52], using copper cathodes in air, have observed a 1 μm crater to be composed of a ring of 0.1 μm craters. Measuring the current and lifetime for the sub-spots they found currents of 0.6A per spot and lifetimes of 1 μs , giving current densities of 10¹⁴ Am².

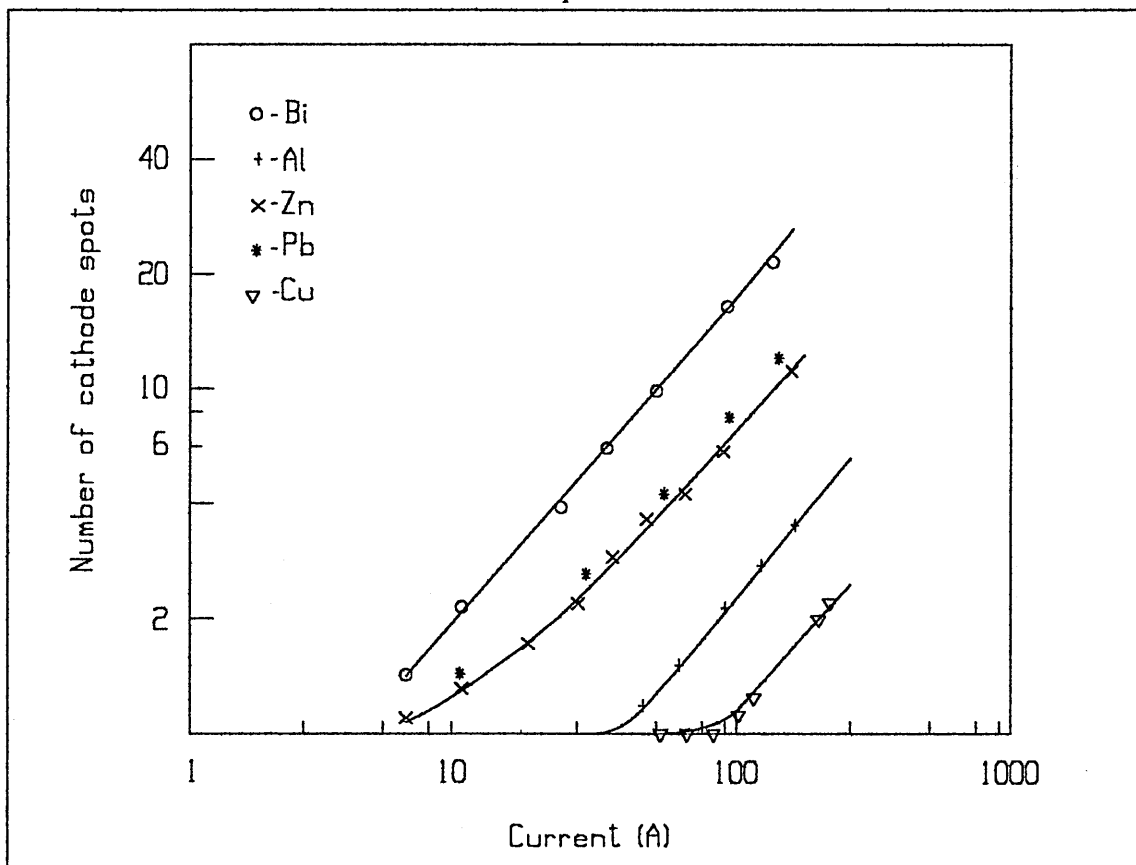


Figure 2.3, Number of cathode spot as a function of arc current after Ref. 60.

Whilst this work was not performed under low pressure conditions it is of relevance as the basis for further work by Djakov and Holmes [34, 60], who, performing similar measurements under vacuum on a variety of cathode materials found a micro structure of one or more cells with current densities between 1×10^{10} and 5×10^{10} Am⁻² (this work is summarised in Figure 2.3).

A number of theories have been put forward to explain and quantify spot splitting. That of Djakov and Holmes [61] explains the formation of the ring of sub-spots by considering each spot as moving under the influence of the remaining spots. Calculations for the growth of ring diameters with time have been made which fit well with experiment. Sena [58] explains sub-spot fission and spot micro structure by considering the repulsive electrostatic forces between two dipoles in competition with the attractive magnetic forces between two current carrying conductors. An identical explanation is offered by Harris [24]. Both authors draw upon this model to make predictions for spot

parameters: in the case of Harris predictions are made of the sub-spot sizes and energies of formation that agree well with experiment. Sena makes no calculations for spot splitting but uses the theory to estimate a value for the cathode sheath thickness which is in very good agreement with estimates made from experimental data.

The structure of the spot has a great bearing upon the motion of the spot in a magnetic field and many authors make use of the substructure in conjunction with other effects to explain the retrograde motion of the arc. These are discussed in detail in Chapter 3.

2.5 The type of erosion.

The erosion rates from cathodes has been found to depend on a number of variables; arc current, arcing time, cathode size [63, 65] and gas pressure [62] but most importantly upon spot type [33].

Examining craters left by a type I spot, Rakhovskii [33] found that the track consisted of single craters of approximately 10^{-7} m depth with a radius of the same order. The area occupied by the craters amounted to only 1% of the area of the cathode (consistent with an explosive emission leaping from feature to feature). Investigating the dependence of erosion rate upon arc current Rakhovskii also found (by keeping the current growth rate constant but by increasing the overall current) a constant erosion rate per coulomb for degassed cathodes.

Type II spots exhibit quite different behaviour, they are often made up of groups of thermally active sub-spots and erosion is extremely intense. The average depth of crater caused by a single type II spot is of the order of 2.5×10^{-5} m, with groups of spots producing trails with a depth of 10^{-5} m. Under these conditions the electric transfer factor (erosion per coulomb) depends substantially upon the current [33].

Further evidence that the erosion rate is critically dependent upon spot type comes from studies by Zykova et al. [65] where it is shown that erosion rates are at a minimum when arcing occurs under conditions which allow only type I spots to exist.

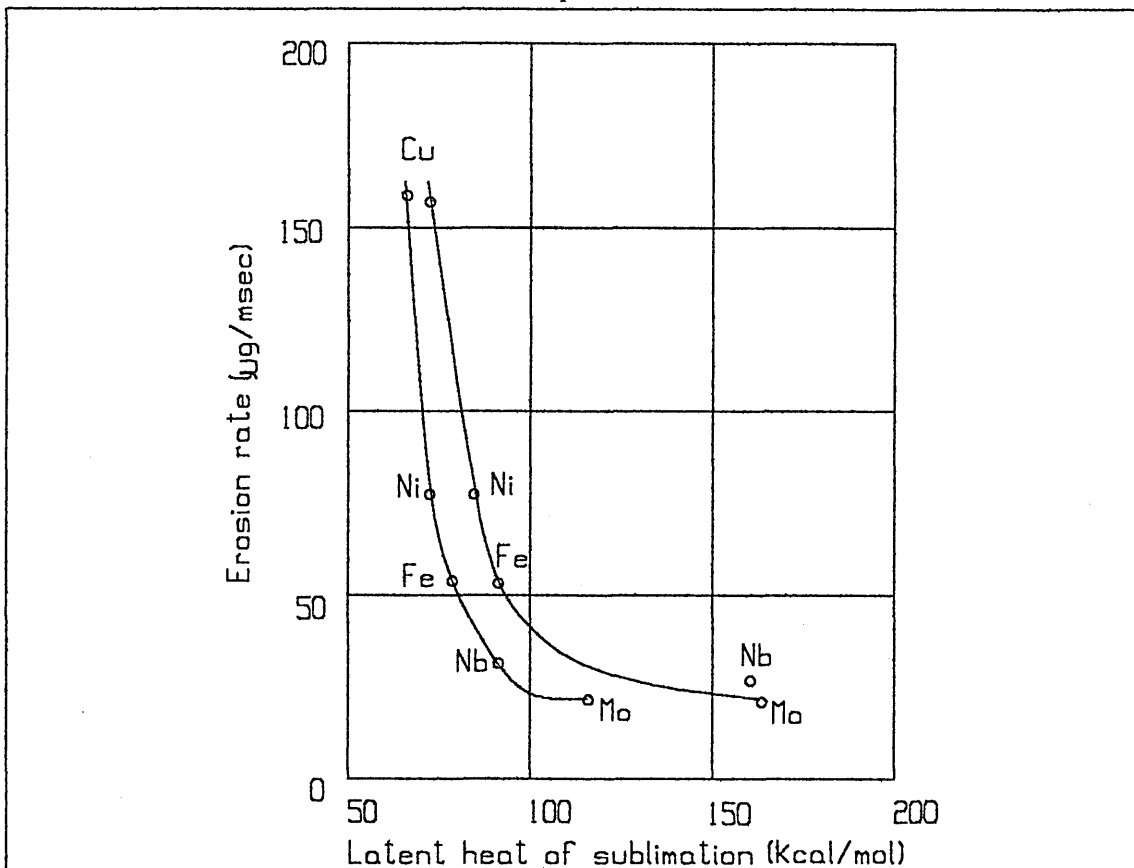


Figure 2.4, Erosion rates as a function of latent heat of sublimation after Ref. 66.

Changing the conditions to allow the operation of a type II spot in conjunction with the type I causes profound increases in erosion rates. Since the fundamental difference between one spot type and another is the change from a field to thermal emission mechanism then there should be a correlation between the thermal properties of the cathode material and the erosion rate [33]. Experiments [66] using degassed cathode materials of differing vapour pressure and latent heat of vaporisation have shown drastically reduced erosion rates with decreasing vapour pressure and increasing latent heat (see Figure 2.4). This would seem to go some way to explaining the difficulties experienced when using dual part cathodes with a steered arc system: the cathode spot dithers at the junction of the two cathode materials, preferring to stay on the material of lower vapour pressure [77].

2.6 Spot motion.

This section discusses experimental studies of spot motion both with and without the application of an external magnetic field.

2.6.1 Random spot motion.

It is generally agreed that the process of crater formation by a cathode spot is a non-stationary process with time [1, 12, 68] but there is a great deal of argument as to the time scale for this process. As mentioned earlier (Section 2.1.4) values reported range from tens of microseconds time scale reported by Rakhovskii [1] to the several nanoseconds given by Jüttner [68]. Many models of the spot require at least order of magnitude estimates for spot life time for any valid conclusions to be drawn from them, particularly in the case where there is some debate about the main source of spot heating (ionic bombardment or Joule heating, see Sections 3.1.1 and 3.2.2). The introduction of a "diffusion constant" by a number of authors [67, 68, 69, 70] goes some way to allowing estimates to be made for the mean spot life time dependent upon two other parameters; the mean crater radius and a constant of spot displacement.

The spot diffusion constant for random spot motion in two dimensions is defined as,

$$\alpha = \frac{s^2}{2\tau} \quad (2.6)$$

Where s is the mean elementary spot displacement in two dimensions and τ is the mean elementary time step. This definition appears to have been adopted [73] after some early misunderstandings in the literature [69, 71], which is discussed below. The following two sections examine the mean spot displacement and the related constant of spot displacement, respectively, in more detail.

2.6.1.1 The mean spot displacement.

The parameter s' is defined above as the mean spot displacement or elementary step in two dimensions and is thus related to the elementary step in one dimension by

$$s' = s\sqrt{2} \quad (2.7)$$

Hence the factor of two appearing in the denominator of Equation 2.6. Assuming a proportionality between s' and the crater radius r , then $s' = \gamma r$ (where γ is the constant of spot displacement) then,

$$\alpha = \frac{\gamma^2 r^2}{2\tau} \quad (2.8)$$

Thus with knowledge of the spot radius, diffusion constant and the constant of spot displacement an estimate may be made for the spot life time.

2.6.1.2 The constant of spot displacement.

The value of γ is the subject of some debate. Dependent upon its magnitude Equation 2.8 gives varying values for the time scale of spot formation which, when considered in tandem with the results of the models described in Section 3.2.2, support either ionic bombardment or Joule heating as the main process for spot heating. A small spot displacement (of the order of a crater radius) indicates a value for γ of approximately unity and a time scale too short for Joule heating to be an important process [68, 69] in which case ionic bombardment must be responsible for the large energy input to the spot. A spot displacement of several times the crater radius, on the other hand indicates a sufficiently long time scale for Joule heating to take place [70, 71, 72] (see Sections 3.1.1 and 3.2.2 for a detailed discussion of the mechanisms of spot heating and the models referred to below).

Hantzsche [67, 69] and Jüttner [37, 68] after running pulsed arcs of *ms* time scales on virgin, clean (baked at high temperature for several hours in ultra high vacuum) cathodes made from a number of metals (aluminium, molybdenum, copper and stainless steel-unstated grade) consistently found that the arc craters observed were "formed successively and without interruption", i.e. the arc track consisted of a line of overlapping craters giving a value for γ of unity or less. However the same pulsed arcs run upon cathodes that had been allowed to oxidise in air for a few minutes produced a distribution of dispersed craters.

Daalder [70, 71, 72] performing similar experiments with a continuous arc on clean, vacuum baked cathodes (cadmium, copper and molybdenum) found dispersed patterns of craters with values for γ of between 3.5 and 6.

Jüttner draws the conclusion [68] that on a clean cathode, especially one that has been previously arced upon, the arc uses metal ejected from the sides of arc craters as a new ignition sites, whereas on a contaminated cathode the arc ignites at areas of impurity, i.e. concentrations of adsorbed gas. Therefore, on a clean cathode, the spot moves with steps equal to or less than a crater radius. This corresponds to the behaviour of type I and type II spots observed by Rakhovskii [1] (see Section 2.2).

In a reply to a letter by Hantzsche et al. [69], Daalder [71] argues that this is not the case, as he has demonstrated experimentally, and points out that comparing data from arcs struck on virgin and previously eroded cathodes is likely to be problematic. Daalder also adds that if the difference in behaviour between spots on virgin and eroded surfaces is not clear, particularly in the presence of an external magnetic field then the assumption of an elementary step equivalent to a spot radius is not justifiable.

Hantzsche and Jüttner [69, 68] examining the effect of the application of a transverse magnetic field (which has the effect of steering and "accelerating" the spot) note that the spot produces a track of overlapping craters with $\gamma \approx 1$. They argue that if such a value of γ is produced whilst the arc is being forced to move more rapidly, then it follows that uncontrolled by a magnetic field it will take smaller steps. However, according to the model proposed by Drouet, which is discussed in detail in Section 3.3.1, this is not

necessarily the case. Drouet suggests that the retrograde motion of the arc is due to the effect of the combination of self and applied fields on the spot plasma. The field is enhanced on the retrograde side of the spot leading to a more confined plasma and more intense heating there. Whilst on the prograde side of the spot the field is diminished and the plasma allowed to become more diffuse. In this case the larger the applied field, the smaller the confined plasma on the retrograde side of the spot and the smaller any spot jump is likely to be. The increase in spot velocity with field may then be attributed to a reduction in the spot life time.

In further work Jüttner et al [37] made a more detailed study of pulsed arcs on virgin and previously eroded surfaces under strict experimental conditions and in addition to this studied the effect of heated cathodes upon the elementary spot step. All of these experiments were carried out in UHV on clean, virgin molybdenum which could be heated to a temperature of 1600 K. The arc was produced by a large capacitance that produced 5ms arcs in the range 33 to 40 A. A coaxial geometry was also used to ensure that there was no disturbance to the spot motion from unwanted external magnetic fields.

The first five pulsed arcs gave tracks on different parts of the cathode and were used to study the spot motion on a virgin surface the motion of the spot was recorded for the first *ms* of arc and the results were used to calculate a value of $\alpha/2$ ¹. All the observed tracks were composed of overlapping craters. The next series of arcs were run over the already eroded surface and again values for $\alpha/2$ calculated. The final experiment determined values for the diffusion coefficient for a range of temperatures from 300 K to 1500 K.

Jüttner et al argue that if, as they have observed, craters on a virgin surface are separated by a crater radius ($\gamma = 1$) and if, as Daalder has observed, they are separated by five to six crater radii on an eroded surface ($\gamma = 5.4$) then as $\alpha/2$ is proportional to γ^2 , $\alpha/2$ should change by a factor of 30-60 during the erosion process. This is not observed to be the case. With virgin surfaces the value for $\alpha/2$ was found to be $5 \times 10^{-4} \text{ m}^2 \text{ s}^{-1}$, whilst with eroded surfaces a value of $6.2 \times 10^{-4} \text{ m}^2 \text{ s}^{-1}$ was found.

¹ It is unclear why values for $\alpha/2$ are given as opposed to ones for α .

Values of $\alpha/2$ for a heated cathode were found to lie in the range $(7-9) \times 10^{-4} \text{ m}^2 \text{ s}^{-1}$ over the range of temperatures. Jüttner et al note the weak variation of spot diffusion against temperature with interest, and point out that not only is $\alpha/2$ insensitive to temperature and current [70, 68] but also the fact that the crater radius, r increases rapidly with current. These facts are used to dispute both the Joule heating model and the large elementary step sizes found by Daalder. It is characteristic of Joule heating models that they give a nearly constant values for the ratio of r^2/τ , i.e. this ratio varies with temperature in a similar manner to measured values of $\alpha/2$. Examining Equation 2.8 it can be seen that this implies that γ is approximately constant. Thus a change in temperature from 300 K to 1500 K increasing r by a factor of two should increase the elementary step size S by a factor two accordingly. Increasing the current from 20 A to 80 A increases the average radius by a factor of six for molybdenum so with $I = 80 \text{ A}$, $T = 300 \text{ K}$ and $r = 13 \mu\text{m}$ the craters should be separated by distance of 70–100 μm . As Jüttner et al point out it is hard to imagine a process which ignites new spots in such a fashion, whilst it is easy to conceive of the position of new craters being related to crater size if the craters overlap.

In summary, it seems probable that the spot separation is so strongly dependent upon surface contamination that discrepancies between measured values for γ may be explained by the smallest amount of contamination [37]. As Jüttner et al note only intense heating (over 1600 K) in UHV or previous intense arcing seems to be able to remove such stubborn surface contamination as an oxide coating.

2.6.1.3 The cathode spot diffusion constant.

The diffusion constant of random spot motion has been measured by number of authors for a variety of cathode materials [67, 68, 69, 72] and the results of these measurements are summarised in Table 2.3. However, to allow any meaningful comparison to be made between values obtained the definition of α needs some examination.

Daalder [71] notes that the experimental method used by Hantszche et al. [69] leads to measured values of \bar{R}^2/t being obtained, where \bar{R} (the mean spot displacement, derived

from the theoretical model of spot motion described in detail in Section 3.2.4) is described by,

$$\bar{R} = \left(\frac{\pi s^2 t}{4 \tau} \right)^{1/2} \quad (2.9)$$

Whereas the method used by Daalder measures α as defined in Equation 2.6.

Examining Equations 2.6 and 2.9 it can be seen that ,

$$\bar{R}^2/t = 0.79 s^2/\tau = 1.57 s^2/\tau = 1.57 \alpha \quad (2.10)$$

According to Daalder, Hantzsche et al now take the experimental value for \bar{R}^2/t to be approximately equivalent to s^2/τ (or more strictly \bar{R}^2/t is approximately equal to r^2/τ , i.e. from Equation 2.8 with a value of unity for γ) this discrepancy is now used to reconcile differences in experimental values obtained for α . Daalder explains that Hantzsche et al. have defined the diffusion constant as s^2/τ , whilst he has defined it as $s^2/2\tau$, he argues that measurements made for suitably long observation periods $t \gg \tau$ will obviously be twice the value determined by himself due to this erroneous definition. However, according to the relationships shown as Equation 2.10 it would seem that the experimental values obtained by Hantzsche et al. are, in fact, in error by a factor of 1.57 higher than those obtained by Daalder, and not by the factor of 2 given by Daalder. This seems to indicate an error in the definition of α by Hantzsche et al, although it seems unlikely that experimental errors will allow a factor of this magnitude to be distinguished.

Examining Table 2.3 above several points become apparent (the difference between the results of Daalder and Hantzsche and Jüttner notwithstanding). Firstly, as was mentioned briefly above, the diffusion constant shows a very weak, if any, dependence upon current [68, 70].

Table 2.3

Summary of diffusion constants found

Author	Mo x10 ⁻³ m ² s ⁻¹	Cu x10 ⁻³ m ² s ⁻¹	Cd x10 ⁻³ m ² s ⁻¹	Al x10 ⁻³ m ² s ⁻¹	SS x10 ⁻³ m ² s ⁻¹	Hg x10 ⁻³ m ² s ⁻¹	Virgin (V) Eroded (E) Not Known (N)	Current (A)	Temp. (K)
Jüttner [50]	14	1.3					V	20-200	300 K
Jüttner [68]	4	2		9	1		V	20-200	300 K
Jüttner [75]	4	2		9	3		V	20-200	300 K
Schmidt [76] ²						1.6	N	3.5-8	300 K
Hantzsche[69]	1.3- 2.6				0.6		V	Not Given	300 K
Daalder [71]	0.74						V	59.5	300 K
Daalder [71]		0.65					V	45	300 K
Daalder [71]		0.65					V	18	300 K
Daalder [71]		0.65					V	9	300 K
Daalder [71]			0.59				V	7.9	300 K
Daalder [71]			0.51				V	4.5	300 K
Daalder [71]			0.83				V	1.8	300 K
Daalder [71]				1.4			V	21.6	300 K
Jüttner [37]	1.12						V	33-40	300 K
Jüttner [37]	1.04						V	33-40	300 K
Jüttner [37]	1.14						V	33-40	300 K
Jüttner [37]	1.06						V	33-40	300 K
Jüttner [37]	1.24						E	33-40	300 K
Jüttner [37]	1.5						E	33-40	900 K
Jüttner [37]	1.34						E	33-40	1100 K
Jüttner [37]	1.72						E	33-40	1300 K
Jüttner [37]	1.7						E	33-40	1500 K

² Calculated by Daalder (71) from data obtained by Schmidt (76)

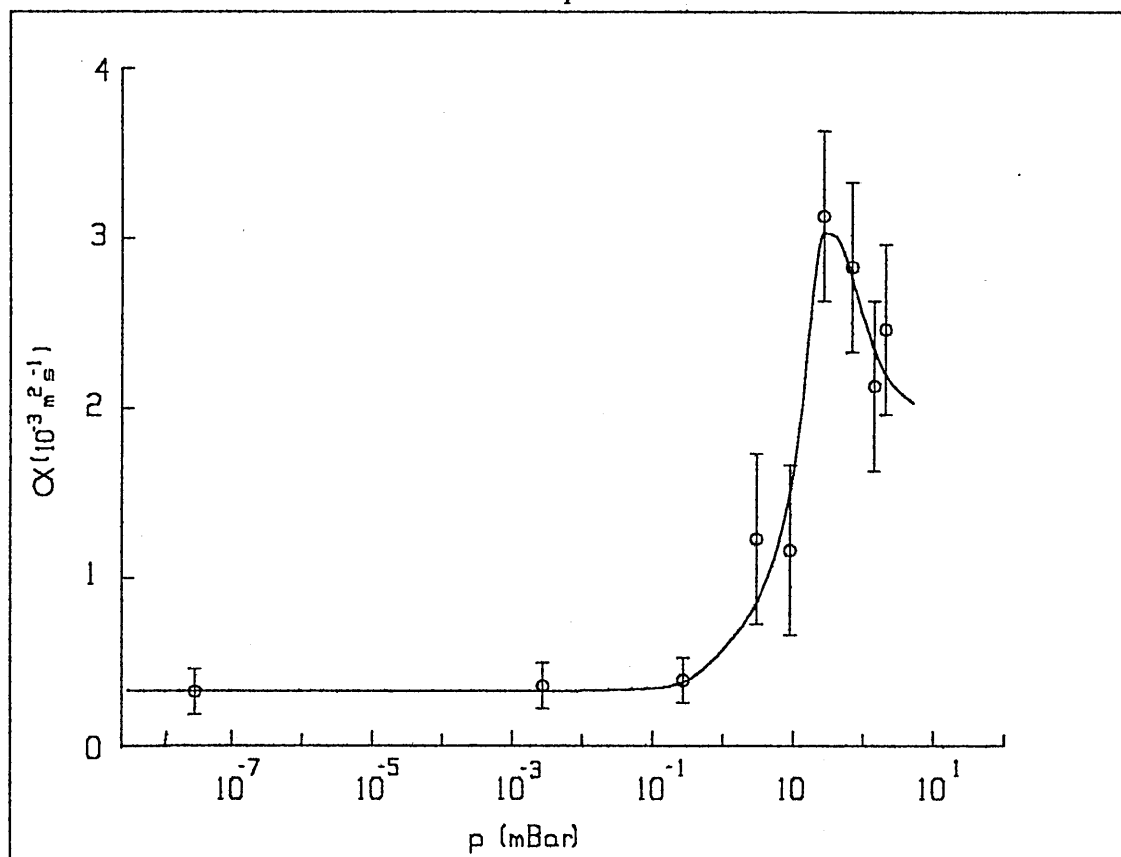


Figure 2.5, Change in diffusion constant with background of argon, after Ref. 73

Jüttner et al [37] note that any change in α with current is only just outside the range of experimental uncertainty for their work, whilst the limited number of results from Daalder [70] show no current dependence at all for copper and a very indeterminate change in that for cadmium. It should be noted that in all the work currents were intentionally kept low to avoid the possibility of multiple spot formation. Secondly, α shows only a very weak dependence on global cathode temperature: an increase by factor of 1.4 in α for a fivefold increase in temperature [37]. Thirdly, and finally, both Daalder [70] and, surprisingly, Hantzsche et al [69] consider α to be weakly material dependent. This is understandable in the light of Daalder's experimental results but does not seem to be supported by those reported by the numerous results of Hantzsche et al. [67, 69] and Jüttner et al [37, 50, 68, 74] in whose work a range of values from 6×10^{-4} (for stainless steel) to 1.4×10^{-2} (for molybdenum) can be seen. Even excluding early, possibly erroneous work, the range is still of an order of magnitude (approximately 10^{-3} ,

for stainless steel to 10^{-2} for aluminium) this is commented on by Hantzsche et al. who say that the α value obtained for aluminium is worthy of re-examination.

Finally, more recent work by Anders and Jüttner [73] examining the effect of background pressure of argon gas upon the value of the diffusion constant for a copper cathode is summarised in Figure 2.5. Although the original graph used Pascals as the unit of measurement of pressure on the x-axis, it has been reproduced here with this axis scaled to milliBar, this is to enable easier interpretation of results presented in Chapter 5. It can be seen that below a pressure of approximately 10^{-1} mBar α has an extremely weak dependence upon pressure of argon, this result has a large bearing upon work presented in Chapter 5.

2.6.2 The arc motion in a magnetic field.

Without the influence of a constraining magnetic field the arc jumps about at random over the cathode surface. With the application of a transverse magnetic field, however, the arc rather surprisingly moves in the non-amperian or retrograde direction $(-\hat{J} \wedge \hat{B})$, [43] for field values of up to approximately one Tesla and in chamber pressures below a certain critical value (1-45 mBar, dependent upon gas).

2.6.2.1 Measurements of arc velocity.

The velocity dependence of the arc upon self magnetic field was investigated by Sherman et al. [44] the results of which are shown in Figure 2.6. An almost linear dependence on field strength is observed for values of field up to 2×10^{-2} T, whilst for fields of above 4×10^{-2} T the velocity increases more slowly to a threshold of approximately 30ms^{-1} (experiments were conducted on a copper cathode and at a base pressure of 10^{-8} mBar). Similar results have been reported by Swift et al. [43] who observed the motion of the arc on a titanium cathode at a pressure of 10^{-6} mBar around a circular track whilst steered by an externally applied field.

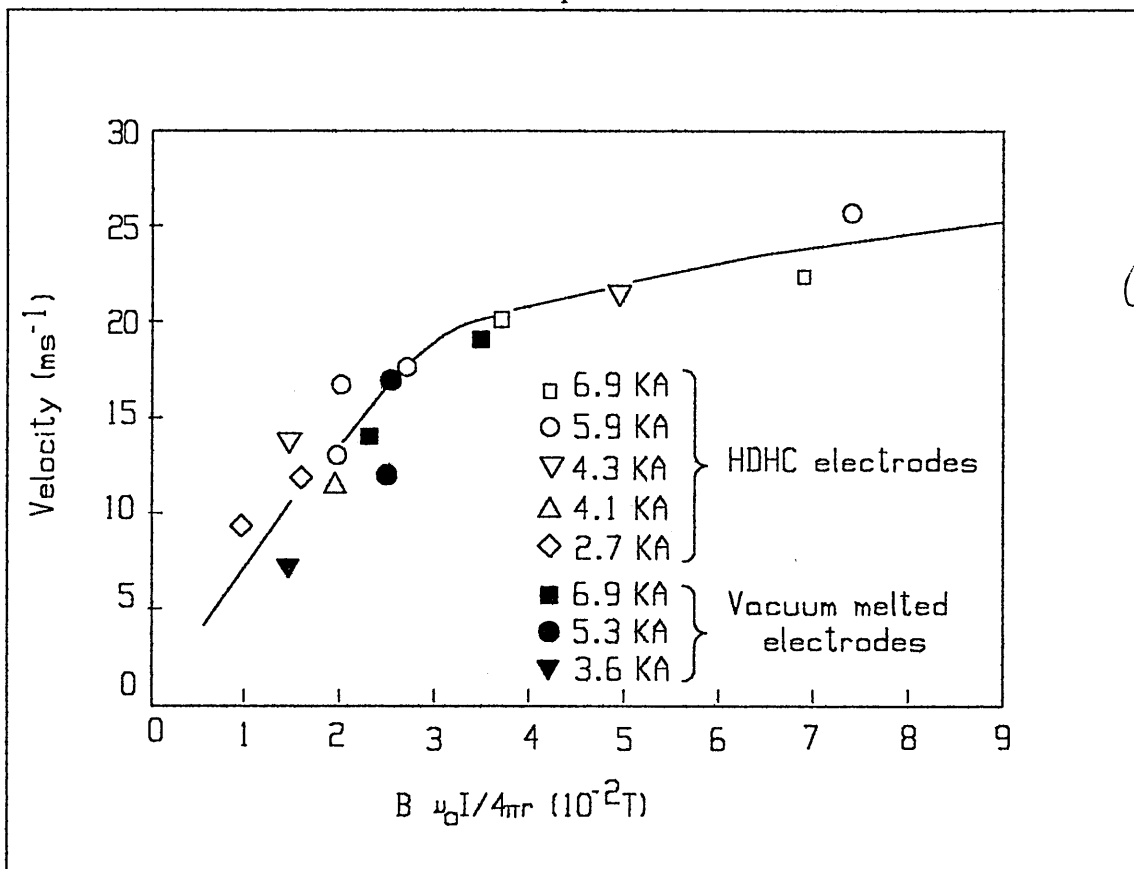


Figure 2.6, Arc velocity as a function of inherent magnetic field after Ref. 44.

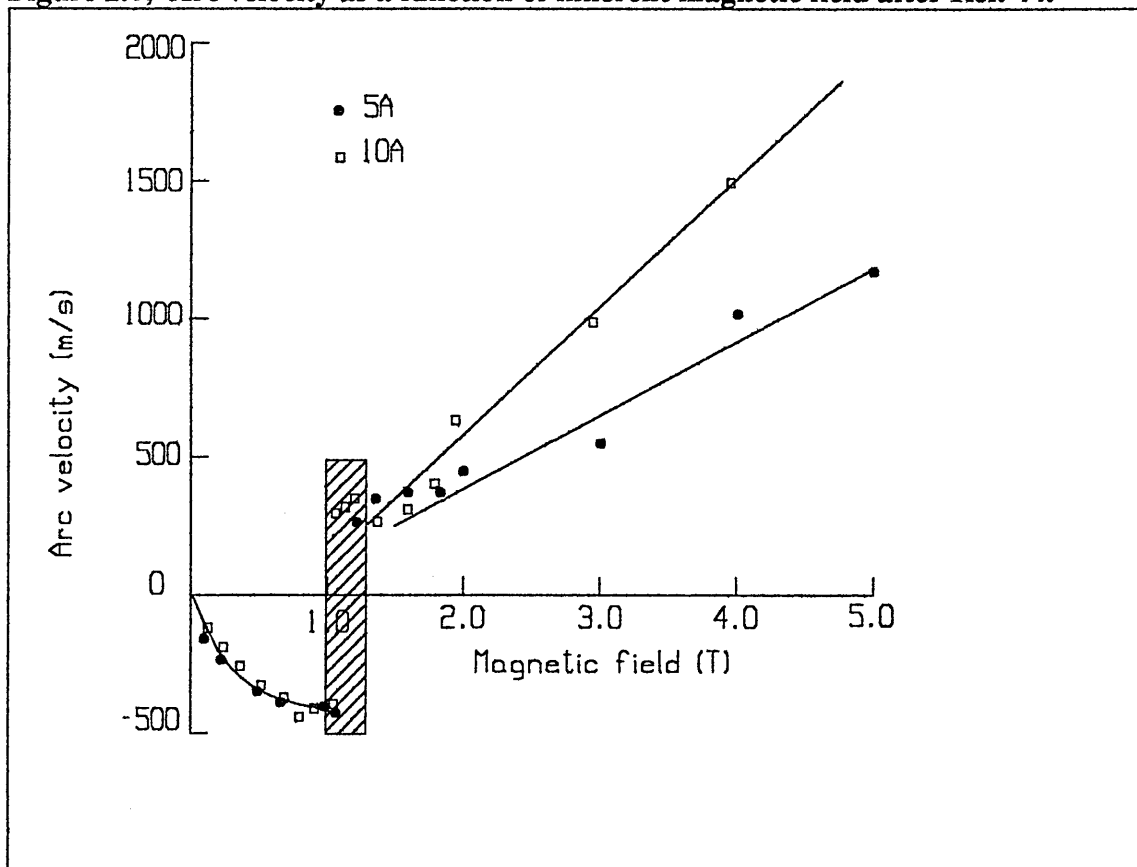


Figure 2.7, Arc velocity as function of transverse field after Ref. 45.

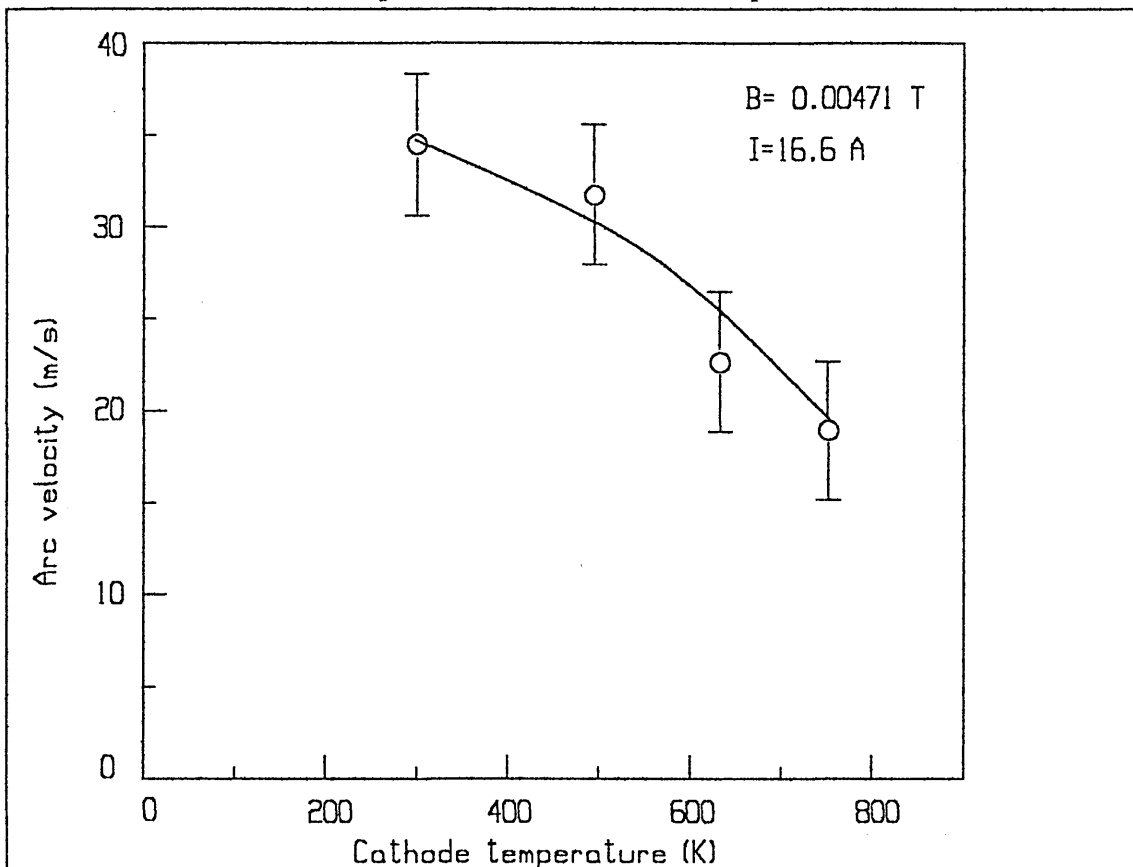


Figure 2.8, Arc velocity as a function of cathode temperature after Ref. 46.

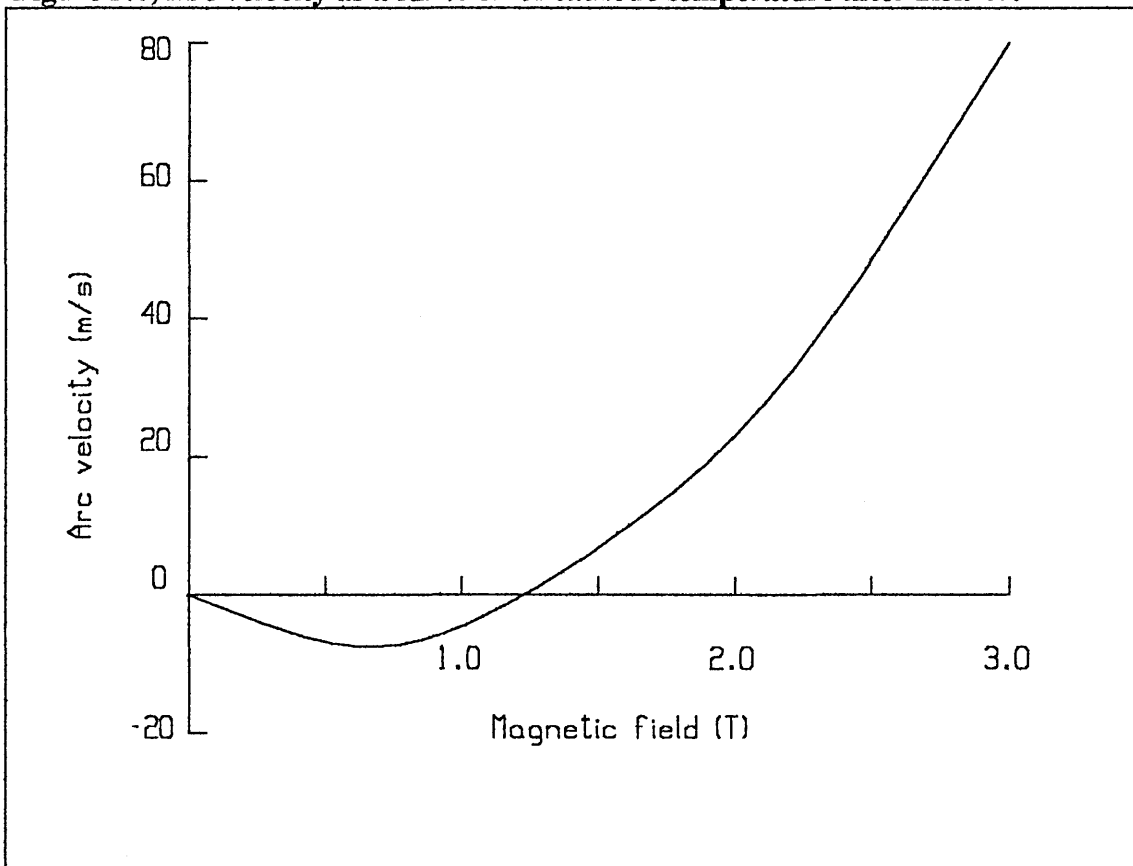


Figure 2.9, Predicted arc velocity as a function of magnetic field after Ref. 42.

The velocity of the arc at higher field strengths (up to 5 T) was the subject of work by Robson [45], examining Figure 2.7, the transition from retrograde to amperian motion can be seen to occur very sharply at approximately one Tesla, thereafter a linear dependence is shown. Similar investigations [43, 46] are in broad agreement with these results.

Fang et al. [46] investigating arc velocities for type II spots in the presence of an applied field found that the velocity of the arc decreased with increasing cathode temperature, see Figure 2.8 (the residence time of the spot at a particular site increasing due to the more favourable conditions produced by pre-heating of the cathode).

In further work [42, 47] Fang also demonstrates that retrograde velocity has a complex dependence upon arc voltage, gas pressure, thermal conductivity and cathode material. A theoretical prediction is derived (shown in Figure 2.9) for velocity that, whilst fitting with observed trends, (see Figure 2.7) shows no sign of the discontinuity from retrograde to prograde motion that occurs at approximately one Tesla.

2.6.2.2 The effects of surface roughness and contamination.

Arc velocity is, perhaps, one of the most frequently measured cathode spot parameters, consequently the relative effects of surface roughness and contamination upon arc motion have been discussed by a number of authors. Fang [42] favours the level of contamination and oxidation of the cathode as the main influence upon spot velocity, showing a dependence on the number of arcing operations (the velocity falling from 30 ms⁻¹ after one arcing operation to 4 ms⁻¹ after 50 operations). Jüttner [37] also inclines toward this explanation, noting the preference shown by arcs for tracking along scratches on the cathode (the effects of these scratches significantly reduced after thorough cleaning indicating the influence of contaminants in the scratches). Fang claims that the contribution of surface roughness to the change in velocity is within the range of experimental scatter and therefore relatively unimportant. Work by Fu [8, 38], however, would appear to contradict this view. Using cathodes of a controlled level of contamination, but differing levels of roughness, Fu demonstrates that the arc velocity

changes by at least an order of magnitude with surface roughness (see Figure 2.10 for a summary of the experimental results).

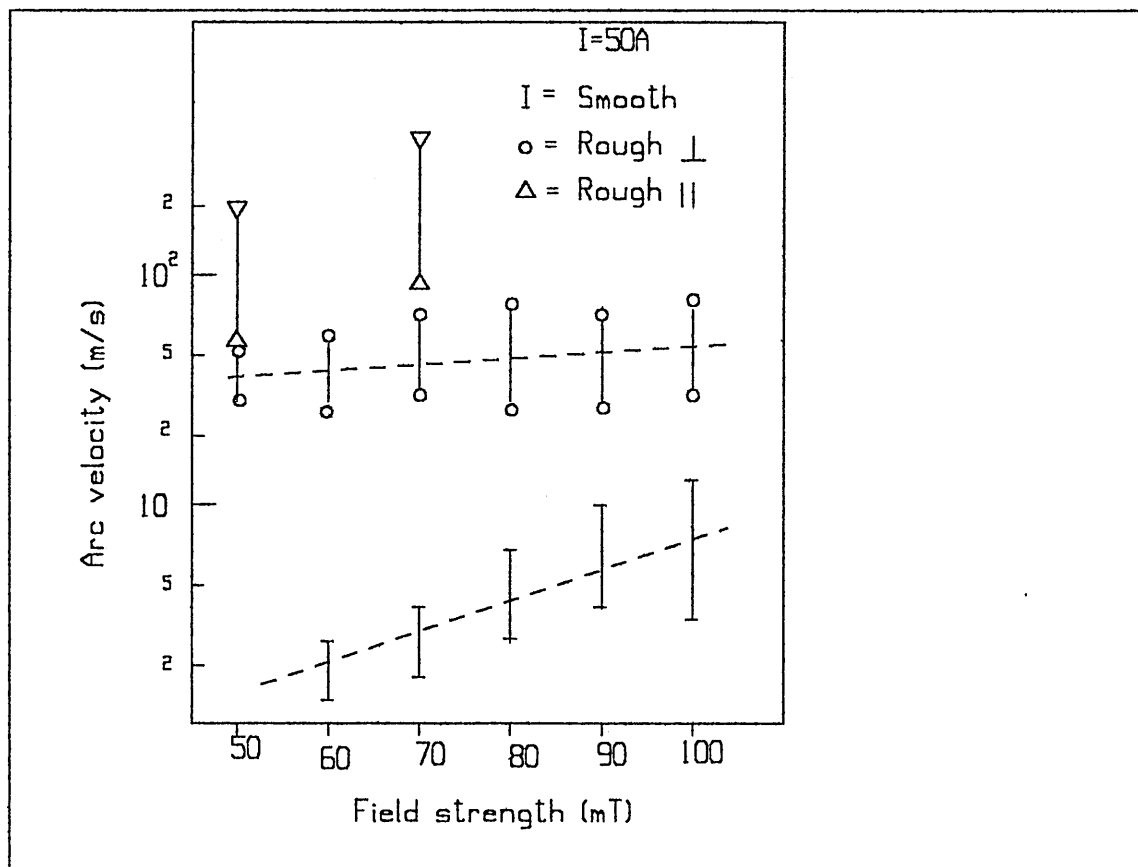


Figure 2.10, Arc velocity as a function of cathode roughness after Refs. 8 and 38.

One factor that becomes apparent from these investigations is how dependent spot velocity is upon the spot type which in turn is dependent upon surface condition. However experimenters do not always identify the type of spot under scrutiny. Further work is required to clarify this dependence whilst fixing or controlling the levels of the remaining parameters. This is discussed in more detail in Chapter 5. It is also worth noting the wide range of values quoted in Section 2.1.4 for spot lifetime, tens of nanoseconds to tens of microseconds. Spot type will almost certainly be one factor responsible for this discrepancy [36].

2.7 Summary.

Some of the fundamental spot parameters and their measured values have been discussed in this chapter. It is readily seen that there is a large range of experimental methods and results available from the literature and the validity of the results is not always easy to judge. Four points, however, remain clear; the first is that spot type is critical to almost all spot parameters and hence must be considered when making experimental measurements of any kind. The second is that the spot substructure has at least an order of magnitude effect upon self magnetic fields and current density, and is likely to be of great significance when trying to model spot motion. Thirdly the effects of surface roughness and surface contamination (although these may broadly considered to be linked to spot type) upon spot velocity, erosion rates and crater size must also be taken into consideration when designing an experiment. Finally, although this is a reiteration of the previous point it warrants special mention. An experiment designed to measure the value of the spot diffusion constant must take account of several factors. Firstly the condition of the cathode must be considered, i.e. whether it is eroded or not and the degree to which it is contaminated. Secondly the influence of an external magnetic field and the effect this might have upon the elementary spot step should be taken into account. Thirdly any possible effect that a background pressure of gas might have should be noted. Finally, and not least, it should be ensured that the quantity that is measured is related correctly to the definition of α given in equation 2.6. Ecker [12] observes that the reason for so much dispute over the nature and properties of the cathode spot is perhaps that researchers are arguing different aspects of the same phenomena without realising the fact.

References.

- [1] V.I. Rakhovskii,
IEEE Trans. on Plasma Science, **PS4(2)**, 81, (1976).
- [2] A.E. Guile, B. Jüttner,
IEEE Trans. on Plasma Science, **PS8(3)**, 259, (1980).
- [3] J. Mitterauer,
Proc. 2nd Inter. Conf. Gas Discharges, London, **IEE PUB90**, 215, (1972).
- [4] J. Mitterauer, P. Till, E. Fraunschiel, M. Haider,
VIIth Inter. Symp. on Discharges and Electrical Insulation in Vacuum,
Novosibirsk, USSR, 83, (1976).
- [5] V.V. Kanzel, V.I. Rakhovskii,
Proc. 6th Inter. Symp. Discharges and Electrical Insulation in Vacuum,
Swansea, 265, (1974).
- [6] F.R. Schwirzke,
IEEE, Trans. on Plasma Science, **19(5)**, 690, (1991).
- [7] L.A. Sena, L.I. Pranevychius, G.N. Fursey,
Proc. Xth Int. Conf. Phen. Ioniz. Gases, Oxford, contributed papers, 105, (1971).
- [8] Y.H. Fu, R.P.P. Smeets,
IEEE, Trans. on Plasma Science, **17(5)**, 727, (1989).
- [9] S. Anders, B. Jüttner,
IEEE, Trans. on Plasma Science, **19(5)**, 705, (1991).
- [10] V.F. Pucharev,
J. Phys. D Appl. Phys., **24**, 685, (1991).
- [11] A. Marlewski,
Zeszyty Navkowe Politechniki Poznanskiej, Elektryka, **29**, 9, (1985).
- [12] G. Ecker,
in "Vacuum arcs, Theory and application.", J.M. Lafferty-Editor,
Wiley-Interscience, (1980).

- [13] E. Hantzsche,
Proc. 12th Int. Conf. Phen. Ionized Gases, Eidhoven, 237, (1975).
- [14] D.D. Gruich, M. Mirrakhimov, T.D. Radjabov, M. Asliddinova,
Proc. 12th Int. Conf. Phen. Ionized Gases, Eidhoven, 236, (1975).
- [15] A.E. Guile, B. Jüttner,
IEEE, Trans. on Plasma Science, **PS8(3)**, 259, (1980).
- [16] B. Jüttner,
Beitr. Plasma Physik., **22**, 453, (1982).
- [17] B. Mazurek, J.D. Cross,
J. Appl. Phys., **63(10)**, 4899, (1988).
- [18] A. Hull,
Phys. Rev., **126(5)**, 1603, (1962).
- [19] J. Mitterauer, P. Till, E. Fraunschiel, M. Haider,
Proc. 7th Int. Vac. Congr., 3rd Intern. Conf. Solid Surfaces, Vienna,
2479, (1977).
- [20] P.N. Chistyakov, A.L. Radionovskii, N.V. Tatrionova, N.E. Novikov,
D.S. Treshchikova,
Sov. Phys. Tech. Phys., **14(6)**, 807, (1969).
- [21] A.A. Plyutto, V.N. Ryzhkov, A.T. Kapin,
Sov. Phys. JETP, **20**, 328, (1965).
- [22] W.D. Davis, H.C. Miller,
J. Appl. Phys., **40**, 2212, (1969).
- [23] O. Lloyd,
10th Inter. Conf. Phen. Ionized Gases, Oxford, **1**, 184, (1971).
- [24] L.P. Harris,
VIIIth Int. Symp. Disch. Electr. Insul. Vac., Albuquerque, **F1**, 106, (1978).
- [25] J. Kutzner, H.C. Miller,
IEEE, Trans. on Plasma Science, **17(5)**, 688, (1989).

- [26] B. Ya Moizhes, V.A. Nemchinskii,
Sov. Phys. Tech. Phys., **25**, 43, (1980).
- [27] C. Wieckert,
Beitr. Plasma Physik., **27**, 309, (1987).
- [28] V.L. Sizonenko, P.I. Markov, L.I. Kiselevskii, G.G. Shergin,
Sov. Phys. Tech. Phys., **29**, 1259, (1984).
- [29] I.I. Aksenov, I.I. Konovalov, V.G. Padalka, V.L. Sizonenkov,
Sov. J. Plasma Phys., **11**, 787, (1985).
- [30] K. Riemann,
IEEE, Trans. on Plasma Science, **17**(5), 641, (1989).
- [31] S.J. Mackeown,
Phys. Rev., **34**, 611, (1929).
- [32] H. Jäger, U. Seydal, H. Wadle,
Phys. Lett., **55A**(8), 481, (1976).
- [33] V.I. Rakhovskii,
IEEE, Trans. on Plasma Science, **18**(3), 677, (1990).
- [34] B.E. Djakov, R. Holmes,
J. Phys. D Appl. Phys., **7**, 569, (1974).
- [35] A.G. Parfynov,
IEEE, Trans. on Plasma Science, **PS13**(5), 277, (1985).
- [36] A.I. Bushik, B. Jüttner, H. Pursch,
Beitr. Plasma Phys., **19**, 177, (1979).
- [37] B. Jüttner, H. Pursch, V.A. Shilov,
J. Phys. D Appl. Phys., **17**, L31, (1984).
- [38] Y.H. Fu,
J. Phys. D Appl. Phys., **22**, 94, (1989).
- [39] G. Ecker,
Z. Naturforsch., **26a**, 935, (1971).

- [40] G. Ecker,
Z. Naturforsch., **28a**, 417, (1973).
- [41] G. Ecker,
Z. Naturforsch., **28a**, 428, (1973).
- [42] D.Y. Fang,
J. Phys. D Appl. Phys., **15**, 833, (1982).
- [43] P.D. Swift, D.R. Mckenzie, I.S. Falconer,
J. Phys. D Appl. Phys., **66**(2), 505, (1989).
- [44] J.C. Sherman, R. Webster, J.E. Jenkins, R. Holmes,
J. Phys. D Appl. Phys., **8**, 249, (1972).
- [45] A.E. Robson, A. von Engel,
Phys. Rev., **93**, 1121, (1954).
- [46] D.Y. Fang, A. Nurnberg, U.H. Bauder,
J. Nucl. Mat., **111** and **112**, 517, (1982).
- [47] D.Y. Fang,
XIth Int. Symp. Discharges and Insulation in Vacuum, 187, (1982).
- [48] E. Hantzsche, B. Jüttner,
IEEE, Trans. on Plasma Science, **PS13**(5), 231, (1985).
- [49] J.E. Daalder,
IEEE, Trans. Pow. App. Sys., **PAS93**, 1747, (1974).
- [50] B. Jüttner,
Beitr. Plasma Phys., **19**, 25, (1979).
- [51] G.P. Smith,
J. Appl. Phys., **S1**,3657, (1980).
- [52] M.G. Drouet, S. Grouber,
IEEE, Trans. Pow. App. Sys., **PAS95**, 105, (1976).
- [53] G.A. Lyubimov, V.I. Rakhovskii,
Sov. Phys. USP., **21**(8), 693, (1978).

- [54] V.I. Rakhovskii,
Measurement techniques, **26**, 865, (1983).
- [55] V.F. Pucharev, A.M. Murzakayev,
J. Phys. D Appl. Phys., **23**, 26, (1990).
- [56] M.G. Drouet,
Jap. J. Appl. Phys., **20**(6), 1027, (1981).
- [57] J. Prock,
IEEE, Trans on Plasma Science, **PS14**(4), 482, (1986).
- [58] L.A. Sena,
Sov. Phys. Tech. Phys., **15**(9), 1513, (1971).
- [59] B. Jüttner,
IEEE, Trans. on Plasma Science, **PS15**(5), 474, (1987).
- [60] B.E. Djakov, R. Holmes,
J Phys. D Appl. Phys., **4**,504, (1971).
- [61] B.E. Djakov, R. Holmes,
Proc. 1st Int. Conf. on Gas Discharges, London, 468, (1971).
- [62] I.I. Aksenov, I.I. Konovalov, V.F. Perslin, V.M. Khoroshikh, L.F. Shipilinskii,
High Temp., **26**(3), 315, (1988).
- [63] J.E. Daalder,
J. Phys. D Appl. Phys., **8**, 1647, (1975).
- [64] J.E. Daalder,
J. Phys. D Appl. Phys., **9**, 2379, (1976).
- [65] N.M. Zykova, V.V. Kantsel, V.I. Rakhovskii, I.F. Seliverstova, A.P.Ustimets,
Sov. Phys. Tech. Phys., **15**, 1844, (1971).
- [66] V.V. Kantsel, T.S. Karakina, V.S. Potokin, V.I. Rakhovskii,
Sov. Phys. Tech. Phys., **9**, 1593, (1965).
- [67] E. Hantzsche,
Beitr. Plasma Phys., **17**, 65, (1977).

- [68] B. Jüttner,
J. Phys. D Appl. Phys., **14**, 1265, (1981).
- [69] E. Hantzsche, B. Jüttner, H. Pursch,
J. Phys. D Appl. Phys., **16**, L173, (1983).
- [70] J.E. Daalder,
J. Phys. D Appl. Phys., **16**, L177, (1983).
- [71] J.E. Daalder,
J. Phys. D Appl. Phys., **16**, 17, (1983).
- [72] J.E. Daalder,
J. Phys. D Appl. Phys., **11**, 1667, (1978).
- [73] S. Anders, B. Jüttner,
IEEE, Trans. on Plasma Science, **19**(5), 705, (1991).
- [74] B. Jüttner,
Beitr. Plasma Phys., **21**, 217, (1981).
- [75] B. Jüttner, H. Pursch,
Proc. 4th Int. Symp. on Switching Arc Phenomenon, Lodz, Poland, 209, (1981).
- [76] E. Schmidt,
Ann. Phys., **6**, 246, (1949).
- [77] L. Donohue, J. Cawley, J.S. Brooks,
Surf. Coat. Tech., **63**, 49, (1994).

Chapter Three

Theoretical models of the arc

Over the last few decades a considerable amount of research has been performed into the motion of the cathodic arc, and as a consequence a large number of theoretical and empirical models have been formulated to predict various aspects of the arc's behaviour. This chapter gives an overview of the relevant models and where such models share common origins they will be described together in general terms. Broadly speaking there are two types of model; those that describe the formation of a random spot and those that describe the motion of the spot under the influence of an external magnetic field. The models of the random spot aim to produce a self consistent theory that charts the evolution of a single spot crater from either a smooth surface or a conical protrusion, whilst models of the steered arc attempt to explain the mechanism by which the spot is steered by an applied magnetic field. Of particular interest to this work are; the two models in Section 3.2.2 (both of which attempt to support a different spot heating mechanism, this has bearing on work presented in Chapter 5) and the three models of the spot motion as a random walk in two dimensions (two of these models describe the random arc and are presented in Section 3.2.4, the third model describes both the random and steered spot motion and is presented in Section 3.3.5). A large number of physical factors have been considered when setting up these models. By way of introduction this chapter describes these inputs and discusses any problems incumbent with their use.

3.1 An introduction to spot models.

A great many physical parameters need to be considered when building a model of the cathode spot such as surface roughness, surface material, surface contamination, anode voltage and current density. The following section describes various thermal inputs to

the spot. Not all parameters are used by each model and there is some contention as to the relative importance attributed to some of the processes. It is also interesting to note at this stage the extremely dynamic nature of the cathode spot and the likelihood that whilst one process might dominate spot heating at the formation of the crater an entirely different mechanism might be responsible for the heating of any micro-protrusion at the time of the spots ignition.

3.1.1 Heating processes.

3.1.1.1 Ionic bombardment.

Energy is input at the cathode surface by ion bombardment from the plasma cloud. The level of heating resulting from this depends on several parameters particularly the accommodation and ion back flow coefficients and the rate of ion neutralisation at the cathode surface. The two accommodation coefficients describe the proportions of the ion's kinetic and neutralisation energy that are given up to the cathode. These are assumed by most authors, for convenience, to be unity [1, 2, 3, 4] as there is no accurate experimental data available about them. The ion back flow coefficient (the proportion of ions created in the ionisation zone that are accelerated back towards the anode) takes a value between zero and unity although many authors, again for simplicity, assume this quantity to be unity [1, 5, 6]. Similarly there is no data pertaining to the rate of ion neutralisation at the cathode surface and models generally assume that all ions have been singly ionised within the plasma cloud and are then all neutralised at the cathode [2]. As a consequence the actual number of ions colliding with the anode can be calculated from the fraction of the total arc current carried by these ions, generally between 7% and 12% of the total current [7].

3.1.1.2 Joule heating.

The cathode is heated by the passage of electrons through it. This is most intense at the cathode spot where the electrons are "funnelled" through an extremely small area. Considering the very high current densities observed (see Section 2.3) the onset of thermal runaway might be expected. Thermal runaway occurs when the current density in a conductor is high enough to produce heating in the metal thus causing an increase in electrical resistivity, this in turn leads to greater heating and further rises in resistivity.. This, however, is not observed to any great degree at the cathode spot.

Three arguments have been forwarded to explain the absence of runaway. Jüttner [8] argues that Joule heating is not a major factor in cathode heating and that thermal

runaway is, therefore, not possible (see Section 3.2.2). Hantzsche [9] notes that in the first instance the mechanism for electron emission cooling at the spot (see section 3.1.2.1) is temperature dependent and, therefore the process is self limiting (there existing a limit to the maximum achievable stationary temperature) and secondly that the time scale for crater formation (10ns) is far too short for thermal runaway to occur (of the order of 100ns). Ecker [10] also offers a comparison of thermal and spot formation time scales (T_{th} and T_{res} respectively) to include the possibility of runaway only if $T_{res} > T_{th}$ this condition is not satisfied with calculated values for T_{th} for copper being of the order of 60ns, whilst spot residence times are observed of the order of 10-30ns.

3.1.1.3 Nottingham heating.

The Nottingham effect may both heat or cool a surface [11]. It is caused by the difference in temperature between the electrons emitted at a surface and those supplied by an electric circuit to replace them. Whether the spot is heated or cooled by this effect is determined by the temperature at the emitting area of the spot. Above an inversion temperature (calculated from the cathode work function and applied electric field) the cathode is cooled by the effect, below the temperature it is heated. Although generally the temperature at the cathode spot is much higher than the inversion temperature, the effect is still of importance as the change in the amount of energy being lost from the cathode with the variation in spot temperature is of significance when calculating the energy balance at the spot [10].

3.1.2 Cooling processes.

3.1.2.1 Electron emission.

The cathode spot may emit electrons in three ways dependent upon the temperatures and electric field gradients present at the spot.

(i) Field emission: the application of an electric field of sufficient magnitude to the cathode surface allows electrons to tunnel through the modified potential barrier and escape the cathode surface. As has been mentioned earlier (see Section 2.2.1), cathodes that are subject to macroscopic fields of insufficient strength to cause field emission do, in fact, exhibit this phenomenon. This is due to a combination of field enhancement by microscopic surface features and lowering of the effective work function of the surface by contaminants [12, 13]. It is generally agreed that pure field emission occurs only in the explosive type I spot on fresh, contaminated surfaces and that the emission mechanisms change as the spot type becomes predominantly type II (see Section 2.2).

(ii) Thermal emission: the electrons within the material are raised to such a temperature that they have a finite probability of the surmounting the potential barrier and escaping the cathode surface. This emission mechanism is dominant in the type II cathode spot, the longer spot residence time giving the plasma cloud time to heat the spot to a temperature at which thermal emission is possible (see section 2.2).

(iii) Thermo-field emission is a combination of the two previous effects. Several formulae have been derived (some specifically for application to arc theory) that give net electron emission due to both effects from a surface at a given temperature and subject to a given electric field.

Cathode spots tend not to exist entirely as type I or type II, rather there is change from predominantly type I to predominantly type II as the cathode is arced upon: the surface cleaned and protrusions eroded [17]. Similarly the emission mechanism from the spot at the various stages of its life is either dominated by field or thermal emission, and hence, various combinations of formulae for the two separate mechanisms or a combined thermo-field expression are used by a number of authors to give a value for the arc current [1, 2, 9, 10, 14].

3.1.2.2 Neutral particle loss.

Energy loss from the spot occurs by way of neutral particle evaporation and macro particle ejection. The ejection of macro particles would appear to present no problems and is described by Prock [1]. The evaporation of neutrals, however, is not easy to describe. Ecker notes that the actual mass loss through evaporation is smaller (by up to 20%) than the losses predicted by the Langmuir equation [10]. This is possibly due to the effect of ions returning from the plasma cloud and bombarding the molten cathode spot not being considered when evaporation rates have been calculated.

3.1.2.3 Heat conduction.

Heat is conducted away from the spot into the body of the cathode. This is normally considered by the Fourier equation but work by Till et al. [3] proposed that this is not valid for very fast systems (of the order of picoseconds) and so developed an extension of the Fourier equation based upon the description of a Thomson cable. The extension considers heat conduction by a system of thermal waves, analogous to electric waves propagated in a cable and introduces the concept of a distributed thermal inductance and resistance within the conducting medium. This modification produces significant changes to modelling of all thermally dependent effects and could, therefore, have considerable effects upon models of spot formation.

3.1.2.4 Heat radiation.

Heat is radiated away from the spot (described by the Stefan-Boltzmann equation). Most authors concur that this is a second order effect and, therefore, negligible [1, 8, 10]. However Mitterauer and Till [2] do consider radiation as a factor in their model.

3.1.2.5 Latent heats.

Heat is lost supplying energy for the latent heats of fusion and evaporation. The temperature at the solid liquid interface is a constant for a given material and therefore the latent heat of fusion is constant. The temperature at which the molten surface boils

however, is governed by the pressure at the surface, and as the latent heat of vaporisation is dependent upon temperature some correction must be applied to arrive at an approximate value of the heat of vaporisation, e.g. linear interpolation [1].

3.1.2.6 Nottingham cooling.

Above the inversion temperature (which is usually the case at the cathode spot) the Nottingham effect cools the spot (see section 3.1.1.3).

3.1.3 Summary.

There appears to be little contention as to which processes are occurring at the spot (most models attempting to describe the evolution or steady state of the spot crater use some or all of the thermal inputs described above). Conflict arises as to importance of each effect, e.g. the argument that ion bombardment dominates the heating processes and that Joule heating is relatively unimportant [8] (see Section 3.2.2) and the relegation of heat radiation to a second order effect [1]. It would seem that the dynamic nature of the spot coupled with the differences between the two types of cathode spot leads to a situation where certain mechanisms dominate different types of spot at different stages of their life cycles, Joule heating and field emission dominating the early part of the spot development to be replaced by ionic bombardment and T-F emission in the latter stages of the life cycle [10].

3.2 Models of the evolution of a random cathode spot.

More complex models of the random cathode spot [1, 2, 8] attempt to specify typical spot parameters such as current density, spot size etc. from the inputs described above. Simpler ones may attempt to quantify a specific contribution to spot operation by any one of these inputs [3, 14, 15, 17, 18]. Described below are several theories used for modelling the spot.

The first section presents a geometry used by a number of authors. It is based upon a molten hemispherical crater (assuming the previous destruction of any surface feature) and lends itself to computer based numerical solution using most or all of the heating and cooling mechanisms listed above (see Figure 3.1).

The second section presents two models that, which although appearing to be simplified versions of the hemispherical crater models, are in fact fundamentally different. The first of the models supposes that ionic bombardment is the main process responsible for spot heating whilst the second argues that Joule heating is the dominant process. This argument, which is ongoing and the subject of considerable debate in the literature, is important not only to establish fundamental processes at the spot but also as an indication of other spot parameters (see Section 2.6).

The third section presents a model of the destruction of a micro-protrusion and demonstrates very effectively the influence of surface roughness upon the behaviour of the spot (see Figure 3.3).

The fourth model presented explains the motion of the cathode spot as a stochastic process. These models are closely linked with Care's model of the motion of the spot as a biased random walk which is described in Section 3.3.5.

3.2.1 Computer based numerical solutions.

Two of the hemispherical crater theories [1, 2] attempt to produce self consistent time dependent models which chart the development of the spot in terms of the temperature distribution across the spot, its diameter and current density. The key feature of these models is that the spot is viewed as a dynamic process with the contributions from

different heating and cooling processes changing on a very short time scale (picoseconds). The effect of changing various initial conditions such as crater radius or electric field can be studied yielding useful information upon feasible states of existence of the spot, e.g. the temperature, spot size, and field strengths which may cause the onset of thermal runaway. Both models consider the crater (which is assumed to have been created by previously by pressure from the plasma) as three distinct regions; the solid layer, the liquid layer and the region above the cathode (see Figure 3.1). The spot is then modelled by way of mass, energy and particle balance.

Several predictions are made by each model. That of Prock [1] gives values for the minimum crater radius and associated formation time, the magnitude and current dependence of spot velocity, the spot splitting current and the erosion rates of several materials. All results agree well with experiment. Mitterauer and Till [2] also give results for several parameters; the temperature distribution, vapour pressure and velocity of melting and evaporation. These allow the determination of a number of spot characteristics. More importantly, predicted values for crater radii produced after certain lengths of time compare well with those produced experimentally by pulsed discharges of the same duration.

There are limitations in both of the models described above. Firstly the uncertainty in a large number of the constants used, lead to values of unity being assumed for the ion back flow coefficient and accommodation coefficients (see section 3.1.1.1) and secondly, as Mitterauer and Till point out, there is a lack of experimental data regarding the thermo-physical behaviour of metals far above their boiling points. This requires estimates to be made for some parameters. A point of interest Mitterauer and Till [2] fail to address is that of spot lifetime and hence the mean radius of the craters left after the death of a spot, i.e. why, after the crater reaches a certain diameter does it extinguish and another take its place. They do, however, note the theoretical existence of the onset of thermal runaway at a time dependent upon the applied electric field and initial radius (thermal runaway occurring sooner for larger initial craters with a higher applied field). As this phenomenon is not observed to any great extent at the spot (see Section 3.1.1.2)

the possibility exists that the spot movement is connected with the onset of runaway. This being the case this model might offer an insight as to the conditions required for runaway to take place. Prock [1] explains that the termination of the spot occurs as the crater becomes sufficiently large to reduce the heating at the spot and, therefore, decrease the amount of vapour available below the level required by the plasma to survive.

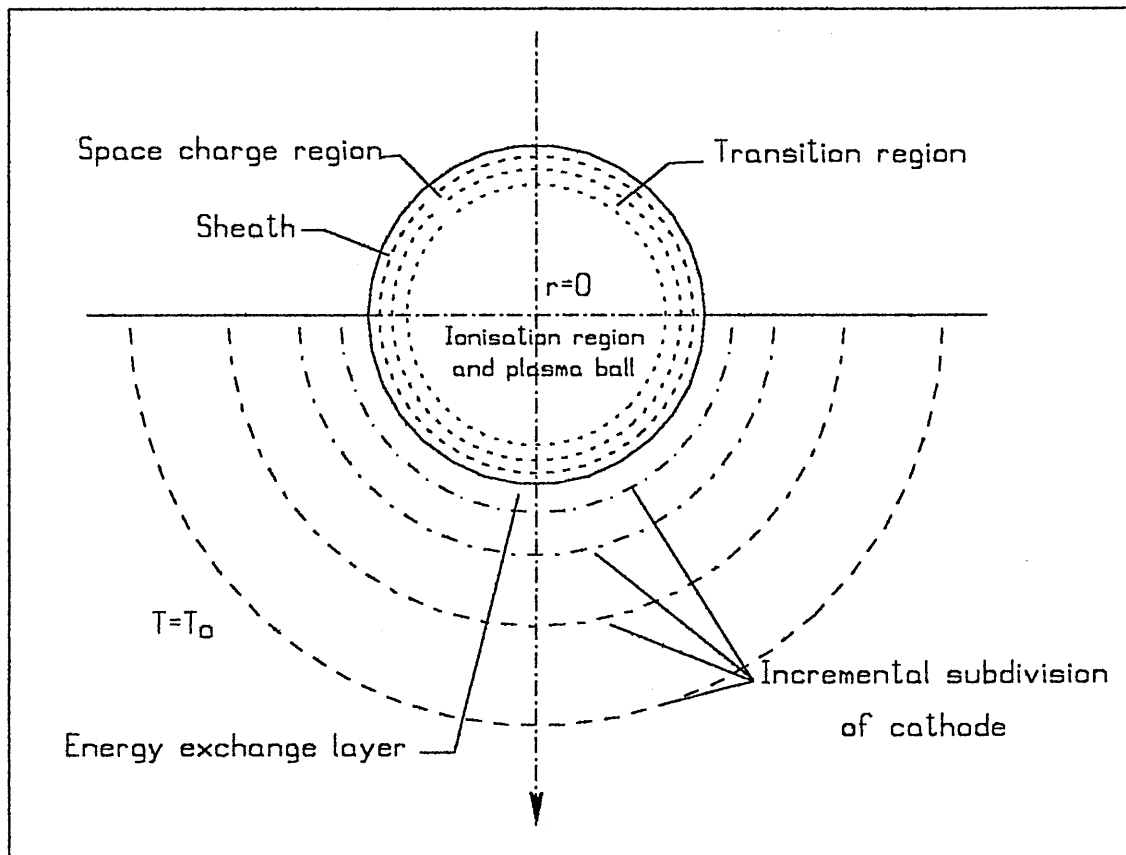


Figure 3.1, Hemispherical crater model after Ref. 1.

3.2.2 Ionic bombardment and Joule heating models.

3.2.2.1 The Joule heating model

The Joule heating model developed by Daalder [40] uses a hemispherical geometry (see Figure 3.2) consisting of a crater of radius r being burrowed into the cathode to a maximum value of $r = r_a$, this is achieved during the formation time $\tau(r_a)$. The electron current I'_{el} flows radially and isotropically into the cathode and is constant for the formation time of the crater and is the only source of heating considered.

The model assumes that once metal in the crater has been reached its molten state by Joule heating it will be removed by the high pressure gradient present at the crater. The time taken for the volume of metal for a crater radius r to reach its melting point and then melt may be calculated, thus giving the crater formation time as a function of radius. If Δt_1 and Δt_2 are the times of melting and fusion respectively then,

$$\tau(r, T_s) = \Delta t_1 + \Delta t_2 \quad (3.1)$$

Where,

$$\Delta t_1 = \int_{T_0}^{T_s} \frac{(2\pi r^2)^2 m_s c_p}{I_{el}^2} \frac{dT}{\rho(T)} \quad (3.2)$$

$$\Delta t_2 = \int_{T_0}^{T_s} \frac{(2\pi r^2)^2 m_s p_s}{I_{el}^2} \frac{dT}{\rho(T_s)} \quad (3.3)$$

Where $\rho(T)$ is the resistance of the layer being considered, m_s is the density of the cathode material, c_p is the specific heat of the solid material and P_s is the heat of fusion.

Considering the change in resistivity with temperature, then according to Wiedmann-Frantz-Lorentz,

$$\rho(T)\lambda = LT \quad (3.4)$$

Where L is the Lorentz constant and λ is taken as a constant for the purposes of this model. Then combining Equations 3.1 to 3.4 gives,

$$\tau(r, T_s) = \frac{(2\pi r^2)^2 m_s \lambda_0}{I_{el}^2 L} \int_{T_0}^{T_s} \frac{c_p}{T} + \frac{P_s}{T_s} dT \quad (3.5)$$

Equation 3.5 thus gives the formation time for a crater of radius r in terms of the crater radius (a dependence to the fourth power), the arc current and the material properties of the cathode. Using the above model crater radii and erosion rates are predicted and compared with experiment.

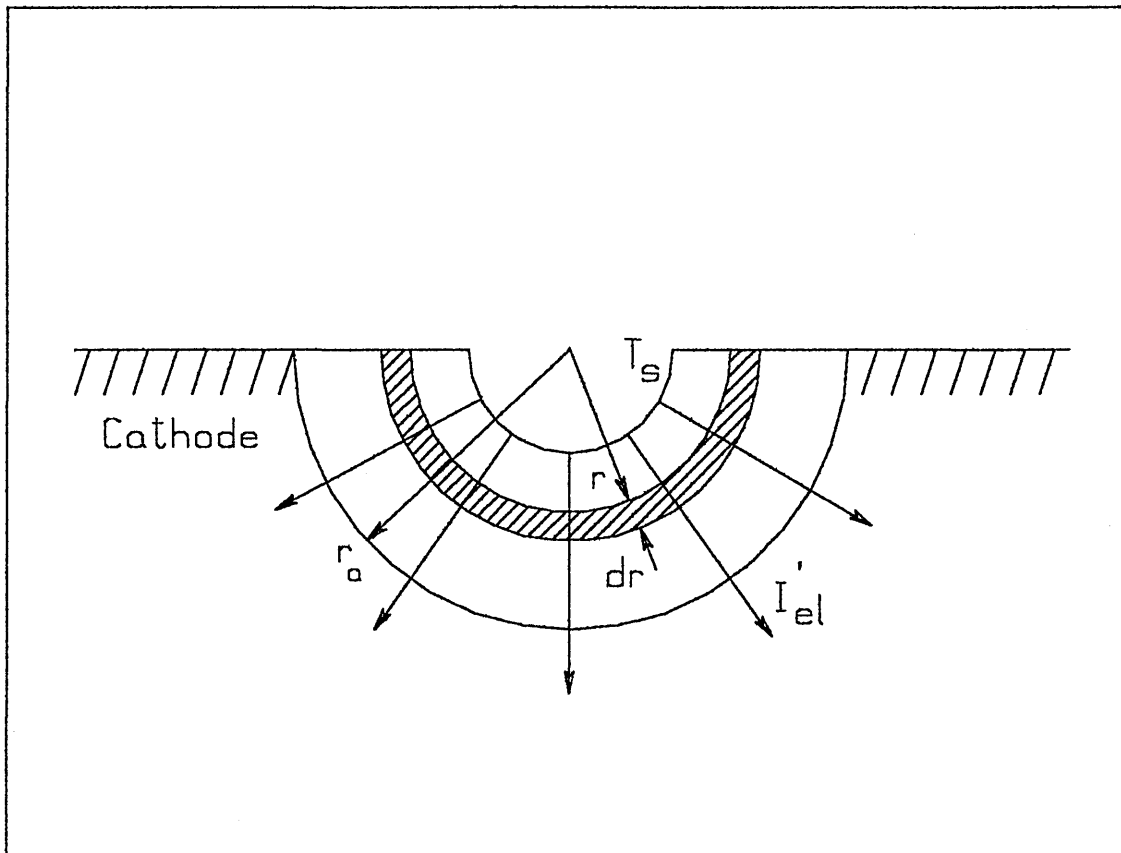


Figure 3.2, Daalder's hemispherical crater after Ref. 40.

Daalder postulates that the crater radius reaches a maximum and the spot will extinguish when the Joule heating in the molten layer is equal to the heat loss by conduction. This occurs as the heat production within the hemispherical shells diminishes with increasing radius, whereas the heat lost through conduction increases until equilibrium is reached. Values of maximum crater radius per amp are calculated for copper, cadmium and tungsten and compared with those measured experimentally. For copper a calculated value of $5.1 \times 10^{-8} \text{ m A}^{-1}$ compares well with the measured value of $5.7 \times 10^{-8} \text{ m A}^{-1}$, however radii calculated for cadmium and tungsten were in error by factors of 2.5 and 0.5 respectively.

Daalder considers erosion of the cathode as the repeated excavation of a crater of radius r_a generated by a current I_{ei} in a time $\tau(r_a)$ in this case he writes the erosion per coulomb as,

$$E_r(r_a) = \frac{2/3 \pi r_a^3 m_s}{I_{ei} \tau(r_a)} \quad (3.6)$$

Substituting in Equation 3.6 with the value for formation time given by Equation 3.5 and the calculated value for r_a allows the calculation of theoretical values for erosion rates for a range of materials. A comparison is made between the experimentally determined value and the predicted rate multiplied by a correction factor. The origins of the correction factor are twofold. Firstly not all evaporated, ionised material leaves the cathode permanently, a substantial proportion recombining with the cathode. Daalder assumes that 50% of the ionised material returns to the cathode. Secondly, the erosion rates are calculated on the basis of 100% electron current, whereas only 90% of the total is carried by electrons, the remainder being carried by ions. Allowing for corrections the differences between measured and predicted values are a factor of between 1.3 and 2. Daalder argues that this is a reasonable agreement considering the calculated value for crater radius was a maximum and, therefore, all erosion rates calculated are a lower limit.

Although reasonable agreement is reached between theory and experiment several points are worth noting. Firstly, the model does not consider any mechanism apart from Joule heating and no theoretical comparison between the various spot heating mechanisms is made. Secondly, the issue of thermal runaway is not addressed, indeed the λ variable is taken as a constant and on the time scale predicted for spot formation by Daalder thermal runaway might be expected. Thirdly the accuracy of the model as it stands relies heavily upon the ratio of number of evaporated and returning ions which is not well documented.

3.2.2.2 The thin layer heating model (ionic bombardment)

This section discusses, in detail, the development of an ionic bombardment model. It is divided into two sections, the first discussing a steady state approximation of heating at the spot and the second the development of the thin layer model. The thin layer model, developed by Jüttner [8], uses a similar geometry to that described above and aims to demonstrate that ionic bombardment is the main process for heating the spot and that Joule heating is of little significance. Jüttner explains this by assuming a very small time scale for crater formation (although the determination of this time scale relies upon the accuracy of experimentally determined values for both the constant of spot displacement and the spot diffusion constant).

(i) Heating of the spot in the steady state.

The spot is defined by the area upon which ions from the plasma cloud are impacting (a circle of radius a), existing within this is a molten pool from which electrons are emitted, defined by a circle of radius r . Expressions are now formulated that give the power inputs to the cathode via Joule heating and ionic bombardment, from these the ratio of two heating processes (P_v/P_s where P_v is the power input at the molten crater of radius r , due to Joule heating and P_s is the power input at the spot, radius a , due to ionic bombardment) may be calculated and the relative contributions to spot heating assessed. P_v is calculated by Jüttner to be,

$$P_v = x r^3 j^2 \quad (3.7)$$

Where x is the resistivity of the cathode material (from $x = x_0 T$), r is the crater radius and j is the current density at the crater. P_s is given by,

$$P_s = \frac{\pi a \lambda (T - T_0)}{F}, \quad (3.8)$$

where a is the radius over which the ions are bombarding, λ is the thermal conductivity of the cathode material, T is the temperature of the spot, T_0 is the ambient temperature and F is a function dependent upon the dimensions of the crater and time. This function tends to unity as time goes to infinity. So in the case of a stationary spot with $t \rightarrow \infty$, combining Equations 3.7 and 3.8 the ratio of the two power inputs becomes,

$$P_v/P_s = \pi^{-3} \lambda^{-1} \frac{x}{T - T_0} \left(\frac{I}{r} \right)^2 \quad (3.9)$$

Jüttner now makes the approximation that $x(T - T_0)^{-1} \sim x_0$, from this then $P_v \sim P_s$ if I/r reaches a critical value

$$\left(\frac{I}{r} \right)_{Crit}^2 = \pi^3 \lambda / x_0 \quad (3.10)$$

As $I/r_c \geq (I/r)_{Crit}$ then, in the stationary case, Joule heating should be the dominant process. However, Jüttner points out that in the case of a highly mobile spot the effect of Joule heating must be reduced. To verify this argument the cathode power

consumption and the crater formation time scale are used to produce the "thin layer heating model".

(ii) The thin layer heating model.

It has been demonstrated experimentally that approximately one third of the power of the arc is dissipated in the cathode [42], this fraction of the total arc power ϕ may be expressed as,

$$\phi = P/IU \quad (3.11)$$

Where P is the power dissipated within the cathode, I is the arc current and U is the arc voltage. Using Equations 3.7, 3.8 and 3.11 Jüttner calculates power inputs to the cathode from Joule heating and ionic bombardment for the stationary case. In both cases the fractional contribution to the cathode heating is at least an order of magnitude lower than the observed fraction of $\phi = 0.3$.

Examining the time scale for the crater formation Jüttner presents an expression for the ratio r^2/τ where r is the crater radius and τ is the time of crater formation, this expression uses formulae derived by Daalder for r and τ [33] and is shown below as Equation 3.12,

$$r^2/\tau = d \times f(T_m, T_0) \quad (3.12)$$

Where d is the thermal diffusivity of the cathode material and $f(T_m, T_0)$ is a slowly varying function of the melting temperature of the cathode material, T_m and the bulk temperature of the cathode, T_0 . This function is of the order of unity (and is taken as such by Litvinov et al [34]) giving,

$$r^2/\tau = d \quad (3.13)$$

Examining experimental results, presented in [8], measuring r^2/τ (α if γ is taken to be unity, where α is the spot diffusion coefficient and γ is the constant of spot displacement as defined in Section 2.6) it can be seen that Equation 3.10 does not hold and, that in fact

$$\alpha = (r^2/\tau)_{\text{exp}} \gg d \quad (3.14)$$

Assuming γ is unity (a spot step of one crater radius) and that Jüttner's measured values for α are correct then the time scale for spot motion is far shorter than the time scale for heat conduction. A model is now proposed to account for both the short time scale of crater formation and the amount of power dissipated in the cathode. Basing his ideas upon earlier work by McClure [35] Jüttner proposes that thin layers ($0.1 \mu\text{m}$) of the cathode on the crater surface are removed either by plasma pressure (in the case of a liquid surface) or sublimed (in the case of a solid layer). This happens much faster than heat may be conducted into the cathode. Craters are therefore formed on a very short time scale (a few nanoseconds) thus excluding the possibility of thermal runaway and preventing Joule heating from making any significant contribution to spot heating. This extremely rapid crater formation also has the effect of reducing the time scale to the point where the factor F in Equation 3.8 is no longer unity and the contribution of ionic bombardment to spot heating is increased accordingly. Approximate calculations by Jüttner show that on the time scales possible within the thin layer heating model give values for ϕ of greater than 0.1, comparable with experimentally determined values

This model, in conjunction with experimental measurements of the spot diffusion constant, provides convincing evidence of the dominance of ionic bombardment as the main spot heating process. This is dependent, however, upon the accuracy of the measured values for α (this is discussed in detail in Chapter 5) and the value of the constant of spot displacement γ (see Section 2.6.1)

3.2.3 Conical protrusion model.

As has been discussed previously (see section 2.6.2), Fu [18] demonstrates experimentally that surface roughness has a profound effect upon arc velocity (see Figure 2.10) which is found to change by an order of magnitude between surfaces of differing roughness. Attempting to confirm this theoretically a model was proposed based upon a specific surface topology which uses a regular cone as a surface feature (see Figure 3.3).

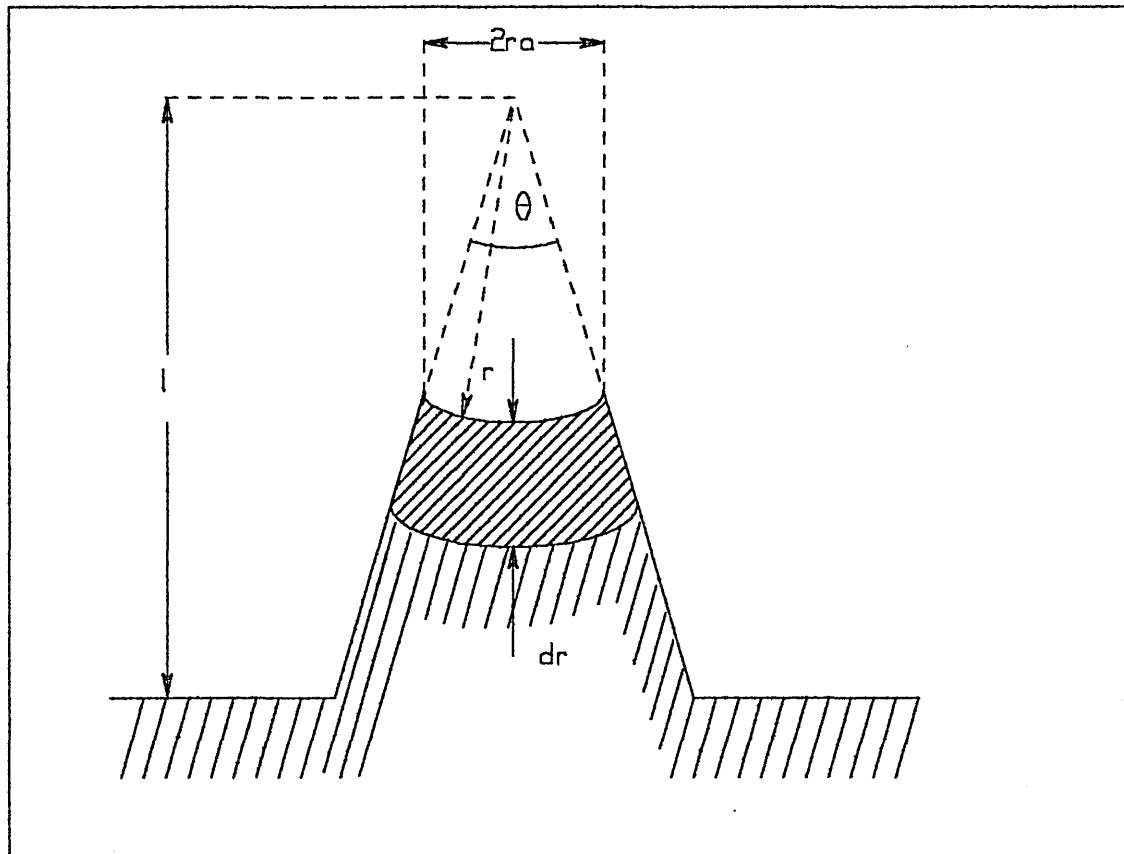


Figure 3.3, Conical protrusion model after Ref. 18.

Mass and energy balance are then used to calculate erosion rates. The model, which is limited in the respect that it only uses Joule heating as an energy source and evaporation as a cooling mechanism and uses a very simplified geometry, gives a good indication of the effects of a protrusion on the rate of erosion. Results from the model show that the amount of matter evaporated from the protrusion, and hence how much material is available to support the arc, is much greater than would be expected from a crater. This,

especially when considered in tandem with electric field enhancement at the protrusion tip, would be expected to have a significant influence upon the favourability of new arc ignition sites in the case of a type I spot. It would be interesting to test these aspects of the model by, perhaps, measurement of the change in evaporation rate on surfaces of differing roughness and the "before and after" examination of a cathode surface to reveal the nature of any erosion occurring at surface protuberances.

3.2.4 Models of the spot motion as a random walk.

Both Hantzsche et al [36, 37] and Daalder [39] have considered the motion of the cathode spot as a random walk and independently come to the same expression to describe the probability density function for the spot's location. The description of the spot motion in such a fashion leads to the definition of a spot diffusion constant (described in detail in Section 2.6.1). The value of this diffusion constant can give information about a number of other spot parameters such as crater formation time and microscopic spot velocity. Dependent upon the value of the crater formation time and mean displacement of the spot weight may be lent to either Joule heating or ionic bombardment as the principal mechanism for spot heating. Of the two models Daalder's [39] has the simpler notation, and for this reason it is chosen as the basis for the description below.

Daalder assumes that the cathode spot starts to move from the origin of an x - y coordinate system. During a time step τ the spot is free to move a step $+s$ or $-s$ along the x axis and a step $+s$ or $-s$ along the y axis. The probability of a step in each direction is assumed to be equal and the movement along each axis independent. The total time t of motion is now defined; the spot, making n displacements, will be in position (x, y) at time t , where $t = n\tau$. Then, provided that n is large and that the displacements along the x and y axes are independent Daalder gives the probability density function of the (x, y) position as,

$$p(x, y) = \frac{1}{2\pi\alpha t} \exp\left(-\frac{x^2 + y^2}{2\alpha t}\right) \quad (3.15)$$

This expression is now transformed from Cartesian to cylindrical co-ordinates thus giving the density function, $p(R)$, of distance, R , from the origin, where $R = (x^2 + y^2)^{1/2}$.

This function is given as,

$$p(R) = \frac{R}{\alpha t} \exp\left(-\frac{R^2}{2\alpha t}\right) \quad (3.16)$$

Where α , the diffusion constant, is defined as $\alpha = s^2/\tau$ (see section 2.6.1). Daalder identifies Equation 3.16 as a Rayleigh distribution which gives the probability of that after time t the spot position is lying in the range between R and $R + dR$. It also follows from this distribution that the mean value of spot displacement is,

$$\bar{R} = \left(\frac{\pi s^2 t}{2 \tau}\right)^{1/2} \quad (3.17)$$

In Section 2.6.1 discrepancies in the definition of the diffusion constant were discussed and the conclusion drawn that correct definition for α (for a step in one dimension) is as defined above by Daalder. It is now noted that during the time step τ a step may be taken in both the x and y directions and, therefore, an elementary step in two dimensions is defined, s' where $s' = s\sqrt{2}$.

Daalder now attempts, experimentally, to confirm that the motion of the spot may be described by a Rayleigh distribution. This is achieved by separate analysis of the spot motion in the x and y directions. The distributions were found to be normal and centred about zero displacement, i.e. the probability of a step in the $+s$ and $-s$ directions is a half

in each direction, this leads Daalder to conclude that the motion of a single cathode spot is a two-dimensional random walk.

Separate work by Anders and Jüttner [13] confirms that this is the case. This is achieved by counting the number of traces, $N(r)$ that intersect an arbitrarily chosen radius r from the starting point of the spot. From this data the fractal dimension, D , of the arc trace is calculated from the equation,

$$N(r) \propto r^{D-1} \quad (3.18)$$

D was found to be $2 \pm 5\%$ a value characteristic of Brownian motion, i.e. a random walk phenomenon.

The formal description of the spot motion of the arc as a stochastic process by two sources is important not only in characterising the motion of a random arc but also as it supports the notion that the motion of the arc in an external magnetic field may be modelled in a similar fashion. Indeed, Hantzsche et al. point out [37] that the motion of an asymmetric random walk, i.e. the motion of the spot under the influence of some external driving force, such as a magnetic field, may be treated by the general form from which the Rayleigh distribution is derived [41].

3.3 Models of the movement of the cathode spot in a magnetic field.

The models described below attempt to explain, and in some cases quantify the movement of the arc in an applied magnetic field. Central to this is the fact that any model must successfully explain the retrograde (or non-amperian) motion of the arc. Important effects discussed below are; the superposition of the applied and self magnetic field of the spot, the action of the applied field upon the positive space charge and emitted electrons and the discrete nature of the motion of the arc. Considerable space is spent discussing the model developed by Care [19], firstly as it considers the arc movement as a stochastic process taking place in two dimensions (this is in a manner similar to the models of Hantzsche et al [36, 37] and Daalder [38, 39], which are

discussed in Section 3.2.4 except that in this instance the random motion of the arc is also influenced by an applied magnetic field) and secondly because predictions made by the model are compared directly with experimental work described in Chapter 5 and also with the work of Hantzsche et al [36, 37] and Daalder [38, 39] mentioned above.

3.3.1 Asymmetric confinement.

Drouet [20] explains the retrograde motion of the arc by assuming an asymmetric confinement of the arc plasma by a combination of applied transverse field component and the self field generated by the electron current from the spot (see Figure 3.4). A subspot structure is assumed to exist thus increasing the current densities and self fields at the subspots by at least two orders of magnitude. The transverse component of the applied magnetic field is then enhanced by the self field on the retrograde side of the spot tightly confining the plasma cloud and diminished by the self field on the prograde side allowing the plasma cloud to expand (see Figure 3.5). This has the effect of causing more intense ion bombardment and, therefore, more intense heating on the retrograde side of the spot and hence more favourable conditions for electron emission and new spot ignition.

Calculations performed using this theory show that (assuming typical subspot parameters for copper) at applied fields of greater than one Tesla the effect of the self field is overcome and the arc starts to move in the amperian direction, as is observed experimentally. This idea is supported in principle by several authors [14, 21] who note that the cathode spot lifetime is proportional to the local magnetic field. Drouet's model raises several interesting points. Firstly the maximum step a spot can jump is limited to the radius of the confined size of the cloud. Secondly it indicates the existence of the subspot structure with the associated increased current densities. And finally the reason for the change in the direction of the motion of the arc at high applied fields is explained succinctly.

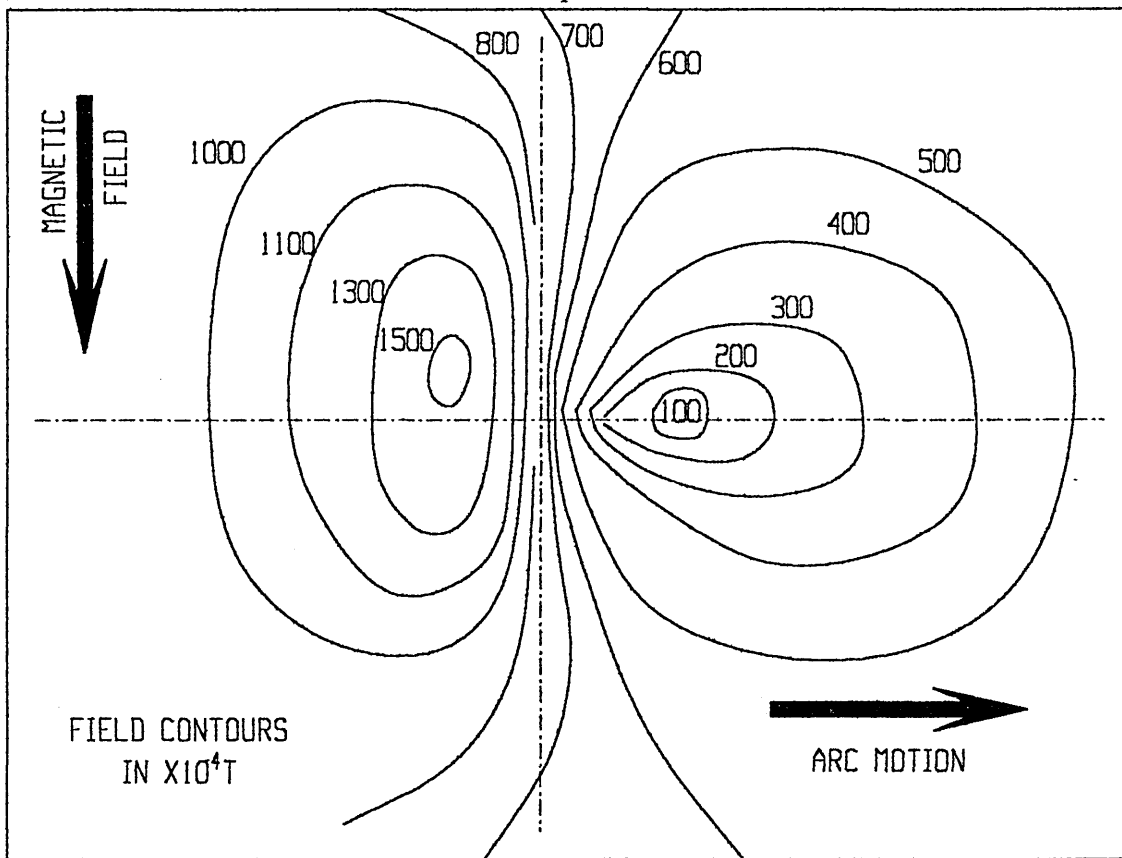


Figure 3.4, Change in applied field near spot due to self-field after Ref. 20.

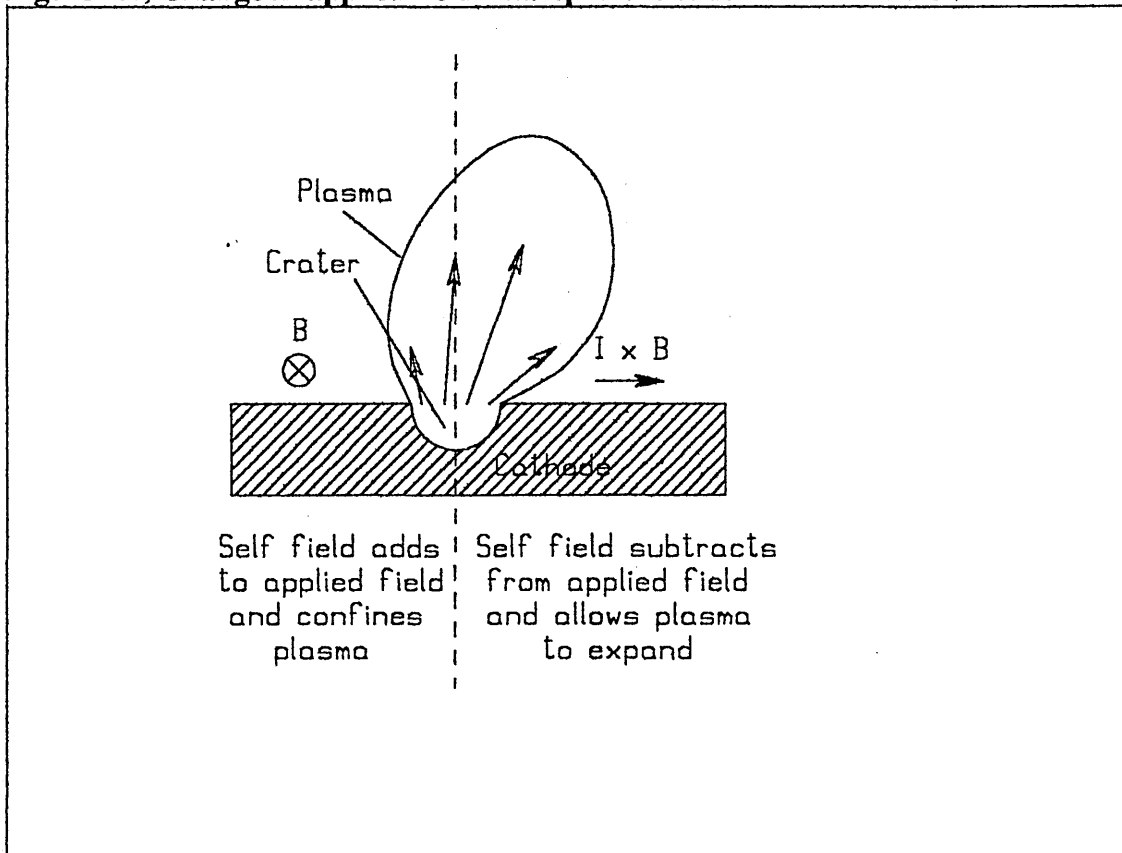


Figure 3.5, Asymmetric confinement of the spot after Ref. 20.

3.3.2 Movement of the space charge.

Several models use the movement of the positive space charge above the cathode surface as the reason behind retrograde motion. Harris [22] models the cathode spot as a collection of cells (see Figure 3.6) which are described as disc shaped areas of plasma that hover a short distance above the cathode surface. The substructure of the spot is held in equilibrium by opposing electrostatic and magnetic forces between each cell, i.e. treating each cells as a set of parallel dipoles there exists an electrostatic repulsive between the dipoles proportional to r^{-4} (where r is the distance between the dipoles), this is opposed by the attractive magnetic force produced when considering each cell as a current carrying element, this attractive force is proportional to the current carried by each segment, the length of the segment and to r^{-2} .

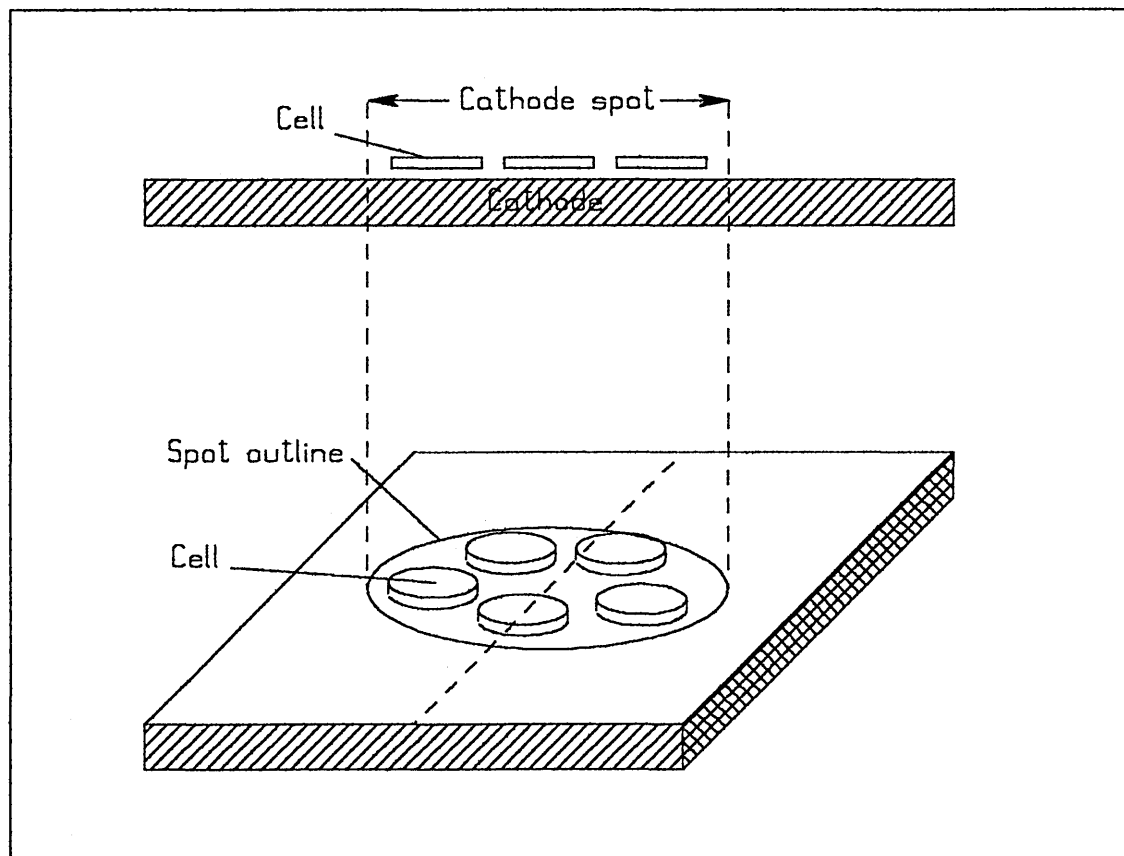


Figure 3.6, The spot considered as a group of cells after Ref. 22.

The discs are assumed to be comprised of two regions (see Figure 3.7) a negative space charge that lies close to the cathode surface and the positive space charge lying further out. The effect of applying an external field to the discs is for the Lorentz force to cause a shift in the position of the electron cloud relative to the position of the positive space charge, but without a shift in the locus of electron emission. This leads to the exposing of the retrograde side of the positive space charge which enhances the electron emission in the area where the electron cloud has receded and the suppression of electron emission at the prograde side of the spot where the electron cloud has advanced. The net effect produced is a re-balancing of the cell and a shift in the main locus of electron emission, i.e. the spot, to the retrograde side. Harris uses his model to calculate values for spot size and energies of formation that agree well with experiment.

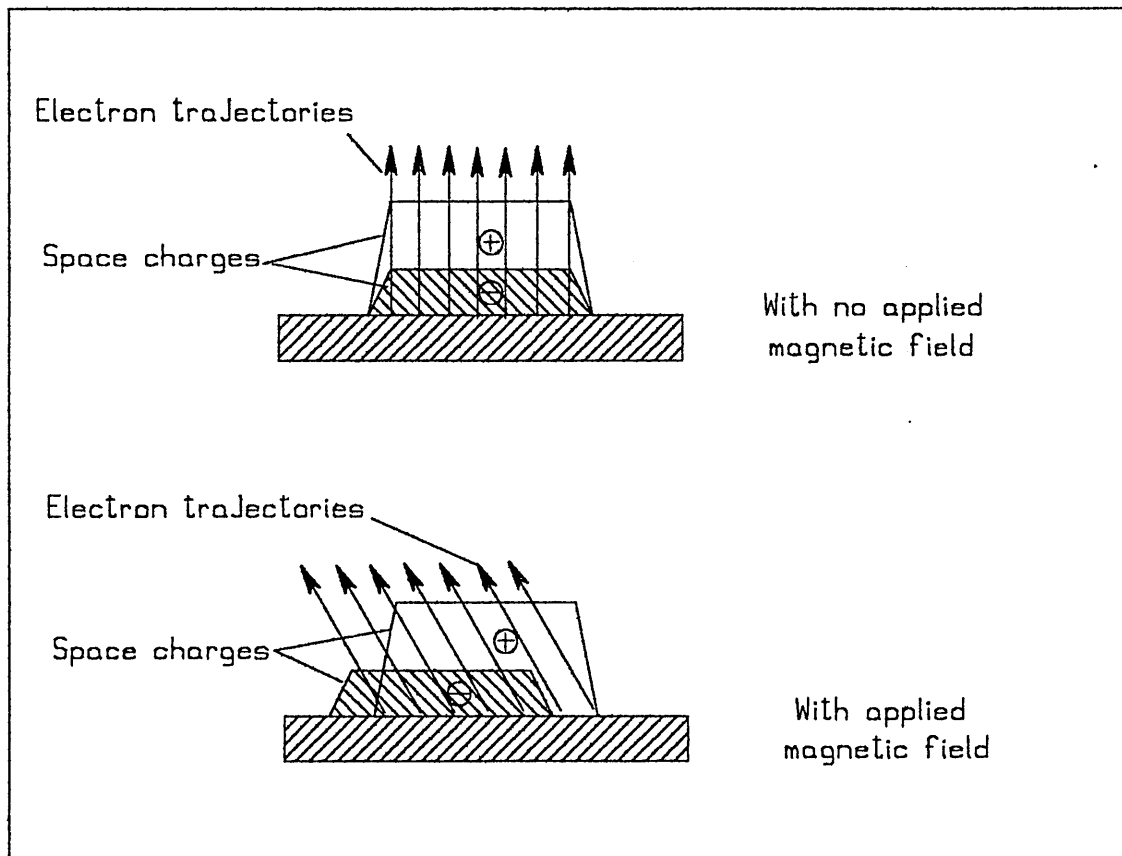


Figure 3.7, The movement of the space charge after Ref. 22.

3.3.3 Movement of the spot plasma.

The movement of the spot may be explained in terms of the spot plasma which bombards the surface with ions and thus heats it to favourable conditions for spot ignition. Nevskii [23] explains spot motion by considering the ions that are, in the absence of a magnetic field, assumed to be swept away with the vapour stream. The application of a field will cause the ions to move under the influence of a Lorentz force along a circular trajectory until a collision occurs. If the collision occurs at the first half revolution, then the ion will transfer its momentum to the spot plasma in the direction opposite to the Amperian force. The stream of ions from the cathode spot should give rise to a body force in the retrograde direction (see Figure 3.8). Expressions are derived for the velocity of the spot as a function of magnetic field and pressure which agree well with experiment. Additionally the mechanism of direction reversal is examined and a value calculated for the pressure at which the arc motion changes from prograde to retrograde, this also agrees well with the experimental value.

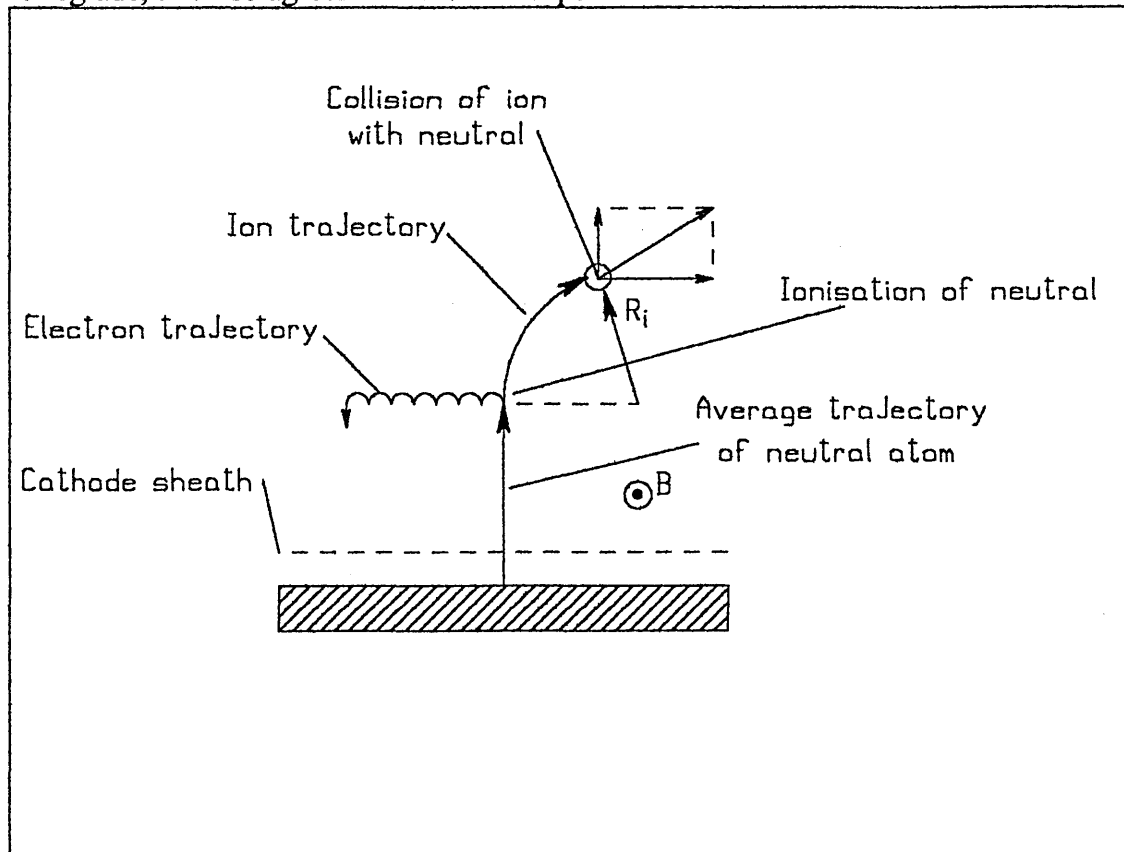


Figure 3.8, The transfer of momentum from ions to the spot plasma after Ref. 23.

3.3.4. Bending of the plasma column.

Three models regard the arc as a flexible plasma column that is fixed at one end (the spot) but free to flex along its length (see Figure 3.9).

Perhaps the first model to examine arc motion with regard to the arc column was that of Robson and von Engel [27]. In this instance the arc column is assumed to be deflected in the Lorentzian direction and be strongly curved in the vicinity of the cathode. The force then acting upon the cathode spot is the sum of the applied field and the self field generated by the curved current carrying element shown on Figure 3.10. Retrograde motion occurs if the self field exceeds the applied field, this is feasible only if the spot dimensions are small enough to give high enough self fields, in the light of recent experimental work investigating the sub structure of the spot this would seem to be the case (see Section 2.3).

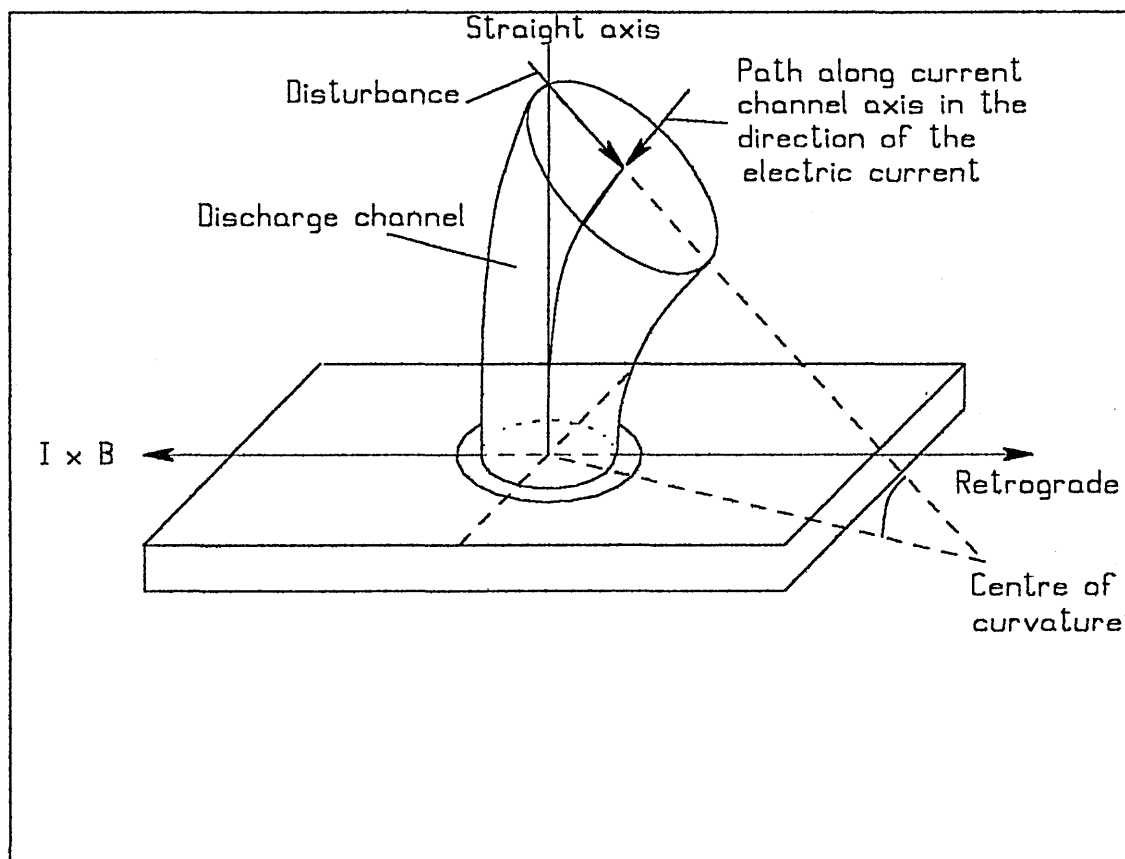


Figure 3.9, The plasma stream fixed at the spot but free to move after Ref. 24.

This model explains some interesting features of spot motion. Robson motion of the arc is the tendency of the arc to drift away from the true direction of retrograde motion when the applied magnetic field is non-parallel to the cathode surface [26]. This is explained in terms of the existence of a current component flowing parallel to the cathode surface giving rise to a force perpendicular to the retrograde direction. The absence of retrograde motion when observing a purely thermionic arc is to be expected as the current densities are much smaller in these cases. But perhaps the most interesting observation is effect on the arc velocity of decreasing the electrode separation, this will tend to force the arc column on to the cathode therefore decreasing the radius of curvature of the arc and increasing the retrograde velocity. This is increase in arc velocity with decreasing electrode separation is observed to occur experimentally.

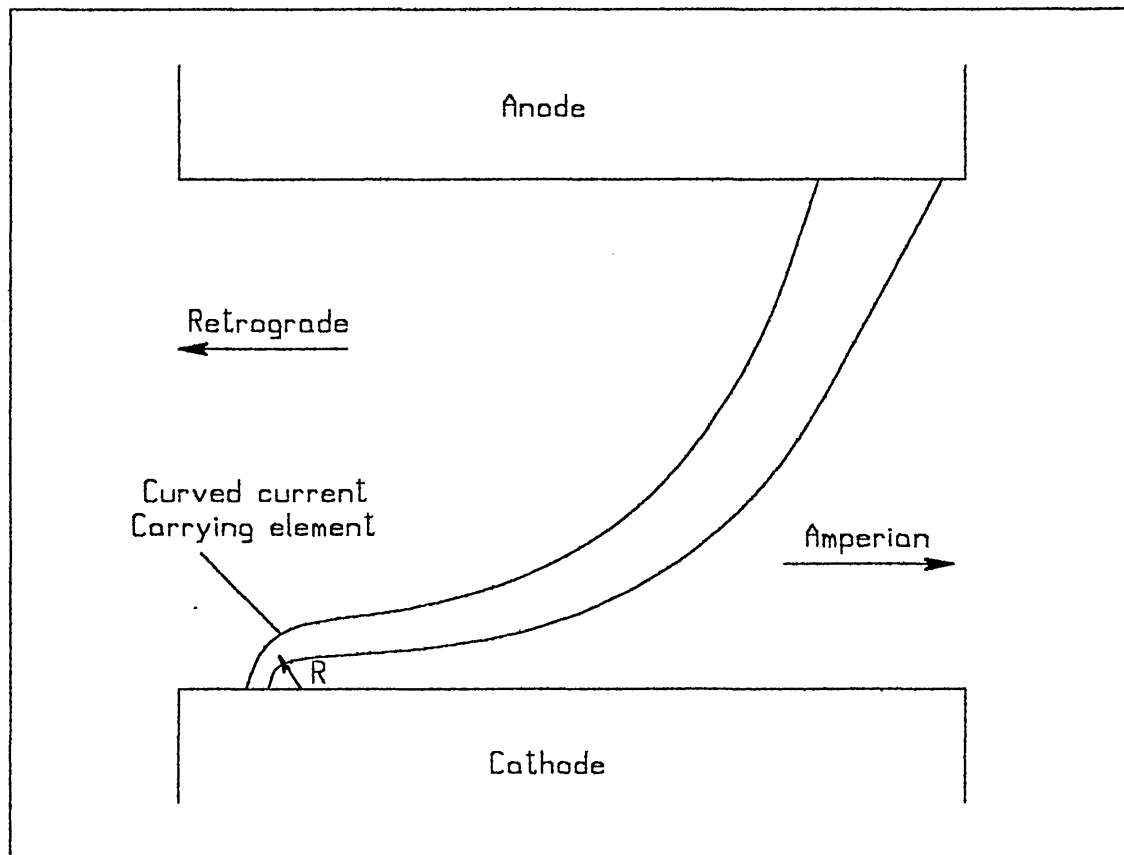


Figure 3.10, the plasma stream showing a current carrying element after Ref. 27.

The model of Hong and Allen [25], is based upon that of Robson and von Engel described above. It uses electrodynamic theory to describe the arc column and views the resultant force upon the spot as the sum of forces in the retrograde and Lorentzian directions. The arc column bends in the Lorentzian direction under the influence of an applied magnetic field, this has two main effects; firstly to produce a force on the arc column in the Lorentzian direction and secondly to distort the current density across the spot. The distortion of the current density profile gives rise to a force in the retrograde direction, the greater the applied field the more severely the column is bent and the greater the magnitude of the retrograde force. A limit is reached at which the column will bend no more and further increases in the applied field serve only to increase the force in the Lorentzian direction. This happens until both forces are balanced and any further increase in field results in Lorentzian motion.

This model qualitatively explains a number of features of arc motion including the temperature dependence of arc velocity, the pressure dependence of arc velocity and the material and surface condition dependence of arc motion. Also discussed is the importance of the current density at the spot, using this model retrograde motion is only predicted with current densities of the order of 10^{12} Am⁻², this value is at the upper end of experimentally observed magnitudes for current density.

Finally a model proposed by Schrade [24] calculates the force per unit length acting upon a current carrying channel due to self and applied magnetic fields and comes to several interesting conclusions. In the first instance, the resultant force upon a straight column is zero, all forces being balanced, however if there is a small disturbance of the column resulting in it being bent then the resultant force becomes non-zero. In the case that the resultant force is in the opposite direction to the disturbance then the channel is driven back to its original position and becomes stable again. Alternatively, if the force is in the direction of the perturbation then the column is driven down into contact with the cathode surface, heating the surface there and creating a new spot and extinguishing the old. In the case of an applied magnetic field the conditions for instability in the column

are more favourable in the retrograde direction and new spots are more likely to be created in this direction.

This model also qualitatively explains Robson drift [26] in terms of the direction of the force resultant from the inclined field. This force reinforces a perturbation in the column not in the true retrograde direction but at a slight angle to it, giving rise to motion in this direction.

3.3.5 A stochastic model of steered arc motion.

The final model for arc motion described in this chapter is that of Care [19]. As mentioned previously special attention will be paid to this model as later experimental work attempts to determine some parameters defined by it (see Chapter 5).

The cathode spot is considered as moving on a two dimensional surface and confined to the vertices of a grid upon this surface . The 'forces' acting upon the spot arise from the two components of the applied magnetic field, the normal field component B_N and the transverse field component B_T . It is these components and their effect on spot motion that will be the subject of Chapter 5. The arc moves with a velocity proportional (approximately) to the transverse field component in the retrograde direction, and is confined to move near to the normal component zero (see section 4.1). This second observation is attributed to a restoring "force" which depends upon the normal field component and also the velocity of the arc (and hence the transverse component).

In the geometry chosen the driving field B_T is assumed to act in the x direction and is independent of x and y . The confining field B_N is assumed to independent of y but dependent upon x . The field is chosen to have normal component zero along the line $x=0$. The arc is considered initially to lie at time step s on one of the vertices of a two dimensional square grid (i,j) , where i, j and s are integers.

The probabilities of moving in any direction from this point are now defined; $P^{(2)}$ and $P^{(4)}$ are defined as the probabilities of retrograde and prograde motion respectively and $P^{(1)}$ and $P^{(3)}$ are defined as motion away from the $x=0$ line in the positive and negative direction respectively. To produce motion in the retrograde direction $P^{(2)}$ and $P^{(4)}$ are

assumed to be unequal. To give a confining effect of the spot to $x=0$, $(P^{(1)}-P^{(3)})$ is assumed to be linearly dependent upon i , i.e. the further way from $x=0$ the spot moves the more likely it is to move towards $x=0$.

Using the model described above a Fokker-Planck equation is derived describing the time dependent probability density of the spot position,

$$\frac{\partial \phi}{\partial t} = \left[D_y \frac{\partial^2 \phi}{\partial y^2} + D_x \frac{\partial^2 \phi}{\partial x^2} \right] + \left[c \frac{\partial \phi}{\partial y} \right] + \left[f(x) \frac{\partial \phi}{\partial x} + \frac{\partial f}{\partial x} \phi \right] \quad (3.19)$$

Term (1) Term (2) Term (3)

Where $\phi(x, y, t)$ is the probability density for the arc position and,

$$\begin{aligned} D_y &= a(P^{(2)} + P^{(4)}) & D_x &= a(P^{(1)} + P^{(3)}) \\ c &= b(P^{(4)} - P^{(2)}) & f(x) &= b(P^{(3)} - P^{(1)}) \end{aligned} \quad (3.20)$$

Examining Equation 3.19 above a physical interpretation may be made as follows. If no magnetic field is present then the terms c and $f(x)$ go to zero and only term (1) of the equation is left, i.e. the arc diffuses out from its starting position at a rate governed by the diffusion coefficients D_x and D_y . If the transverse component of a magnetic field, B_T is applied then the variable c in term (2) becomes non-zero, this has the effect of driving the arc along the y axis with a mean velocity c with the random diffusive motion of the spot superimposed upon this mean velocity. Introducing the normal field component, B_N the function $f(x)$ in term (3) becomes non-zero, this is interpreted as inducing a velocity which tends to restore the spot to the $x=0$, i.e. the spot is confined to the normal field zero by the normal field component.

Assumptions described above are now quantified. The velocity c is made directly proportional to the transverse field component B_T , this is approximately true over certain ranges of transverse field [43]. The confinement function $f(x)$ is made proportional to

3.4 Summary.

The field of arc modelling covers such a large vista of types of model, aspects of the arc to model and inputs to the model that is often difficult place any review of these models in perspective. It is the purpose of this summary to briefly list the models reviewed in this chapter and to place them in context with the remainder of the thesis. Although some may not be directly relevant to later work they do provide important background detail and give some indication of the diversity of problems and possible solutions associated with modelling this phenomenon.

Initially reviewed in this chapter were the thermal inputs to a great many spot models. Although not many models use all of these inputs, indeed many use only one or two, it is important to consider them as fundamental processes occurring at the spot to a lesser or greater extent. As is seen later in the chapter the relative importance of some of these inputs is the subject of lively debate.

The second part of the chapter is dedicated to models of the random arc, these were, in order;

(i) Computer based simulations of the spot as a hemispherical crater.

These models attempted to produce computer based, time dependent, numerical solutions of the evolution of a number of spot parameters.

(ii) Ionic bombardment and Joule heating models.

Both of these models regarded the spot as a hemispherical crater heated by one main energy source. As the names suggest the ionic bombardment model regarded the primary energy source as ionic bombardment and Joule heating of relatively little importance. Conversely the Joule heating model thought ionic bombardment as a secondary effect and Joule heating as the main source of energy.

(iii) The conical protrusion model.

This model concentrated upon a regular cone as a surface feature on the cathode. The only source of energy used was Joule heating. This model demonstrated the preferential erosion rates given by eroding a conical structure in an attempt to explain the arc's preference for surface features.

(iv) Models of the spot as a random walk.

These models modelled the spot motion as stochastic process. Through these models the important concept of a spot diffusion coefficient is introduced in parallel to experimental work presented in Chapter 2.

Each of these models aims to examine a different aspect of spot behaviour. Whilst perhaps the most complete and self consistent of them are the computer based solutions, the other models all note and attempt to describe one or two observations of the spot's behaviour. In most cases with a high degree of success.

The third and final part of the chapter deals with models of the magnetically steered spot. Unlike the previous section this one has the common theme that all the models' (except the last) primary function is to explain the retrograde motion of the spot. The models are, in order.

(i) Asymmetric confinement of the spot plasma.

Here the retrograde motion is explained by a combination of self and applied fields combining favourably on the retrograde side of the spot to confine the plasma and subtracting on the prograde side of the spot to produce a diffuse plasma.

(ii) Movement of the space charge.

Several authors use the movement of the space charge to explain retrograde motion. The magnetic field causes a deviation in the path of emitted electrons leading to an

exposed positive space charge. The rebalancing of the charges causes a net motion of the spot in the retrograde direction.

(iii) Movement of the spot plasma.

The applied field will cause ions to move in a circular radius. If the ions collide with particles in the plasma before one half revolution the a net force in the retrograde direction will be imparted to the plasma. New spot ignition is more likely to occur, therefore on the retrograde side of the spot.

(iv) Bending of the plasma column.

Several authors consider the plasma column as fixed at the spot end but free to flex along its length. This column though normally stable can be bent to such an extreme by the application of a magnetic field that it may contact the cathode on the retrograde side of the spot causing new spot ignition there.

(v) A stochastic model of the arc.

This model does not attempt to explain the retrograde motion of the spot. Rather it uses empirically derived constraints upon the spot motion to derive a time dependent probability density plot of the spot's position. The constraints upon the spot motion are dependent upon the applied normal field gradient and transverse field component.

Again this section attempts to demonstrate the diversity of spot models. Although most share a common aim there are many reasons offered to explain the phenomenon of retrograde motion and all require more detailed empirical evidence to confirm or disprove them. As has been discussed in Chapter 2 empirical evidence of spot behaviour is difficult to obtain at a microscopic level. However a number of experiments may be conducted to test the validity of Care's model. This work is the subject of the remainder of this thesis.

References.

- [1] J. Prock,
IEEE Trans. on Plasma Science, **PS14**(4), 482, (1986).
- [2] J. Mitterauer, P. Till,
IEEE Trans. on Plasma Science, **PS15**, 488, (1987).
- [3] P. Till, M. Haider, J. Mitterauer in,
"Progress in cybernetics and systems research"
(Eds. R. Trappel, F.D.P. Hanika, R. Thomlinson), Washington D.C., Hemisphere
10, 435, (1982).
- [4] B. Jüttner,
Beitr. Plasma Phys., **19**, 25, (1979).
- [5] D.Y. Fang,
J. Phys. D Appl. Phys., **15**, 833, (1982).
- [6] D.Y. Fang,
IEEE Trans. on Plasma Science, **PS11**(3), 110, (1983).
- [7] C.W. Kimblin,
J Appl. Phys., **44**(7), 3074, (1973).
- [8] B Jüttner,
Beitr. Plasma Phys., **22**, 453, (1982).
- [9] E. Hantzsche,
IEEE Trans. on Plasma Science, **PS11**(3), 115, (1983).
- [10] G. Ecker in,
"Vacuum arcs, Theory and application.", J.M. Lafferty-Editor,
Wiley-Interscience, 1980.
- [11] F.M. Charbonnier, R.W. Struger, L.W. Swanson, E.E. Martin,
Phys. Rev. Lett., **13**, 397, (1964).

- [12] L.A. Sena, L.I. Pranevychius, G.N. Fursey,
Proc. Tenth Int. Conf. Phen. Ioniz. Gases, Oxford, C.P. 105, (1971).
- [13] S. Anders, B. Jüttner,
IEEE Trans. on Plasma Science, (5), 705, (1991).
- [14] E. Hantzsche,
Beitr. Plasma Phys., **22**, 325, (1982).
- [15] E. Hantzsche, Zeszyty Naukowe Politechniki Poznanskiej,
Elektryka, **29**, 79, (1985).
- [16] A.I. Bushik, B. Jüttner, H. Pursch,
Beitr. Plasma Phys., **19**, 177, (1979).
- [17] B.E. Djakov, R. Holmes,
J. Phys. D Appl. Phys., **7**, 569, (1974)
- [18] Y.H. Fu,
J. Phys. D Appl. Phys., **22**, 94, (1989).
- [19] C.M. Care,
J Phys. D Appl. Phys., **25**(12), 1841, (1992).
- [20] M.G. Drouet,
Jap. J. Appl. Phys., **20**(6), 1027, (1981).
- [21] I.G. Kesaev in,
"Cathode processes in the mercury arc", Consultants Bureau, New York, (1964).
- [22] L.P. Harris,
Proc. Tenth Int. Symp. on Disch. and Insul. in Vacuum, 106, (1981)
- [23] A.P. Nevskii,
Sov. Phys. Tech. Phys., **14**(6), 803, (1969).
- [24] H.O. Schrade,
IEEE Trans. on Plasma Science, **17**(5), 635, (1989).
- [25] J.S. Hong, J.E. Allen,
Europhysics conference abstracts, **1GC**(3), 2033, (1992).

- [26] A.E. Robson,
J. Phys. D Appl. Phys., **11**, 1917, (1978)
- [27] A.E. Robson, A. von Engel,
Phys. Rev., **93a**, 653, (1954).
- [28] B.E. Djakov, R. Holmes,
Proc. First Int. Conf. on Gas Discharges, London, 468, (1970.)
- [29] I.G. Kesaev in,
"Cathode processes in the electric arc", Nauka-Moscow, (1968).
- [30] R.L. Boxman, S. Goldsmith, I. Izraeli, S. Shalev,
IEEE Trans. on Plasma Science, **PS11(3)**, 138, (1983).
- [31] I.I. Beilis, G.V. Levchenko, V.S. Potkin, V.I. Rakhovskii, I.N. Rykalin
Fizika i Himia Orabotki Metalov, **3**, 19, (1966).
- [32] B. Jüttner
J. Phys D Appl. Phys., **14**, 1265, (1981)
- [33] J. Daalder,
J. Phys. D Appl. Phys., **11**, 1667, (1978).
- [34] E.A. Litvinov, G.A. Mesyats, A.A. Starobinets,
8th Int. Symp. on Disch. and Insul. in Vacuum, Albuquerque, **D3-1**, (1978).
- [35] G.W. McClure,
J. Appl. Phys., **45**, 2078, (1974).
- [36] E. Hantzsche,
Beitr. Plasma Phys., **17**, 65, (1977)
- [37] E. Hantzsche, B. Jüttner, H. Pursch,
J. Phys. D Appl. Phys., **16**, L173, (1983).
- [38] J.E. Daalder,
J. Phys. D Appl. Phys., **16**, L177, (1983).
- [39] J.E. Daalder,
J. Phys. D Appl. Phys., **16**, 17, (1983).

- [40] J.E. Daalder,
PhD Thesis, Eindhoven University of Technology, 66, (1978).
- [41] S. Chandrasekhar,
Rev. Mod. Phys., **15**, 1, (1943)
- [42] J.E. Daalder,
J. Phys. D Appl. Phys., **10**, 2225, (1977).
- [43] P.D. Swift, D.R. Mckenzie, I.S. Falconer, P.J. Martin,
J. Appl. Phys., **66**(2), (1989).

Chapter Four

The design of the steered arc system

This chapter describes the design and construction of an experimental steered arc system that was used to perform experimental work discussed in Chapter 5. The system consists of two major components; a vacuum chamber and associated pumping system and an array of electromagnetic arc steering coils. The system was designed with two objectives in mind, these are discussed individually below.

(i) Earlier steered arc systems, as described in Chapter 1, have limited control of the arc's position and confinement. This has two consequences. Firstly, the arc covers a limited amount of the cathode surface, approximately 40% in the case of the Interatom machine (calculated from photographs of the machine in operation). This is costly in terms of materials and engineering time particularly when coating processes are scaled up to a commercial level. Secondly, poor arc confinement can lead to complete loss of control of the arc spot (especially at junctions between dissimilar metals on multi-part cathodes [1]). This may cause periods of random arcing leading to increased macro-particle emission and an inferior coating [2]. The novel design of steering system proposed here, which uses a pair of electromagnetic coils, hopes to alleviate some of the problems associated with steered arc systems. This is achieved in two ways; the arc is steered upon a path of continuously variable radius and the magnitude of the confining and driving elements of the magnetic field [3] are controllable independently of the radius of the arc path. Control of the arc radius theoretically allows usage of the entire cathode surface: on a commercial scale this would have the advantages of increasing cathode usage and so reduce machine down time. Additionally problems of intense cathode heating at points of extreme erosion would be avoided. Control of the driving and confining field components allows greater positional control of the arc spot and reduces the likelihood of loss of control of the spot.

(ii) The model developed by Care [3], which is described in detail in Section 3.3.5, describes the motion of the cathode spot in terms of a biased stochastic process. The level of bias within the model depends in turn upon the magnitudes of the transverse and normal magnetic field components (the driving and confining fields). As mentioned above the magnitudes of these components are controllable with the system described in this chapter (although not independently). This enables several experiments to be conducted to test the validity of Care's model. These experiments are described and the results analysed in Chapter 5.

The following chapter is divided into two parts; the first describes the modelling, design and construction of the electromagnetic coil array, the second the design and construction of the vacuum chamber and associated systems.

4.1 The electromagnetic steering array.

4.1.1 Confinement of the cathode spot.

Work by Swift et al [4, 5] demonstrated experimentally that the spot of a cathodic arc sits preferentially at the point on the cathode where the component of the magnetic field normal to the surface is zero. Figure 4.1 shows the positional dependence of the normal and transverse field components across a diameter of a circular cathode and coil. The position of the cathode spot is indicated by the erosion shown upon the cathode surface.

The motion of the spot along this trajectory is hypothesised to be due to the action of a restoring force F , provided by the magnetic field B , and acting upon the positive space charge, $+q$. As Swift et al. note, the existence of the space charge, $+q$, (through which a current of j passes) is confirmed experimentally and several models have been proposed to explain its existence (see Section 2.1). The velocity of the spot is then given by¹,

$$\mathbf{v} \sim -\mathbf{j} \wedge \mathbf{B} \quad (4.1)$$

This leads to a force on q , F , where,

$$\mathbf{F} \sim \mathbf{v} \wedge \mathbf{B} \quad (4.2)$$

And so from the triple vector product identity,

$$\mathbf{F} \sim q \left[|\mathbf{B}|^2 \mathbf{j} - (\mathbf{B} \cdot \mathbf{j}) \mathbf{B} \right] \quad (4.3)$$

¹ The negative sign of this proportionality indicates the retrograde motion of the spot and is introduced on an empirical basis, i.e. Swift et al do not attempt to construct a theoretical model that leads to Equation 4.1.

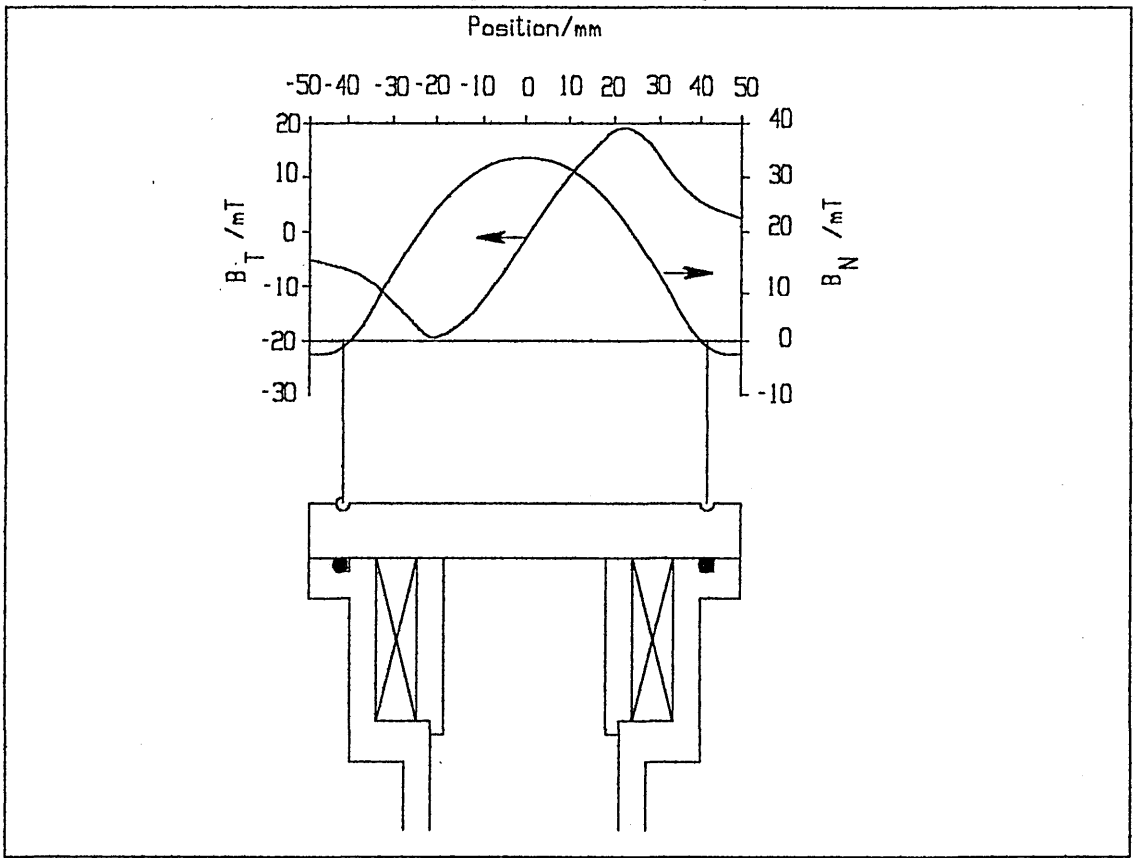


Figure 4.1, Profiles of the magnetic field components from a single coil after Ref. 4.

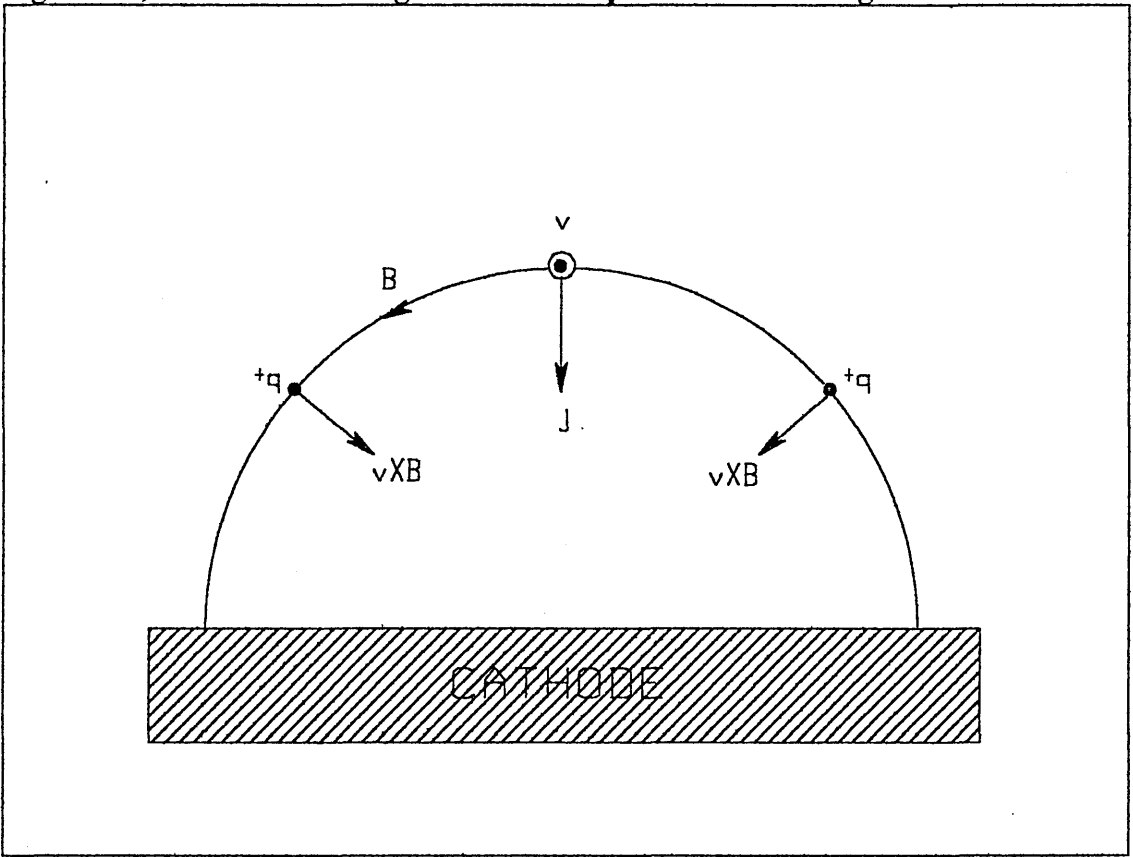


Figure 4.2, The restoring force acting upon the positive space charge after Ref. 4.

Examining Figure 4.2 it can be seen that the force on the charge q acts to restore the space charge to the position of the normal field zero. As the space charge is the source of ions providing one major source of heating at the spot (see Sections 3.1 and 3.2) then it seems reasonable to assume that the cathode spot will follow the movement of the space charge.

Previously, when permanent or electromagnets have been used to steer an arc, figures are usually quoted for the peak strength of the normal field component as a measure of the level of arc control [4, 5, 6]. Indeed Swift [5] notes that whilst the space charge is most likely to be found at the locus of the normal field zero it does in fact deviate some distance either side of it, the magnitude of these deviations decreasing with increasing normal field strength. But the normal field strength at a point is approximately equal to the normal field gradient multiplied by the deviation from the radius normal zero.

Following Swift's reasoning: the magnitude of the restoring force to the zero rises more rapidly with distance from the zero the steeper the normal field gradient. This dependence of confinement upon normal field gradient is an essential feature of the model by Care [3].

These observations provide the basis for the design of the steering system described in the following section.

4.1.2 A two coil steering system.

Using a single coil, as shown in Figure 4.1, the normal zero, on a fixed plane perpendicular to the axis of the coil, defines a circular path of fixed radius. Altering the current to the coil merely serves to scale the magnitude of the generated field, and hence field gradient, without altering its geometry in the plane of interest. An alteration in the range between the plane of interest and the coil does produce a change in the radius of the normal field zero. However, attempting to control the arc by this method would result in weak confining fields at large coil ranges, with probable loss of arc control.

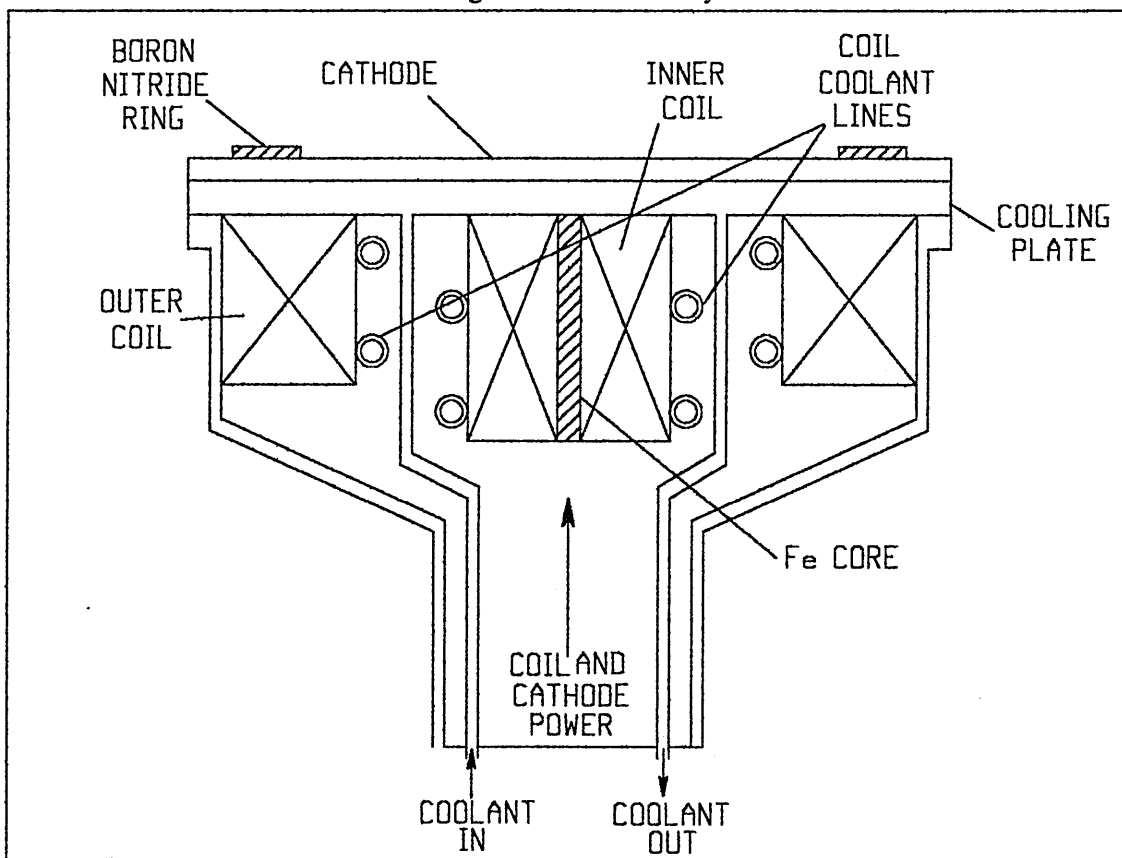


Figure 4.3, Schematic diagram of coil assembly.

A novel steering system is proposed here using two or more concentric coils, see Figure 4.3. By varying the relative currents to these coils it is theoretically possible to move the normal component zero to virtually any point on the radius of the cathode whilst controlling the magnitudes of the normal (and hence normal field gradient) and transverse field components at the zero.

Examining Figures 4.4 and 4.5 (which are plotted using data obtained as described in Section 4.1.3) it can be seen that a coil that is long and thin (with respect to the cathode to coil range) produces a bell shaped profile for the normal field component with zeros occurring at a point where the normal field gradient is almost at its minimum. A shorter wider coil, however, gives an almost flat profile for most of the curve falling sharply to zero at a point just outside the radius of the coil.

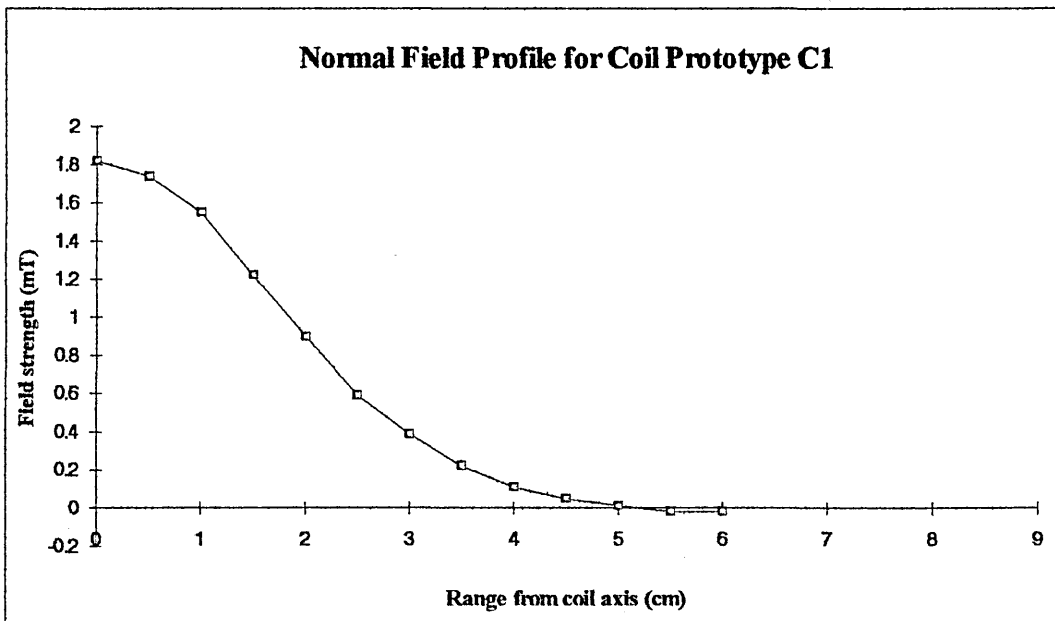


Figure 4.4, Normal field profile of long, thin coil without iron core.

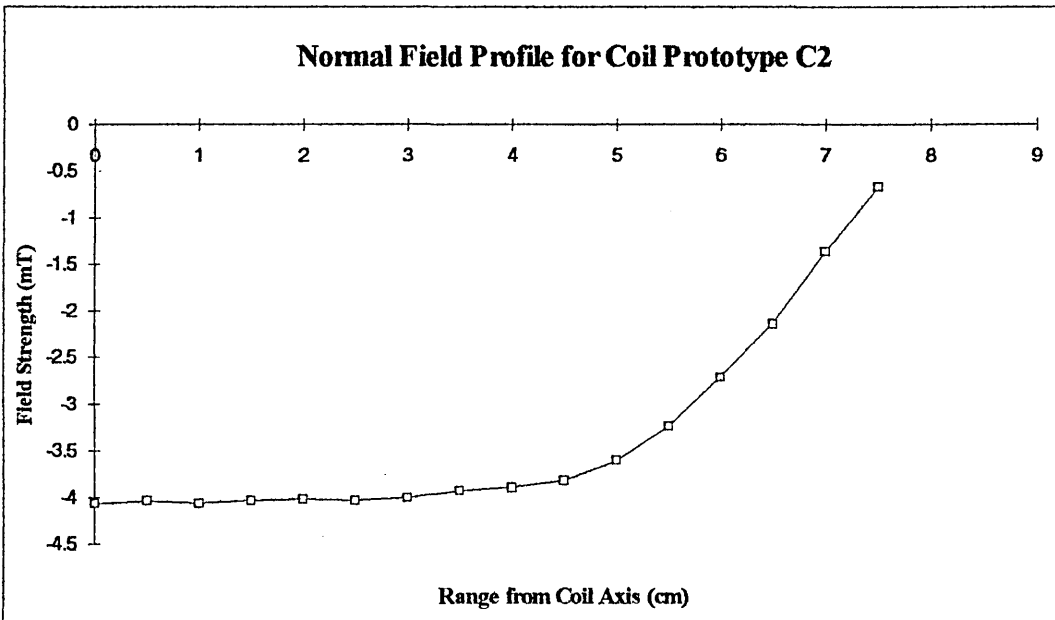


Figure 4.5, Normal field profile of short, wide coil without soft iron core.

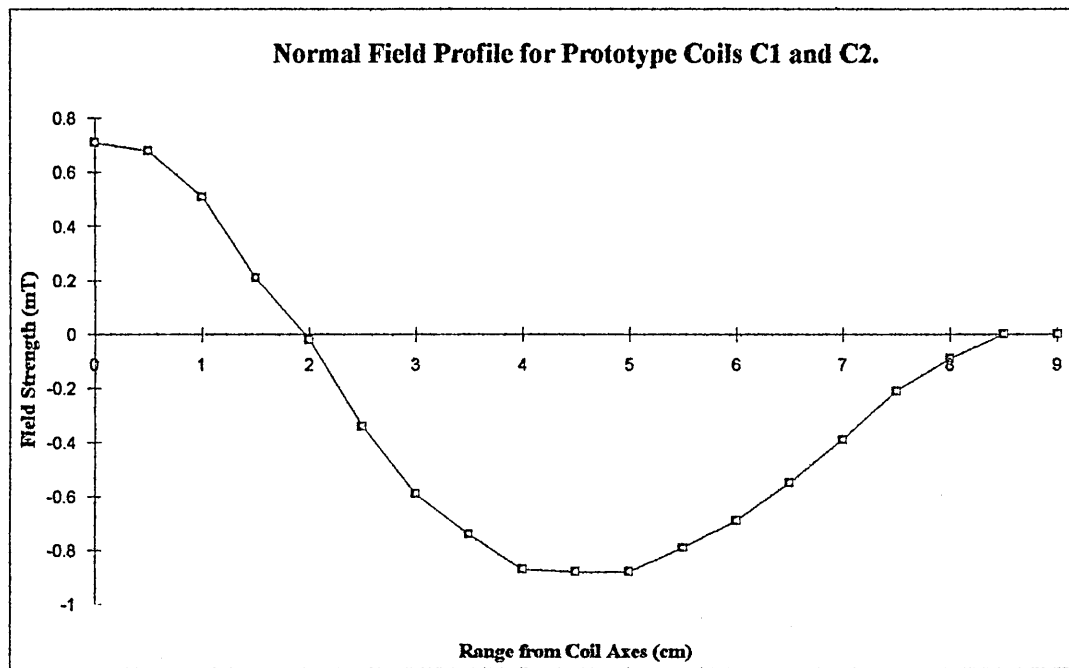


Figure 4.6, Using a reverse biased outer coil to shift the normal component zero.

Assuming, then, that the narrower inner coil has a current applied to it to give a positive field, of the shape described above, at the cathode surface. A current of the opposite polarity may be applied to the outer coil which will, when superimposed on the inner coil profile, produce a negative shift in it (see Figure 4.6). By the correct choice of the ratio of inner and outer coil currents the inner coil profile may be shifted and the normal zero located where required. This has the additional advantage that in most cases the zero is moved to a point where the normal field gradient is much steeper than that produced by an equivalent single coil.

To ensure that steering coils were of the correct geometry it was decided to model the fields for a system of two or more coils. This enabled various designs of coils to be tested before construction. Key factors were the ability to achieve the required control over the normal zero position, the normal field, the transverse field components and to fit into the limited space available.

To model the fields two computer programs were written, both attempting to predict transverse and normal field components and zero crossing points of the field. The first of

these was based upon the dipole approximation of a coil and the second used the Biot-Savart equation describing the field produced by a current carrying element. It soon became apparent that at the coil to cathode distances of interest, a sufficiently accurate model must be able to describe the near field geometry. The description of a coil as a dipole is a far field approximation and was consequently rejected. Conversely, the Biot-Savart equation described the field profiles from a system of two coils with great accuracy and was initially employed to design the coil array.

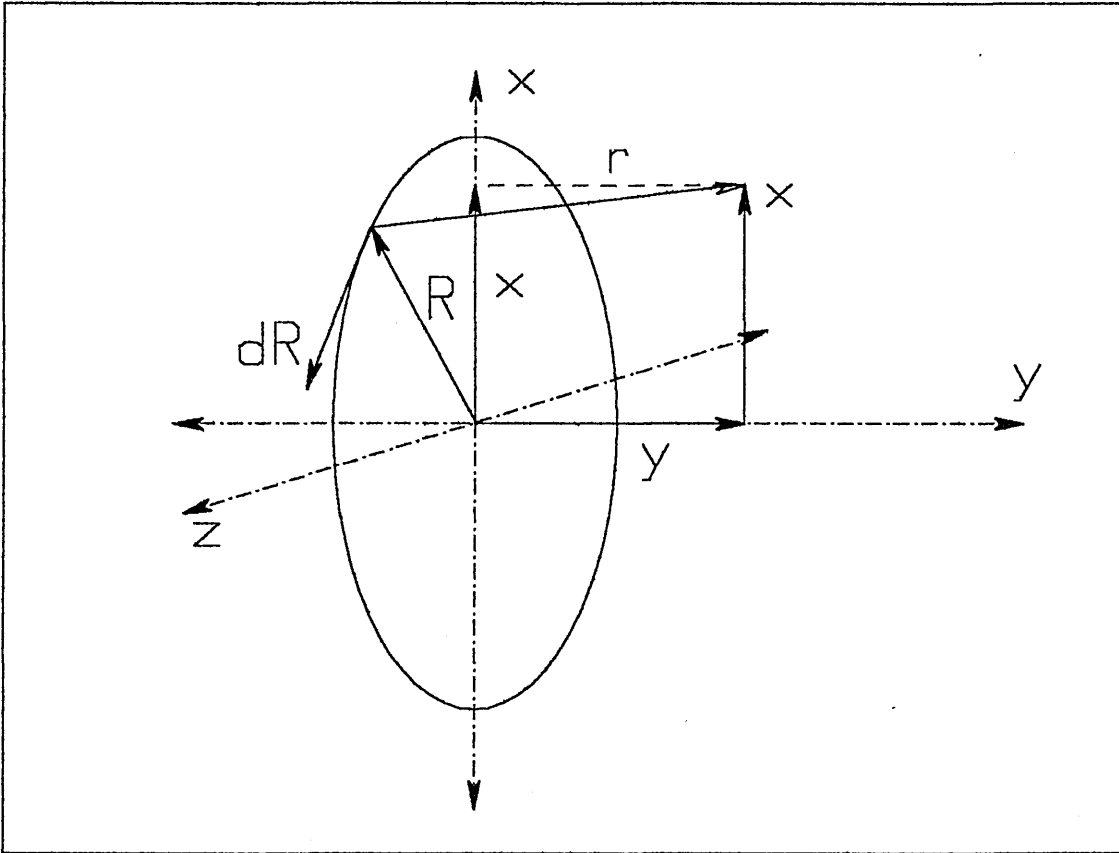


Figure 4.7, The geometry used by Higbie [7] to model a current carrying loop.

4.1.3 Modelling of the coil fields.

Higbie [7], using the geometry shown in Figure 4.7, derives an expression for the y component of the magnetic field from a current loop for any off axis point. Following his methodology a similar expression is derived below for the x component (see Appendix I). It is interesting to note that distances are expressed in terms of a ratio with the radius of the current carrying loop. This allows the field profile for a reference coil to be calculated at a number of ranges, stored as a look up table and scaled to give the field shapes for any coil.

The resulting equations are

$$dB_x = \frac{m}{R} \frac{\delta \cos\theta}{(\rho^2 + \delta^2 + 1 - 2\rho\cos\theta)^{3/2}} d\theta \quad (4.4)$$

And,

$$dB_y = \frac{m}{R} \frac{(1 - \rho\cos\theta)}{(\rho^2 + \delta^2 + 1 - 2\rho\cos\theta)^{3/2}} d\theta \quad (4.5)$$

Where dB_x and dB_y are the magnetic field components in the x and y directions respectively,

$$m = \frac{\mu_0 NI}{4\pi} \quad (4.6)$$

and,

$$\delta = \frac{x}{R} \quad \text{and} \quad \rho = \frac{y}{R} \quad (4.7)$$

The total field components may then be found by performing the following summations,

$$B_x(\rho, \delta) = \frac{m\Delta\theta}{R} \sum_i \frac{(\delta \cos\theta_i)}{(\rho^2 + \delta^2 + 1 - 2\rho \cos\theta_i)^{3/2}} \quad (4.8)$$

and,

$$B_y(\rho, \delta) = \frac{m\Delta\theta}{R} \sum_i \frac{(1 - \rho \cos\theta_i)}{(\rho^2 + \delta^2 + 1 - 2\rho \cos\theta_i)^{3/2}} \quad (4.9)$$

Where,

$$\theta_i = \frac{\Delta\theta}{2}, \frac{3\Delta\theta}{2}, \frac{5\Delta\theta}{2} \dots \dots \dots 2\pi - \frac{\Delta\theta}{2} \quad (4.10)$$

The size of step to be used for the numerical integrations is dependent upon how well the integration converges. This was examined by performing the calculations with the current loop divided into 10, 20 and 40 arcs: the results in each case for the predicted field strengths were the same to within four figures. A step size of 36° was, therefore, used. A full listing of the program is given in Appendix II.

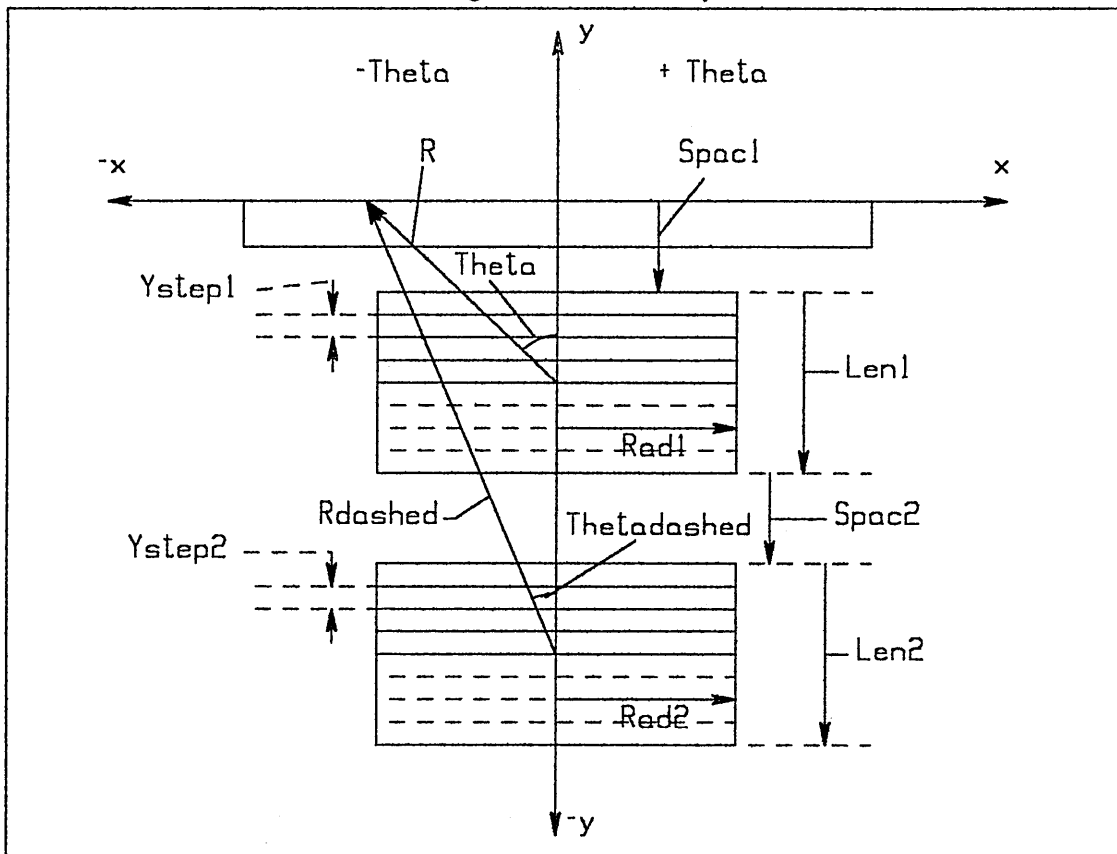


Figure 4.8, The geometry used to model a two coil system.

4.1.4 Testing of the field modelling program.

To test the accuracy of the model described above the normal magnetic field profiles were measured, using a Hall effect Gauss/Tesla meter, across the diameters of several arrangements of single and dual coils with varying ratios of inner and outer coil currents. The results were then compared with those obtained from the model. The details for this, and other experiments described in this chapter are summarised in Appendix III. Examining Figures 4.9 and 4.10 it can be seen that the predicted profiles compare very favourably with experiment for a range of conditions with the important parameters of normal field zero and field gradient at the zero accurately predicted (further comparisons between predicted and experimental profiles are included as Figures AIII.1 and AIII.2 in Appendix III). The Biot-Savart model was therefore initially used to investigate prototype coil design.

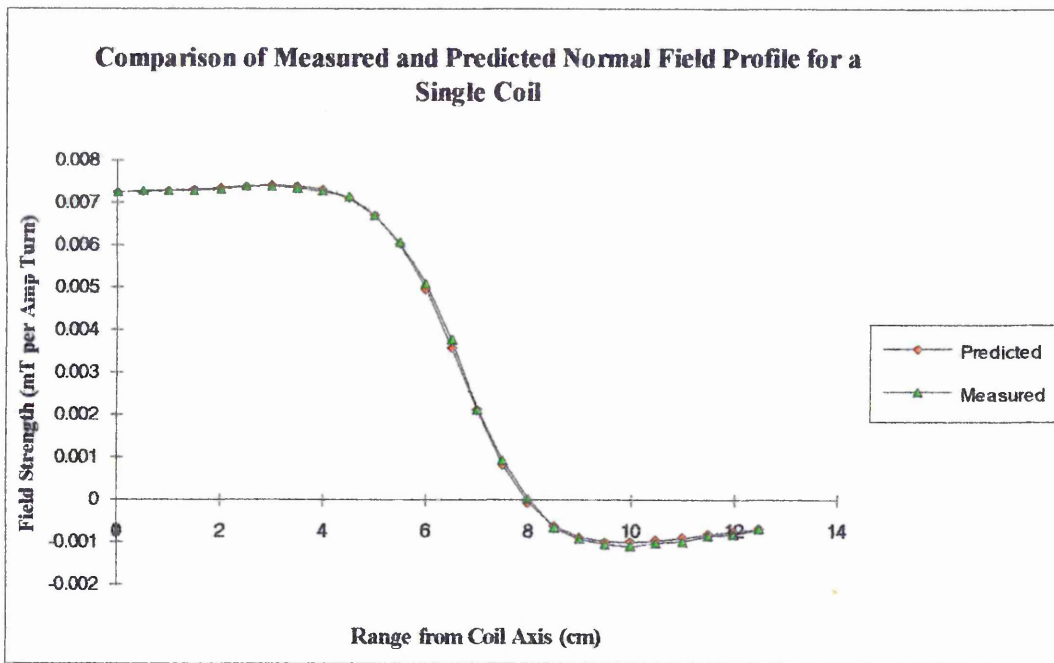


Figure 4.9, Field profiles for a single coil.

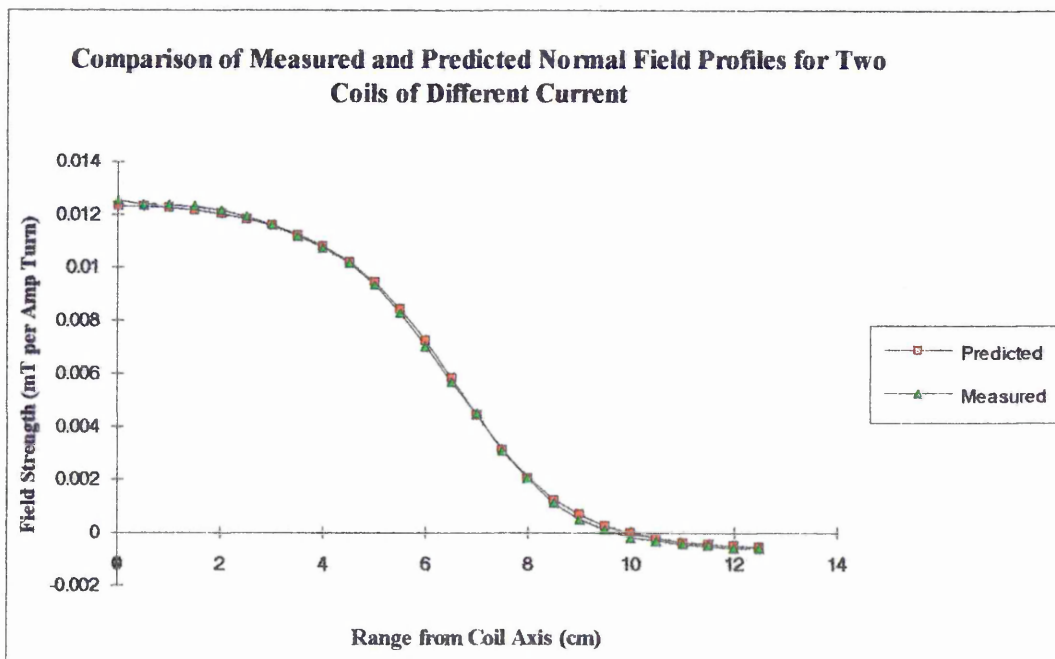


Figure 4.10, Field profiles of two coils carrying different currents.

4.1.5 The design of the coils.

Using the Biot-Savart model various coil configurations were investigated subject to restrictions imposed by the space within the cathode assembly (see Figure 4.3). It soon became apparent that purely electromagnetic coils of a suitable power would not fit into the space available. However the addition of a soft iron core to the centre of the inner coil was found to give an improvement to the normal and transverse field strengths of between four and five times without significantly altering the profile of the normal field component (see Figure 4.11). The use of the core does, however, lead to a distortion of the normal field profile produced by the outer coil (see Figure 4.12) although this does not appear to affect the performance of the assembly as a whole (see Figure 4.13).

The addition of the core, whilst not affecting the principle of the steering system, meant that the Biot-Savart program was no longer able to accurately predict the normal field gradient and zero position. This, however, was not of great significance at this stage of the design: the basic geometry remaining little changed and the increased field strength provided by the core allowing more leeway in the coil operating currents, i.e. the range of operating fields and hence normal field gradients and zero positions were greatly increased by the use of a core.

Control of the arc still required accurate knowledge of the normal field gradient and zero position. These were determined by a semi-empirical method. The field profiles of both prototype coils were measured individually and each profile curve fitted with a polynomial fitting routine. Relative coils currents required to fix the normal field zero at the position required are found by solving the two equations. Absolute coil currents needed to give the required field gradients are found by differentiating the two functions, calculating the gradient at the zero and multiplying the relative coil currents by a constant factor. A computer program was written to perform this task.

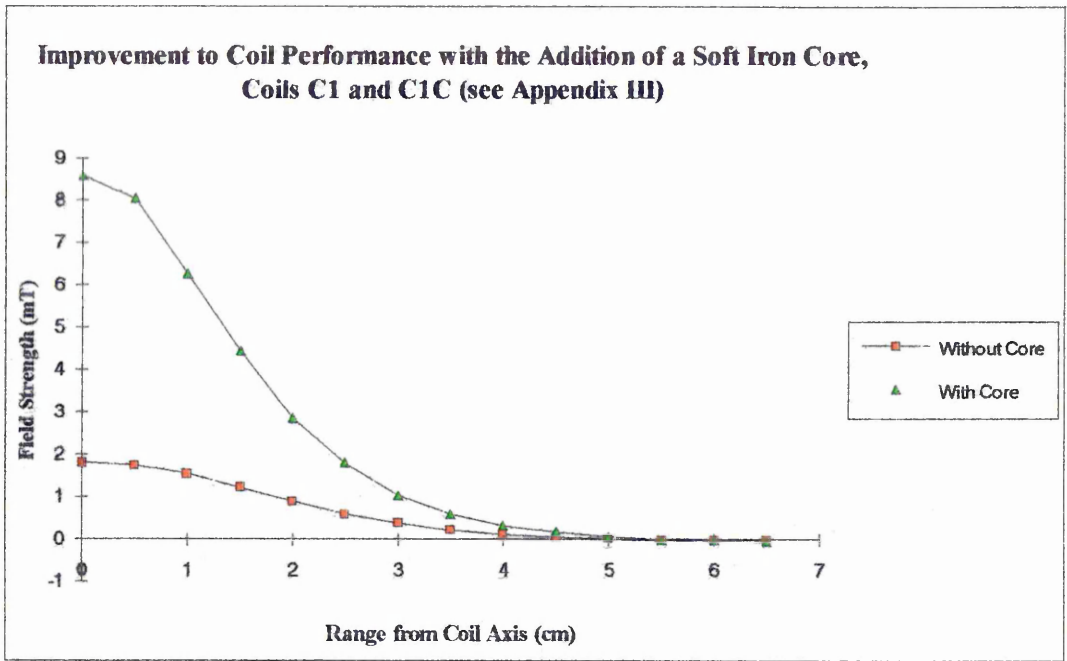


Figure 4.11, Change in normal field magnitude of inner coil due to core.

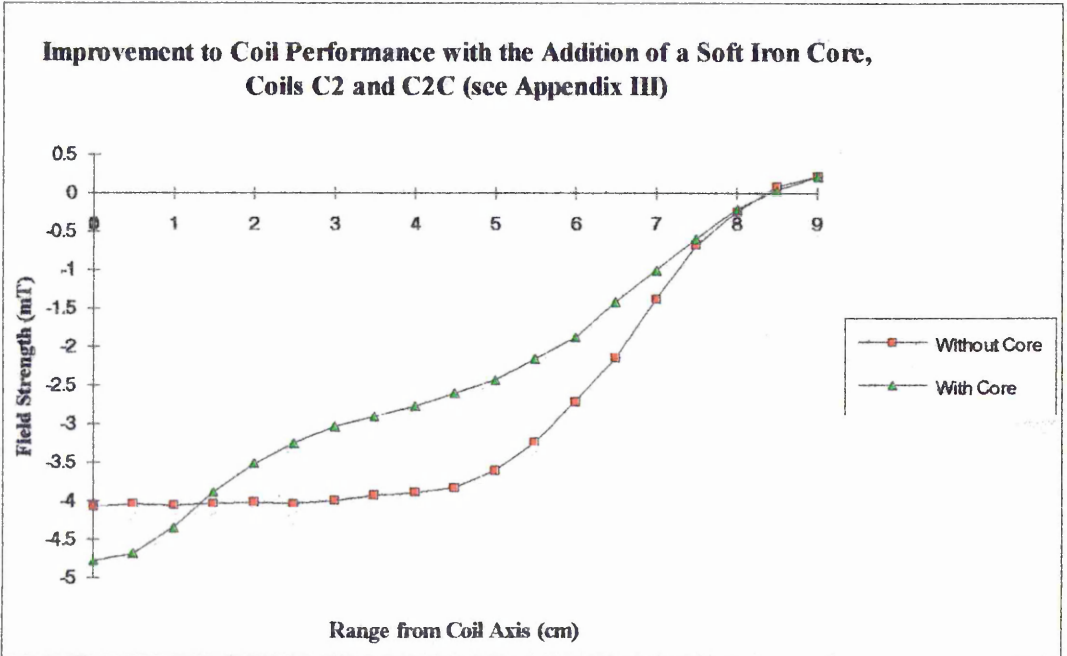


Figure 4.12, Distortion of normal field profile of outer coil due to addition of core.

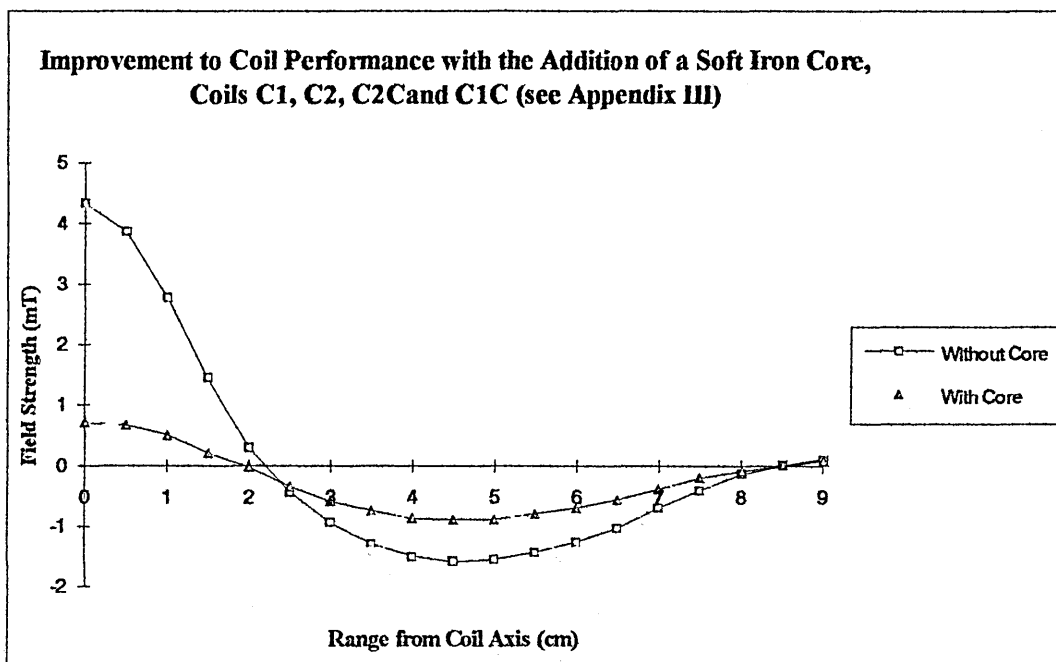


Figure 4.13, Change in profile of two coil system with a soft iron core.

This method was tested for accuracy by using the program to predict coil currents required to produce a range of field gradients and varying normal field zero positions, these were then used to drive the prototype coils. The field profiles produced were measured and compared with those predicted by the program. Examining Figure 4.14 it can be seen that the normal field zero and field gradient are accurately predicted, with some small amount of systematic error possibly due to slight alterations in coil measurement range (further comparisons between predicted and measured profiles are included as Figures AIII.3 and AIII.4 in Appendix III). The method is, therefore, suitable for predicting required coil currents and was used to calculate the ratios of currents needed to position the normal field zero for future work. The predicted ratios are compared with experimentally measured values in Table 4.1 below.

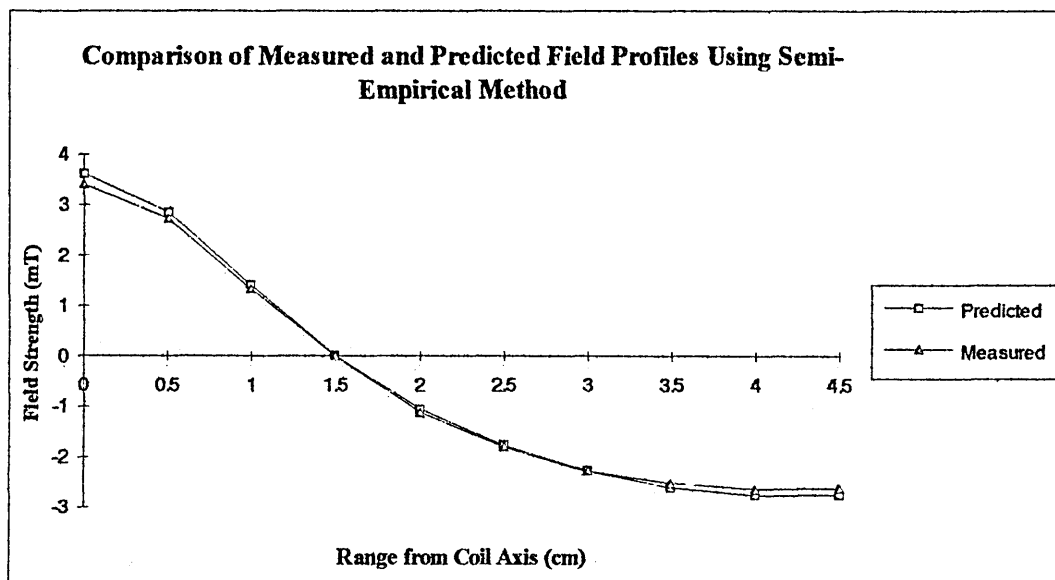


Figure 4.14, Measured and predicted field profiles for a gradient of 2.5 mTcm⁻¹ and normal zero position of 1.5 cm.

Table 4.1

Comparison of measured and predicted coil current ratios

Zero Position (cm)	1.5	2.0	2.5	3.0	3.5
Ratio C3C:C4C (predicted)	1.79	2.56	3.49	6.25	10.75
Ratio C3C:C4C (measured) ±5%	1.88	2.52	3.48	6.04	10.0

4.1.6 The manufacture of the coils.

The prototype coils (C3C and C4C) were found to be of a geometry and power capable of producing the field profiles required, they were therefore duplicated in a form suitable for enclosure within the cathode assembly. Both coils were wound from 1.7 mm diameter enamelled copper wire on brass formers and encased in brass jackets to allow the attachment of copper, water-cooling pipes to dissipate heat produced whilst operating at high coil currents. Figure 4.3 shows a schematic diagram of the coils housed in the cathode assembly. Figure 4.15 shows a dimensioned sectional drawing of the coils themselves. Both coils were equipped with a thermocouple embedded in the middle of the windings to monitor coil temperature and safeguard against overheating. Initial trials showed that the coils were capable of operating to the required specification for long enough periods of time to allow experiments to be conducted.

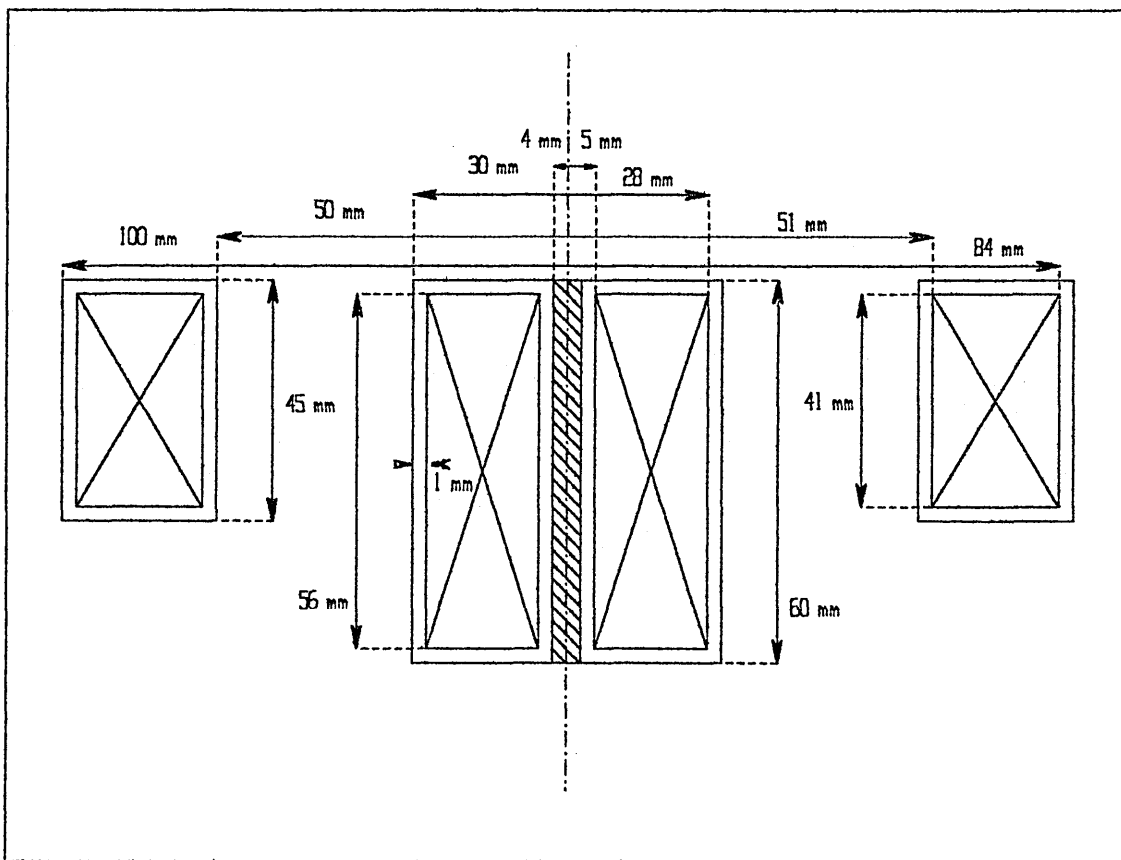


Figure 4.15, Dimensions of steering coils.

4.2 The arc chamber and associated systems.

This section describes the design and construction of the experimental chamber and the nature of the associated control systems and power supplies. The system as a whole is represented by Figure 4.16 as a block diagram. The major features of this diagram will be discussed individually below.

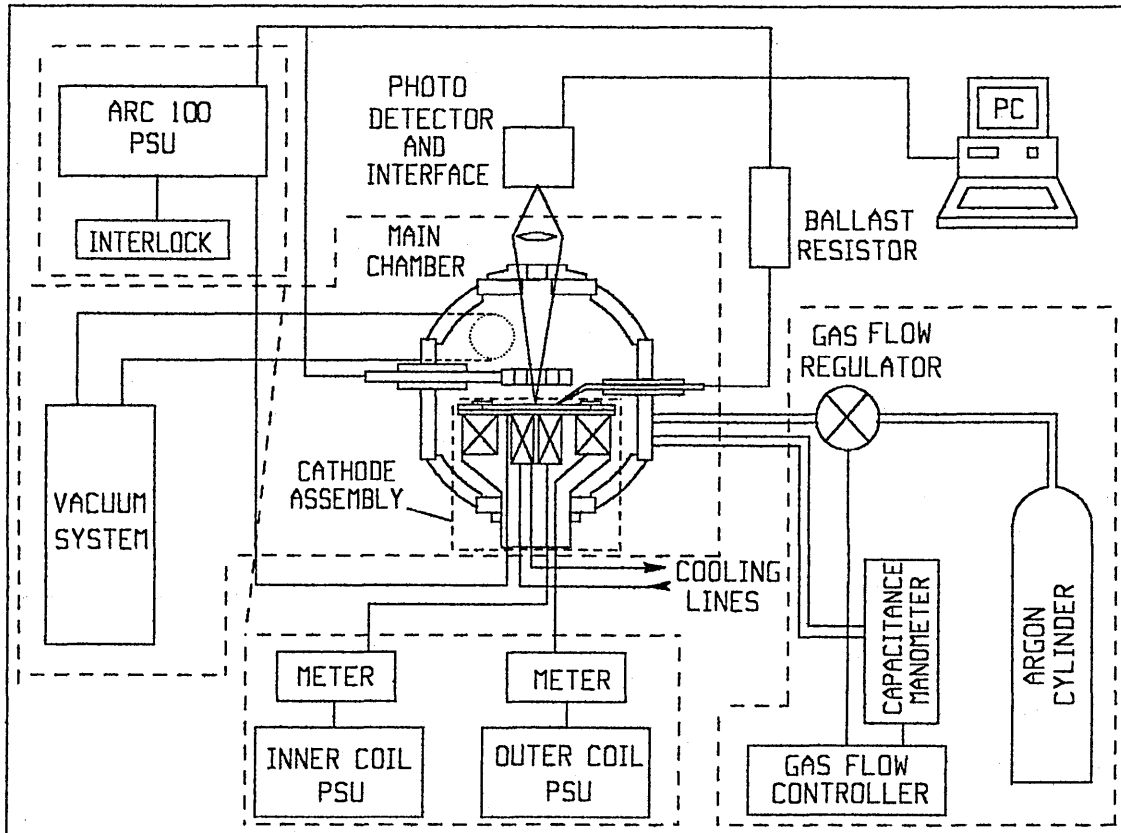


Figure 4.16, Schematic diagram of the steered arc system.

4.2.1 The main chamber and pumping system.

A sketch of the main chamber is shown in Figure 4.17 and a photograph of it in Figure 4.18. It and the cathode assembly were designed by Dr R. New and manufactured by Messrs R. Day and G. Robinson at engineering facilities at The Materials Research Institute, Sheffield Hallam University. It consists of a cylindrical aluminium chamber mounted upon the modified base plate of an existing Genevac unit. The pumping system for the unit comprises a 20 cm throat diffusion pump backed by a rotary pump which

gave a pumping capability of approximately 1300 ls^{-1} . Access to the chamber is via a circular top plate by which the chamber is also connected to earth. Four ports are mounted on the side of the chamber at 90° intervals, these consist of square plates through which a number of feed-throughs are mounted.

The first of these provides access for the cathode assembly shown in detail in figure 4.3. The second is installed with a circular viewing port allowing optical measurements to be made. The third is mounted with a water cooled electrical feed-through that supplies current and supports the circular spoked anode: the anode was made in this fashion to enable a direct line of sight from the viewing port to a range of arc track radii. The final port is mounted with three feed-throughs these consist of; an electrical feed-through, a gas feed-through and a connection to a pressure transducer. The electrical feed-through, which incorporates a rotary motion, is connected to anode potential through a ballast resistor thus allowing the arc to be struck by making a momentary short between the supply voltage and earth via a monal spike (the resistor ensures that the current passed is low enough to prevent the spike from welding to the cathode).

The entire system achieved a good seal and during operation the chamber consistently attained a residual pressure of below 10^{-5} mBar.

4.2.2 The power supplies.

Three units were used to supply power to the system, two to supply current to the steering coils and one to supply power to the arc. The inner coil was driven by a constant current P.S.U. with feedback stabilisation and was capable of delivering currents of up to 20 Amps. The outer coil was similarly supplied by a unit capable of delivering up to 10 Amps.

The main arc current was generated by a commercially produced arc supply: the "ARC 100" unit manufactured by ELMA Technik GMBH. This supply gave fixed current outputs of between 0 and 100 Amps at potentials of up to 100 Volts. The "ARC 100" also featured a low voltage opto-coupler interlock that required a 5V signal to enable the system thus allowing control of the unit via a remote switch.

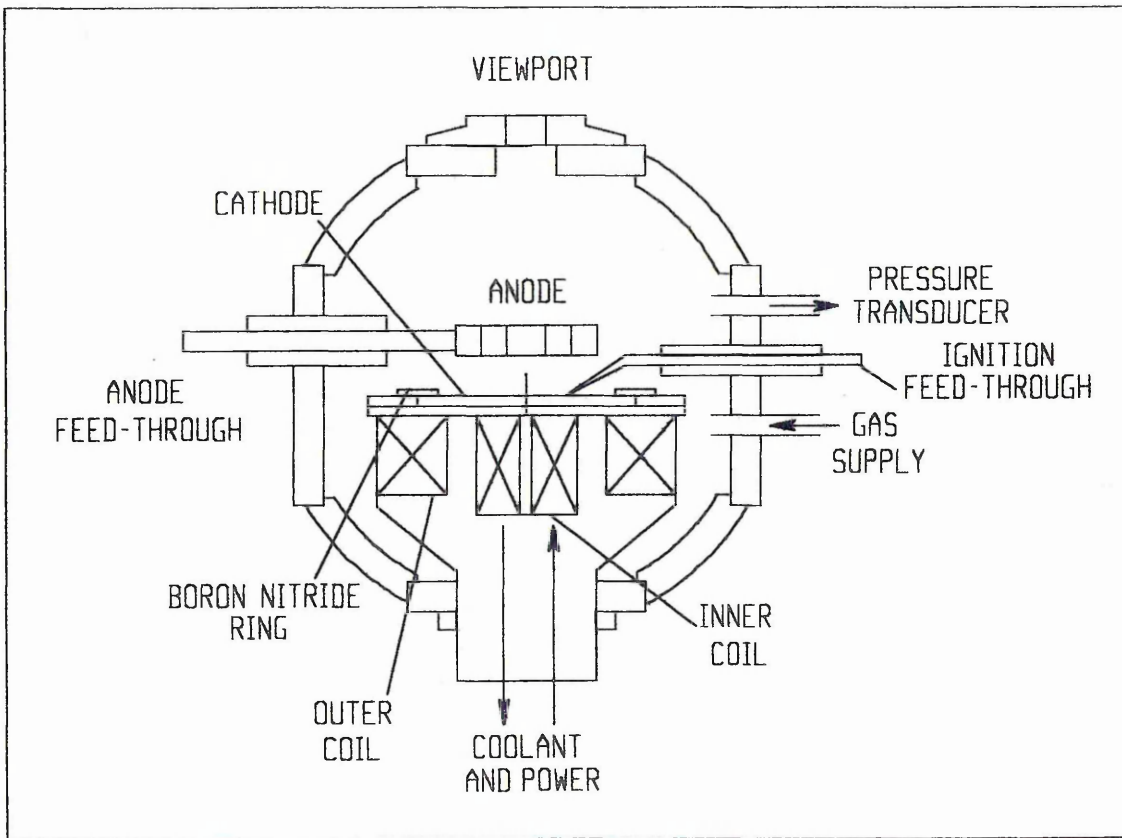


Figure 4.17, Schematic of the main chamber.

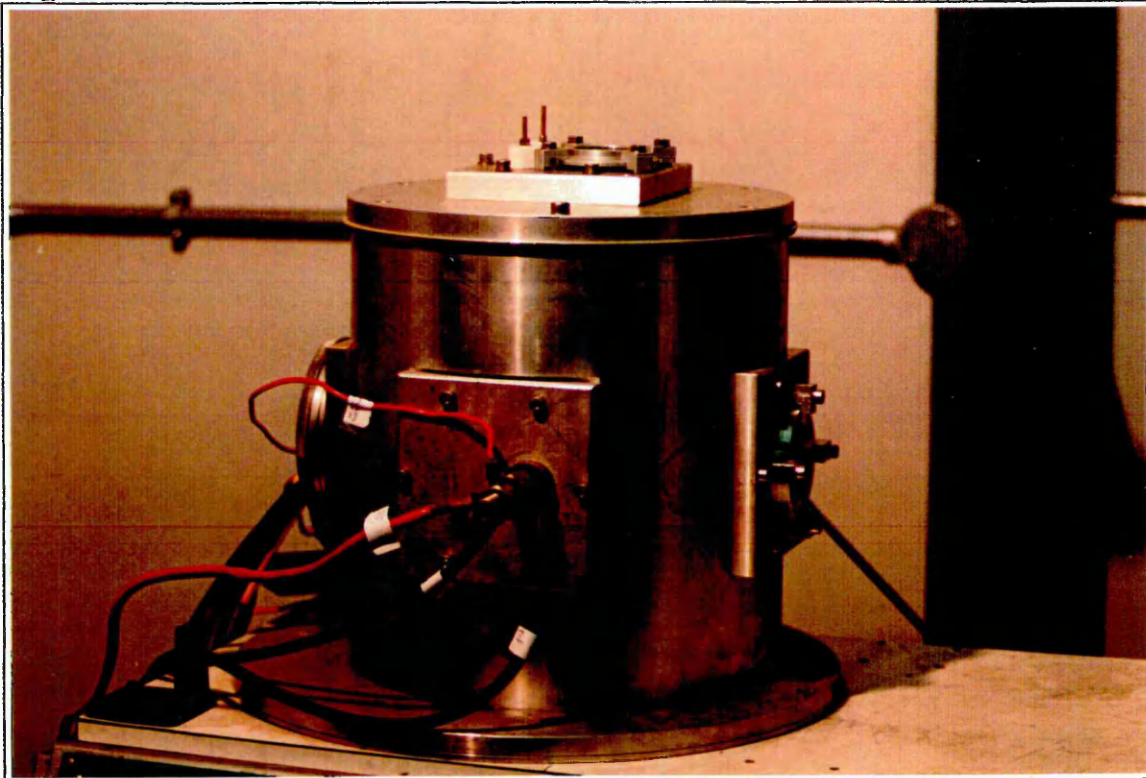


Figure 4.18, Photograph of the main chamber.

4.2.3 The gas flow control system.

The background pressure of argon within the system was critical to later experiments (see Chapter 5). It was initially (for the first experiment described in Chapter 5) controlled manually by the setting of a needle valve feed through to the base of the chamber. This method of control, although giving a stable background pressure for the duration of the early experimental work was found to be unsatisfactory for two reasons. Firstly, manual control of the valve was time consuming and for later experiments other conditions required frequent monitoring to ensure accurate data collection. Secondly, manual control was more easily established at higher pressures, operating at these pressures the diffusion pump had a tendency to stall thus causing instabilities in pumping speeds. For later experiments the pressure was therefore controlled using a feedback system comprising a pressure transducer, a control unit and an automatic gas admit valve.

The gas pressure controller employed was an MKS 250. This controller enabled the setting of a fixed chamber pressure to a high degree of accuracy (0.25% of reading) over a 4 decade range dependent on the output from a suitable choice of pressure transducer.

The transducer chosen was the MKS Baratron 122A, an absolute pressure gauge of the capacitance manometer type. This type of gauge was selected for 3 reasons; firstly, the operational range of the gauge is large, in this case 2.25×10^{-4} mBar to 0.75 mBar, secondly, the gauge gives an absolute measure of pressure (no corrections are required for differing gas types) and finally the accuracy of the gauge is very high: 0.5% of reading.

Gas flow control was established with an MKS 248 solenoid control valve. This valve afforded proportional control over the gas flow, and consequently, with opening threshold levels correctly set at the control unit, gave a very stable control of the chamber pressure. All components described above were manufactured by MKS Instruments Inc.

Using the above system and operating at 0.75×10^{-3} mBar of argon the variations in chamber pressure did not exceed 1% of the reading.

4.2.4 The cathode assembly.

The cathode assembly, shown in Figures 4.19 and 4.20, served three functions; firstly to house the electromagnetic steering system, secondly to provide a secure electrical and physical mounting point for the cathode (whilst enabling the cathode to be changed easily) and finally to provide cooling for the cathode and coil system. To allow easy access to the coils and cooling network and prevent the risk of flooding the pumping system, the assembly was designed to be sealed from atmosphere around its narrower cylindrical end: the inside of the assembly thus being at atmospheric pressure.

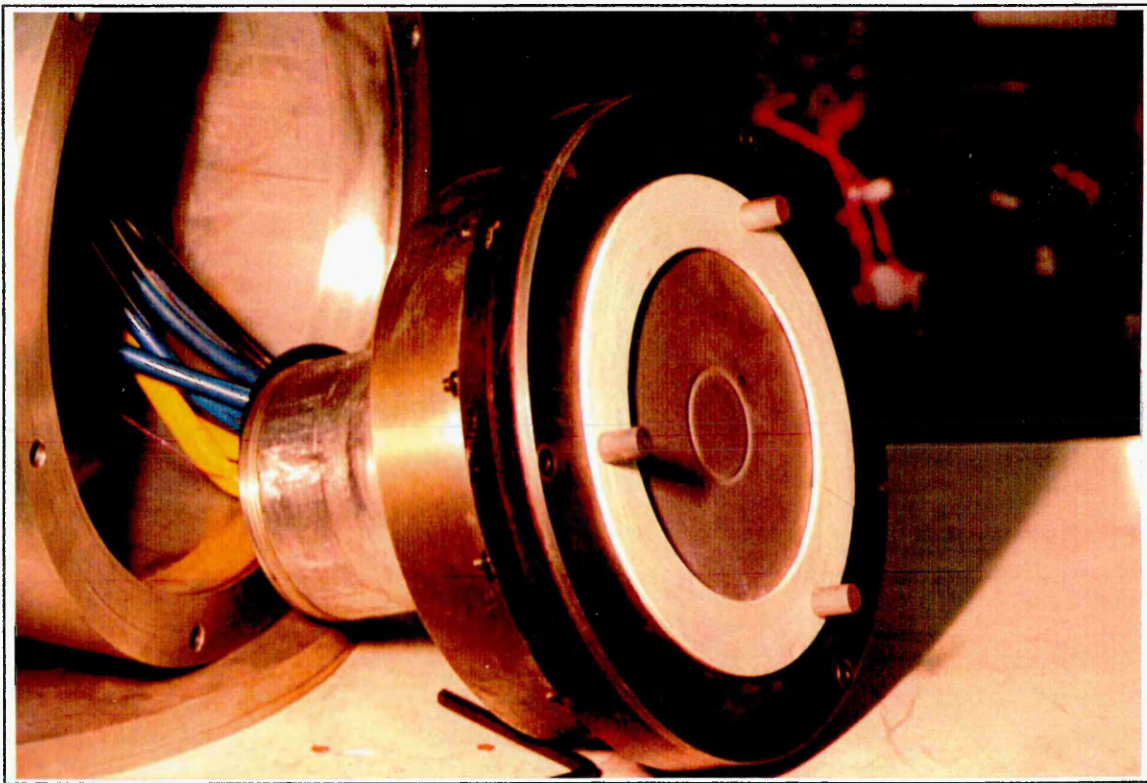


Figure 4.19, A photograph of the cathode assembly.

The cathode consisted of a 5mm by 150mm disc of the material under investigation. It was secured in place by an aluminium ring which was fixed to the assembly by a number of counter sunk bolts around its circumference. The union between the retaining ring and cathode was covered by a disc of amorphous boron nitride, this served the dual

functions of confining the arc to the cathode during random arcing and preventing the arc burrowing at the junction between the two metals. This part of the assembly is shown in detail in Figure 4.20.

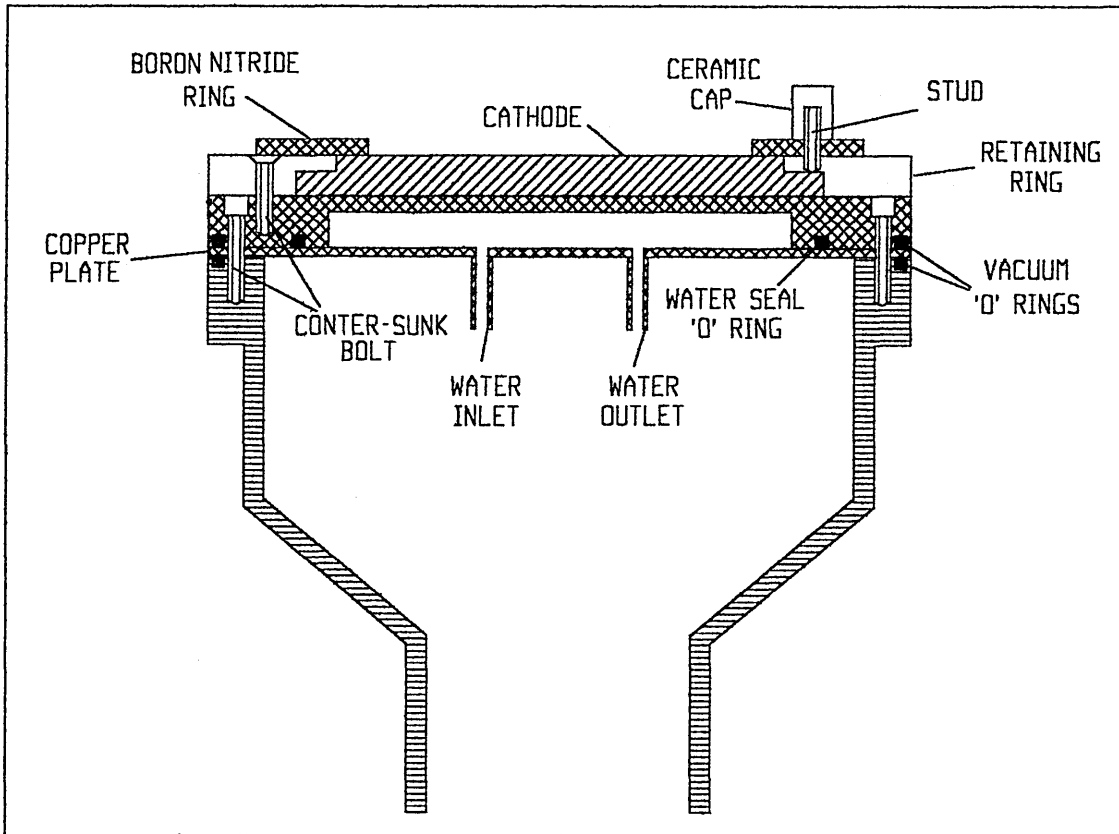


Figure 4.20, Detailed sketch of the cathode mounting.

The cathode and retaining ring were mounted upon a copper cooling plate which also served as the vacuum seal (by way of two large 'o' rings) between the main body of the assembly and the cathode mounting. The plate consisted of a hollow disc sealed by a circular sheet of copper through which the water inlet and outlets were mounted. The temperature of the outlet water was constantly monitored by a thermocouple to guard against overheating, although temperature rises in the coolant during operation were rarely more than a few degrees. Power was supplied to the cathode by direct connection to the cooling plate. This connection was made by way of three push on 'bullet' connectors, the male sides of which were tapped and braised into the copper plate. Three connections , using narrower gauge wire, were employed due to space restrictions.

The electromagnets were cooled in two ways; firstly, mounting directly onto the cooling plate provided some cooling on the front face of the coils and secondly two spirals of copper tubing were braised onto the brass coil jacketing, this tubing was connected into the cooling plate water supply.

4.3 Summary of system and system performance.

The preceding chapter has described the design and development of a two coil electromagnetic arc steering system and experimental chamber.

The coils were initially designed by use of the Biot-Savart model which allowed accurate predictions to be made of the field profiles generated by a system of one or more purely electromagnetic coils. Subject to restriction imposed by the space available within the cathode assembly a soft iron core was added to the centre of the inner coil to produce the required field strengths. The addition of a core, whilst not significantly affecting the field geometry for the purposes of overall design, required the use of an alternative to the Biot-Savart model that described field parameters accurately enough to produce the finished coils. Consequently a semi-empirical method was used to describe the coil currents needed to give normal field component gradients and zero positions necessary to control the arc within the required range of values. The use of these two methods has allowed the production of the steering system with the minimum of engineering time.

The completed system allows the running of a random or steered arc upon a cathode of 14cm diameter in an accurately controlled background of argon gas. Initial tests were made, using a titanium cathode, to investigate the limitations of the system regarding the range of radii that control of the arc was maintained, the minimum current at which stable arcs were achievable and the range of pressures at which the arc would operate, these are discussed below.

Control of the arc was established over a range of radii from approximately 1cm to 5cm. The level of control at the varying radii was dependent upon the field gradient

achievable at the normal field zero, this in turn was limited by the range of coil currents available. This range of control was limited only by restrictions upon the sizes of coils that would fit inside the cathode assembly. Future designs taking this into consideration would allow steered arc coverage of the entire cathode.

The stability of the arc whilst being steered was of critical importance during later experimental work. The range of arc currents and argon pressures over which the arc ran without extinguishing was therefore investigated. It was found, for titanium, that a current in excess of 70 amps and argon pressures upwards of 0.75×10^{-3} mBar gave a stable arc in both the random and steered modes. It was decided to operate the system at the minimum current, thus reducing the risk of spot splitting. Using manual control the lowest stable pressure achievable was 15×10^{-3} mBar, fitting of the automatic control unit gave stable arc behaviour at a pressure of 0.75×10^{-3} mBar.

References.

- [1] L. Donohue, J. Cawley, J.S. Brooks,
Surf. Coat. Tech., **63**, 49, (1994).
- [2] P.C. Johnson,
Physics of Thin Films, **14**, 129, (1989).
- [3] C.M. Care,
J Phys. D Appl. Phys., **25**(12), 1841, (1992).
- [4] P.D. Swift, D.R. Mckenzie, I.S. Falconer, P.J. Martin,
J. Appl. Phys., **66**(2), (1989).
- [5] P.D. Swift,
J. Appl. Phys., **67**(4), (1990).
- [6] C.F. Morrison,
U.S. Patent No. 4,724,058, (1988).
- [7] J. Higbie,
Am. J. Phys., **46**(10), 1075, (1978).

Experimental studies of arc motion

As mentioned previously in Chapters 2 and 3 the arc has been modelled successfully as a stochastic process. Models by Hantzche et al, Daalder and Anders et al. [1, 2, 3] have defined the arc spot diffusion coefficient and constant of spot displacement for a random arc. These have been measured by various experimental techniques and values for a range of materials have been determined.

A model proposed by Care [4] has further developed this idea by regarding the motion of the steered arc as a random walk biased by the two components of the applied magnetic field; the transverse field component B_T and the normal field gradient B'_N . The confinement of the arc to the path defined by the normal field zero is governed by both of these components whilst the motion of the arc along the zero is dependent upon the transverse field component alone.

This chapter describes experimental work designed to measure the motion of the arc in the directions of confinement and retrograde motion. This allows the predictions made by the stochastic model to be tested and values for the spot diffusion coefficient and macroscopic velocity to be determined. The chapter is divided into four main parts which are discussed individually below.

- (i) Section 5.1 is an introduction to the chapter and serves to describe the stochastic model in more detail.

- (ii) Section 5.2 describes the measurement of the distribution of orbital radii of the spot as a function of transverse field strength and normal field gradient. This allows the determination of the measure of spot confinement to the normal zero by the applied field. The measured distribution is compared to that predicted by the stochastic model.

(iii) Section 5.3 describes the measurement of the distribution of spot transit times around its orbit. This allows the determination of the spot diffusion coefficient and macroscopic velocity. The measured distribution is compared to that predicted by the stochastic model. This experiment is repeated for a range of cathode materials.

(iv) Section 5.4 describes the distribution of spot transit times around its orbit as a function of applied transverse and normal field components. This allows the determination of the dependence of spot velocity upon transverse field component and the magnetic field dependence of the spot diffusion coefficient.

Due to the highly sensitive nature of spot behaviour it was decided to fix as many experimental conditions as possible whilst studying the motion of the spot.

Although the coils were capable of positioning the normal field zero over a range of values, for the purposes of the following experiments a radius of 2 cm was chosen. This choice of radius enabled the largest range of field gradients to be employed whilst allowing an unobstructed view of the arc track from the view port.

Similarly a fixed background pressure of argon was chosen. This was initially 15×10^{-3} mBar but, as mentioned in Chapter 4, difficulties with stalling of the diffusion pump made it necessary to employ an electronic gas control system and operate at a reduced pressure of 0.75×10^{-3} mBar. Hence the experiments detailed in Section 5.2 are conducted at the higher pressure while those in Sections 5.3 and 5.4 are conducted at the lower pressure.

For titanium the minimum stable arc current was found to be 70 amps. All experiments using titanium as a cathode material were conducted at this current. Later experiments using other cathode materials necessitated the use of higher arc currents. These will be discussed in Section 5.3.

5.1 Introduction.

The stochastic model is described briefly in Section 3.3.5. This introduction will describe the solution to the model in detail, paying particular attention to the natures of the probability density functions for spot position in the directions of confinement and motion.

The equation for the time dependent probability density for the arc spot is given in Chapter 3 as Equation 3.19. The equation may be solved analytically if the two assumptions initially made (regarding the dependence of arc velocity and confinement) are written,

$$c = k_c B_T \quad (5.1)$$

Where c is the mean arc velocity, k_c is a constant and B_T is the transverse field component. And,

$$f(x) = k_f B'_N B_T x \quad (5.2)$$

Where k_f is a constant and B'_N is the normal field gradient. The first of these statements assumes a linear change in the arc velocity with transverse field component. This is a reasonable assumption over a limited range of B_T [5]. The second is a simplifying assumption that leads to confinement of the arc near to the normal component zero by a 'restoring force' which is dependent upon the normal and transverse field components. The solution to Equation 3.19¹ is then,

¹It should be noted that in presenting the solution to the stochastic model the assumption has been made (for the purposes of this thesis) that the diffusion constants in the directions of motion and confinement are the same. Hence the omission for Equation 3.19 of the term from the ratio of the two constants.

$$\begin{aligned} \phi(x, y, t) = & \frac{1}{2\pi L^2} \sqrt{\frac{1}{2t/t_0}} \exp\left[-\frac{(y/L + c^*t/t_0)^2}{4t/t_0}\right] \\ & \times \exp\left[-\frac{(x/L)^2}{2}\right] \sum_{m=0}^{\infty} \frac{(-1)^m}{2^{2m}(m!)} \exp[-2mt/t_0] H_{2m}\left(x/(\sqrt{2}L)\right) \end{aligned} \quad (5.3)$$

Where t_0 , the characteristic time and L , the mean distance diffused by the arc in time t_0 , are defined by,

$$t_0 = 1/(k_f B'_N B_T) \quad L = \sqrt{D_x t_0} \quad (5.4)$$

$H_n(x)$ is a Hermite polynomial of order n , and the dimensionless quantity c^* is given by,

$$c^* = ct_0/L \quad (5.5)$$

The behaviour of this solution may be demonstrated in the directions of retrograde motion and confinement by superimposing a mean arc velocity c upon the distribution and then examining the evolution of the function with time, i.e. the distribution is viewed via a frame of reference moving at the mean arc velocity.

At long times and substituting for c^* the equation becomes,

$$\phi(x, y, t) = \frac{1}{2\pi L^2} \sqrt{\frac{1}{2t/t_0}} \exp\left[-\frac{(y + ct)^2}{4D_x t}\right] \exp\left[-\frac{1}{2} \frac{x^2}{(D_x/k_f B'_N B_T)}\right] \quad (5.6)$$

This occurs as the only surviving term of the Hermite polynomial at long times is the $m=0$ term, which is equal to unity.

This simplified equation allows the arc behaviour in each direction to be easily examined. In the direction of confinement (the x direction) the probability density function spreads out with time to become a Gaussian of fixed width at long times. The width of this Gaussian is governed by the diffusion constant of the material being arced upon, the normal field gradient and the transverse field component.

In the direction of motion the arc moves at a mean velocity (determined by the transverse field component) and diffuses about its mean position, unconfined, at a rate governed by the diffusion coefficient.

The nature of these probability density functions will be discussed in detail at the beginning of the section describing their experimental measurement.

5.2 Measurement of the arc confinement.

5.2.1 Introduction.

Examining Equation 5.3, it follows that, at long times, the probability density function in the x direction becomes a Gaussian with half width L , i.e.

$$\phi(x,t) = \frac{1}{\sqrt{2\pi}L} \exp\left[-\frac{1}{2}\left(\frac{x}{L}\right)^2\right] \quad (5.7)$$

The probability of finding the spot a certain distance from the track centre should have a normal distribution with a width proportional to $1/\sqrt{B_T B'_N}$ (see above).

This section describes the experimental measurement of the distribution of arc radii as a function of the transverse field component, B_T and the normal field gradient B'_N and its comparison with that predicted by Equation 5.7.

5.2.2 Experimental details.

Using the apparatus shown in Figure 5.1 (and described in detail in Chapter 4) measurements were made of the distribution of arc radii for a number of different field gradients and transverse fields.

The ratio of coil currents was set to give a normal zero of 2 cm. By varying the magnitudes of the currents the radius was maintained but B_T and B_N' were adjusted. Approximately 100 photographs of orbits of the arc were taken for each of 11 settings of the steering field. This was performed by maintaining a stable steered arc and using a still 35 mm camera with a fast automatic motor wind to expose as many frames as possible for the duration of the arc. The exposure time was calculated to 'capture' approximately one whole orbit of the arc. The radius of the arc track was then measured from the negatives.

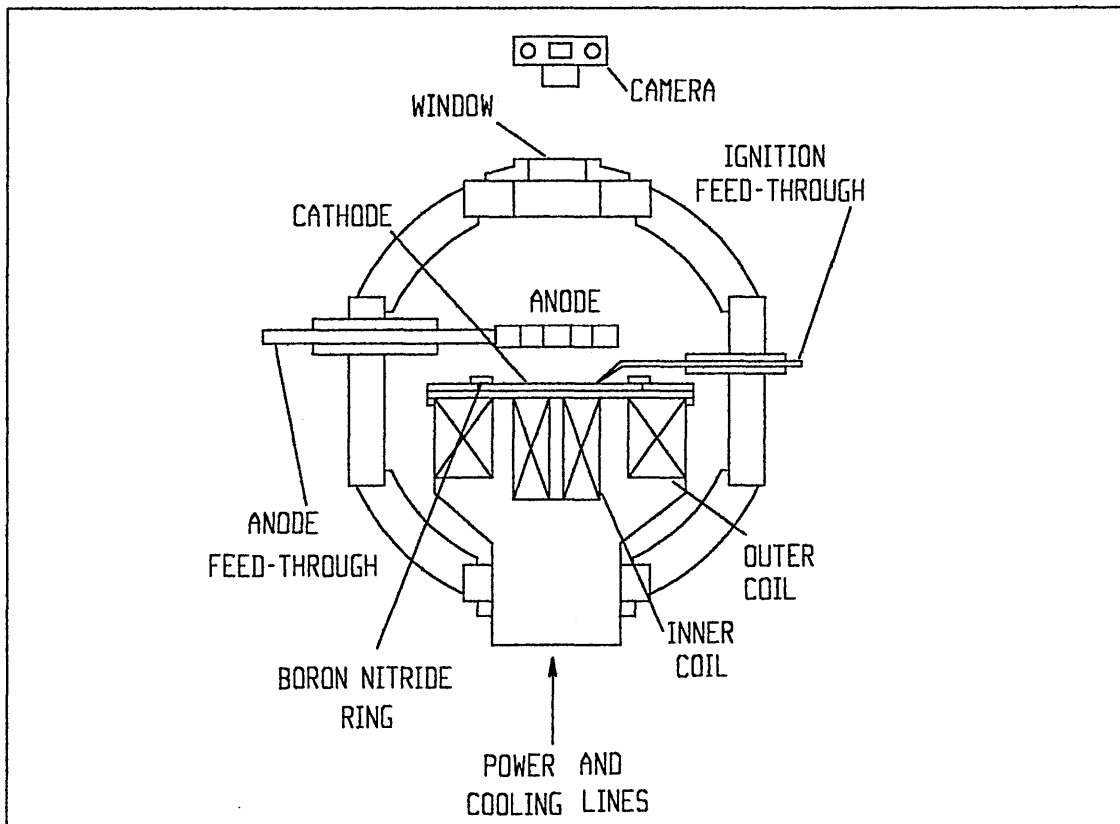


Figure 5.1, Schematic of experimental apparatus.

This was achieved accurately by using a photographic enlarger to project the negatives onto a ruled screen, from which a measurement could be taken. To ensure a fixed frame of reference and a constant scale of enlargement the spoked anode was left in a fixed position for the duration of the measurements. This meant that an outline of the anode could be drawn from the first of the negatives allowing the subsequent projections to be accurately aligned and enlarged. Measurements were made from the centre of the arc orbit to a fixed point on its radius, this was done for two reasons. Firstly, the measurement across the diameter of the arc would result in the determination of convolution of two distributions of confinement (one at either end of the diameter). Secondly, the use of a fixed point excluded the influence of any error in the determination of the centre of rotation of the arc. This centre was determined by running the arc for several hundred orbits on a very tight confinement whilst holding open the camera shutter. The resulting negative gave a very clear circular path from which the position of the centre could be calculated.

From the measurements the standard deviation of the radius was determined (as a measure of arc confinement) for the given magnetic field conditions. In addition to this 430 photographs were taken at a 12th coil setting to allow a more detailed study of the distribution of radii to be made and thus a more accurate comparison to the model to be made.

5.2.3 Results and Discussion.

Table 5.1 shows the results of the measurement of the standard deviation of the track radius at different field settings, the standard error in these measurements and the coil currents required to achieve the field settings. Equation 5.7 predicts that a graph of standard deviation versus $(B_T B'_N)^{-1/2}$ should be a straight line that passes through the origin. Figure 5.2 shows the data plotted in such a fashion. The relationship is linear to 1% confidence and intercepts the y axis at the origin to within error (0.04 ± 0.18 mm). The data does, however, exhibit a degree of scattering about the best fit line that, whilst

not invalidating the confidence of fit and the value of the intercept, warrants some explanation and is therefore discussed at the end of this section.

Although this is consistent with the theoretical prediction it is not possible with the present steering system to be sure if the magnetic field dependence is unambiguously $(B_T B'_N)^{-1/2}$. This is due to the fact that with the present coil set-up B'_N and B_T are approximately proportional to each other and consequently it is impossible to alter the setting of one without altering the setting of the other. The separation of the dependence is discussed as a suggestion for future work in Chapter 6.

Figure 5.3 shows the distribution of the 430 radii measured at field settings of $B_T=7.81$ mT and $B'_N=810$ mTm⁻¹. The solid curve is the normal distribution with the same standard deviation and mean as the measured data. The broken lines show normal distributions with the same mean as the data and standard deviations that differ from that of the data by plus and minus the standard error, thus attempting to show distributions that could be reasonably expected from the data. It can be seen that the measured distribution is somewhat narrower than the equivalent normal distribution. Furthermore the measured distribution has a skew of 0.5 which indicates a distribution that is loaded on the left of the median. In this case more orbits of smaller radius have been measured than would be expected from the theoretical prediction.

There are two factors that offer an explanation for this discrepancy. The first is that the simplified field geometry used by the stochastic model has not adequately described the degree of confinement. Alternatively, and more probably, changes arising in the magnetic field profile have increased the magnitude of the arc confinement and thus caused a more 'pinched' distribution. The changes in the applied field are due to the arc burrowing a track into the cathode and thus reducing the range between arc and electromagnets. Although, in the case of this experiment, this reduction in range is only of the order of millimetres, the effect is considerable taken that the coil to spot distance starts at approximately 11 mm.

Table 5.1

Summary of experimental results and settings.

S.D. of arc radii (mm)	Standard error in S.D.	No. of readings in data set	B'_N mTm ⁻¹	B_T mT	Inner coil current (A)	Outer coil Current (A)
2.52	0.26	96	545	5.17	6.93	2.75
2.32	0.18	175	635	5.69	7.7	3.0
1.83	0.17	121	663	5.94	8.19	3.25
1.71	0.13	170	717	6.69	8.8	3.5
1.45	0.15	100	769	6.94	9.45	3.75
1.56	0.08	431	810	7.81	10.22	4.0
1.31	0.14	89	911	8.44	11.35	4.5
1.36	0.14	89	992	9.29	12.68	5.0
1.38	0.13	122	1066	9.89	13.86	5.5
1.04	0.09	138	1161	10.33	15.12	6.0
1.1	0.1	125	1213	11.2	16.38	6.5
1.1	0.11	103	1270	11.69	17.64	7.0

100

100

100

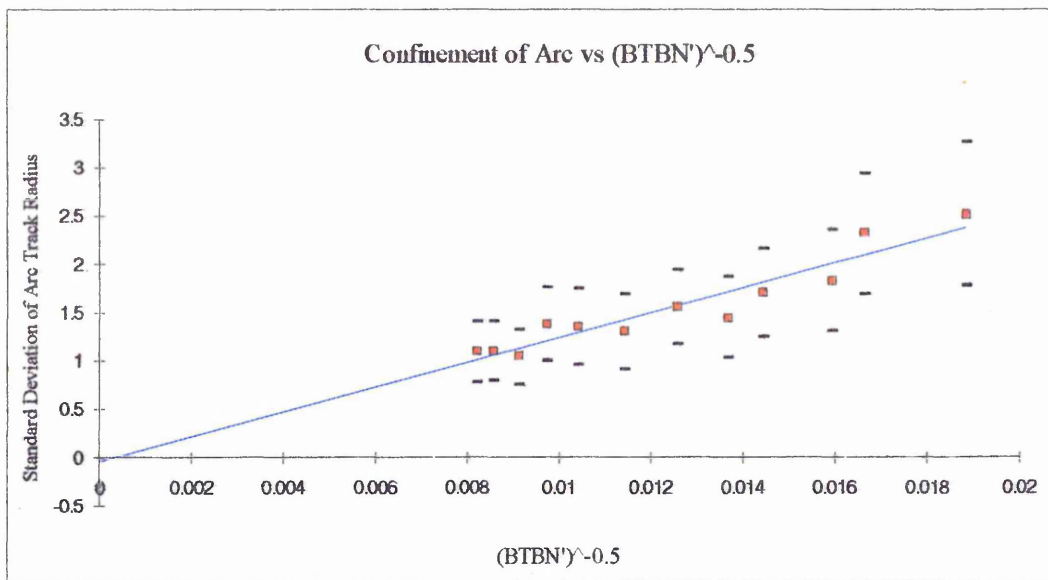


Figure 5.2, Experimental data with best fit straight line.

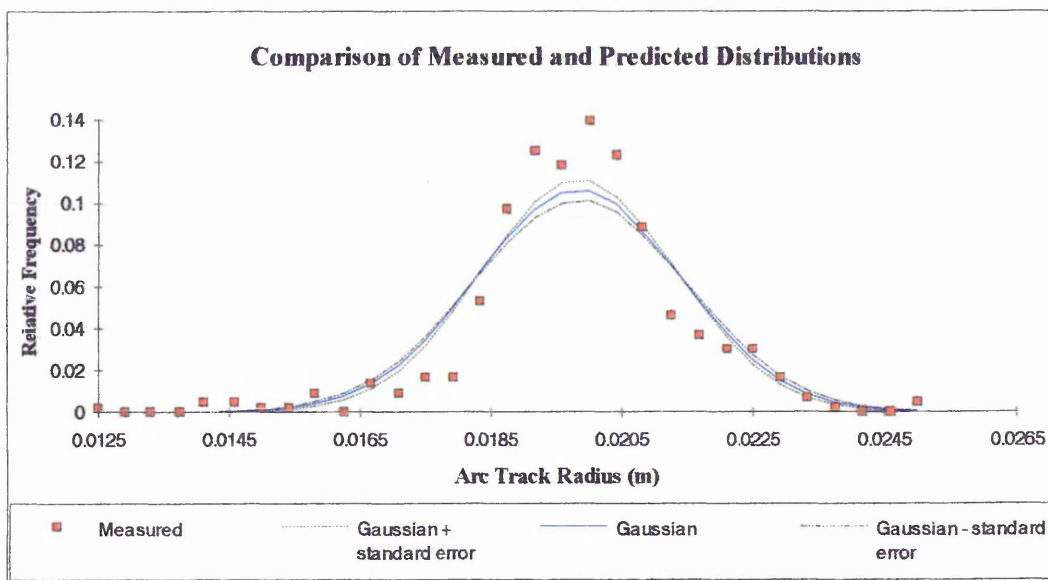


Figure 5.3, A plot of the measured distribution and a normal distribution with the same mean and standard deviation as the measured distribution.

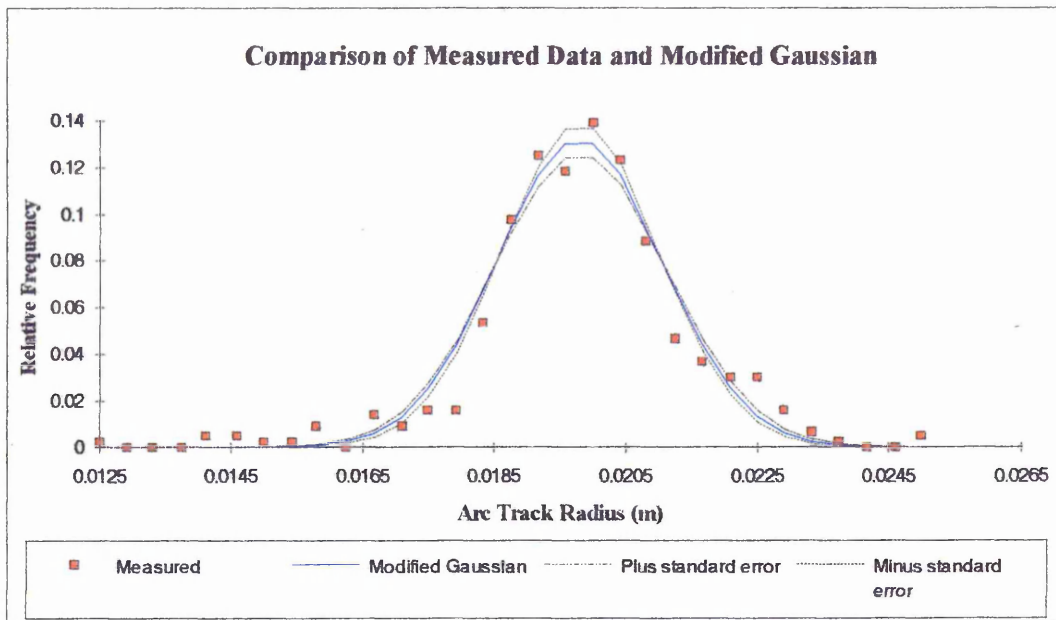


Figure 5.4, A plot of the measured distribution and a normal distribution with the same mean as the measured distribution, but corrected standard deviation.

Initial field measurements were made with an unused flat cathode and gave $B_T=7.81$ mT and $B'_N=810$ mTm⁻¹. Some 120 or so measurements were made at this stage with little or no erosion of the cathode. At a later stage of the experiments the remaining 310 measurements were made. By this time a track 2.5 mm deep had been eroded in the cathode and the field profile altered significantly. The normal field gradient at the zero was found to have changed by 25%, whilst the transverse field was found to have increased by 22% (these changes are discussed in detail in Section 5.3). This leads to an increase of approximately 19% in the level of arc confinement.

It seems reasonable to assume that measurements made initially have been carried out with a weaker degree of confinement and thus loaded the measured distribution in the wing areas. Conversely, the later measurements have been conducted with a higher degree of confinement and are responsible for the loading near the centre of the distribution. The measured distribution consists, therefore, of two superimposed distributions. The normal distribution is calculated from the standard deviation and mean

of the measured data and falls somewhere between fitting well in the wings of the distribution and fitting well at its centre. Unfortunately negatives of the orbits were catalogued only according to the applied field and not chronologically and it is impossible to test this theory properly. However, some idea of whether this is the case may be gained by plotting the measured distribution with a normal distribution of the same mean as the data but with a standard deviation corrected by 19% (the degree of change in the arc confinement).

It can be seen that the fit is much improved at the centre of the distribution with the solid curve giving a good fit and the standard error curves bracketing the scatter of the measured data at this point. As would be expected the fit at the wings of the distribution is not as good as that previously obtained, particularly at small radii. This would seem to support the argument given above.

This effect of increased confinement is also probably responsible for the degree of scatter shown the data plotted in Figure 5.2. Data was initially collected across a range of five field settings to determine the field dependence of the arc confinement and consequently a track was eroded into the cathode. Further coil settings were then used to provide a more complete picture of this dependence by 'filling in' the larger gaps on the x-axis, it is likely that the increased field strengths occurring at this stage of cathode erosion would give levels of confinement above that which would be expected. Thus causing an offset in a subset of the data plotted in Figure 5.2. This increased confinement will also have been observed to a lesser extent with the earlier readings although the effect will have been less noticeable. The large experimental error shown on Figure 5.2 is the result of the sum of the statistical error shown in Table 5.1 and the maximum possible experimental error due to the change in confining field strength.

Confinement of the arc would merit further, more detailed, study and is discussed in Chapter 6.

5.3 Measurement of the distribution of orbital transit times.

5.3.1 Introduction.

The stochastic model predicts that the motion of the arc in the direction of the driving field will be a movement at a uniform velocity v^2 with a random diffusive motion superimposed [4]. By assuming a one dimensional motion and that at time $t=0$ the arc is at $y=0$ the probability density function, $h(x, t)$, for spot position in the x direction may be given by [6, 7],

$$h(y,t) = \frac{1}{(4\pi\alpha t)^{1/2}} \exp\left[-\frac{(y-vt)^2}{4\alpha t}\right] \quad (5.8)$$

Where α is an empirical diffusion coefficient and v the spot velocity.

Experimental work described later in this chapter observes the passage of the spot past a fixed point on the arc's orbit to allow distributions of spot transit times to be measured. The theoretical distribution of transit times may be obtained from Equation 5.8 above [6,7]. If $g(y_0, t)$ is the probability that the arc is beyond the point $y=y_0$ at time t then,

$$g(y_0, t) = \int_{y_0}^{\infty} h(y, t) dy = \frac{1}{2} \left(1 - \operatorname{erf} \left(\frac{(y_0 - vt)}{(4\alpha t)^{1/2}} \right) \right) \quad (5.9)$$

Experiments described in detail in Section 5.3.2 measure the probability distribution $pf(t)$ of the time t , taken for the arc to undertake its first crossing of the point y_0 . If the

² The notations for the diffusion constant and velocity have been changed here from those initially used by Care [4] to that used by Hantzche et al, Daalder and Jüttner [1, 2, 3] this has been done to avoid future confusion.

arc crosses the point y_0 without reversal, the probability distribution $pf(t)$ of the time, t , taken for the arc to cross y_0 is given by,

$$p(\tau) = \frac{\partial g}{\partial t} \Big|_{t=\tau} = \frac{\alpha(v\tau + y)}{4\sqrt{\pi\alpha^3\tau^3} \exp\left(\frac{-(v\tau + y)^2}{4\alpha\tau}\right)} \quad (5.10)$$

In work described below the approximation that $pf(t)=p(t)$ has been made, i.e. that the arc crosses the observation point without reversal. Predictions made by Equation 5.10 for the distribution of spot transit times may now be compared with those measured experimentally.

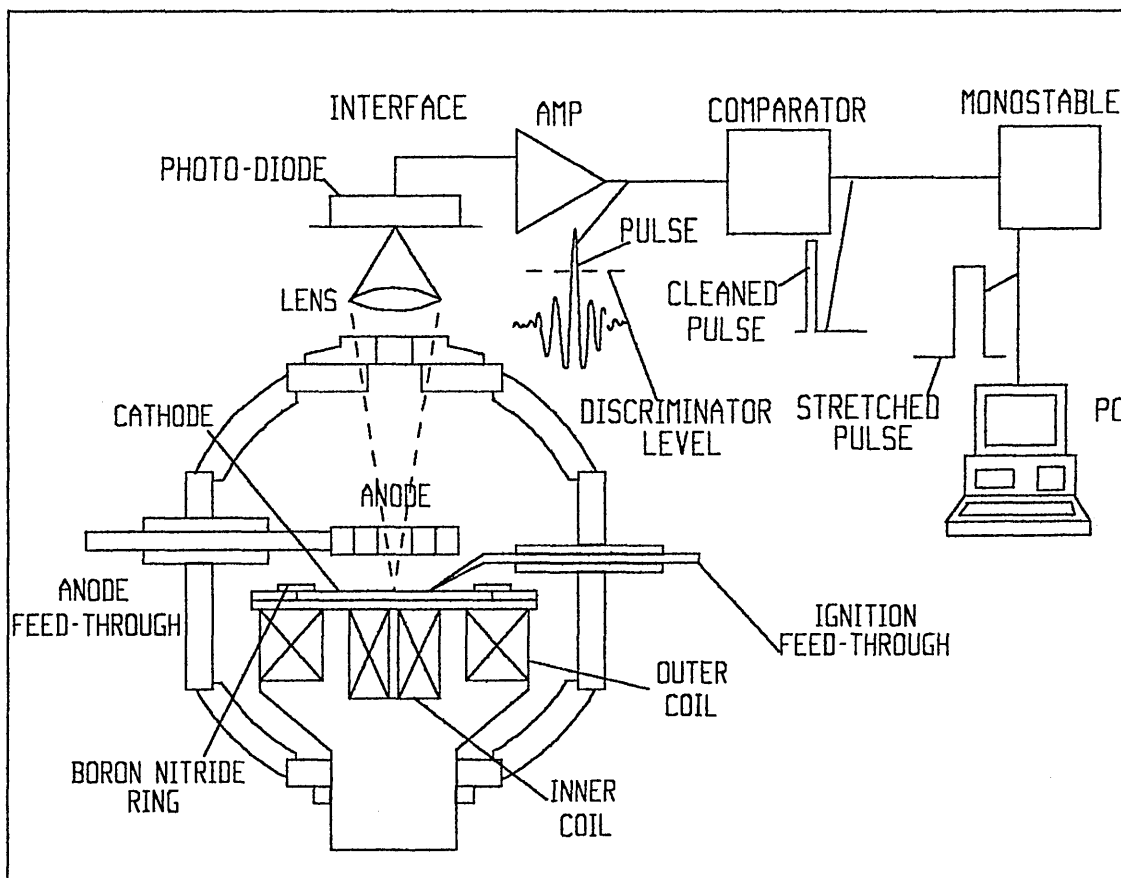


Figure 5.5, Equipment used to measure the arc orbital transit time.

5.3.2 Experimental details.

Using the equipment shown in Figure 5.5 measurements were made of the distribution of arc transit times for a number of cathode materials. This section describes the hardware and software used to collect the data, the cathode materials used and the experimental conditions under which measurements were made.

5.3.2.1 The arc detection equipment.

The arc was imaged onto a large area photo-diode by a lens. The lens was chosen to give a magnification of approximately 0.25 thus reducing the size of the deviations of the arc from its mean orbital radius. The active area of the diode was masked apart from a 0.1mm, slit extending horizontally across its face. This allowed the passage of the arc to be detected at a fixed point on its orbit whilst ensuring that large deviations from the mean arc radius were also detected.

The current signal from the diode was converted to a voltage and amplified by a large gain, low noise circuit specifically designed for photo-diode applications [8] (see Figure 5.6). The output from the amplifier, which is shown as trace TR1 in Figure 5.7, took the form of a sharp pulse upon detection of the arc spot combined with a quantity of background noise present due to 'stray' light from the arc striking the detector.

This signal was then cleaned using a comparator set at a level that discriminated between the pulse and the background noise. This level is shown on Figure 5.7 as trace TR2. The output from the comparator was now a short square edged pulse of 0 to 5 Volts. This pulse was then stretched to approximately 10% of the orbital period using a monostable multivibrator that locked its trigger input for the duration of the output pulse. This was done to avoid the possibility that the arc might be detected making a random move back into the detection area.

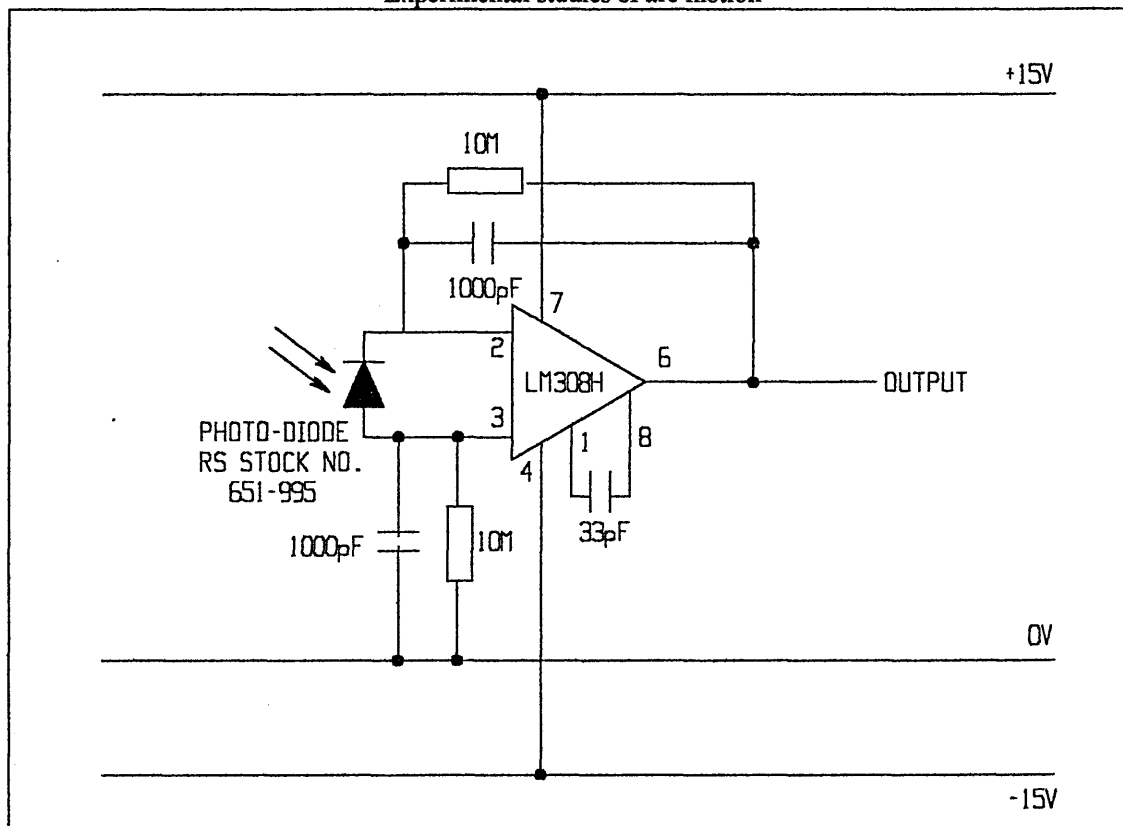


Figure 5.6, Low noise current to voltage converter and amplifier used.

The signal from the monostable was now a TTL compatible 0 to 5 Volts signal that enabled it to be monitored and timed using a computer. The interface was achieved using a National Instruments AT-MIO-16 general purpose interface board which could be controlled using software written using the National Instruments Lab Windows package. This package and the software written to control the board and monitor the signal are described in detail below.

5.3.2.2 The arc timing software.

Lab Windows is a window based general interfacing package that allows the capture, analysis and visual display of a large range of external signals. Using pre-written library routines the user may configure a number of interface boards to capture analogue or digital signals or use them to trigger various counters and timers on the boards.

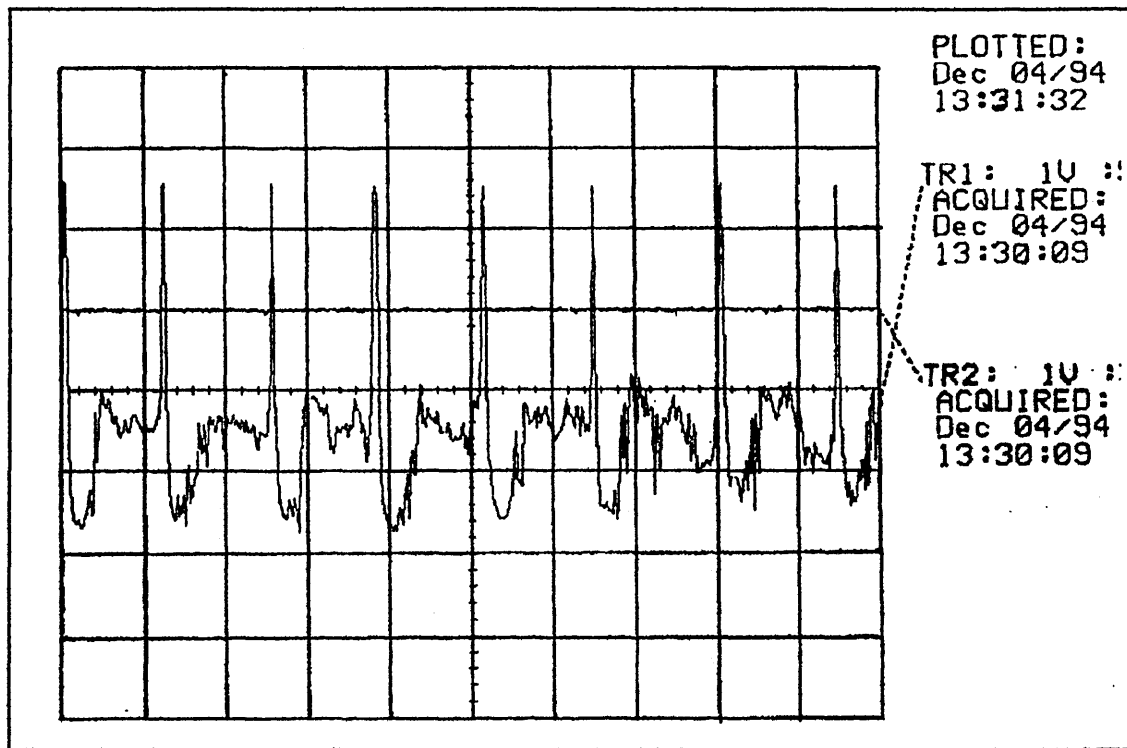


Figure 5.7, The signal from the amplifier upon detection of the arc.

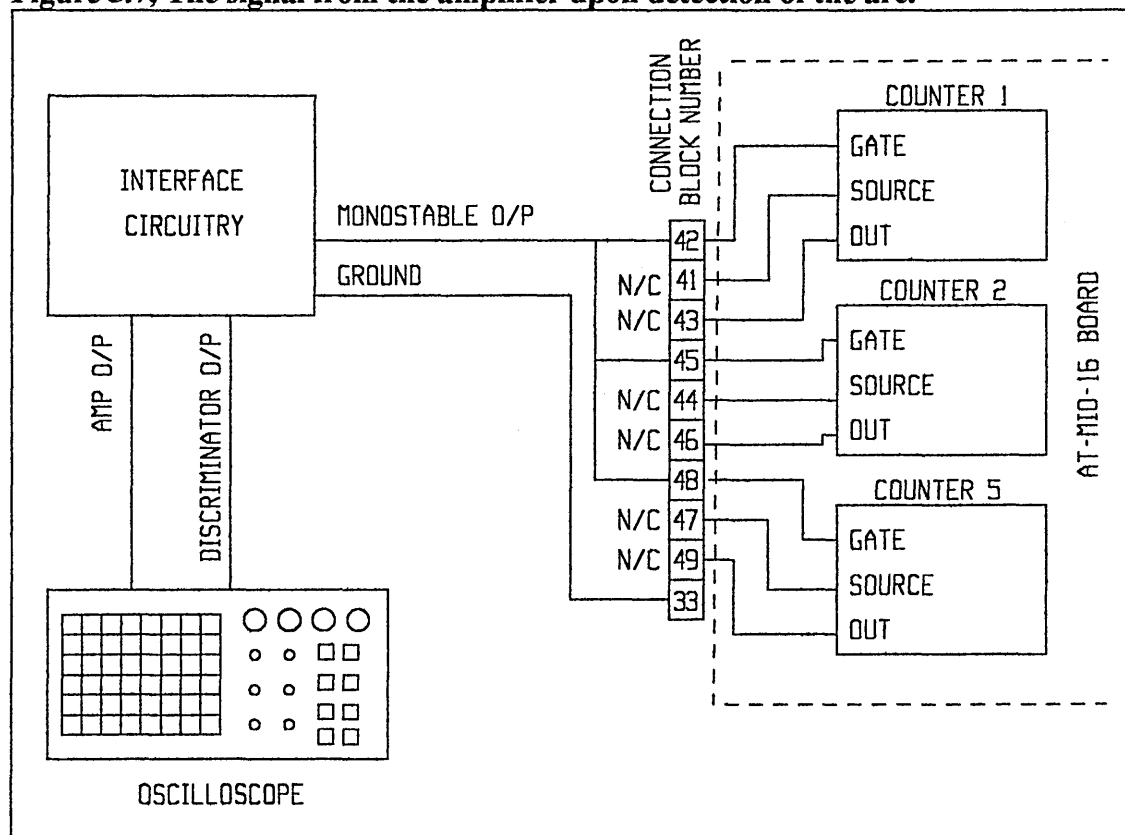


Figure 5.8, External connections to the AT-MIO-16 board.

In this case the signal is used to trigger the counters clocked by the three 1 MHz clocks available on the AT-MIO-16 board and hence time the period between pulses.

Figure 5.8 shows the external connections from the detection circuit to the clocks on the interface board, whilst Figure 5.9 shows the timing diagram for the states of the counters. A full listing of the timing program, 'arctime' is given in Appendix II.

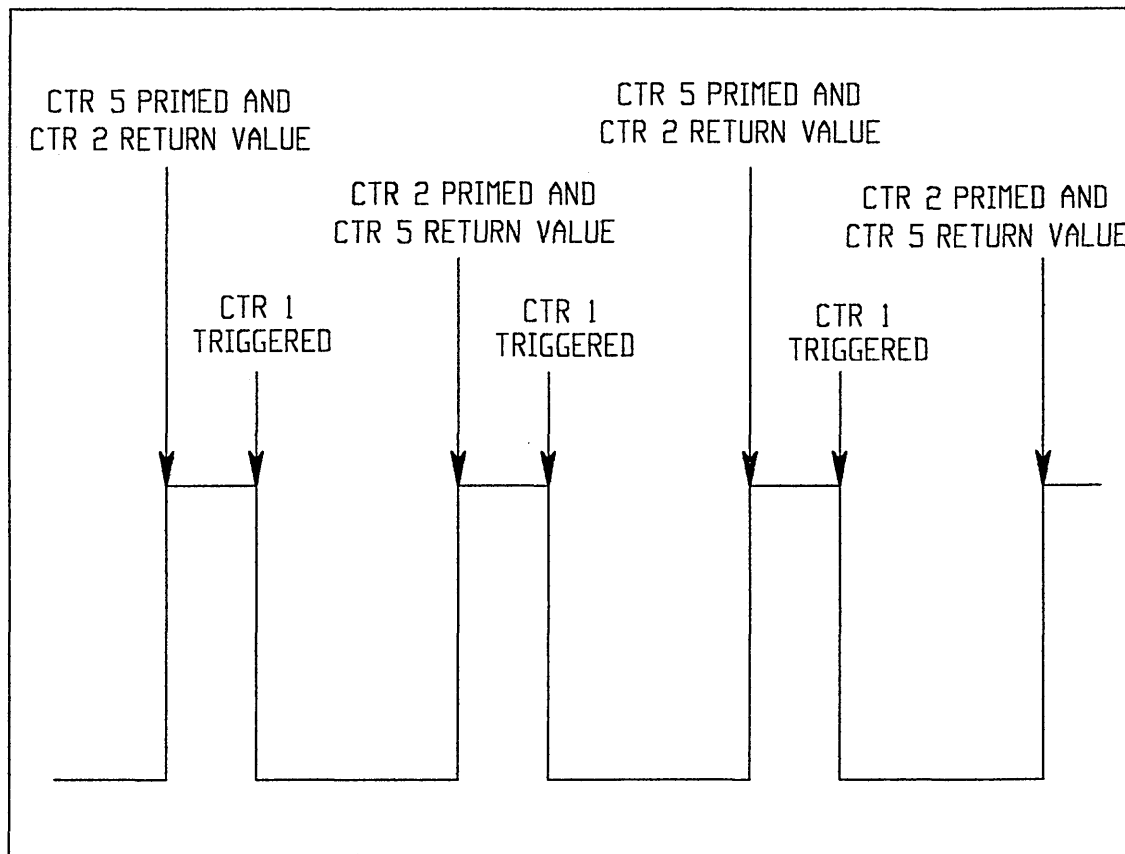


Figure 5.9, The sequence of counter triggering.

The three counters on the AT-MIO board are labelled counters 1, 2 and 5. In this application counters 2 and 5 are used to time the periods between pulses (using the rising edges) whilst counter 1 is used coordinate the process. This is performed by ensuring that the respective counter is zeroed and primed by the time counter 1 detects the falling edge of the previous pulse.

As can be seen in Figure 5.9, counter 1 is configured to detect the falling edge of a pulse and acts to delay the program until the first pulse is detected (CTR.EvRead()).

This also ensures that both counters are detecting different, successive pulses. As soon as the falling edge of the last pulse is detected counter 2 is read (CTR.EvRead()). The first time this occurs no useful data is obtained and the instruction merely serves to prime the counter for successive measurements. Counter 2 is then initiated to measure the period between one rising edge and the next (CTR.Period()), i.e. the next time the counter is read it returns the measured period as the variable *perTEMP%*. The program then pauses until another falling edge is detected and then counter 5 is activated in a similar manner to counter 2 thus ensuring that all pulses are measured in succession. Counters 2 and 5 both use a 1MHz clock to time the periods so ensuring sufficient resolution. A typical orbit is approximately 10 ms thus giving a precision of $\pm 0.1\%$

The timing routine is contained within a loop that allows 1000 operations thus collecting nearly 2000 measurements of the arc orbital period. This data are then saved for analysis by a different program.

5.3.2.3 The experiments.

Experiments were performed upon a number of cathode materials, these were,

- (i) 4 x ASTM B265-79, Grade 2 titanium.
- (ii) 1 x ASTM B551-85, Grade 702 zirconium.
- (iii) 1 x Grade 316 stainless steel.
- (iv) 1 x 99.99% pure aluminium.

Stainless steel and aluminium were chosen as work has been performed on the diffusion coefficient of a random arc on these materials allowing a comparison of values obtained to be made. Titanium and zirconium were chosen as they are widely used in the PVD industry and, as yet, have not had their diffusion coefficients determined.

Attempts were also made to employ molybdenum and copper as cathode materials but unfortunately a stable arc could be struck on neither material. In the case of copper this

was because the cathode quickly became contaminated with aluminium sputtered from the walls of the vacuum chamber. This phenomena was not observed to occur with any of the other cathode materials. In the case of molybdenum, the arc supply could not deliver a sufficiently large current (at the electrode spacing used) to maintain an arc for more than a few seconds.

Some early experiments also attempted to use carbon in graphite form as a cathode material. Whilst highly stable arcs were struck which were successfully steered by the coils the spot moved so slowly (approximately $1 \times 10^{-3} \text{ms}^{-1}$) that the likelihood was that the steering coils would have overheated before sufficient measurements could be made. Future work, using modified steering coils, could include the study of the arc's motion on graphite, its extremely slow motion allowing detailed observation to be made.

For the duration of this experiment conditions were kept as stable as possible. This was done to examine and possibly correct for the effects, observed in the previous experiment, of the change in spot behaviour due to the increasing field magnitudes caused by cathode erosion. All measurements were made at a fixed pressure of 1 mTorr of argon and fixed magnetic field settings of $B_T = 11.2 \text{ mT}$ and $B_N' = 1061 \text{ mTm}^{-1}$. The normal zero was set at 19 mm radius. Where possible the arc current was kept fixed for a particular cathode material (stainless steel requiring a higher current than titanium), although two different currents were used for zirconium. This was done to investigate the effect of arc current upon diffusion coefficient, this is a weak dependence according to the literature (see Section 2.6).

Using the methods detailed above experimental 'runs' were made on the cathode under investigation. A typical run consisting of the measurement of the periods of 2000 spot orbits. A number of such runs were made on each cathode (twenty five in the case of titanium, by which time the arc became less stable and more difficult to trigger. The apparatus had to be opened periodically to allow the viewing port to be cleaned, this resulted in contamination of the cathode which significantly affected the motion of the arc. It was determined experimentally that the velocity approached a steady state value,

and hence that the cathode was clean, after 4 runs (see Section 5.3.3.3). Consequently after pumping down, 4 runs were used to condition the cathode, with results being extracted from the fifth (see Figure 5.10).

As mentioned in Section 2.6 the cleanliness of the cathode is vitally important to the measurement of the diffusion coefficient. Some authors [2, 9] use high temperature vacuum bake out as a cleaning process if a virgin metal surface is required or, in the case that the surface condition is unimportant repeated use of the arc itself.

Measurements were made on 4 titanium cathodes. A total of 25 runs were carried out on each cathode. After 5 runs the apparatus was opened for cleaning and the track erosion was measured using a laser 'tally-surf' profiler. This allowed the determination of the magnetic field profile relevant to each phase of the experiment (this is discussed in more detail in Section 5.3.4.1). All runs were carried out at an arc current of 70A

Experiments were carried out on one cathode of each of aluminium, zirconium and stainless steel. In all cases the cathodes were cleaned by thorough random arcing. In this instance the random arc was used to clean the cathode in preference to the steered arc as the method obscured the view port less rapidly. For aluminium two runs were carried out at an arc current of 70A. Six runs were achieved with zirconium, three at 70A and three at 100A. For stainless steel two runs were carried out at 100A. Between runs using cathodes of differing materials the chamber was thoroughly cleaned of all deposits left by the previous arcing operations.

5.3.3 Analysis of results.

The experiments described in the preceding section yielded a large amount of data concerning the distribution of spot transit times on a variety of cathode materials. This section describes the sorting of these data into a form where they may be analysed and the analysis of the collated data.

5.3.3.1 The distributions of spot transit times.

Each experimental run yielded 2000 values for the spot transit time. These data were saved sequentially in the form of an ASCII file by the program 'arctime'. Using another piece of software, again written using the Lab windows package, the data were imported and analysed. The program 'datnorm' (a full listing is given in Appendix II) performed three major functions; firstly the data were filtered, secondly they were ordered into frequency bins and finally a normal distribution of the same mean and standard deviation as the data was calculated.

Filtering of the data was performed to eliminate erroneous readings occasionally returned by the program 'arctime'. These erroneous readings occurred for one of two reasons. Firstly the spot might be detected on its first passage by the detector, missed on its next but then detected again on its third orbit (the spot moving at the extreme maximum or minimum orbital path). This gave readings approximately twice that expected. The second reason for error remains unexplained: the counters returning a period value of 0. This cannot be explained by the spot moving back into line of sight of the detectors as the setting of the monostable circuit prevents this event from being detected. One possible explanation is that counter 1 is being triggered by the falling edge of a pulse (thus allowing the timing of the next pulse to begin) but then counter 2 or 5 is not detecting the next rising edge. This is possibly due to some interference on the signal, the experimental rig being situated in an extremely electrically noisy environment. The errors rarely constituted more than 1% of the total data and were easily filtered by setting an upper and lower pass limit.

The data were then sorted into bins to allow the plotting of a frequency histogram and subsequent comparison with the theoretical distribution. The division of the data into 17 bins gave a relatively smooth distribution whilst retaining some finer detail. These histogram data were saved to file to allow parameter fitting by another program.

The standard deviation, mean and skew (third moment of the distribution) were also calculated by the program. This allowed the determination of the normal distribution

Supplementary Table 1. The characteristics of the study population

Table 1 shows the characteristics of the study population. The mean age of the study population was 67.5 years (range 50–85 years). The majority of the study population were male (70.5%), and the majority were married (78.5%). The majority of the study population were employed (65.5%), and the majority were living in a city (75.5%). The majority of the study population were of high educational attainment (75.5%). The majority of the study population were of high income (75.5%). The majority of the study population were of high social class (75.5%). The majority of the study population were of high health status (75.5%). The majority of the study population were of high quality of life (75.5%).

Table 1. Characteristics of the study population

Table 1 shows the characteristics of the study population. The mean age of the study population was 67.5 years (range 50–85 years). The majority of the study population were male (70.5%), and the majority were married (78.5%). The majority of the study population were employed (65.5%), and the majority were living in a city (75.5%). The majority of the study population were of high educational attainment (75.5%). The majority of the study population were of high income (75.5%). The majority of the study population were of high social class (75.5%). The majority of the study population were of high health status (75.5%). The majority of the study population were of high quality of life (75.5%).

Table 1 shows the characteristics of the study population. The mean age of the study population was 67.5 years (range 50–85 years). The majority of the study population were male (70.5%), and the majority were married (78.5%). The majority of the study population were employed (65.5%), and the majority were living in a city (75.5%). The majority of the study population were of high educational attainment (75.5%). The majority of the study population were of high income (75.5%). The majority of the study population were of high social class (75.5%). The majority of the study population were of high health status (75.5%). The majority of the study population were of high quality of life (75.5%).

with the same mean and standard deviation as the measured data. The normal distribution data were saved to file to allow comparison to the theoretical distribution by another program.

5.3.3.2 Fitting of the data to the theoretical distribution.

The distributions given by program 'datnorm', described above, can now have a theoretical distribution fitted to them. This is achieved by altering the velocity and diffusion coefficient parameters until the best possible fit between the measured and theoretical distribution. The distance travelled by the arc on its orbit, y , is assumed to be constant, i.e. the arc makes a number of oscillations about the mean radial path in the course of an orbit thus giving a mean orbital distance.

The parameters ν and α for the best fit are chosen by the program 'smirnov' a full listing of which is given in Appendix II. This program was modified from a prewritten pascal subroutine [15] to work under the Quick Basic language. The program uses a grid search method to successively approximate the values for velocity and diffusion coefficient. Initial guesses are made for the values of ν and α based upon earlier results obtained. A step size for each coefficient is then determined (initially one tenth the value of the coefficient). The program then steps through values of ν and α testing for the goodness of fit at each point until a local minimum is found. The point of the minimum and the two bracketing it are then used to determine the minimum of the parabola that passes through the three points. This point having been found the size of the steps taken is reduced on the basis of the number of steps required to find the previous minimum. The process is repeated until the change in the goodness of fit with each iteration is below some predetermined level (~1% in this case).

The goodness of fit test used was changed from the conventional χ^2 test for the comparison of measured frequencies used in the prewritten program to the Kolmogrov-Smirnov (K-S) test for the comparison of measured and continuous distributions [10]. The formula for the calculation of χ^2 test is given by,

$$\chi^2 = \sum \frac{(O - E)^2}{E} \quad (5.11)$$

Where E is the expected value and O the observed value. The K-S test calculates the absolute maximum deviation, D , between the normalised cumulative distributions of the continuous function and measured distribution and is given by,

$$D = \text{Max}_{i=1}^n |F_i - S_i| \quad (5.12)$$

Where F_i is the theoretical cumulative distribution and S_i is the measured cumulative distribution. The advantage of this method is that the curve is equally fitted at every data point instead of, as is the case with χ^2 , weight being given to fitting in the wings of the distribution. This occurs due to the division by the expected value during the calculation of χ^2 shown in Equation 5.11, i.e. in areas of low frequency where errors are likely to become apparent, higher values for χ^2 are returned than would be expected from similar deviations in areas of higher frequency.

After being minimised the D value may then be compared with tabulated or calculated threshold values given at various confidence levels. For the hypothesis that the experimental data are other than from the theoretical distribution to be rejected the D value returned by the K-S test must lie below the tabulated or calculated threshold value. For large n the critical statistic D_{crit} is defined by,

$$D_{crit} = 1.63/\sqrt{n} \quad (5.13)$$

at the 1% confidence level, where n is the number of samples. The D value between the theoretical distribution and the normal distribution of the same mean and standard

deviation as the measured data is also calculated. This gives some means of comparison of the relative goodness of fit obtained.

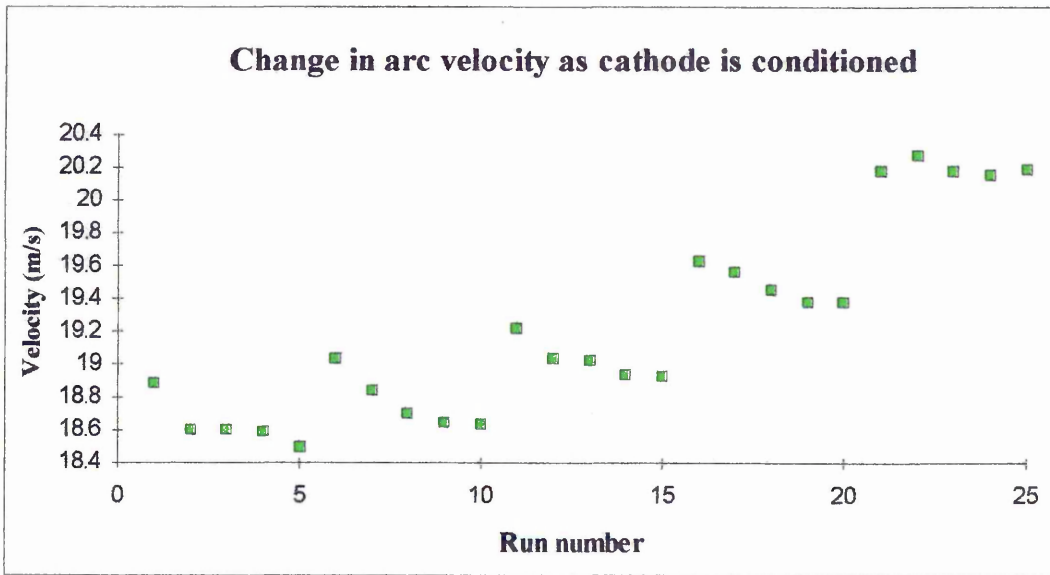


Figure 5.10, The arc velocity stabilising as the cathode is conditioned.

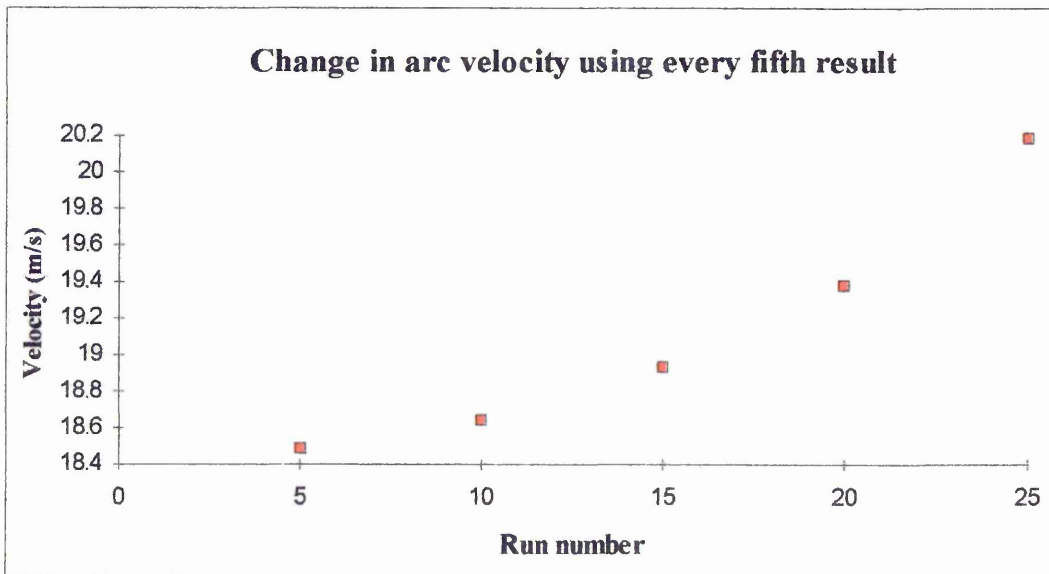


Figure 5.11, The change in arc velocity using stable velocities.

5.3.4 Results and discussion.

The fitting process described above was performed upon all data sets obtained and values for ν and α determined. Figure 5.10 shows a plot of arc velocity versus run number for cathode number 4 and includes all results taken, whilst Figure 5.11 shows the same plot using every fifth result. It can be seen clearly that for the initial four runs of each set, while the cathode is being conditioned, the velocity is higher than would be expected but tends towards a stable value at the approximately the fifth run. In two cases at runs 20 and 25 the final velocity is, in fact, higher than the fourth, this is to be expected as the general trend of increasing velocity on the clean cathode becomes apparent. This behaviour is indicative of a change from the faster type I spot found on contaminated or oxidised surfaces to the slower type II spot found on virgin surfaces. The same may be said for the measurements taken of the diffusion coefficient which are shown as Figures 5.12 and 5.13. In this case the diffusion coefficient settles at a small peak between one set of five runs and the next. This rise in diffusion coefficient may be due in part to a localised rise in the temperature of the cathode surface near the path of the arc. Jüttner et al [9] observe a change in the diffusion coefficient by a factor 1.4 for a change in global cathode temperature from 300K to 1500K. Local heating in this case is very intense due to the confined nature of the spot motion and it reasonable to assume that this heating is responsible for the slight rise in spot diffusion.

Considering the initial results discussed above there are few relevant data to be obtained from readings taken during the cleaning process, therefore all work described here uses either every fifth result (in the case of titanium cathodes) or thorough random arcing (in the case of all other metals) to ensure that any oxide layer or surface contamination is removed and meaningful measurements made.

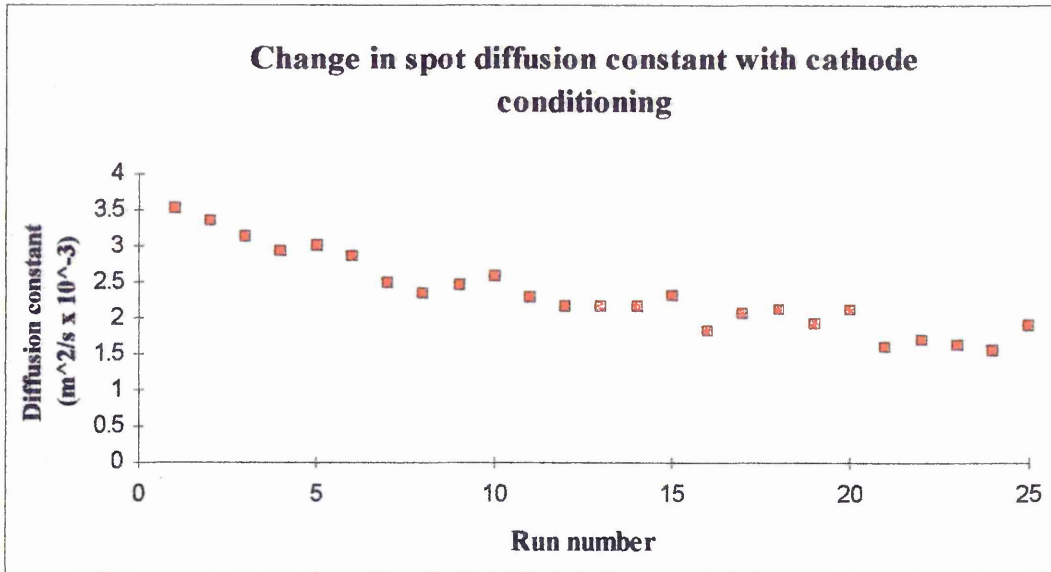


Figure 5.12, The diffusion coefficient stabilising as the cathode is conditioned.

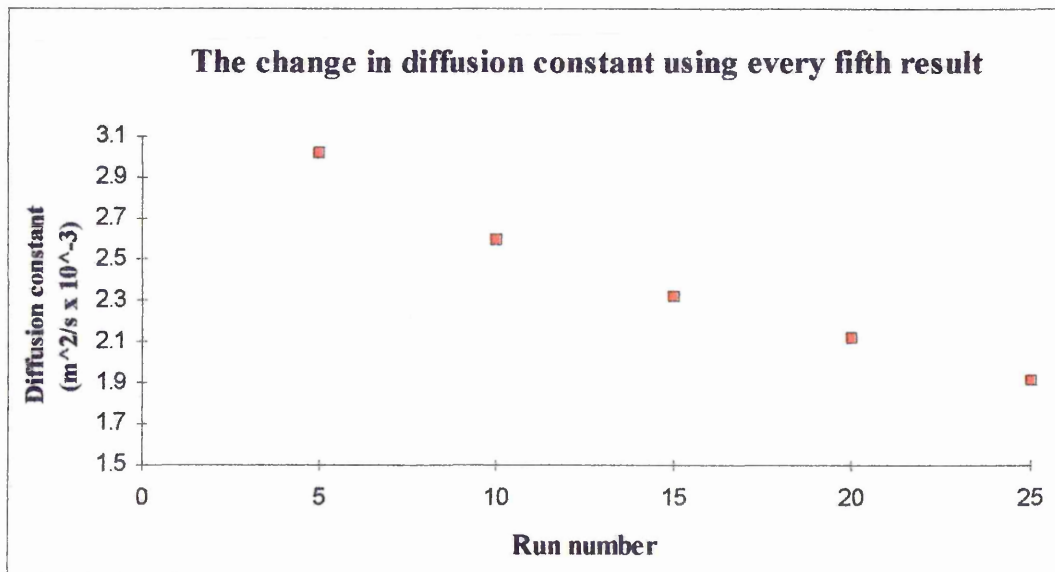


Figure 5.13, The change in diffusion coefficient using stable values.

Table 5.2 Summary of experimental data from titanium cathodes

□ Run number	D_{Model} ($\times 10^{-2}$) $D_{Crit} = 2.7$	D_{Normal} ($\times 10^{-2}$) $D_{Crit} = 2.7$	Current (A)	v (ms^{-1})	α ($\times 10^{-3} m^2s^{-1}$)
Cathode 1					
5	1.14	3.32	70	18.97	2.5
10	1.43	4.1	70	19.27	1.9
15	2.1	8.5	70	19.63	2.2
20	1.68	6.2	70	20.36	1.8
25	1.63	5.9	70	20.78	1.8
Cathode 2					
5	0.7	1.9	70	19.1	3.3
10	1.38	3.82	70	19.34	2.9
15	1.59	12.2	70	19.33	2.5
20	1.76	12.6	70	19.89	2.0
25	1.3	17.6	70	20.63	1.9
Cathode 3					
5	0.69	1.58	70	18.76	3.0
10	1.1	2.8	70	18.63	3.0
15	1.5	4.2	70	19.22	2.2
20	0.9	3.5	70	19.59	1.85
25	1.55	4.8	70	20.1	1.79
Cathode 4					
5	0.57	1.95	70	18.49	3.0
10	0.86	2.8	70	18.64	2.6
15	1.46	4.78	70	18.93	2.4
20	1.71	5.04	70	19.38	2.1
25	1.23	3.8	70	20.19	1.9
Mean values across 4 cathodes					
5	-----	-----	70	18.83	3.1
10	-----	-----	70	18.97	2.8
15	-----	-----	70	19.28	2.3
20	-----	-----	70	19.81	2
25	-----	-----	70	20.43	2.1

Tables 5.2 and 5.3 summarise the experimental data collected. Table 5.2 shows those collected from the 4 titanium cathodes used and presents mean values (taken across the 4 cathodes) for the spot velocity and diffusion coefficient at every fifth run. Table 5.3 shows the values for spot velocity and diffusion coefficient obtained from zirconium,

stainless steel and aluminium cathodes. Both tables give values obtained for the critical statistic for goodness of fit D_{Crit} between the measured data and the fitted model and the measured data and the normal curve with the same mean and standard deviation as the data.

Table 5.3

Summary of experimental results for zirconium, stainless steel and aluminium

□ Run number	D_{Model} ($\times 10^{-2}$) $D_{Crit} = 2.7$	D_{Normal} ($\times 10^{-2}$) $D_{Crit} = 2.7$	Current (A)	v (ms^{-1})	α ($\times 10^{-3} m^2s^{-1}$)
Zirconium					
1	0.97	3.1	70	15.2	4.8
2	1.14	3.67	70	15.2	4.6
3	1.64	5.84	70	15.1	4.3
4	1.27	3.84	100	17.5	4.9
5	2.23	5.35	100	17.3	5.1
6	2.56	5.55	100	17.6	4.6
Stainless steel					
1	0.95	4.55	100	9.9	2.5
2	1.48	5.73	100	9.9	2.8
Aluminium					
1	3.3	12.1	70	8.9	7.7
2	4.02	17.2	70	9.2	7.0

In all cases the value of D between the measured distribution and that predicted by the stochastic model (D_{Model}) was better than the D value between the normal curve and experiment (D_{Normal}). In nearly all cases the value of D_{Model} was below the critical value for a sample of 2000 and consequently the hypothesis that the experimentally measured data is from a distribution other than that predicted by the model is rejected in these cases with a 1% confidence interval. But, in some of the fit tests between experiment and the corresponding normal distribution (particularly at earlier runs, i.e. a shallow erosion track) values below the critical level were also returned. However, visual

inspection of these cases and indeed all measurements (see Figure 5.14) reveals that although a reasonable value of D_{Normal} is returned the measured distributions have a characteristic positive skew (third moment about the mean) that can only be exhibited by the stochastic model.

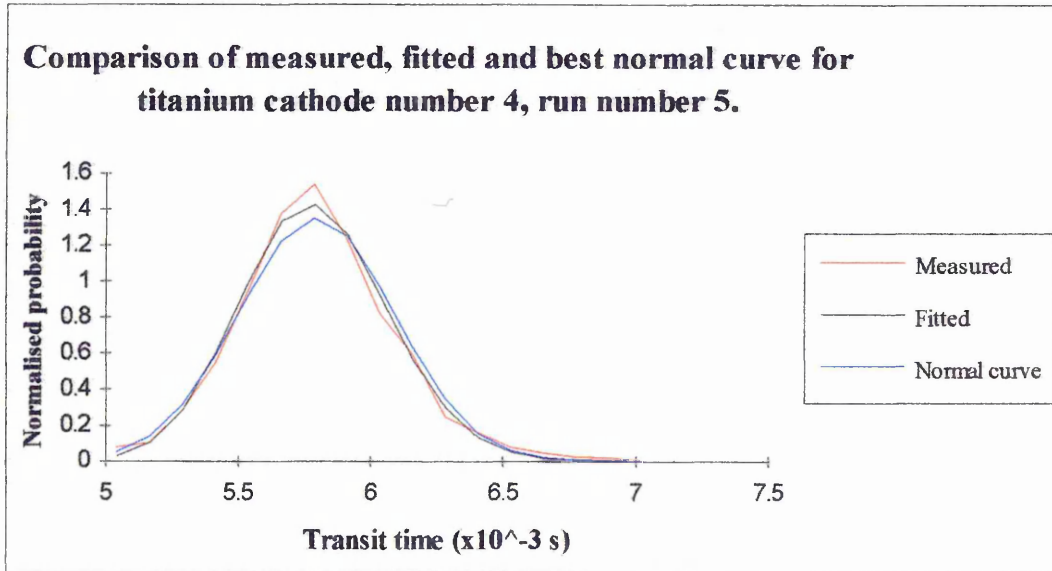


Figure 5.14, Results of fitting the stochastic model to measured data for titanium.

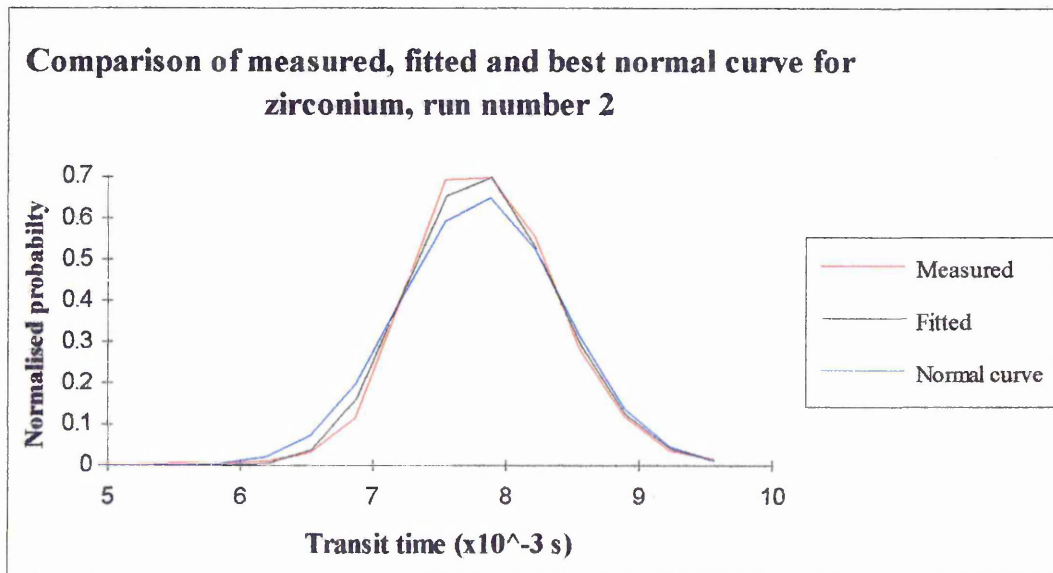


Figure 5.15, Results of fitting the stochastic model to measured data for zirconium.

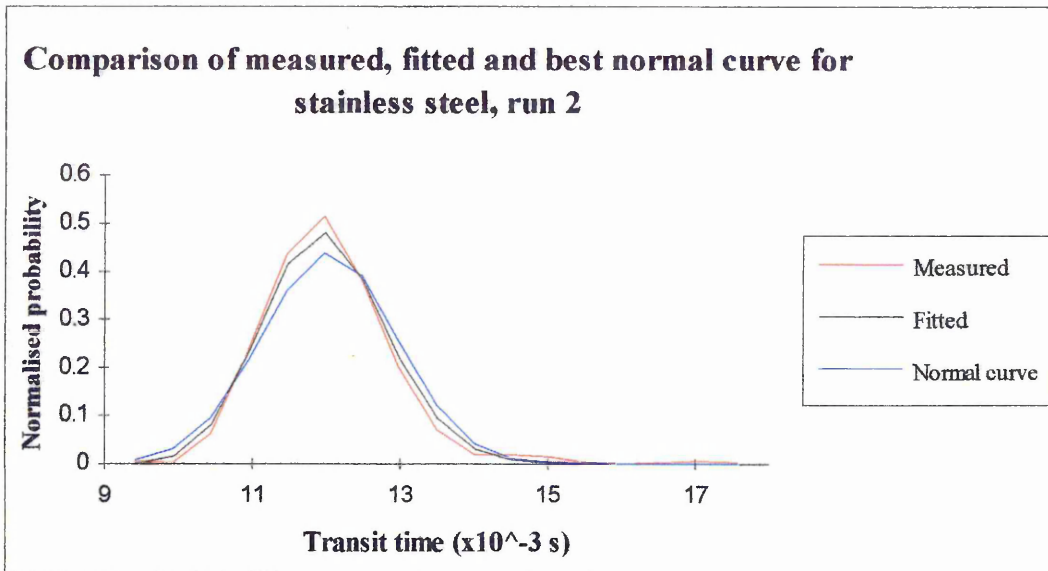


Figure 5.16, Results of fitting the stochastic model to measured data for stainless steel.

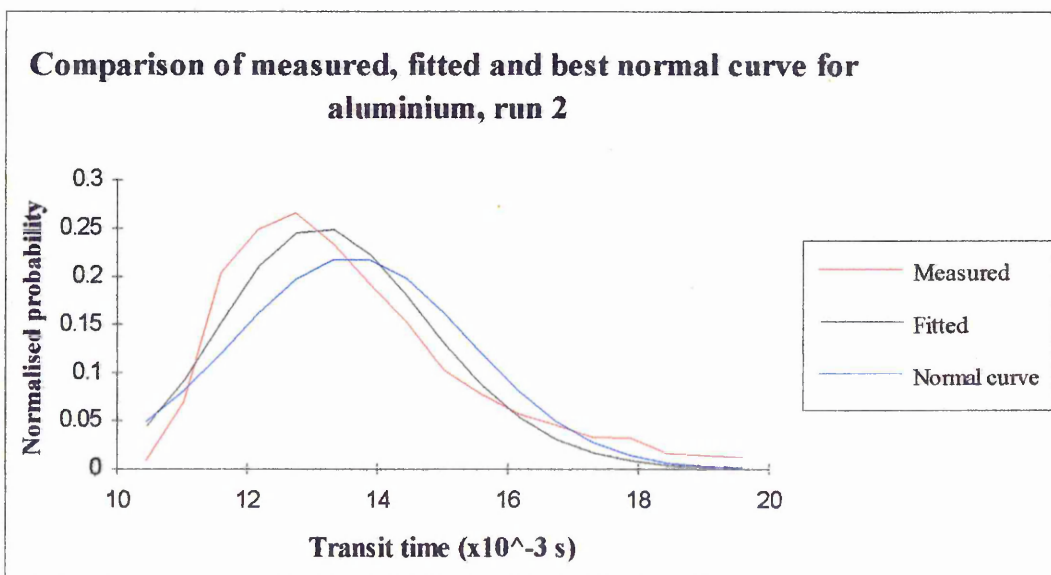


Figure 5.17, Results of fitting the stochastic model to measured data for aluminium.

In the case of aluminium the velocity distributions were broader, considerably more skewed and with a lower mean velocity than those measured for other materials. Correspondingly the D_{Model} values were higher and consistent with rejection of the hypothesis at a 10% confidence interval. The D_{Normal} for aluminium were extremely high and the hypothesis accepted, i.e. the fit rejected.

As a deeper and deeper track is eroded the D_{Normal} values begin to rise significantly above the critical value and any fit is consequently rejected. However the D_{Model} values (which also rise slowly) remain below the critical level in the cases of titanium, zirconium and stainless steel but rise slightly above it in the case of aluminium.

Accepting that in the majority of cases a good fit has been obtained and that accurate values for the spot velocity and diffusion coefficient have been determined, the magnitude of these parameters on a flat cathode and the change in magnitudes with erosion of the cathode (and consequent change in field profile) will be discussed below.

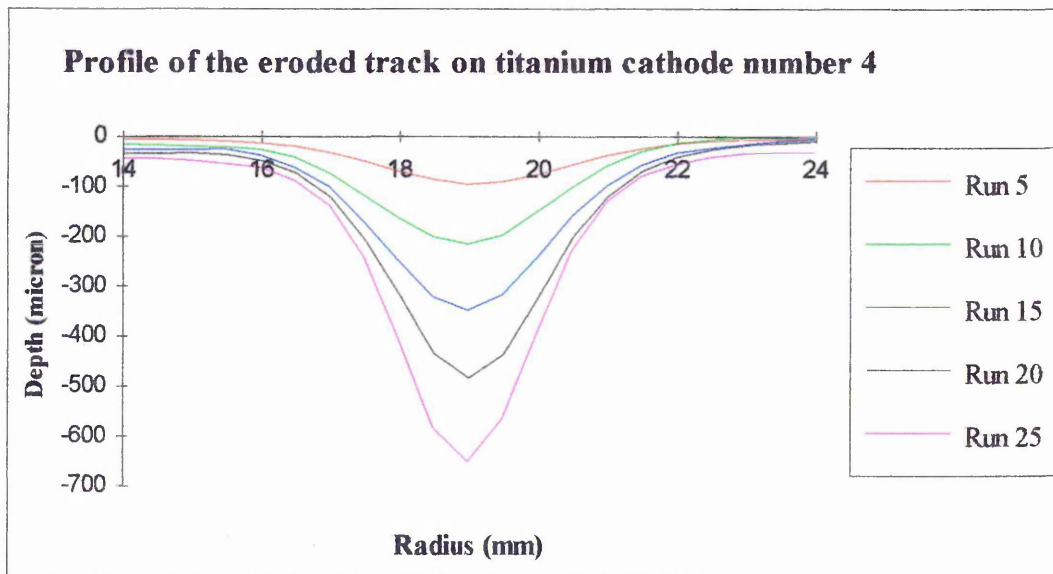


Figure 5.18 The erosion of the track by the cathode spot.

5.3.4.1 The change in the field profiles

During the process of making measurements of the spot motion the arc erodes a deeper and deeper track into the cathode. The deepening of the track decreases the distance between the magnetic coils and the arc spot thus increasing the normal field gradient and transverse field component.

These changes were quantified in the following fashion. Firstly the field profile was measured at a number of erosion depths by using thin plastic sheets as spacers thus giving the change in transverse and normal field components as a function of depth at a number of radii (every 0.5 mm). The erosion profile of the cathode was then measured by means of a laser tally surf depth profiler (manufactured by UBM GmbH.) after every fifth run (see Figure 5.18). The field profile data were then curve fitted using a polynomial fitting routine to allow values for field components to be interpolated at any depth. Altered field profiles were then calculated by determining the new field component magnitude at a number of points (every 0.5 mm) across the eroded profile.

Figure 5.19 shows the transverse field profile after every fifth run. Whilst Figures 5.20 and 5.21 show the change in normal field gradient and transverse field magnitude, respectively, at the same points.

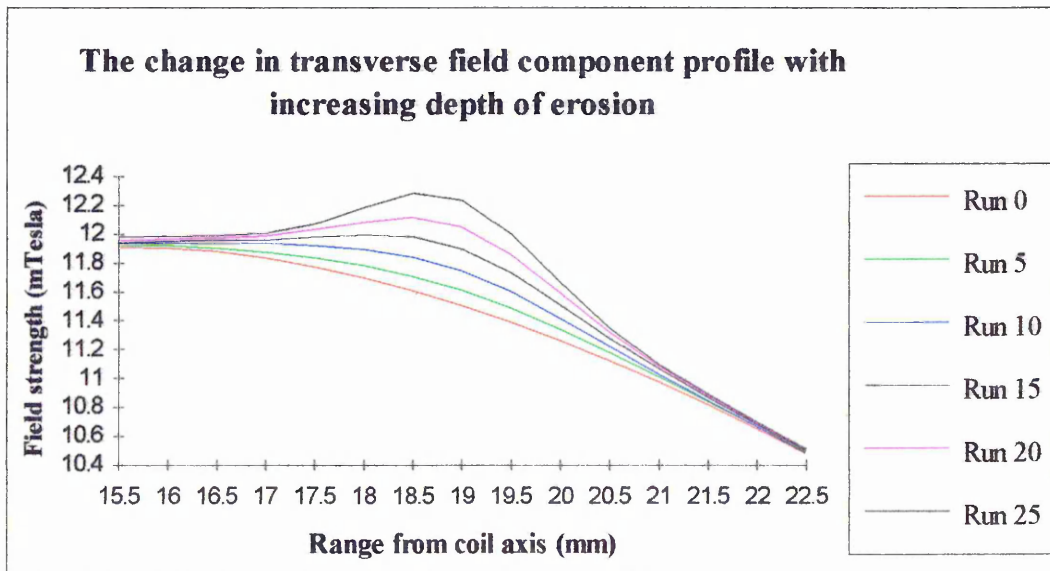


Figure 5.19, The increase in transverse field strength with depth of erosion.

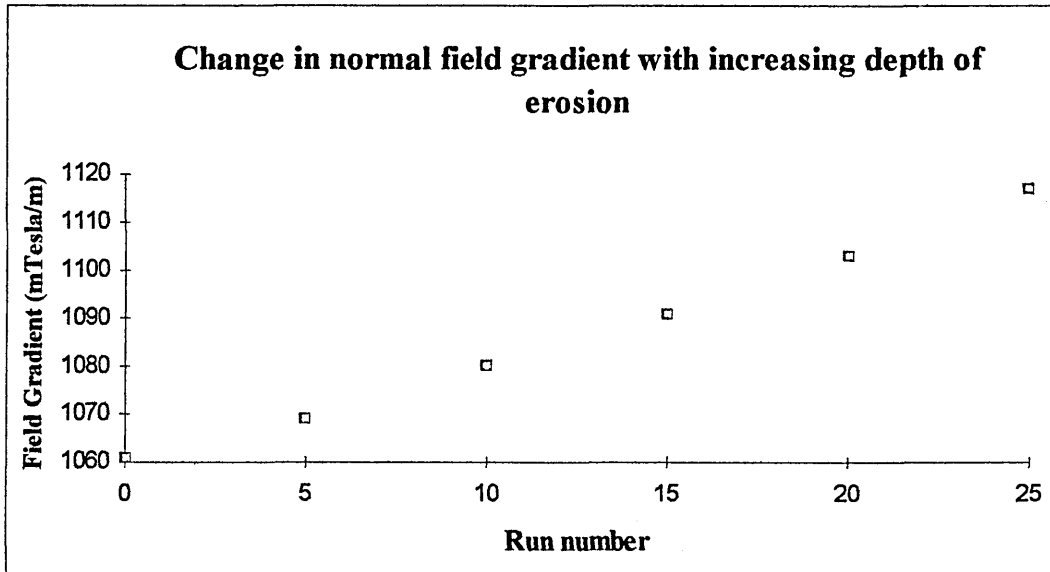


Figure 5.20, The increasing normal field gradient with increasing track depth.

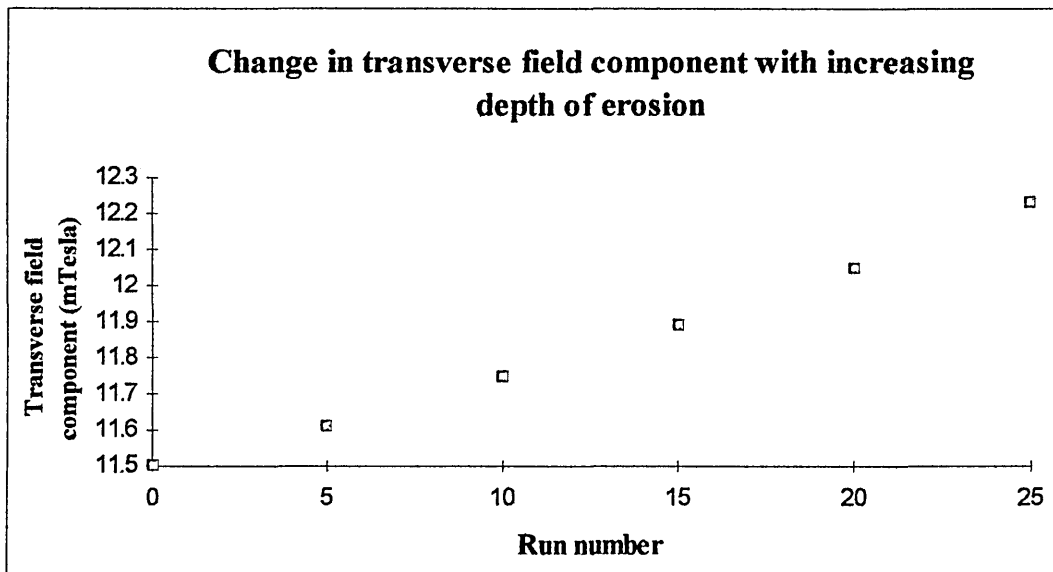


Figure 5.21, Increase in transverse field component with track depth.

5.3.4.2 The spot velocity.

Table 5.2 above, gives the mean spot velocity over the 4 cathodes at every fifth run, i.e. the mean spot velocity was determined by the fitting routine described above for each cathode at every fifth run, the four results (one for each cathode) were then averaged to give a mean velocity at every fifth run.

The spot velocity increases as the arcing process erodes a track into the cathode. Figure 5.22 shows the results for the mean spot velocities given in Table 5.2 plotted against transverse magnetic field strength (determined as described in (i) above). Error bars are estimated from the sum of squares of the differences between the 4 sets of data and are slightly larger than would be expected due to the presence of a systematic error. This error is probably due to inconsistencies in the mounting of the cathode assembly, i.e. the coils were mounted slightly eccentrically with reference to the axis of the cathode, consequently any rotation in the cathode upon reassembly would mean that the arc would track over a shifted circular trench thus altering the field profile presented to it.

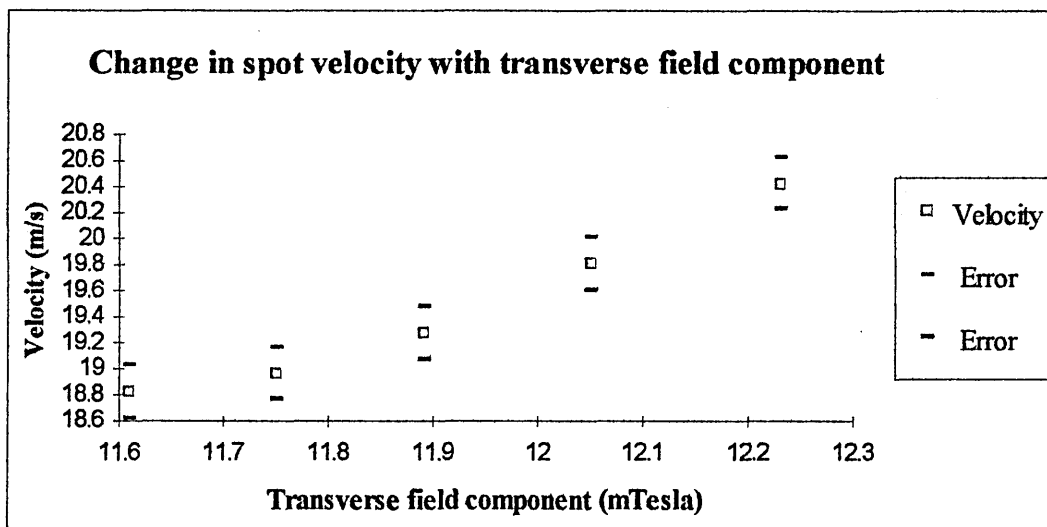


Figure 5.22, The change in spot velocity with transverse field.

From Swift et al [5] an approximately straight line would be expected with a gradient of around 1 ms^{-1} per mTesla. Although a straight line may be fitted to this data within

Week 11: The Great Depression

The Great Depression was a severe economic downturn that began in 1929 and lasted until the mid-1930s. It was characterized by a sharp decline in economic activity, widespread unemployment, and deflation. The stock market crash of 1929 is often cited as the starting point of the depression.

The causes of the Great Depression are still debated, but several factors are widely cited. These include the stock market crash, a sharp decline in consumer spending, and a series of banking failures. Additionally, the Federal Reserve's monetary policy, which aimed to maintain the gold standard, is believed to have exacerbated the crisis.

The impact of the Great Depression was devastating. Unemployment reached unprecedented levels, and many people lost their homes and businesses. The government's response, including the New Deal, aimed to provide relief and stimulate economic growth. However, the depression did not end until the United States entered World War II in 1941.

The Great Depression also led to significant changes in government policy and economic thought. The New Deal introduced a series of programs and reforms that reshaped the role of the federal government in the economy. It also led to the development of Keynesian economics, which emphasized the importance of government intervention during economic downturns.

The Great Depression remains a critical period in American history, serving as a stark reminder of the potential consequences of economic instability. It also highlights the importance of government action in addressing economic crises and the need for a robust safety net for citizens during difficult times.

Keynesian Economics and the Role of Government



The New Deal: A Response to the Great Depression

The New Deal was a series of programs and reforms introduced by President Franklin D. Roosevelt in response to the Great Depression. It aimed to provide relief to the unemployed, stimulate economic growth, and reform the financial system. Key programs included the Social Security Act, the National Industrial Recovery Act, and the Agricultural Adjustment Act.

error, closer inspection would indicate that the dependence is not linear. All subsets of the velocity data exhibiting the same trend of spot velocity increasing more rapidly with increasing erosion and transverse field. However the tangent to the curve at the first data point does appear to have such a gradient of approximately $1 \text{ ms}^{-1}\text{mT}^{-1}$. It is possible that the increase in normal field gradient with depth of erosion is confining the arc more tightly thus reducing the mean orbital distance covered by the spot, i.e. the excursions of the spot from the mean orbital radius are reduced and the spot is required to cover a smaller component in the radial direction. Thus it will appear that the arc velocity has increased

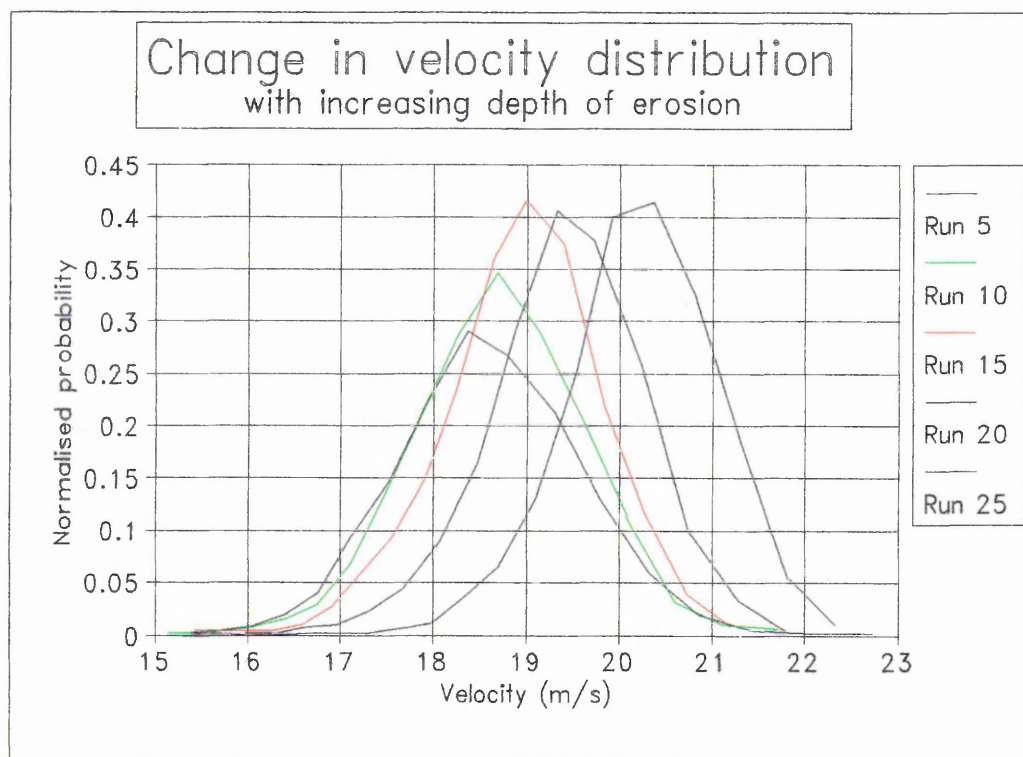


Figure 5.23, The change in transit time profile with increased erosion.

The increase in velocity is therefore likely to depend upon two factors. Firstly the natural increase in velocity due to the increase in transverse field component and secondly the reduction in mean orbital distance due to the increase in normal field gradient. It is also possible that the formation of the arc track may provide some further

confinement of the spot. This and suggestions for further work to examine reasons why such confinement would exist are discussed in detail in Chapter 6.

Figure 5.23 shows a plot of the velocity distributions at every fifth run. The change in the nature of the profile can be clearly seen with the profile shifting to higher velocity and becoming narrower (decreased diffusion coefficient) with increasing depth of erosion and field magnitudes. The change in diffusion coefficient with erosion is discussed in detail in the following section.

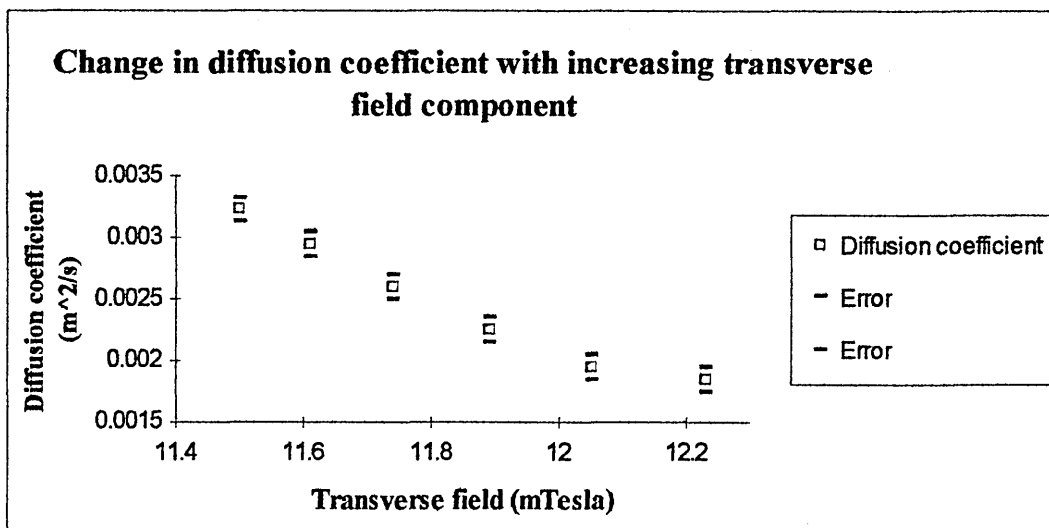


Figure 5.24, Decreasing trend of diffusion coefficient with increasing depth of erosion.

5.3.4.3 The diffusion coefficient.

As was discussed in detail in Section 2.6.1.3 the diffusion coefficient of the randomly moving cathode spot has been determined by a number of authors [1, 2, 9, 11, 12, 13, 14]. Jüttner and Daalder both use high speed photography to analyse brief periods of spot motion upon a surface to determine the rate of spot diffusion in UHV. The experiments described in this section were conducted in a stabilising background of 0.75×10^{-3} mBar of argon although experimental evidence suggests that below a critical value (0.1 mBar for argon) the diffusion coefficient is unaffected by gas pressure [3].

The diffusion coefficient of every fifth distribution for each of the cathodes was determined using the fitting routine described in Section 5.3.3.2. The results were averaged over the four cathodes and plotted against transverse magnetic field in a similar manner to the velocity data described above. Examining Figure 5.24 it can be seen that values found for titanium decrease with erosion/transverse field in the range $3.0 \times 10^{-3} \text{ m}^2\text{s}^{-1}$ to $1.9 \times 10^{-3} \text{ m}^2\text{s}^{-1}$, but the rate of change appears to decrease with increasing erosion/magnetic field. Values for α determined for other materials were limited in number and determined without significant erosion of the cathode.

Table 5.4
Summary of diffusion coefficients found

Author	Ti ($\times 10^{-3} \text{ m}^2\text{s}^{-1}$)	Zr ($\times 10^{-3} \text{ m}^2\text{s}^{-1}$)	Al ($\times 10^{-3} \text{ m}^2\text{s}^{-1}$)	SS ($\times 10^{-3} \text{ m}^2\text{s}^{-1}$)	Current (A)
Current work	3.23 ³	4.6	-----	-----	70
Current work	-----	4.9	7.4	2.7	100
Daalder [2]	-----		1.4	-----	21.6
Jüttner [12]	-----	-----	9	1	20-200
Jüttner [13]	-----	-----	9	3	20-200
Hantzsche [1]	-----	-----	-----	0.6	Not given

The values for α measured are summarised in Table 5.4, along with values found for α by previous authors. In the case of titanium the value given is that extrapolated back

³This value is extrapolated from the available data.

from the measured data to the point where a flat cathode existed. This was achieved by using a polynomial fitting routine which allowed the diffusion coefficient at run 0 to be estimated. In the other cases values are averaged from the data available. It is interesting to note the small change in α with current for zirconium: a mean value of $4.6 \times 10^{-3} \text{ m}^2\text{s}^{-1}$ for the first three runs at 70A and a mean value of $4.9 \times 10^{-3} \text{ m}^2\text{s}^{-1}$ for the next three runs at 100A. This weak dependence is confirmed in the literature [1, 14]. In addition to this some of the results given for other authors are for virgin metal surfaces whereas those determined in this work are for an eroded surface. However investigations by Jüttner et al [9] on virgin and eroded cathodes show that there is very little change in α with erosion (i.e. surface texture, not erosion depth) with changes just exceeding the uncertainty of the measurements.

In comparing values for α two factors must be considered. Firstly some of the measured diffusion is attributable to motion in the radial direction, i.e. changes in the path length travelled by the spot leading to a spread in the velocity distribution. Secondly a correction factor of approximately 0.625 must be applied to Jüttner's results (see Section 2.6.1.3).

The first of these factors would explain the observed trend of α with erosion and consequent increase in transverse field and normal field gradient. As discussed in the previous section any increase in these field components leads to greater confinement of the arc and hence a smaller contribution to the diffusion coefficient from radial motion. The fact that α appears to tend towards a stable value at later runs and higher fields would seem to suggest that the contribution from radial motion is being minimised at these points by the increase in spot confinement. This increase may not all be attributable to increased field strengths but may be due in part some other phenomena noted in Section 5.3.4.2 (ii) above. This would imply a contribution from radial motion of the order or 40%, the value for α changing by this amount from run 0 to run 25 (estimates of this contribution to α to made by considering the possible spread of orbital distances also give values of 40-50%). In the light of this assumption it would seem more valid to

compare the results presented here for an eroded cathode with the results of other authors. This matter is discussed in detail in Chapter 6 where suggestions are made for future work to test this theory.

Allowing for these factors there is good agreement between the results of Jüttner and the results presented here for aluminium and between the results of Jüttner and Pursch and our results for stainless steel. Later work by Hantzsche et al. show an order of magnitude difference between results for stainless steel. The difference between these results could well be due to a different grade of stainless steel being used (the grade used by Hantzsche et al. is not stated).

5.4 The field dependence of the diffusion coefficient.

According to the stochastic model the diffusion coefficient α in direction of retrograde motion should have no dependence upon the transverse field component or the normal field gradient (see Equation 5.2). This section briefly describes a short experiment conducted to test the existence of any such dependence.

5.4.1 Experimental details.

Using the equipment and software described in detail in Section 5.3.2 velocity distributions were measured for a range of coil settings (and hence transverse field strengths and normal field gradients). All experiments were conducted on a titanium cathode in a background pressure of 0.75×10^{-3} mBar of argon, at an arc current of 70A and with the normal field zero set at 19 mm.

Thirty runs were conducted (the first four of each group of five were used to condition the cathode). Each run again consisted of the timing of 2000 orbits of the arc spot. At every fifth run the coils were adjusted to the required field setting and data collected. At the thirtieth run the coils were reset to the currents used at run five. This allowed an estimate for the overall trend in the diffusion coefficient to be made at a constant field

(i.e. the trend of α with depth of erosion) and an approximate correction applied to data collected at different field settings.

The results were analysed by software as described in Section 5.3.3 and the best fit values for ν and α obtained for each field setting. Table 5.5 shows the field settings used and the values for ν and α calculated.

Table 5.5
Values of ν and α obtained at different magnetic field settings

Run number	B'_N (mTesla m ⁻¹)	B_T (mTesla)	ν (m s ⁻¹)	α (m ² s ⁻¹)
5	1270	11.69	20.5	2.82
10	1213	11.2	20.0	2.61
15	1161	10.33	19.42	2.25
20	1066	9.89	18.85	2.43
25	992	9.29	18.32	2.71
30	1270	11.69	23.0	2.05

5.4.2 Results and discussion.

Figure 5.25 shows the values obtained for α plotted against transverse field, the two points at 11.69 mTesla being the fifth and thirtieth runs. Examining this graph several points become apparent. Firstly it is possible that the diffusion coefficients obtained for runs 5 to 30 are the same within error (one result in three would be expected to lie outside one standard deviation from the mean). Secondly the α value obtained for run 30 is substantially lower than those for the previous 25 runs. This would seem to indicate that the possible trend (noted in Section 5.3.4.3) of decreasing α with depth of erosion due to some confining effect of the track is being exhibited here. Thirdly,

assuming that there is a trend apparent within runs 5 to 25, this would seem to show an initial decrease in α with decreasing transverse field up to run 15 (in opposition to the trend observed in Section 5.3.4.3). This followed by an increase in α with decreasing transverse field for runs 20 and 25. Finally the values for transverse field given are those measured for a flat cathode: some correction to these values (up to 10% in the case of run 30) must be expected.

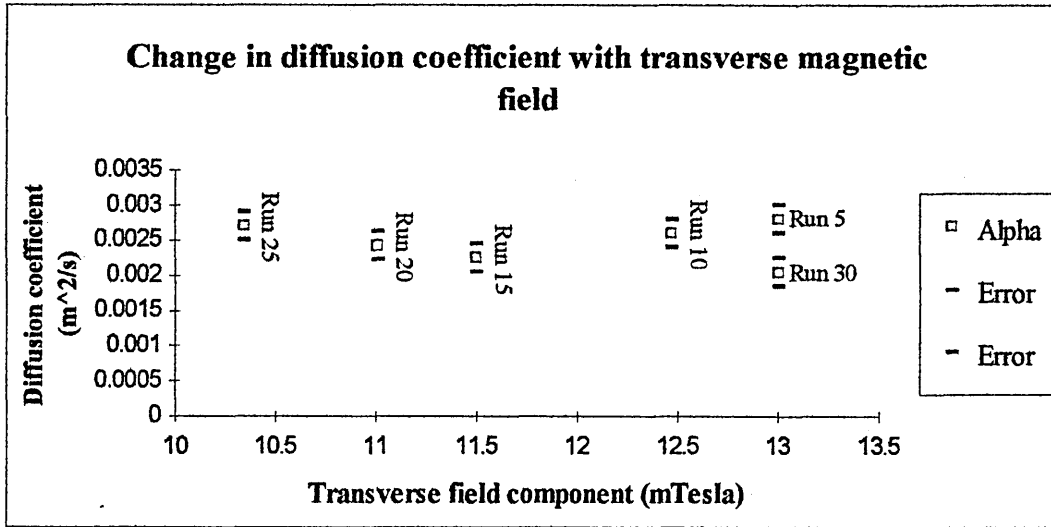


Figure 5.25, Change in diffusion coefficient with magnetic field.

Considering these facts one possible explanation for the observed trend is as follows. For runs 5 to 15 the transverse field magnitude and normal field gradient are high. The spot is thus well confined and, as a track is eroded and the spot confined further, the amount of diffusion is reduced. At some point between runs 15 and 20 a field setting is reached where the spot is no longer so well confined that it must reside in the eroded track and can play upon the flat cathode surface. This would have two consequences; firstly the magnitude given in Figure 5.25 for transverse field at these points is likely to be a more accurate measure of the field there, i.e. whilst the spot is moving outside the track there is no artificial increase in the magnetic field to be considered. Secondly if the existence of the trench does have some confining effect upon the spot then this

The first part of the course covers the basic concepts of set theory, including the definition of a set, the operations of union, intersection, and complement, and the properties of sets. We then move on to the study of functions, which are mappings from one set to another. This includes the definition of a function, the domain and range of a function, and the properties of functions. The second part of the course covers the study of real numbers, including the properties of real numbers, the decimal representation of real numbers, and the operations of addition, subtraction, multiplication, and division. We also study the properties of exponents and radicals, and the properties of logarithms.

Chapter 1: Set Theory

1.1. The Concept of a Set

1.2. Operations on Sets

$$A \cup B$$



1.3. Properties of Sets

1.4. Functions

1.5. The Real Number System

Chapter 2: Real Numbers

The real number system is the foundation of most of the mathematics we study. It includes the rational numbers, which can be expressed as fractions, and the irrational numbers, which cannot be expressed as fractions. We study the properties of real numbers, including the properties of addition, subtraction, multiplication, and division. We also study the properties of exponents and radicals, and the properties of logarithms. The real number system is a complete ordered field, which means that it has all the properties of a field, and it is also ordered. This means that we can compare real numbers, and we can find the least upper bound of a set of real numbers. The real number system is also complete, which means that every Cauchy sequence of real numbers converges to a real number. This property is essential for many of the results in calculus and analysis.

confinement will be lost when the spot moves out of the trench. These two effects may combine to decrease the amount of confinement of the spot and so more diffusive behaviour is exhibited. At run 30 the spot is again confined to the trench by a stronger field (also now increased by the depth of the track) and the amount of diffusion reduced accordingly.

Considering the number of effects at work upon the spot during this experiment it is hard to draw a firm conclusion pertaining to the change in spot diffusion in the direction of driven motion with magnetic field or even whether there are any changes. There remain a number of experiments to be performed to separate the dependencies of spot diffusion upon spot confinement, spot confinement upon track depth and the erosion profiles produced by differing field profiles. This section is the subject of discussion in Chapter 6 where possible further work is suggested to test these dependencies.

5.5 Summary of chapter.

This chapter has presented experimental work designed to examine the dependence of motion of the arc spot upon applied magnetic field. The results of these experiments have subsequently been compared to a new stochastic model of arc motion.

Three experiments have been performed. Firstly the dependence of the confinement of the spot in the radial direction upon transverse field component and normal field gradient has been tested for a titanium cathode (experiment 1). Secondly the distribution of spot orbital transit times has been measured for four titanium cathodes and one cathode each of zirconium, 316 stainless steel and aluminium. The arc velocities and spot diffusion coefficients for these materials have been determined (experiment 2). Finally the change in spot diffusion coefficient with magnetic field has been measured (experiment 3).

Comparisons with the stochastic model have been very favourable with several aspects of the model comparing well with experiment. This comparison has been limited in some respects by the unforeseen high rate of cathode erosion and consequent change in field profiles. This has led to efforts being made to account for the change in magnetic fields. This has been successful in the case of experiment 2, limited success has been achieved in the case of experiment 1 and further work is required in the case of experiment 3.

In the case of experiment 1 (spot confinement) the predicted straight line relationship between confinement and a function of the transverse field component and normal field gradient is observed within error. This straight line also passes through the origin, as would be expected, within error. The predicted profile of spot confinement as a Gaussian is not observed when considering the raw data. However, considering the change in field profile with erosion, corrections to the expected degree of confinement give a good comparison.

Experiment 2 (spot transit times) compares very well with predictions made by the stochastic model. The measured data were accepted as being from the predicted distributions within a 1% of a type 1 error in all cases but one (aluminium). The mean spot velocities and spot diffusion coefficients have been measured for a number of

materials. New data for the diffusion coefficients of titanium and zirconium are presented. Additionally diffusion coefficients for aluminium and stainless steel have been determined and compared with measurements made by other authors. Whilst good agreement is reached between results for both materials in some cases there is an order of magnitude difference in some instances. In the case of stainless steel this may be attributable to a different grade of material being used.

Experiment 3 whilst possibly showing no change in diffusion coefficient with magnetic field (as predicted by the stochastic model) is limited by a lack of data. Several possible trends are observable within this data although further work is recommended to examine the dependencies of spot diffusion upon and spot confinement and spot confinement upon track depth.

References

- [1] E. Hantzsche, B. Jüttner, H. Pursch,
J. Phys. D Appl. Phys., **16**, L173, (1983).
- [2] J.E. Daalder,
J. Phys. D Appl. Phys., **16**, 17, (1983).
- [3] S. Anders, B. Jüttner,
I.E.E.E. Trans. on Plasma Science, **19**(5), 706, (1991).
- [4] C.M. Care,
J. Phys. D Appl. Phys., **25**(12), 1841, (1992).
- [5] P.D. Swift, D.R McKenzie, I.S. Falconer, P.J. Martin,
J Appl. Phys., **66**(2), 505, (1989).
- [6] P. Walke, R. New, C.M. Care,
Accepted for publication in Surf. Coat. Tech.,
Proceedings of ICMCTF 1994, San Diego, (1994).
- [7] C.M Care,
Internal communication.
- [8] R.S. Data sheet No. F14784.
- [9] B. Jüttner, H.Pursch, V.A. Shilov,
J. Phys. D Appl. Phys, **17**, L31, (1984).
- [10] Basic statistical methods for engineers and scientists,
J.B. Kennedy, A. Neville, 3rd edition, Harper andRow, New York, (1986).
- [11] B. Jüttner,
Beitr. Plas,a Phys., **19**, 25, (1979).
- [12] B. Jüttner,
J. Phys D Appl. Phys., **14**, 1265, (1981).
- [13] B. Jüttner, H. Pursch,
Proc. 4th Int. Symp. on switching arc phenomenon, Lodz, Poland, 209, (1981).

- [14] J.E. Daalder,
J. Phys D Appl. Phys., **16**, L177, (1983).
- [15] Philip R. Bevington, D. Keith Robinson,
"Data reduction and error analysis for the physical sciences",
Second Edition, McGraw-Hill, New York, (1992).

Chapter Six

Summary and further work.

The purpose of this chapter is two fold; firstly to summarise experimental work performed (presented in Chapters 4 and 5) and secondly to offer suggestions for further work which would possibly elaborate upon results presented here. In addition to this several ideas are presented for further work that whilst not directly related to work presented here would be of interest in as much as it would add to existing experimental evidence concerning such controversial parameters as the spot displacement and spot residence time.

6.1 Summary.

Chapter 4 described the design and construction of a novel two coiled electromagnetic steering system and associated vacuum and control system. The two coil system allowed the arc to be steered on a circular path of continuously variable radius thus giving possibilities of the even erosion of the entire cathode surface and the development of multi-part cathode system. It was noted that scaled up to a commercial level this process could offer many advantages.

Such a system was initially modelled by employing a computer program, using a numerical solution of the Biot-Savaart model to give off axis field values for two coaxial coils. The model was shown to be very accurate with errors typically less than 1%. Due to physical restrictions it became apparent that a purely electromagnetic system of coils of a suitable power would not fit inside the space available within the vacuum chamber and consequently a soft iron core was added to boost the coils outputs. Whilst the addition of the core was shown to dramatically improve coil performance it did not severely affect the coil geometries thus allowing the basic design modelled previously to be used. This new system was modelled on a semi-empirical basis (using field profiles measured from the coils at a fixed coil current) with sufficient accuracy to allow the production of prototype coils.

The associated vacuum system was constructed from an existing Genevac unit. It consisted of a circular aluminium chamber with a number of side ports. The arc current was supplied by a commercial supply capable of delivering 100 A at up to 100 V. The background gas pressure of argon was controlled by either a manually controlled needle valve (in the case of early experiments) or a commercially available feedback system. This consisted of a capacitance manometer pressure transducer, an automatic proportional solenoid gas valve and a feedback control unit

The complete system was able to provide complete control over the arc for a range of orbital radii from 1 cm to 5 cm and for a practical range of argon background pressures from 1 mTorr to 20 mTorr. It was anticipated that this initial design could be improved to extend the range of arc control thus encompassing the entire cathode.

Chapter 5 described three experiments performed to test the motion of the arc under the influence of an applied steering field and compared the results of these experiments with new model arc motion.

The distribution of the orbital radii of the arc spot was measured. According to the stochastic model the arc is confined by a function of the normal field gradient and transverse field component. This relationship between the arc confinement and this function should be linear and pass through the origin. The probability density function for the arc position in the direction of confinement, i.e. the radial direction, should be a normal distribution.

Approximately 100 photographs were taken of complete arc orbits at each of eleven field settings. In addition to this 430 photographs were taken of the arc at a 12th setting to allow a more detailed investigation of the distribution of arc radii.

The standard deviation of the arc radius was calculated at each of the field settings and was plotted against the function of the steering fields. The relationship was shown to be linear and pass through the origin within error, thus in agreement with the stochastic model (although not unambiguously).

The distribution of arc radii at the twelfth setting was plotted and compared with a normal distribution of the same mean and standard deviation as the data. The measured data were noticeably skewed and a good comparison was not observed for the bulk of the distribution. This was explained by way of the change in magnetic profile with depth of erosion. A new, modified distribution was plotted that was in much closer agreement with the central part of the distribution thus supporting this supposition

The distributions of spot transit times were measured for four cathode materials; titanium, zirconium, aluminium and 316 stainless steel. The stochastic model predicts the probability density function for the spot position in the direction of driven motion and gives a modified distribution if the spot were to be observed moving past a fixed position.

Experiments were performed upon 4 titanium, 1 zirconium, 1 stainless steel and 1 aluminium cathodes. All measurements were made at a fixed argon pressure, arc radius and confinement and where possible the arc current was kept constant. In the case of titanium twenty five runs were made on each cathode. It was shown that the first four runs of each group of five (the chamber being opened for inspection every fifth run) exhibited type I spot behaviour and consequently the data from these runs were not used. Every fifth run gave a valid distribution of 2000 orbital transit times. With all other cathode materials as many runs as possible were made with the random arc being used to clean the cathode.

Frequency histograms of the data were produced. These histograms were then compared to theoretical distributions predicted by the stochastic model. Comparison was made via the Kolmogorov-Smirnov test for comparing continuous functions with grouped data (the chi-squared test being shown to be unsuitable for this application). In all cases for titanium, zirconium and stainless steel the fit was accepted at 1% confidence, thus strongly supporting Care's model. In the case of aluminium one fit was accepted at 10% confidence, whilst the other was narrowly rejected at this level. The determination of the fit also returned values for the mean spot velocity and spot diffusion coefficient.

Also measured were the change in arc velocity and spot diffusion with cathode erosion and consequent change in magnetic field strength. These parameters (averaged over the four titanium cathodes) were plotted against increasing run number, erosion depth and transverse field component. It was noted that the mean arc velocity increased more rapidly with transverse field than would be expected, whilst the spot diffusion coefficient decreased with transverse field when a constant value would be expected. The high rate of velocity change was explained by an increase in confinement of the spot as a track was eroded on the cathode, although not all this increase could be attributed to an increase in the magnetic field strength. The change diffusion constant was similarly explained by an increase in the level of arc confinement.

Results for diffusion coefficients measured for aluminium and stainless steel were compared with those determined by other authors. Good agreement was shown between measurements by some authors and the present work, whilst an order of magnitude difference existed between others. The diffusion coefficients of titanium and zirconium had not previously been measured and new results for these materials were presented.

The change in spot diffusion coefficient was measured as a function of magnetic field. According to the stochastic model the magnitude of the diffusion constant should not change with the magnitude of the steering field. The spot diffusion coefficient was measured for five different settings of the steering coils, data being collected at every fifth run on a titanium cathode. The measured spot diffusion coefficients were then plotted against the transverse field component. Whilst the possibility existed that the data was flat within error it was also possible that the diffusion coefficient was being affected by a similar confining effect as noted above. Further work was recommended here before any firm conclusions could be drawn.

In conclusion it may be said that the majority of the work detailed in Chapter 5 would seem to support Care's description of the motion of the cathodic arc spot as a stochastic process. It now remains to test the level of this support by examining the distributions of

spot positions more rigorously to allow a more detailed comparison to be made. Suggestions for how such investigations could be made are raised below.

6.2 Recommendations for future work.

Examining the results presented in Chapter 5 several areas for further and more detailed study become apparent, these are discussed below. In addition to this several ideas are discussed for work that might have been performed had this project moved in a different direction.

(i) A third steering coil.

The addition of a third, coaxial, steering coil would allow the independent control of the transverse and normal fields whilst maintaining a fixed normal zero. This would enable further experiments to be conducted on the confinement of the arc with a view to separating the dependence of the spot confinement on the normal field gradient and transverse field component. It would therefore be possible to test the accuracy of Care's assumption of the nature of the spot confinement.

It would also be advantageous to use more accurate and less time consuming method of measuring the spot's orbital radius than a still camera. The use of a photo-diode array would not only alleviate these problems but would enable simultaneous measurement of many thousands of orbital radii and transit times. This would have two immediate advantages. Firstly, the extent of any additional confinement effect as a track is eroded could be directly monitored. Secondly, the effect of this confinement upon the spot diffusion coefficient and velocity could be simultaneously measured.

On a practical basis, the use of this system with commercial coating apparatus would allow even erosion of the cathode by a spot of predetermined confinement and independently controlled velocity. The spot may be swept over the whole cathode whilst maintaining a velocity that deters the production of macro particles.

(ii) Machined trenches.

Another area that warrants closer inspection is the effect of the trench upon the confinement of the spot and any consequent effect this has on the spot diffusion and mean path length and velocity. One possible solution to this is to artificially create trenches of suitable geometries whilst exploiting the controllable nature of the coils to change the field geometry at the bottom of the trench, i.e. the coils could be set to correct for the current depth of erosion thus keeping fields constant as the track is eroded. In tandem with experiments proposed above in (i) any effect of the physical presence of the trench could be determined and quantified. This would allow determination of the dependencies of spot diffusion and velocity upon a number of parameters whilst correcting for the change in spot confinement.

It would also be of interest and require a minimum of extra preparation to examine the macro particle production of a cathode as a function of the trench depth and steering fields. This information would be of value to commercial coaters enabling the fine tuning of steering arrays for the minimum production of macro particles.

(iii) 'Before and after' microscopic study of cathodes.

If the spot indeed ignites at surface features and continues as a type I spot until all contamination and surface features have been removed then it would be of interest to follow this process. Using a scanning electron microscope it would be possible to perform 'before and after' microscopy on a small section of the cathode surface and study the evolution of the arc track upon a fresh cathode.

The cathode could be initially stamped with two marks (made by, for example, a micro-hardness indenter). This would allow the correct orientation of the target after arcing and the indexing, before arcing, of a number of prominent surface features. These features catalogued and the cathode cleaned by high temperature bake out a number of short (microsecond) arc pulses could be played upon the cathode surface. After each pulse the cathode would be removed and the indexed features studied.

This experiment would provide valuable information upon the location and nature of arc ignition and the transition from type I to type II spot formation.

In addition to this the experiment could be repeated with eroded cathodes and prominent crater edges indexed by the same method. Studies could then be made of the mean spot displacement which is important in determining the rate of spot diffusion (see Section 2.6.1).

(iv) High speed photography.

Several runs were made by another author using the apparatus described in Chapter 4 and employing a segmented cathode (see Section 1.1.3). In these instances high speed motion photography was used very successfully to monitor the motion of the spot. It would be useful to make such films of the spot moving on the steered path and from these films calculate the spot diffusion coefficient. This would serve two purposes; firstly it would give some means of testing the accuracy of the experiments and secondly the diffusion in the radial and driven directions could be separated and its dependence upon spot confinement determined.

(v) The production and testing of a commercial steering array.

One of the purposes of the construction of a two coil system was as an improved design on existing commercially available steering systems. The increased cathode usage, particularly with those made of more exotic materials, has definite economic advantages not only in terms of materials saved but also in reduced engineering time. It is a logical and straight forward step to scale up a two or three coil system for use on a commercial coating chamber and evaluate the performance of such system.

The system could be designed by a commercial finite element package tailored for magnetic field modelling (such packages are readily available). It is anticipated that such system would be of a rectangular geometry, the majority of commercial coating units employing long rectangular cathodes, and could be of a purely electromagnetic nature or a combination of electromagnetic coils and either ferrite cores, permanent magnets or both.

The evaluation of such a system would consist of consideration of several factors. The level of macro particle emission, the cathode usage in terms of the percentage of bulk material used, the deposition rate and the quality of coatings delivered from such a system would have to be evaluated and compared with conventional systems. It would also be interesting to see whether any process parameters need to be changed to give the same quality coating. Finally the amount of down time and engineering time saved through increased cathode usage would have to be assessed and compared with the cost of the installation of the array.

Appendix I

The Biot-Savart Model.

This appendix gives the full derivation for the magnetic field components B_x and B_y for any point (x,y) from a plane coil (for a schematic of the geometry used see Figure 4.7). Using the geometry shown in Figure 4.8, then the coils may be divided into a number of current carrying loops shown in Figure 4.7.

The current element $d\underline{l} = d\underline{B}$ so,

$$\underline{r} = \underline{x} + \underline{y} - \underline{R} \quad (\text{AI.1})$$

The Biot-Savart law gives,

$$dB = m \frac{(d\underline{l} \times \underline{r})}{r^3} \quad (\text{AI.2})$$

Where,

$$m = \frac{\mu_0 NI}{4\pi} \quad (\text{AI.3})$$

But,

$$\begin{aligned} r^2 &= (\underline{x} + \underline{y} - \underline{R}) \cdot (\underline{x} + \underline{y} - \underline{R}) \\ &= x^2 + y^2 + R^2 - 2Rx \cos\theta \\ &= R^2(\delta^2 + \rho^2 + 1 - 2\rho \cos\theta) \end{aligned}$$

So,

$$r^3 = R^3(\delta^2 + \rho^2 + 1 - 2\rho\cos\theta)^{3/2}$$

Where,

$$\rho = \frac{x}{R} \text{ and } \delta = \frac{y}{R}$$

Dealing with the y component,

$$(d\underline{l} \times d\underline{r})_y = [d\underline{R} \times (\underline{x} - \underline{y} - \underline{R})]_y$$

But,

$$(d\underline{R} \times \underline{y})_y = 0$$

And,

$$(d\underline{l} \times \underline{r})_y = d\underline{R} \times (\underline{x} - \underline{R})$$

$$= R^2(1 - \rho\cos\theta)d\theta \quad (\text{AI.4})$$

Now in the x direction,

$$(d\underline{l} \times \underline{r})_{x,z} = [d\underline{R} \times (\underline{x} + \underline{y} - \underline{R})]_{x,z}$$

But $d\underline{R} \times \underline{x}$ and $d\underline{R} \times \underline{R}$ have zero component in the plane of the coil, i.e. the x, z plane, so,

$$(d\underline{l} \times \underline{r})_{x,z} = d\underline{R} \times \underline{y}$$

Now,

$$\begin{aligned} |d\underline{R}| &= |\underline{R}| \times |\underline{\theta}| \\ &= yRd\theta \\ &= r^2\delta d\theta \end{aligned}$$

This may contain a component in the z direction, so resolving in the x direction gives,

$$(d\underline{l} \times \underline{r})_x = R^2\delta \cos\theta d\theta \quad (\text{AI.5})$$

From Equations AI.1 to AI.5,

$$dB_x = \frac{m}{R} \frac{\delta \cos\theta}{(\rho^2 + \delta^2 + 1 - 2\rho\cos\theta)^{3/2}} d\theta \quad (\text{AI.6})$$

And,

$$dB_y = \frac{m}{R} \frac{(1 - \rho\cos\theta)}{(\rho^2 + \delta^2 + 1 - 2\rho\cos\theta)^{3/2}} d\theta \quad (\text{AI.7})$$

These equations may be solved by the numerical integrations,

$$B_x(\rho, \delta) = \frac{m\Delta\theta}{R} \sum_i \frac{(\delta \cos\theta_i)}{(\rho^2 + \delta^2 + 1 - 2\rho\cos\theta_i)^{3/2}} \quad (\text{AI.8})$$

And,

$$B_y(\rho, \delta) = \frac{m\Delta\theta}{R} \sum_i \frac{(1 - \rho\cos\theta_i)}{(\rho^2 + \delta^2 + 1 - 2\rho\cos\theta_i)^{3/2}} \quad (\text{AI.9})$$

Where,

$$\theta_i = \frac{\Delta\theta}{2}, \frac{3\Delta\theta}{2}, \frac{5\Delta\theta}{2} \dots \dots \dots 2\pi - \frac{\Delta\theta}{2} \quad (\text{AI.10})$$

Appendix II

Program documentation

Program: ARCTIME
Author: P.Walke.
Last modified: 18th May 1994
Function: Times the periods between arc orbits
Program uses the 3, 1Mhz clocks on ATMIO16 to wait for signal on lines 1, 2 and 5,
once triggered each clock then times the interval between the first trigger and the next.

```
REM DEFINE VARIABLES
DIM SHARED period$(4000), sumdif$(8), totdif$(8), sortper$(3000)
DIM fs AS STRING * 9
DIM ffn AS STRING * 11
drive$ = "a:"
ext$ = ".dat"
n% = 2000
n2% = 4000
REM CONFIGURE CLOCKS
i..dummy% = CTR.Config(2, 1, 1, 0, 0, 0)
i..dummy% = CTR.Config(2, 2, 0, 3, 0, 0)
i..dummy% = CTR.Config(2, 5, 0, 3, 0, 0)
REM DATA COLLECTION
WHILE dummy% = 0
  CLS
  INPUT "Enter 1 to start data collection"; dummm2%
  FOR i% = 0 TO 999
    REM START COUNTER 1 COUNTING EVENTS AT GATE 1
    i..dummy% = CTR.EvCount(2, 1, 11, 0)
    REM WAIT UNTIL AN EVENT OCCURS AT GATE 1
    WHILE event% = 0
      i..dummy% = CTR.EvRead(2, 1, dummm%, event%)
    WEND
    REM RESET COUNTER 1
    event% = 0
    i..dummy% = CTR.Reset(2, 1, 1)
    REM READ TIME AT COUNTER 2
    i..dummy% = CTR.EvRead(2, 2, dummm2%, pertemp1%)
    cnt% = cnt% + 1
    period$(cnt%) = CINT(pertemp1%)
  
```

```
REM CONFIGURE COUNTER 2 TO MEASURE PERIOD WITH 1MHZ CLOCK
  i..dummy% = CTR.Period(2, 2, 1)
REM START COUNTER 1 COUNTING EVENTS AT GATE 1
  i..dummy% = CTR.EvCount(2, 1, 11, 0)
REM WAIT UNTIL AN EVENT OCCURS AT GATE 1
  WHILE event% = 0
    i..dummy% = CTR.EvRead(2, 1, dumm%, event%)
  WEND
REM RESET COUNTER 1
  event% = 0
  i..dummy% = CTR.Reset(2, 1, 1)
REM READ TIME AT COUNTER 5
  i..dummy% = CTR.EvRead(2, 5, dumm2%, pertemp2%)
  cnt% = cnt% + 1
  period#(cnt%) = CINT(pertemp2%)
REM CONFIGURE COUNTER 5 TO MEASURE PERIOD WITH 1MHZ CLOCK
  i..dummy% = CTR.Period(2, 5, 1)
NEXT i%
PRINT "done"
BEEP
CALL StdDev(period#(), cnt%, meanie#, sd#)
PRINT "Mean and SD"; meanie#, sd#
REM OUTPUT FILE TO DISK
INPUT "File name please"; fs$
z% = ffmt(ffn$, "%s<%s%>%s", drive$, fs$, ext$)
h% = 1
h% = OpenFile(ffn$, 2, 0, 1)
FOR i% = 0 TO n% - 1
  zz% = FmtFile(h%, "%s<%f", period#(i%))
NEXT i%
i..dummy% = CloseFile(h%)
cnt% = 0
WEND
```

Program: DATNORM
Author: P.Walke
Last modified: 18th May 1994
Function: Produces distribution of experimental data

Program reads in a series of 2000 orbital periods collected by program "arctime" and sorts them into data bins. A histogram is plotted of the data and mean standard deviation and skew of the distribution is calculated. A normal distribution of the same mean and SD as the measured distribution is also calculated. The distributions are saved for later use by program "smirnov".

REM DIMENSION VARIABLES

REM \$INCLUDE: 'arc.inc'

DIM SHARED period#(4000), ax#(50), hist%(50), sortper#(4000), probx#(50)

DIM SHARED hist2#(50), avge#(10), index#(10), dummy#(10), temp#(300)

DIM fs AS STRING * 9

DIM ffn AS STRING * 11

drive\$ = "a:"

ext\$ = ".dat"

cnt% = 0

no% = 2000

CLS

REM IMPORT DATA

INPUT "Enter file name"; fs\$

z% = fmt(ffn\$, "%s<%s%s%s", drive\$, fs\$, ext\$)

x% = OpenFile(ffn\$, 1, 2, 1)

n% = ScanFile(x%, "%s>%4000f[x]", period#())

n% = CloseFile(h%)

REM FILTER OUT ERRONEOUS READINGS

FOR i% = 0 TO no% - 1

IF period#(i%) > 4000 AND period#(i%) < 8000 THEN

sortper#(cnt%) = period#(i%)

cnt% = cnt% + 1

ELSE

END IF

NEXT i%

REM CALCULATE THE STANDARD DEVIATION OF DATA IN TEN BLOCKS

REM TO CHECK FOR TREND IN DATA

nopoint% = CINT((cnt% - 1) / 10)

start% = 0

ending% = nopoint% - 1

count% = 0

FOR i% = 0 TO 9

FOR j% = start% TO ending%

tot# = tot# + sortper#(j%)

temp#(count%) = sortper#(j%)

count% = count% + 1

NEXT j%

```
count% = 0
CALL StdDev(temp#(), nopoint%, meanbit#, standbit#)
avge#(i%) = tot# / (nopoint% - 1)
tot# = 0
index#(i%) = i%
start% = start% + nopoint%
ending% = ending% + nopoint%
NEXT i%
REM CHECK GRADIENT OF ANY TREND
CALL LinFit(avge#(), index#(), 10, dummy#(), grad#, inter#, rsquare#)
CALL Mean(sortper#(), cnt%, meanone#)
FOR i% = 0 TO cnt% - 1
  sortper#(i%) = sortper#(i%) - ((grad# * i% + sortper#(0)) - meanone#)
NEXT i%
REM DISPLAY USER INTERFACE
h% = LoadPanel("arc.uir", arc)
i..ret% = DisplayPanel(h%)
WHILE ctrl% <> arc.st
  i..ret% = GetUserEvent(0, h%, ctrl%)
WEND
REM PLOT SD TO CHECK FOR TREND
i..ret% = SetCtrlVal(h%, arc.rsq, rsquare#)
i..ret% = SetCtrlVal(h%, arc.grad, grad#)
i..ret% = PlotY(h%, arc.gr, avge#(), 10, 4, 2, 1, 1, 15)
WHILE ctrl% <> arc.pf
  i..ret% = GetUserEvent(0, h%, ctrl%)
WEND
i..ret% = DeletePlots(h%, arc.gr)
i..ret% = ConfigureAxes(h%, arc.gr, -1, 0!, 1!, 1, 0!, 1!)
REM CALCULATE DISTRIBUTION PARAMETERS AND PLOT HISTOGRAM
ctrl% = 255
CALL MaxMin1D(sortper#(), cnt% - 1, maxi#, dum%, mini#, dum2%)
CALL StdDev(sortper#(), cnt% - 1, meanie#, stand#)
CALL Moment(sortper#(), cnt% - 1, 3, m3#)
skew# = m3# / (stand# ^ 3)
CALL Histogram(sortper#(), cnt% - 1, mini#, maxi#, hist%(), ax#(), 17)
binw# = ax#(1) - ax#(0)
REM CALCULATE NORMAL DISTRIBUTION
FOR i% = 0 TO 16
  hist2#(i%) = hist%(i%) / (binw# * (cnt% - 1))
  xpos# = .5 * ((ax#(i%) - meanie#) / stand#) ^ 2
  probx#(i%) = (1 / (SQR(2 * 3.14159) * stand#)) * EXP(-1 * xpos#)
NEXT i%
REM PLOT HISTOGRAM
i..ret% = PlotXY(h%, arc.gr, ax#(), hist2#(), 17, 4, 4, 0, 0, 1, 4)
WHILE ctrl% <> arc.pf
  i..ret% = GetUserEvent(0, h%, ctrl%)
WEND
```

REM PLOT NORMAL DISTRIBUTION

i..ret% = PlotXY(h%, arc.gr, ax#(), probx#(), 17, 4, 4, 0, 0, 1, 15)

REM DISPLAY DISTRIBUTION PARAMETERS

i..ret% = SetCtrlVal(h%, arc.mn, meanie#)

i..ret% = SetCtrlVal(h%, arc.sd, stand#)

i..ret% = SetCtrlVal(h%, arc.sk, skew#)

i..ret% = SetCtrlVal(h%, arc.N, cnt% - 1)

REM HARDCOPY/DONE ROUTINE

ctrl% = 255

WHILE ctrl% <> arc.ok

 i..ret% = GetUserEvent(0, h%, ctrl%)

 IF ctrl% = arc.hc THEN

 i..ret% = OutputPanel(-1, "", 1, h%)

 END IF

WEND

REM SHUT DOWN PANEL

i..ret% = CloseInterfaceManager

REM SAVE DISTRIBUTIONS

INPUT "File name please, y-data"; fs\$

z% = fmt(ffn\$, "%s<%s%s%s", drive\$, fs\$, ext\$)

h% = 1

h% = OpenFile(ffn\$, 2, 0, 1)

FOR i% = 0 TO 16

 zz% = FmtFile(h%, "%s<%i,", hist%(i%))

NEXT i%

i..dummy% = CloseFile(h%)

INPUT "File name please, x-data"; fs\$

z% = fmt(ffn\$, "%s<%s%s%s", drive\$, fs\$, ext\$)

h% = 1

h% = OpenFile(ffn\$, 2, 0, 1)

FOR i% = 0 TO 16

 zz% = FmtFile(h%, "%s<%f,", ax#(i%))

NEXT i%

i..dummy% = CloseFile(h%)

INPUT "File name please, normal data"; fs\$

z% = fmt(ffn\$, "%s<%s%s%s", drive\$, fs\$, ext\$)

h% = 1

h% = OpenFile(ffn\$, 2, 0, 1)

FOR i% = 0 TO 16

 zz% = FmtFile(h%, "%s<%f,", probx#(i%))

NEXT i%

i..dummy% = CloseFile(h%)

END

Program: Smirnov
Author: Modified from a Birmingham University FORTRAN library
routine by
P.Walke.
Last modified: 10th January 1994
Function: Fits experimental and theoretical distributions

Program uses a grid search method to fit the variables k and v between measured distributions, normal distributions and Care's model. The fit is either convoluted with the distribution of orbital radii or straight fit with fixed radius. The Kolmogorov-Smirnov test is used to test for goodness of fit.

REM DECLARE SUBROUTIES AND DEFINE VARIABLES

DECLARE SUB normal ()

DECLARE SUB graphik ()

DECLARE SUB funct ()

DECLARE SUB kscal ()

DECLARE SUB norks ()

DIM SHARED xf(50), yf(50), yft(50), x(50), pr(50), xpol(50)

DIM SHARED prpol(50), norprob(50), deltaa(3), area

DIM SHARED gx(50), binwid, delx, k1prev, k2prev, maxy, maxpr, passv

DIM SHARED passk, binwid2, npts%, ks, fks, nfree%, free, k(3), x

DIM SHARED meanie, stand, norad%, maxpos, nks, ans3\$

npts% = 17

norad% = 30

nterms% = 1

nfree% = 16

x = .1185

free = nfree%

ans1\$ = "y"

ans\$ = "y"

ans2\$ = "y"

CLS

INPUT "Enter directory name"; dir\$

CLS

WHILE ans2\$ = "y"

CLS

INPUT "Enter filename for data "; filenam1\$

CLS

INPUT "Convoluted (y/n)"; ans3\$

ans3\$ = LCASE\$(ans3\$)

REM ENTER DATA TO GENERATE NORMAL DISTRIBUTION

CLS

INPUT "Enter mean arc period "; meanie

INPUT "Enter standard deviation of arc period "; stand

meanie = meanie / 1000000

stand = stand / 1000000

CLS

REM GIVE FIRST GUESS AS STARTING POINT FOR SEARCH

INPUT "Enter first guess for velocity"; k(1)

INPUT "Enter first guess for diffusion constant"; k(2)

REM CALCULATE INITIAL GRID SIZE

deltaa(1) = k(1) / 20

deltaa(2) = k(2) / 50

CLS

PRINT "Importing data...Please wait"

fil1\$ = "c:\d\paul\arcdata\" + dir\$ + "\x" + filenam1\$ + ".dat"

fil2\$ = "c:\d\paul\arcdata\" + dir\$ + "\y" + filenam1\$ + ".dat"

OPEN fil1\$ FOR INPUT AS #1

OPEN fil2\$ FOR INPUT AS #2

FOR i% = 1 TO npts%

INPUT #1, xf(i%)

INPUT #2, yf(i%)

xf(i%) = xf(i%) / 1000000

NEXT i%

CLOSE #1

CLOSE #2

REM IMPORT DISTRIBUTION OF RADII

fil3\$ = "c:\d\paul\arcdata\p(r).dat"

OPEN fil3\$ FOR INPUT AS #1

FOR i% = 1 TO norad%

INPUT #1, x(i%), pr(i%)

IF pr(i%) > maxpr THEN

maxpos = x(i%)

END IF

NEXT i%

CLOSE #1

REM CALCULATE NORMAL DISTRIBUTION

CALL normal

REM NORMALISE EXPERIMENTAL DISTRIBUTION

CLS

binwid = xf(2) - xf(1)

FOR i% = 1 TO npts% - 1

area = area + (binwid * ((yf(i% + 1) + yf(i%)) / 2))

NEXT i%

FOR i% = 1 TO npts%

yf(i%) = yf(i%) / area

NEXT i%

REM NORMALISE DISTRIBUTION OF RADII

binwid2 = x(2) - x(1)

FOR i% = 1 TO norad% - 1

area2 = area2 + (binwid2 * ((pr(i% + 1) + pr(i%)) / 2))

NEXT i%

FOR i% = 1 TO norad%

pr(i%) = pr(i%) / area2

NEXT i%

```
REM FIT FOR k AND v
WHILE ans1$ = "y"
FOR j% = 1 TO 2
  IF j% = 1 THEN passv = passv + 1
  IF j% = 2 THEN passk = passk + 1
  k1prev = k(1)
  k2prev = k(2)
  ks = 0
REM CALCULATE THEORETICAL DISTRIBUTION
CALL funct
REM CALCULATE K-S GOODNESS OF FIT FACTOR
CALL kscal
ks1 = fks
fun = 0
delta = deltaa(j%)
REM FIND AN AREA OF CHANGING GRADIENT
PRINT "Thinking about pass 1"
DO
  k(j%) = k(j%) + delta
  CALL funct
  CALL kscal
  ks2 = fks
  LOOP WHILE (ks1 - ks2) = 0
REM CHECK THAT THE DIRECTION OF STEP IS TOWARDS A MINIMUM
PRINT "Thinking about pass 2"
IF (ks1 - ks2) < 0 THEN
  delta = -1 * delta
  k(j%) = k(j%) + delta
  CALL funct
  save = ks1
  ks1 = ks2
  ks2 = save
END IF
CLS
REM INCREMENT OR DECREMENT k AND v UNTIL K-S FACTOR INCREASES
PRINT "Thinking about pass 3"
DO
  fun = fun + 1
  k(j%) = k(j%) + delta
  CALL funct
  CALL kscal
  ks3 = fks
  cond = ks3 - ks2
  IF cond < 0 THEN
    ks1 = ks2
    ks2 = ks3
  END IF
  PRINT "Thinking about pass 4"
  LOOP WHILE cond < 0
```

```
CLS
REM FIND THE MINIMUM OF A PARABOLA DEFINED BY THREE POINTS
PRINT "Thinking about pass 5"
dum1 = ks1 - ks2
dum2 = ks3 - ks2
IF dum2 <> 0 THEN
  delta = delta * (1 / (1 + (dum1) / (dum2))) + .5
END IF
k(j%) = k(j%) - delta
sigma = deltaa(j%) * SQR(2 / (free * (ks3 - 2 * ks2 + ks1)))
REM DECREASE STEP SIZE ACCORDING TO NUMBER OF STEPS MADE
PREVIOUSLY
deltaa(j%) = deltaa(j%) * fun / 3
CALL funct
CALL kscal
ks = fks
maxy = 0
REM FIND MAXIMUM AND MINIMUM OF DISTRIBUTIONS
FOR i% = 1 TO npts%
  IF yft(i%) > maxy THEN maxy = yft(i%)
  IF yf(i%) > maxy THEN maxy = yf(i%)
NEXT i%
REM CALCULATE EXPERIMENTAL-NORMAL K-S VALUE
CALL norks
nks = fks
REM PLOT FUNCTIONS FOR COMPARISON BY EYE
CALL graphik
NEXT j%
CLS
PRINT "Do you wish to recalculate?"
ans1$ = INPUT$(1)
WEND
REM SAVE FITTED DATA
INPUT "Output filename please"; filenam4$
nam4$ = "c:\d\paul\arcdata\fitted\" + filenam4$ + ".dat"
FOR i% = 1 TO npts%
  xf(i%) = xf(i%) * 1000
NEXT i%
REM NORMALISE FITTED DISTRIBUTIONS
area3 = 0
binwid = xf(2) - xf(1)
FOR i% = 1 TO npts% - 1
  area3 = area3 + (binwid * ((yf(i% + 1) + yf(i%)) / 2))
NEXT i%
FOR i% = 1 TO npts%
  yf(i%) = yf(i%) / area3
  yft(i%) = yft(i%) / area3
  norprob(i%) = norprob(i%) / area3
NEXT i%
```

```
stand = (k(1) / meanie) * stand
OPEN nam4$ FOR OUTPUT AS 3
PRINT #3, USING "##.##;.#####;#.####"; k(1); k(2); stand
FOR i% = 1 TO npts%
  PRINT #3, USING "##.#####;#.#####;#.#####;#.#####"; xf(i%);
yf(i%);yft(i%);norprob(i%)
NEXT i%
CLOSE #3
PRINT "Another go?"
ans2$ = INPUT$(1)
CLS
WEND
```

REM CALCULATES VALUE OF THEORETICAL FUNCTION

SUB funct

REM TESTS WHETHER CONVOLUTION REQUIRED

IF ans3\$ = "y" THEN

delx = k(1) * binwid

nback% = INT(((maxpos - x(1)) / delx) - .5)

nforw% = INT(((x(30) - maxpos) / delx) - .5)

nosteps% = nback% + nforw% + 1

xint = maxpos - nback% * delx

REM FUNCTION CONVOLUTED WITH RADII DISTRIBUTION

FOR i% = 1 TO nosteps%

FOR k% = 1 TO 30

IF xint >= x(k%) AND xint <= x(k% + 1) THEN

grad = (pr(k% + 1) - pr(k%)) / (x(k% + 1) - x(k%))

prpol(i%) = pr(k%) + grad * (xint - x(k%))

xpol(i%) = xint

END IF

NEXT k%

xint = xint + delx

NEXT i%

FOR i% = 1 TO npts%

yft(i%) = 0

FOR k% = 1 TO nosteps%

pow = (((-1 * (xf(i%) * k(1)) + xpol(k%)) ^ 2) / (4 * k(2) * xf(i%)))

IF pow <= 0 THEN

PRINT "Pow is less than zero, hit any key"

a\$ = INPUT\$(1)

END IF

temp = ((k(2) * (xf(i%) * k(1) + xpol(k%))) * (EXP(-1 * pow))) /

(4 * SQR(3.141593) * (k(2) * xf(i%)) ^ 1.5)

gx(k%) = temp * prpol(k%)

NEXT k%

REM NUMERICAL INTEGRATION

FOR k% = 1 TO norad% - 1

yft(i%) = yft(i%) + (delx * ((gx(k% + 1) + gx(k%)) / 2))

NEXT k%

```
NEXT i%
REM IF CONVOLUTION NOT REQUIRED STRAIGHT FUNCTION
CALCULATION
ELSE
FOR i% = 1 TO npts%
  pow = (((-1 * (xf(i%) * k(1)) + x) ^ 2) / (4 * k(2) * xf(i%)))
  yft(i%) = ((k(2) * (xf(i%) * k(1) + x)) * (EXP(-1 * pow))) / (4 * SQR(3.141593) *
(k(2) * xf(i%)) ^ 1.5)
NEXT i%
END IF
CLS
END SUB
```

```
REM PLOT FUNCTIONS TO ALLOW VISUAL COMPARISON
```

```
SUB graphik
SCREEN 9
VIEW (0, 0)-(600, 220)
WINDOW (xf(1), 0)-(xf(npts%), maxy)
COLOR 4
PSET (xf(1), yf(1))
FOR i% = 2 TO npts%
  LINE (xf(i% - 1), yf(i% - 1))-(xf(i%), yf(i%))
NEXT i%
COLOR 9
PSET (xf(1), yft(1))
FOR i% = 2 TO npts%
  LINE (xf(i% - 1), yft(i% - 1))-(xf(i%), yft(i%))
NEXT i%
COLOR 14
PSET (xf(1), norprob(1))
FOR i% = 2 TO npts%
  LINE (xf(i% - 1), norprob(i% - 1))-(xf(i%), norprob(i%))
NEXT i%
COLOR 7
LOCATE 17, 1
PRINT "Pass number "; passv; " for velocity"
PRINT "Pass number "; passk; "for Diffusion constant"
PRINT "Velocity, v= "; k(1); ", changed by "; k(1) - k1prev
PRINT "Diffusion constant, k= "; k(2); ", changed by "; k(2) - k2prev
PRINT "Kolmogorov-Smirnov deviation model to data is"; ks
PRINT "Kolmogorov-Smirnov deviation normal curve to data is"; nks
COLOR 15
PRINT "Hit any key when ready"
a$ = INPUT$(1)
SCREEN 0
END SUB
```

REM CALCULATE THE K-S GOODNESS OF FIT COEFFICIENT

SUB kscale

cumy = 0

cumyft = 0

yftot = 0

yfttot = 0

dval = 0

FOR i% = 1 TO npts%

yfttot = yfttot + yft(i%)

NEXT i%

FOR i% = 1 TO npts%

cumy = cumy + (yf(i%) / yfttot)

cumyft = cumyft + (yft(i%) / yfttot)

cumdum = ABS(cumy - cumyft)

IF cumdum > dval THEN

dval = cumdum

END IF

NEXT i%

fks = dval

END SUB

REM CALCULATE THE K-S GOODNESS OF FIT TO NORMAL DISTRIBUTION

SUB norks

cumy = 0

cumyft = 0

yftot = 0

yfttot = 0

dval = 0

FOR i% = 1 TO npts%

yfttot = yfttot + norprob(i%)

NEXT i%

FOR i% = 1 TO npts%

cumy = cumy + (yf(i%) / yfttot)

cumyft = cumyft + (norprob(i%) / yfttot)

cumdum = ABS(cumy - cumyft)

IF cumdum > dval THEN

dval = cumdum

END IF

NEXT i%

fks = dval

END SUB

REM CALCULATE NORMAL DISTRIBUTION

SUB normal

FOR i% = 1 TO npts%

xp = .5 * ((xf(i%) - meanie) / stand) ^ 2

norprob(i%) = (1 / (SQR(2 * 3.14159) * stand)) * EXP(-1 * xp)

NEXT i%

END SUB

Program: TESCA21
Author: P.Walke
Last modified: 21st October 1991
Function: Predicts field profiles from multi-coil system

Program uses numerical integration of the Biot-Savart law to predict the normal and transverse field components produced by one to three electro-magnetic coils of varying sizes and ranges.

OPTION BASE 0

```

DIM SHARED XCOMP(200), YCOMP(200), RAD(200), XCO(200), YCO(200)
DIM SHARED MAXX.B, MINX.B, MAXY.B, MINY.B, LEN1, LEN2, RAD1, RAD2,
R
DIM SHARED MIN.B, MAX.B, XMIN, XMAX
DIM SHARED SPAC1, SPAC2, STR2, YSTART1, YEND1, YSTART2, YEND2
DIM SHARED YSTEP2, XSTEP1, XSTEP2, XSTART, XEND, XSTEP, YSTEP1
DIM SHARED MOM1, MOM2, BXMAX, BYMAX, BXMIN, BYMIN, XIND,
DIM SHARED TWOPI, POL1$, POL2$, POL3$, YAX, HAFDEL, DELTHET
DIM SHARED MOM3, RAD3, LEN3, SPAC3, STR3, YSTART3, YEND3, YSTEP3,
DIM SHARED THCK2, THCK3, THCK1
DIM SHARED RADSTART1, RADSTART2, RADSTART3, RADSTEP1,
RADSTEP2,
DIM SHARED YMAX, YMIN, YNO, RADSTEP3
DECLARE SUB ENTER ()
DECLARE SUB CALC ()
DECLARE SUB SAVER ()
DECLARE SUB MAIN ()
DECLARE SUB GRAPH ()
DECLARE SUB SCALE ()
DECLARE SUB DELAY ()
CALL MAIN
END

```

REM SUBDIVIDES COILS INTO CURRENT CARRYING LOOPS AND INTEGRATES ROUND THEM

```

SUB CALC
FOR X = XSTART TO XEND STEP XSTEP
  XIND = XIND + 1
  BX = 0: BY = 0
  CLS
  PRINT "CALCULATING BLOCK "; XIND; " OF";
  INT(((XEND - XSTART) / XSTEP) + .5) + 1
  radi = RADSTART1
  FOR R = 1 TO 10
    MOM1 = .00001 / (radi * 10 * (YNO + 1))
    FOR Y = YSTART1 TO (YEND1 + YSTEP1 / 2) STEP YSTEP1
      FOR TH = HAFDEL TO TWOPI STEP DELTHET
        DIVIS = ((X / radi) ^ 2 + (Y / radi) ^ 2 + 1 - (2 * (X / radi) * COS(TH))) ^ 1.5

```

```

IF POL1$ = "N" OR POL1$ = "n" THEN
  BX = BX - (((Y / radi) * COS(TH)) / DIVIS) * MOM1
  BY = BY - (((1 - (X / radi) * COS(TH)) / DIVIS) * MOM1)
ELSE
  BX = BX + (((Y / radi) * COS(TH)) / DIVIS) * MOM1
  BY = BY + (((1 - (X / radi) * COS(TH)) / DIVIS) * MOM1)
END IF
NEXT TH
NEXT Y
radi = radi + RADSTEP1
NEXT R
IF STR2 <> 0 THEN
  radi = RADSTART2
  FOR R = 1 TO 10
    MOM2 = (.00001 / (radi * 10 * (YNO + 1))) * STR2
    FOR Y = YSTART2 TO (YEND2 + YSTEP2 / 2) STEP YSTEP2
      FOR TH = HAFDEL TO TWOPI STEP DELTHET
        DIVIS = ((X / radi) ^ 2 + (Y / radi) ^ 2 + 1 - (2 * (X / radi) * COS(TH))) ^ 1.5
        IF POL2$ = "N" OR POL2$ = "n" THEN
          BX = BX - (((Y / radi) * COS(TH)) / DIVIS) * MOM2
          BY = BY - (((1 - (X / radi) * COS(TH)) / DIVIS) * MOM2)
        ELSE
          BX = BX + (((Y / radi) * COS(TH)) / DIVIS) * MOM2
          BY = BY + (((1 - (X / radi) * COS(TH)) / DIVIS) * MOM2)
        END IF
      NEXT TH
    NEXT Y
    radi = radi + RADSTEP2
  NEXT R
END IF
IF STR3 <> 0 THEN
  radi = RADSTART3
  FOR R = 1 TO 5
    MOM3 = (.00001 / (radi * 5 * (YNO + 1))) * STR3
    FOR Y = YSTART3 TO (YEND3 + YSTEP3 / 2) STEP YSTEP3
      FOR TH = HAFDEL TO TWOPI STEP DELTHET
        DIVIS = ((X / radi) ^ 2 + (Y / radi) ^ 2 + 1 - (2 * (X / radi) * COS(TH))) ^ 1.5
        IF POL3$ = "N" OR POL3$ = "n" THEN
          BX = BX - (((Y / radi) * COS(TH)) / DIVIS) * MOM3
          BY = BY - (((1 - (X / radi) * COS(TH)) / DIVIS) * MOM3)
        ELSE
          BX = BX + (((Y / radi) * COS(TH)) / DIVIS) * MOM3
          BY = BY + (((1 - (X / radi) * COS(TH)) / DIVIS) * MOM3)
        END IF
      NEXT TH
    NEXT Y
    radi = radi + RADSTEP3
  NEXT R
END IF

```

```
XCOMP(XIND) = BX * 1000 * DELTHET
YCOMP(XIND) = BY * 1000 * DELTHET
IF XIND = 1 THEN
  BYMAX = YCOMP(1): BYMIN = YCOMP(1): BXMAX = XCOMP(1): BXMIN =
XCOMP(1)
  END IF
  IF XCOMP(XIND) > BXMAX THEN BXMAX = XCOMP(XIND)
  IF YCOMP(XIND) > BYMAX THEN BYMAX = YCOMP(XIND)
  IF XCOMP(XIND) < BXMIN THEN BXMIN = XCOMP(XIND)
  IF YCOMP(XIND) < BYMIN THEN BYMIN = YCOMP(XIND)
  YIND = 0
  RAD(XIND) = X
NEXT X
IF BXMAX > BYMAX THEN MAX.B = BXMAX ELSE MAX.B = BYMAX
IF BXMIN < BYMIN THEN MIN.B = BXMIN ELSE MIN.B = BYMIN
CLS
BEEP
CALL DELAY
BEEP
CALL DELAY
BEEP
PRINT "CALCULATIONS COMPLETE PLEASE PRESS ANY KEY TO
CONTINUE"
A$ = INPUT$(1)
CLS
END SUB

SUB DELAY
FOR I = 1 TO 10000
NEXT I
END SUB

REM DATA ENTRY SUBROUTINE
SUB ENTER
CLS
LOCATE 2, 1: PRINT "X RANGE"
LOCATE 6, 1: INPUT "ENTER X START "; XSTART
LOCATE 8, 1: INPUT "ENTER X END "; XEND
LOCATE 10, 1: INPUT "ENTER X STEP "; XSTEP
CLS
LOCATE 2, 1: PRINT "INNER COIL"
LOCATE 6, 1: INPUT "ENTER MEAN RADIUS IN CM "; RAD1
LOCATE 8, 1: INPUT "ENTER COIL THICKNESS IN CM"; THCK1
LOCATE 10, 1: INPUT "ENTER LENGTH IN CM "; LEN1
LOCATE 12, 1: INPUT "ENTER SPACE TO CATHODE IN CM"; SPAC1
LOCATE 14, 1: INPUT "POLARITY, (P/N)"; POL1$
CLS
LOCATE 2, 1: PRINT "MIDDLE COIL"
LOCATE 6, 1: INPUT "ENTER RELATIVE STRENGTH OF MIDDLE COIL"; STR2
```

```
IF STR2 <> 0 THEN
  LOCATE 8, 1: INPUT "ENTER MEAN RADIUS IN CM"; RAD2
  LOCATE 10, 1: INPUT "ENTER COIL THICKNESS IN CM"; THCK2
  LOCATE 12, 1: INPUT "ENTER LENGTH IN CM"; LEN2
  LOCATE 14, 1: INPUT "ENTER SPACE TO CATHODE IN CM"; SPAC2
  LOCATE 16, 1: INPUT "POLARITY, (P/N)"; POL2$
ELSE
  RAD2 = 1: LEN2 = 1: SPAC2 = 1: POL2$ = "P"
END IF
CLS
LOCATE 2, 1: PRINT "OUTER COIL"
LOCATE 6, 1: INPUT "ENTER RELATIVE STRENGTH OF OUTER COIL"; STR3
IF STR3 <> 0 THEN
  LOCATE 8, 1: INPUT "ENTER MEAN RADIUS IN CM"; RAD3
  LOCATE 10, 1: INPUT "ENTER COIL THICKNESS IN CM"; THCK3
  LOCATE 12, 1: INPUT "ENTER LENGTH IN CM"; LEN3
  LOCATE 14, 1: INPUT "ENTER SPACE TO CATHODE IN CM"; SPAC3
  LOCATE 16, 1: INPUT "POLARITY, (P/N)"; POL3$
ELSE
  RAD3 = 1: LEN3 = 1: SPAC3 = 1: POL3$ = "P"
END IF
YSTART1 = SPAC1: YSTART2 = SPAC2: YSTART3 = SPAC3
YEND1 = YSTART1 + LEN1: YEND2 = YSTART2 + LEN2: YEND3 = YSTART3 +
LEN3
YNO = 29
YSTEP1 = (YEND1 - YSTART1) / YNO: YSTEP2 = (YEND2 - YSTART2) / YNO:
YSTEP3 = (YEND3 - YSTART3) / YNO
RADSTART1 = RAD1 - (THCK1 / 2): RADSTART2 = RAD2 - (THCK2 / 2):
RADSTART3 = RAD3 - (THCK3 / 2)
RADSTEP1 = THCK1 / 9: RADSTEP2 = THCK2 / 9: RADSTEP3 = THCK3 / 9
BXMAX = 0: BXMIN = 0: BYMAX = 0: BYMIN = 0: XIND = 0: YIND = 0
MAX.B = 0: MIN.B = 0
DELTHET = .31415926#: HAFDEL = .157076963#: TWOPI = 6.2831852#
CLS
END SUB
```

REM PLOTS THE PREDICTED FIELD PROFILES

SUB GRAPH

SCREEN 9

VIEW (0, 0)-(600, 250)

IF YMAX > 0 THEN

WINDOW (XSTART, (YMIN + YMIN / 20))-(XEND, (YMAX + YMAX / 20))

ELSE

WINDOW (XSTART, (YMIN + YMIN / 10))-(XEND, 3 / 2 * YAX)

END IF

LINE (XSTART, 0)-(XEND, 0)

FOR I = XSTART TO XEND

LINE (I, (ABS(YMIN) + ABS(YMAX)) / 40)-(I, -(ABS(YMIN) + ABS(YMAX)) / 40)

```
NEXT I
FOR I = XSTART TO XEND STEP .1
  LINE (I, (ABS(YMIN) + ABS(YMAX)) / 80)-(I, -(ABS(YMIN) + ABS(YMAX)) /
80)
NEXT I
IF YMAX > 0 THEN
  LINE (0, YMIN)-(0, YMAX)
  FOR I = YMIN TO (YMAX + YAX / 2) STEP YAX
    LINE (-.1, I)-(.1, I)
  NEXT I
ELSE
  LINE (0, YMIN)-(0, YAX)
  FOR I = YMIN TO (YAX + YAX / 2) STEP YAX
    LINE (-.1, I)-(.1, I)
  NEXT I
END IF
INDEX = 1
PSET (XSTART, YCO(1)), 4
FOR X = XSTART TO XEND STEP XSTEP
  LINE -(X, YCO(INDEX)), 4
  INDEX = INDEX + 1
NEXT X
INDEX = 1
PSET (XSTART, XCO(1)), 3
FOR X = XSTART TO XEND STEP XSTEP
  LINE -(X, XCO(INDEX)), 3
  INDEX = INDEX + 1
NEXT X
LOCATE 21, 1: PRINT "RAD1="; RAD1; ", LEN1="; LEN1; ", THCK1="; THCK1; ",
SPC1="; SPAC1; ", POL1="; POL1$; ", REL STR1 =1"
LOCATE 22, 1: PRINT "RAD2="; RAD2; ", LEN2="; LEN2; ", THCK2="; THCK2; ",
SPC2="; SPAC2; ", POL2="; POL2$; ", REL STR2 =" ; STR2
LOCATE 23, 1: PRINT "RAD3="; RAD3; ", LEN3="; LEN3; ", THCK3="; THCK3; ",
SPC3="; SPAC3; ", POL3="; POL3$; ", REL STR3 =" ; STR3
LOCATE 2, 1: PRINT USING "B.MAX IS ##.###^"; MAX.B
LOCATE 3, 1: PRINT USING "BYMAX IS ##.###^"; BYMAX
LOCATE 4, 1: PRINT USING "BYMIN IS ##.###^"; BYMIN
LOCATE 5, 1: PRINT "ALL IN mT PER AMP-TURN"
A$ = INPUT$(1)
SCREEN 0
CLS
END SUB

REM CALLS SUBROUTINES AND REPEATS MAIN PROGRAM
SUB MAIN
CLS
ANS$ = "Y"
DO WHILE ANS$ = "Y" OR ANS$ = "y"
CALL ENTER
```

```
CALL CALC
CALL SCALE
CALL GRAPH
CALL SAVER
PRINT "DO YOU WISH TO RUN AGAIN, (Y/N)": ANS$ = INPUT$(1)
LOOP
END SUB

REM SAVES THE PREDICTED PROFILES
SUB SAVER
CLS
PRINT "DO YOU WISH TO SAVE, (Y/N)": ANS$ = INPUT$(1)
CLS
IF ANS$ <> "N" AND ANS$ <> "n" THEN
  I$ = LTRIM$(STR$(RAD1)): J$ = LTRIM$(STR$(RAD2)): K$ =
  LTRIM$(STR$(LEN1)): L$ = LTRIM$(STR$(LEN2))
  M$ = LTRIM$(STR$(SPAC1)): N$ = LTRIM$(STR$(SPAC2)): O$ =
  LTRIM$(STR$(STR2)): P$ = LTRIM$(STR$(RAD3)): Q$ = LTRIM$(STR$(LEN3)):
  R$ = LTRIM$(STR$(SPAC3)): S$ = LTRIM$(STR$(STR3)):
  TIT1$ = "R1=" + I$ + ",R2=" + J$ + ",R3=" + P$ + ",L1=" + K$ + ",L2=" + L$ +
  ",L3=" + Q$ + ",SP1=" + M$ + ",SP2=" + N$ + ",SP3=" + R$ + ",REL.S.2=" + O$ +
  ",REL.S.3=" + S$ + ",(ALL IN cm)"
  TIT2$ = ",POL1=" + POL1$ + ",POL2=" + POL2$ + ",POL3=" + POL3$
  TITLES$ = CHR$(34) + TIT1$ + TIT2$ + CHR$(34)
  CLS
  INPUT "WHAT DO WISH TO CALL THE FILE"; FILNAME$
  CLS
  FILE$ = "D:\PAULMAGCALC\" + FILNAME$ + ".DAT"
  OPEN FILE$ FOR OUTPUT AS #1
  PRINT #1, TITLES$
  FOR X = (XIND - 1) / 2 TO XIND
    PRINT #1, USING "###.##;##.###^~^~;##.###^~^~;##.###^~^~"; RAD(X);
  YCOMP(X); XCOMP(X); YCOMP(X) + XCOMP(X)
  NEXT X
  PRINT #1, USING
  "##.###^~^~;##.###^~^~;##.###^~^~;##.###^~^~##.###^~^~;##.###^~^~"; BXMIN;
  BYMIN; BXMAX; BYMAX; MAX.B; MIN.B
  CLOSE #1
  PRINT "DATA SAVED AS "; FILE$
  PRINT "PUSH ANY KEY"
  paul$ = INPUT$(1)
  CLS
END IF
END SUB
```

REM SCALES THE DATA FOR THE GRAPH ROUTINE

SUB SCALE

YMAX = MAX.B * 1.1: YMIN = MIN.B * 1.1

IF ABS(YMAX) > ABS(YMIN) THEN MAXB = ABS(YMAX) ELSE MAXB =
ABS(YMIN)

YAX = (MAXB) / 10

NEGY = INT(YMIN / YAX): PTVEY = INT(YMAX / YAX)

IF PTVEY = 0 THEN PTVEY = 1

YMIN = (NEGY - 1) * YAX: YMAX = (PTVEY + 1) * YAX

YMAX = YMAX * 1000

YMIN = YMIN * 1000

YAX = YAX * 1000

FOR I = 1 TO (INT(((XEND - XSTART) / XSTEP) + .5) + 1)

 YCO(I) = YCOMP(I) * 1000

 XCO(I) = XCOMP(I) * 1000

NEXT I

END SUB

Appendix III

A summary of coil parameters and experiments

AIII.1 Coil dimensions and nomenclature.

Listed in Tables AIII.1 and AIII.2 are the coil dimensions and number of windings for the coils used in the experimental rig and in experiments described in Chapter 4.

AIII.1.1 Experimental coils.

Table AIII.1

Details of experimental coils

Coil Parameters	Inner Coil C1	Outer Coil C2	Inner Coil C1C	Outer Coil C2C
Number of Turns	300	300	300	300
Length (cm)	5.5	4.5	5.5	4.5
Inside Diameter (cm)	1.5	12.5	1.5	12.5
Outside Diameter (cm)	5.0	15.5	5.0	15.5
Core Length (cm)	N/A	N/A	5.5	5.5
Core Diameter (cm)	N/A	N/A	1.5	1.5

AIII.1.2 Prototype coils.

Table AIII.2

Details of prototype coils

Coil Parameters	Inner Coil C3	Outer Coil C4	Inner Coil C3C	Outer Coil C4C
Number of Turns	304	417	304	417
Length (cm)	5.64	4.14	5.64	4.14
Inside Diameter (cm)	1.0	16.8	1.0	10.0
Outside Diameter (cm)	5.6	10.0	5.6	16.8
Core Length (cm)	N/A	N/A	6.0	6.0
Core Diameter (cm)	N/A	N/A	0.8	0.8

AIII.2 Experimental details for Biot-Savart model.

Listed in Table AIII.3 below are the experimental details for work described in Section 4.1.4 using the coils detailed above.

Table AIII.3

Summary of experimental conditions for Figures 4.9, 4.10, AIII.1 and AIII.2

Graph Number	Coil C1 Current (A ± 0.005A)	Coil C2 Current (A ± 0.005A)	Coil C1 Range (cm ± 0.5cm)	Coil C2 Range (cm ± 0.5cm)
4.9	1.01	-----	18	-----
AIII.1	0.49	1.02	24	58.5
AIII.2	1.01	1.02	24	58.5
4.10	1.01	2.06	24	65

Figures AIII.1 and AIII.2 below are further examples of field profiles predicted by the Biot-Savart model described in Section 4.1.4.

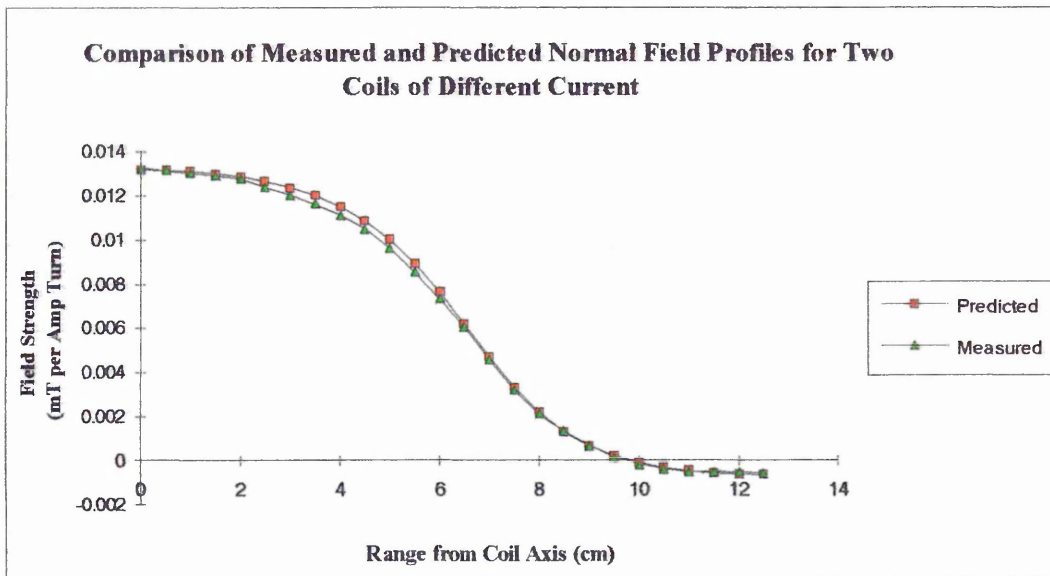


Figure AIII.1, Field profiles for two coils carrying different currents.

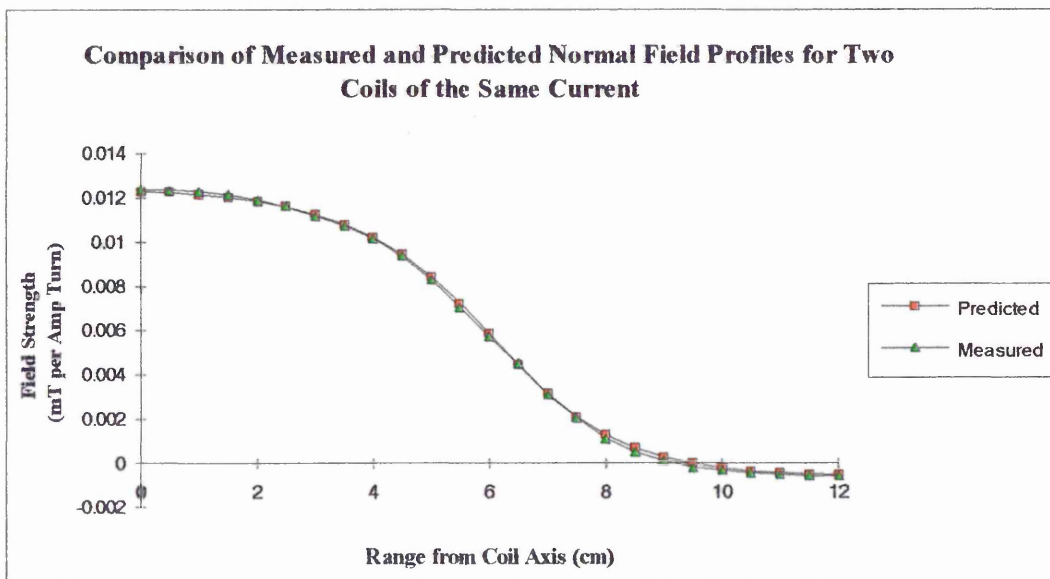


Figure AIII.1, Field profiles for two coils carrying the same currents.

AIII.3 Currents used for testing of the coils.

Listed below in Table AIII.4 are the coils and currents used to produce the field profiles shown in Sections 4.1.2, 4.1.3 and 4.1.4.

Table AIII.4
Summary of coils and currents used

Figure Number	Coil C1 Current (A)	Coil C2 Current (A)	Coil C1C Current (A)	Coil C2C Current (A)	Range (cm)
4.4	2	-----	-----	-----	1.5
4.5	-----	1	-----	-----	1.5
4.6	1	-0.25	-----	-----	1.5
4.11	2	-----	2	-----	1.5
4.12	-----	-1	-----	-0.8	1.5
4.13	1	-0.25	2	-0.5	1.5

AIII.4 Experimental details for semi-empirical method.

Listed in Table AIII.5 below are the predicted currents required to give the specified normal field zero position and field gradient at the normal.

Table AIII.5
Summary of predicted currents.

Figure Number	Field Gradient (mTcm ⁻¹)	Normal Zero (cm)	Coil C3C Current (A)	Coil C4C Current (A)
4.14	2.5	1.5	1.97	1.1
AIII.3	3	2.5	4.01	1.17
AIII.4	2	2	2	0.78

Figures AIII.3 and AIII.4 below are further examples of the semi-empirical method described in Section 4.1.5.

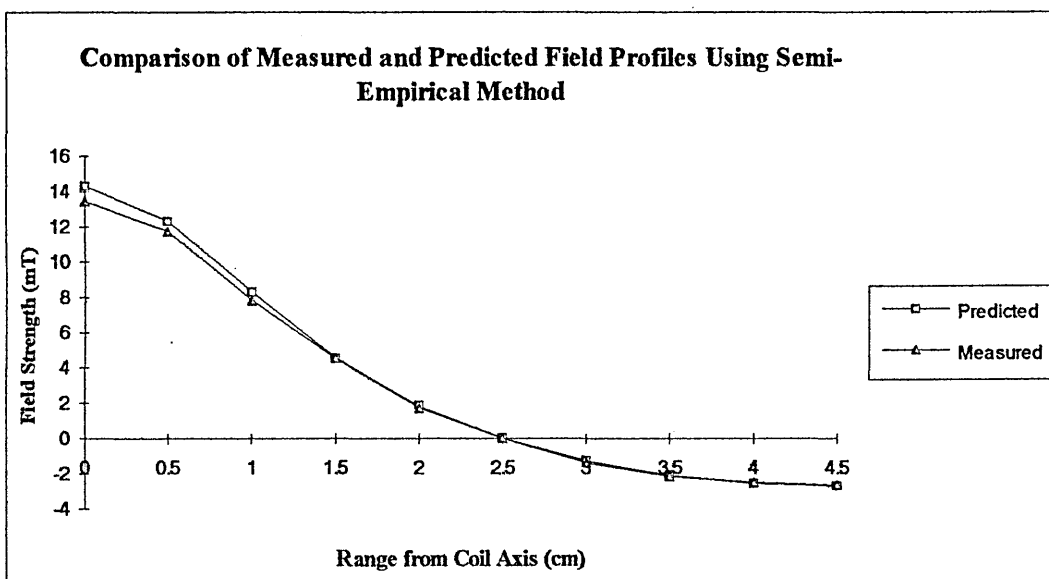


Figure AIII.3, Measured and predicted field profiles for two coil system.

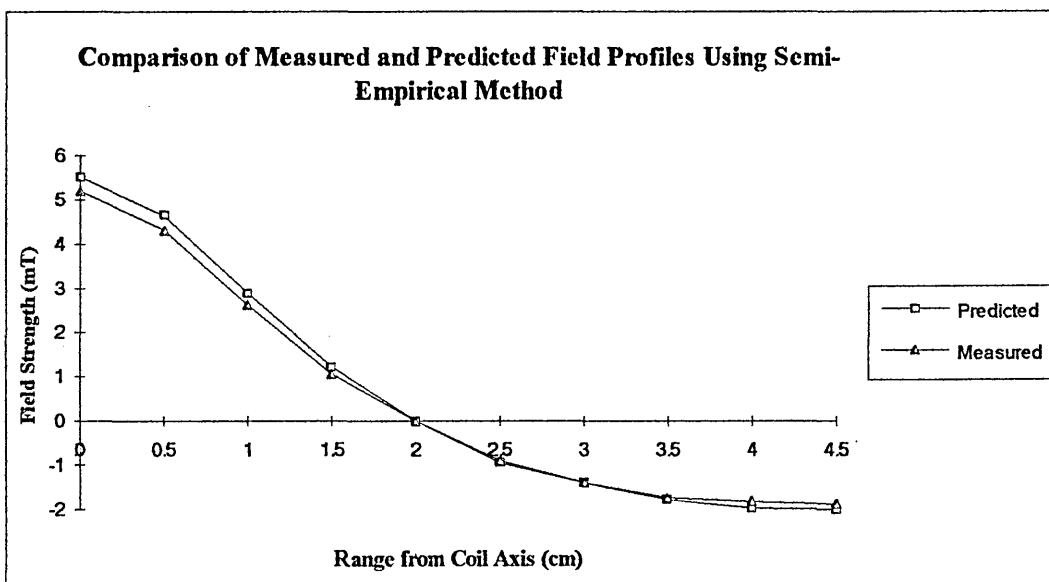


Figure AIII.4, Measured and predicted field profiles for two coil system.